

Université de Limoges
École Doctorale Bio-Santé (ED 524)
[INSERM-U850]

Submitted for the degree of
Doctor of the University of Limoges
Discipline / Specialty: Theoretical Chemistry

Presented and defended by
Tahani OSSMAN

December 2, 2016

**Physical-chemical understanding of membrane partitioning
and permeation at an atomic resolution: towards *in silico*
pharmacology**

Thesis directed by Patrick Trouillas and Nicolas Picard

JURY :

Referees

M. Michal Otyepka, Pr, Department of Physical Chemistry, Palacky University

Mme. Claire Rossi, Dr, FRE 3580 CNRS, Université de Compiègne

M. Luca Monticelli, CR INSERM – HDR, IBCP (CNRS, UMR 5086), Lyon

Examinators

M. Patrick Trouillas, Pr, INSERM UMR 850, Université de Limoges

M. Nicolas Picard, Pr, PU-PH, INSERM UMR 850, Université de Limoges

M. Florent Di Meo, Dr, INSERM UMR 850, Université de Limoges



A mes parents



Il faut toujours viser la lune, car même en cas d'échec on atterrit dans les étoiles
Oscar wild



Acknowledgements

This thesis becomes a reality with the kind support and help of many people. I would like to take this opportunity to express my sincere thanks to all of them, who directly or indirectly have been instrumental to my success during my PhD at Limoges University.

First and foremost, I feel like expressing my deepest gratitude and respect to my advisor Patrick Trouillas. Despite my poorly molecular modeling knowledge, you believed in me and you have given me the opportunity to do my thesis in your lab. I have learned a lot with you. Your door is always open. You patiently support me and inspire me to stretch myself over my limits. Thanks Patrick for all; the great atmosphere that you always try to keep, your human qualities, your patience, your generosity..... As my friends always told me when I speak about you, *I am very lucky to do my thesis with a person and great advisor like you*.

I take this precious opportunity to express my gratitude toward M. Pierre Marquet for giving me the opportunity to work in his team and the financial support to do my PhD studies. It was an honor to me to work in your research group.

I would like also to thank my co-supervisor, Nicolas Picard who has thought me useful things about pharmacological drugs.

I would like to thank all members of the jury; Michal Otyepka, Claire Rossi and Lucca Monticelli. I am sincerely honored that you accepted to review this work and to be part of my jury. I really appreciate your kindnesses and your expertises.

I am grateful to Florent, one of the most talented *theoricien* I have ever met. You devoted your precious time in giving me informations about the various aspects and in making me understanding the different conceptual problems, mainly in our last project. I am extremely appreciative for your technical guidance and support throughout the course of my work. Thank you for your help and comments on the thesis manuscript, they were really helpful.

I would like to express my special gratitude to my officemate:

Le pilote *Gabin*! thanks for your guidance encouragement, your gracious support and for your faith in me at most of stage of this research. You have taught me a lot of useful things about simulations and data analysis. You have always made time to answer small and not so-small questions. Your motivation, your positively comments (mainly when I wrote the publications in English) have really encouraged me to do more. Big thanks to your scripts that made life at work so much easier.

Michal *Mon Petit Coeur*, I have had the pleasure to share office with you. We spent a lot of time together and it was fun. Sharing and discussing ideas with you was always inspiring. You know how to make the office an enjoyable place to work. Warm thanks for traveling from Czech Republic to attend my defense.

Benjamin, I think we have had a great time exchanging discussions. Your i) gateau magique, your ii) ZIPP ZIPP ZIPP with Gabin and iii) your funny expressions and ideas will be great memories when my hair becomes white☺.

Thanks to all other staff at the department; Patricia, Jean Herve, Helene, Khadija, Fida, Cecille, Marie, Danko, Sebastien, Bastien, Julien and Roland for discussions and company during numerous lunches and coffee breaks.

Racha! Thanks for pushing me at the right moments and taking a step back when needed. You always cheered me up and had an open ear when I needed someone to talk. You always were close to me in any situation I was in. Your presence kept me happy during my PhD years.



Hafitha, Mohamad! and Hussein ! It has been a pleasure to meet persons like you. You made my journey in France so much easier and more fun.

This thesis is dedicated to my family who believe in me when I don't believe in myself; for their endless support:

Mama! Papa! I do not think I can express how lucky I am to have you. You are always behind me with your prayers, love and blessings. Without you I would not be where I am today. Thank you for earning an honest living for us.

Hicham! Hazem! Maram! and Riham you are my treasure ☺

To all my nearest friends; Saraa, Flowers and Layla.

Finally, to my dear, who early leave the life. You are a big part of this as well. Your death did not give me the time to thank you for encouraging me and providing tremendous support throughout my life, for having enough faith to follow me to the other side of the world. You were and always will be the one who brought life into me....



Copyright

This work is licensed under a Creative Commons Attribution-NonCommercial-NoDerivatives 4.0 International License.

Available online: <http://creativecommons.org/licenses/by-nc-nd/4.0/>



Contents

Aknowledgments	4
Contents.....	7
List of figures.....	10
List of tables	13
Acronyms	14
Introduction	16
Chapter I. Cell membrane	18
I.1. Introduction.....	18
I.2. Biological membrane composition.....	18
I.2.1. Phospholipids	19
I.2.2. Sphingolipids	21
I.2.3. Sterols	22
I.2.4. Carbohydrates.....	22
I.2.5. Proteins	23
I.3. Molecular shape and lipid phases	23
I.3.1. Lipid polymorphism.....	23
I.3.2. Membrane fluidity and phase transitions.....	24
I.4. Membrane composition of eukaryotic and prokaryotic cells.....	26
I.4.1. Human skin membrane	28
I.4.2. Bacterial membranes.....	29
I.5. Transport across cell membranes	31
I.5.1. Passive permeation	31
I.5.2. Protein-mediated transport	32
I.5.3. Endocytosis and exocytosis.....	32
Chapter II. Theory and methods	33
II.1. Molecular dynamics	33
II.1.1. Equation of motion.....	33
II.1.2. Bonded interactions.....	33
II.1.3. Non-bonded interactions.....	34
II.1.4. Force field	35
II.1.5. Integration Algorithms.....	37
II.2. Environments	37
II.2.1. Ensembles.....	37
II.2.2. Water models	38
II.2.3. Periodic conditions	39
II.3. Potential of the mean force and related properties	40
II.3.1. z-Constraint method	41
II.3.2. Umbrella sampling.....	42
II.3.3. COSMOmic	42
II.4. Diffusion coefficient and autocorrelation function	43
II.5. Analysis of simulation results	44
II.5.1. Lipid order parameter	45
II.5.2. Area per lipid	45



II.5.3. Bilayer thickness	45
II.5.4. Distribution	46
II.5.5. Radial distribution function.....	46
Chapter III. <i>In silico</i> pharmacology: drug membrane partitioning and crossing	48
III.1. Introduction	48
III.2. Glossary of <i>in silico</i> terms	49
III.3. Drug insertion and partitioning into lipid bilayers	50
III.3.1. Anesthetics.....	51
III.3.2. β -blockers.....	52
III.3.3. Non-steroidal anti-inflammatory drugs	52
III.3.4. Antioxidants.....	52
III.3.5. Antiviral drugs.....	53
III.3.6. Antimicrobial peptides	54
III.4. Drug entrance into cytoplasmic media	54
III.4.1. Drug passive diffusion and permeation	54
III.4.2. Facilitated diffusion mediated by membrane transport protein	57
III.5. Membrane proteins for biotransformations	60
III.6. Efflux transport toward drug resistance	62
III.7. Membrane composition.....	63
III.8. Conclusion	66
Chapter IV. Molecule insertion.....	68
IV.1. Preliminary theoretical insights on molecule insertion	68
IV.2. Multidrug Resistance-Associated Protein 4 (MRP4) controls ganciclovir intracellular accumulation and contributes to ganciclovir-induced neutropenia in renal transplant patients.....	74
IV.2.1. Introduction	74
IV.2.2. Materials and Methods	76
IV.2.3. Results.....	79
IV.2.4. Discussion.....	82
IV.2.5. Conclusion	84
IV.3. Interaction of wine anthocyanin derivatives with lipid bilayer membranes	85
IV.3.1. Introduction	85
IV.3.2. Material and methods.....	87
IV.3.3. Results and discussions.....	89
IV.3.4. Conclusion	95
Chapter V. Drug permeation: towards the semi-quantitative elucidation of structure permeation relationship	96
V.1. Introduction.....	96
V.2. Theoretical methodologies.....	98
V.2.1. Inhomogeneous solubility-diffusion model by z-constraint MD simulations.....	98
V.2.2. Technical details on MD simulations	98
V.2.3. Partitioning and free energy profiles	99
V.2.4. Diffusion profiles	99
V.2.5. Resistance and permeation coefficients	101
V.3. Structure-Permeation Relationship	101
V.3.1. Role of polarity	102
V.3.2. Role of sugar moieties	104



V.3.3. Role of pH.....	106
V.3.4. Role of molecular size.....	107
V.4. Conclusion.....	108
Conclusion	109
References.....	111



List of figures

Figure 1: Schematic representation of a lipid bilayer cell membrane and its constituents. Adapted from [2].....	18
Figure 2: Chemical structures of four representative classes of lipids.....	19
Figure 3: Structure of alcohol molecules found in membrane lipid. OH groups that bond phosphates are highlighted.....	20
Figure 4: Chemical structures of sterols.....	22
Figure 5: Lipid shapes and their influence on membrane structure.	24
Figure 6: Scheme illustrating the different phases adopted by lipid bilayers in aqueous medium.	25
Figure 7: Phospholipid distribution in the different membranes in mammals.....	27
Figure 8: Plasma membrane of eukaryotic cells. The graph shows the distribution of phospholipids between the two leaflets of the human erythrocyte membrane.....	27
Figure 9: Human skin layers.	28
Figure 10: Structure of the Gram-positive bacteria (a) and Gram-negative bacteria (b)..	30
Figure 11: Different force field resolutions of a POPC molecule: AA-FF, UA-FF and CG-FF.	36
Figure 12: Water model having 3-sites of interactions.	39
Figure 13: Periodic boundary conditions (PBC).	40
Figure 14: Pictorial description of unassisted (passive) permeation and energetic profile for drug crossing.....	40
Figure 15: 411 known targets of 1732 FDA approved drugs (up to 2015) according to ChEMBL21 dataset sorted by target type. Membrane bound targets consist about 62.4 % are annotated by expansion of triangle.....	49
Figure 16: Pictorial description of unassisted (passive) permeation and energetic profile for drug crossing.....	51
Figure 17: Location of α -tocopherol, ascorbic acid and a prototypical polyphenol (quercetin) in a DOPC lipid bilayer.	53
Figure 18: Predicted (A) Gibbs energy profiles and (B) diffusion coefficients of eight derivatives.....	56
Figure 19: (A) X-ray structure of Glucose transporter type 3 (PDB-ID: 4ZW9 - GLUT3 [217].	59
Figure 20: Scheme of biotransformation of ibuprofen with membrane-bound CYP2C9 and UGT2B7 enzymes.....	61
Figure 21: (A) X-ray structure of a ABC-transporter (PDB-ID: 3G5U, P-glycoprotein.....	63
Figure 22: Formation of nano-domains in (A) ternary and (B) quaternary mixtures.....	66
Figure 23: Chemical structures of studied drugs.....	68



Figure 24: Characteristic snapshot of triamterene and diazepam at their preferred location in DOPC lipid bilayer.	70
Figure 25: A) Location of sulfamethoxazole and its anionic form, sulfamethoxazolate, in the lipid bilayer; and B) Location of morphine and its cationic form, N-protonated morphine, in the lipid bilayer.	70
Figure 26: Location of prednisone in the lipid bilayer membrane.	71
Figure 27: A) location distribution of tacrolimus in lipid bilayer membrane and B) evolution along trajectory of location for several Cs molecules starting from different positions.	72
Figure 28: Predicted depth of drug penetration vs. $\log P$ for a series of eleven drugs.	72
Figure 29: (A) Chemical structure of ganciclovir (GCV)..	75
Figure 30: Ganciclovir intracellular accumulation into (A) Jurkat cells in presence of $50 \mu\text{mol.L}^{-1}$ of the MRP inhibitor MK-571 and (B) HEK293T cells transiently transfected with <i>ABCC4</i> (MRP4) reference and variant (rs15868658) sequences or with an empty vector (pcDNA5/FRT).....	81
Figure 31: Chemical structures of a series of anthocyanin derivatives, based on the malvidin moiety.	87
Figure 32: Definition of the vector V used to determine the orientation of flavonoid moiety in membranes.	88
Figure 33: Location of the quinonoidal forms of malvidin-3- <i>O</i> -glucoside (A_4 , A_7 , and A_5).....	91
Figure 34: Free energy profiles of penetration in the lipid bilayer for (A) malvidin-3- <i>O</i> -glucoside deprotonated forms A_4 , A_7 , and A_5 ; (B) malvidin-3- <i>O</i> -glucoside anionic ($A_{4,7}^-$) and cationic (AH^+) forms; (C) chalcone, hemiketal and pyranoanthocyanin forms; and (D) malvidin aglycone.....	91
Figure 35: Location of the aglycone malvidin in membrane.	93
Figure 36: Charge distribution in the flavylum cation (AH^+), quinonoidal base (A_4) and quinonoid anion ($A_{4,7}^-$) as obtained by two different methods of calculation.....	94
Figure 37: Chemical structures of the 8-member set of compounds studied in this work.	97
Figure 38: (a) Force fluctuation autocorrelation function and double/triple exponential fit in 4 different z-constraint windows and (b) z-dependent diffusion profiles according to fitting procedure.....	100
Figure 39: Profiles of (a) Gibbs energy profiles, (b) diffusion coefficient, and (c) resistance to membrane crossing of benzene (black), glucose (blue) and testosterone (magenta).	103
Figure 40: Profiles of (a) Gibbs energy profiles, (b) diffusion coefficient, and (c) resistance to membrane crossing of quercetin (red) and rutin (cyan).....	105
Figure 41: Profiles of (a) Gibbs energy profiles, (b) diffusion coefficient, and (c) resistance to membrane crossing of MPA (orange) and mycophenolate (purple).	106
Figure 42: Profiles of (a) Gibbs energy profiles, (b) diffusion coefficient, and (c) resistance to membrane crossing of benzene (black), ganciclovir (green) and mycophenolic acid (orange).	107



Figure 43: Diffusion coefficient per region vs. molecular volume in the 5 membrane regions.

.....108



List of tables

Table 1: Most common fatty acids found in membranes.	20
Table 2: Abbreviations of the common phospholipids.	21
Table 3: Lipid composition in human epidermis.	28
Table 4: Parameters for some water models..	39
Table 5: Lipid area (APL) and Luzzati bilayer thickness (<i>DB</i>) of several fluid bilayers at different temperatures].	46
Table 6: Simulation time (in ns) for two representative molecular systems with three types of force field with regular computational facilities (8 CPUs) achievable within a day.	67
Table 7: Location, orientation of drugs studied..	69
Table 8: patient characteristics.	76
Table 9: Variant genotype distributions and allele frequencies in the exploratory group.	79
Table 10: Association of clinical and genetic covariates with neutrophil count evolution in the exploratory group.	80
Table 11: Location, orientation, free energy barriers and dipole moments of malvidin derivatives studied.....	90
Table 12: Calculated maximum free energy differences ($\Delta\Delta G$, kcal.mol ⁻¹) along z-constraint windows.	101
Table 13: Calculated maximum free energy differences ($\Delta\Delta G$, kcal.mol ⁻¹) along z-constraint windows..	102



Acronyms

AA: All-atom
ABC: ATP-binding cassette
ACF: Autocorrelation function
ADME: Absorption, Distribution, Metabolism and Excretion
AMP: Antimicrobial peptide
CG: Coarse-grained
CL: Cardiolipin
CMV: Cytomegalovirus
CNT: Concentrative nucleoside transporter
COM: Center of mass
COX: Cyclooxygenase
Cs: Cyclosporine
CYP: Cytochrome P450
DLiPC: Dilinoeoyl-phosphatidylcholine
DOPC: 1,2-dioleoyl-sn-glycero-3-phosphocholine
GA: General anesthetic
GCV: Ganciclovir
GlpT: Glycerol-3-phosphate:phosphate transporter
GLUT1: Glucose transporter; GST: Glutathione S-transferase
Gram-: Gram negative bacteria
Gram+: Gram positive bacteria
IF: Inward facing
LA: Local anesthetic
LacY: Lactose permease
Ld or L α : Liquid disordered phase
Lo: Liquid ordered phase
logP: Partition coefficient
LPS : Lipopolysaccharide (LPS),
MATE: Multi-antimicrobial extrusion protein
MD: Molecular dynamic
MFS: Major facilitator superfamily
MM/GBSA: Molecular Mechanics / Generalized Born Surface Area
MM/PBSA: Molecular Mechanics / PoissonBoltzmann Surface Area
MPA: Mycophenolic acid
MRP4 : Multidrug Resistance-Associated Protein 4
Msba: Bacterial ABC lipid flippase
NAT: N-acetyltransferases
NBD: Nucleotide-binding domains



NSAID: Non-steroidal anti-inflammatory drug
NSS: 4 Neurotransmitter:sodium symporter
OAT: Organic anion transporter
OF: Outward facing
OM: Outer membrane
PC: Phosphatidyl-choline
PE: Phosphatidyl ethanolamine
PEPT: Peptide transporter
PG: Phosphatidyl glycerol
PI: Phosphatidyl inositol
PIP2: Phosphatidylinositol 4,5-bisphosphate
PMF: Potential of mean force
POPC: 1-Palmitoyl,2-oleoyl-sn-glycero-3-phosphocholine
POPG: 1-Palmitoyl-2-oleoyl-sn-glycero-3-phosphoglycerol
PS: Phosphatidyl serine
QM/MM: Quantum mechanics/Molecular mechanics
ROS: Reactive oxygen species
SC: Stratum corneum
SG: Stratum granulosum
SLC: Solute carrier
SM: sphingomyelin
So or L β : Solid crystalline phase
SULT: Sulfotransferase
Tm: melting temperature
TM: Transmembrane helice
TMD: Transmembrane domain
UA: United-atom
UGT: Uridine 5'-diphosphoglucuronosyltransferase
VGCV : Valganciclovir
 $\Delta G(z)$: Gibbs energy profile
 $D(z)$: Diffusion coefficient
 P : Permeability coefficient
 R : Resistance
 $\xi(z, t)$: Friction coefficient



Introduction

The development of novel drugs is not only a matter of the best therapeutic activity (i.e., pharmacodynamics, PD), but also a matter of how drugs reach its biological target. This mainly concerns drug membrane crossing, i.e., influx. The vast majority of drugs has to cross at least one cellular membrane barrier passively or transporter-mediated. The research on passive transport is particularly strong, as this process can support active (protein-mediated) transport. Also drug toxicity has often been related to drug efflux, in this case mainly membrane transporters are involved.

Nowadays, to correctly tackle this issue, a thorough understanding is required with an atomic resolution. Passive permeation can be decomposed into four successive steps: 1) partitioning into the hydrophobic core of the membrane or binding to the polar head groups; 2) diffusion through each lipid bilayer leaflet; 3) transfer from one to the other leaflet; and 4) partitioning back to the aqueous (inner) compartment. These processes are driven by drug-membrane interactions. The complete physical-chemical understanding of these interactions allows establishment of structure-permeation relationship (SPR). Several experimental techniques have been developed to study these interactions and predict permeability coefficients [1]. There are pros and cons to these experimental techniques, which do not allow a complete understanding at an atomic level.

With the increase of computing power, and the development of force field parameterization, molecular dynamics (MD) has become an alternative and efficient tool to study drug-membrane interactions. MD simulations allow providing accurate atomic-scale interpretations with a femtosecond resolution. In the present work, we have investigated interactions of various drugs with membranes, as well as their positioning, orientation, and passive permeation.

The manuscript is organized as follows: chapter I proposes a brief overview of the different membrane ingredients (section I.2); organization in biological membranes (section I.3); variability in composition according to cell types (section I.4); and the different mechanisms by which drugs can cross membranes (section I.5).

Chapter II introduces the computational methods. The underlying theory and the methodological details are presented in section II.1 and II.2. Another advantage of MD simulations is their capacity to evaluate the Gibbs energy profiles also denoted as potentials of the mean force (PMF). The calculation of Gibbs energy profiles is important to evaluate partition and permeability coefficients; the related methodologies are reported in section II.3. Section II.4 reports the methodology to calculate the local diffusion coefficient. The last section (section II.5) of this chapter refers to the analysis of MD simulations from the resulting coordinate trajectories.

Chapter III is a review on the interactions of several classes of drugs with lipid bilayers and with membrane proteins. The pathway of drug cellular uptake is discussed in details from a theoretical point of view.

The subject of Chapter IV is to establish the relationship between drug chemical structure and interaction/insertion with/in membranes. In section IV.1, we have focused on drugs (e.g., antiviral and immunosuppressant) widely used in renal transplantation and for which interaction with membrane is an essential pharmacological step to rationalize their action and



elimination. To evaluate drug insertion, typical 1 μ s MD simulations were performed. The capacity to insert into lipid bilayers, the stable location and the preferred orientation were systematically evaluated. Among the studied compounds, ganciclovir (GCV) has been shown prone to intracellular accumulation, leading to several adverse hematological effects. To rationalize this issue, the contribution of Multidrug Resistance-Associated Protein 4 (MRP4) in GCV toxicity on neutrophils in renal transplantation was studied by other researchers from our Inserm Unit and published together with the theoretical data on GCV membrane insertion (section IV.2). In this work, MD simulations have supported a better understanding of the mechanism of GCV penetration/crossing in/through lipid membranes.

In the context of xenobiotic-membrane interactions, we also studied the capacity of various anthocyanin derivatives to insert lipid bilayer membranes (section IV.3). Anthocyanins exhibit numerous biological activities (e.g., inhibition of lipid peroxidation in biological membranes), for which their position in bilayer membrane is of particular importance. Based on MD simulations and COSMOmic calculations, position, orientation and Gibbs energy profile through membrane were evaluated.

The last chapter (Chapter V) goes further in the description of drug-membrane interactions by attempting to i) calculate drug permeability of several compounds (including drugs used in transplantation), and ii) provide an overview of drug passive permeation through membrane at the nanoscale resolution. Such evaluation has required calculation of dynamical aspects (i.e., diffusion) of the permeation process. Biased MD (z-constrained) simulations were performed to calculate both ΔG and diffusion profiles. We have studied permeation of several classes of compounds (antivirals, immunosuppressants, antioxidants...); pH effect and influence of substituents have been rationalized based on these compounds at an atomic resolution.



Chapter I. Cell membrane

I.1. Introduction

Biological membranes are vital structural components of living cells. They play a determinant role in cell protection and they control the transport of xenobiotics, including drugs. They include plasma membranes but also various membranes of cell organelles, e.g., mitochondrial and nucleus membranes. Their composition highly depends on one to another cell type, as well as on cell life cycle. The constitutive amphiphilic lipids are the essential compounds, providing membrane their bilayer structure of 6-10 nm thick, with two asymmetrical outer and inner leaflets (Figure 1). However, membranes are constituted of many other ingredients; indeed, cell function depends on a large number of other compounds, e.g., proteins, sterols and glycolipids that are embedded in the lipid bilayer. Biological membranes are described as a mosaic of all these components (fluid mosaic model). Although it was previously described as homogeneous, several studies have suggested that lipid bilayer is highly heterogeneous, and maybe arranged in lateral nano- to micro-domains, which differ in their lipid composition and their behavior. Biological membranes are also highly dynamic and complex systems, which are currently still under careful scrutiny by experimental and computational methods. Lipids and proteins are packed together mainly by noncovalent interactions, namely hydrophobic effects, electrostatic interactions, hydrogen bonding and dispersive interactions (van der Waals forces).

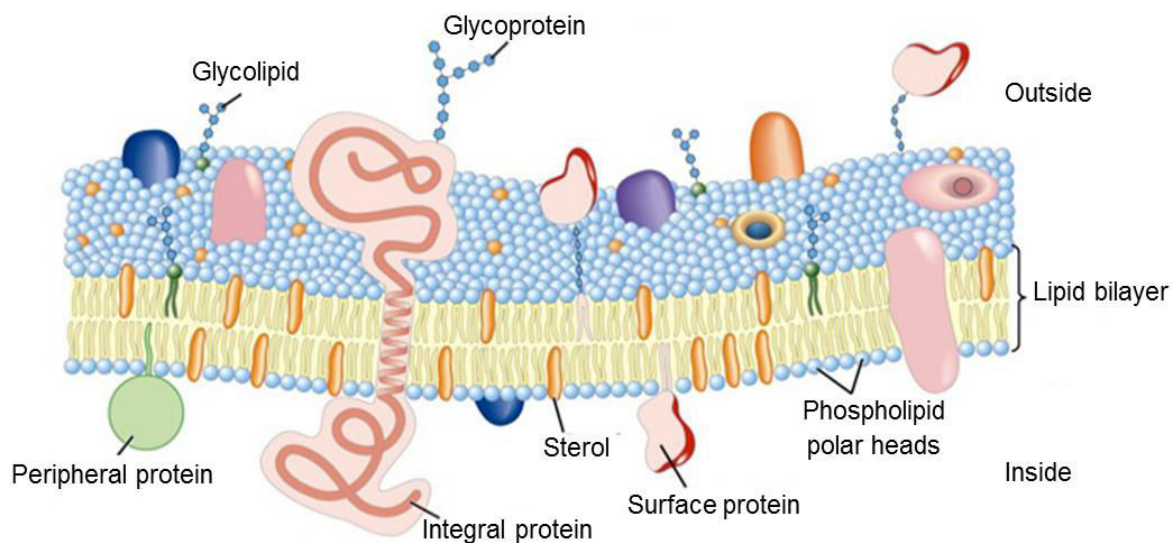


Figure 1: Schematic representation of a lipid bilayer cell membrane and its constituents. Adapted from [2].

I.2. Biological membrane composition

With about 50% of the mass of a biological membrane, lipids constitute the largest part. They exist as different chemical structures and sizes. Membrane lipids are amphiphilic and they can be classified according to their (hydrophobic) fatty acid tails and their polar groups. A large variety of membrane lipids have been identified so far. For instance, some lipids are found exclusively in bacteria (e.g., lipid A [3]), others are almost exclusively found in mitochondrial membranes (e.g., cardiolipin [4,5]). Phospholipids are the most abundant lipids



in living cell membranes, as in mammalian and bacterial cells. Sphingolipids, sterols and glycolipids are also major constituents of biological membranes.

I.2.1. Phospholipids

The main class of phospholipids is glycerophospholipids (40-60% of the total lipid fraction). Glycerophospholipids are constituted of a glycerol backbone attached to two fatty acids and one phosphate group. The fatty acids are linked to the first and second oxygen of glycerol via ester linkage, at positions C1 (sn1) and C2 (sn2), respectively. The third hydroxyl group, at position C3 (sn3), reacts with phosphoric acid and form phosphatidate (Figure 2).

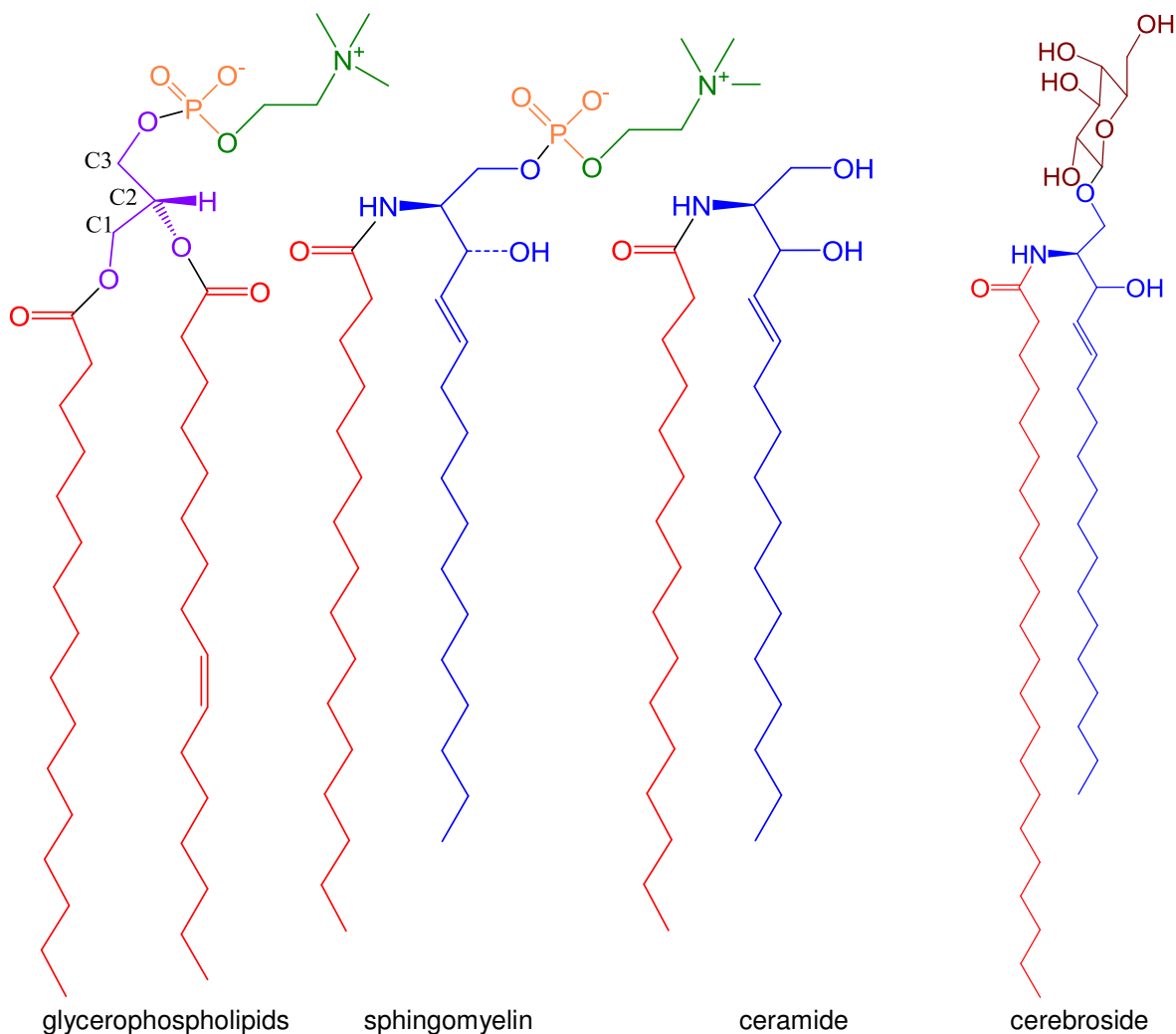


Figure 2: Chemical structures of four representative classes of lipids.

Due to their acidic nature, the phosphatidate can link to an alcohol molecule including choline, ethanolamine, serine, glycerol or inositol (Figure 3). These chemical arrangements make zwitterionic lipids (phosphatidyl-choline - PC and phosphatidyl ethanolamine - PE) or negatively charged lipids (phosphatidyl serine - PS, phosphatidyl glycerol – PG, phosphatidyl inositol - PI, and cardiolipin – CL; a dimer of PG). The ratio of charged lipids and their distribution between the two leaflets of a given lipid bilayer control the net charges of membrane. This can induce a surface potential that may dramatically affect biological processes [6–8].



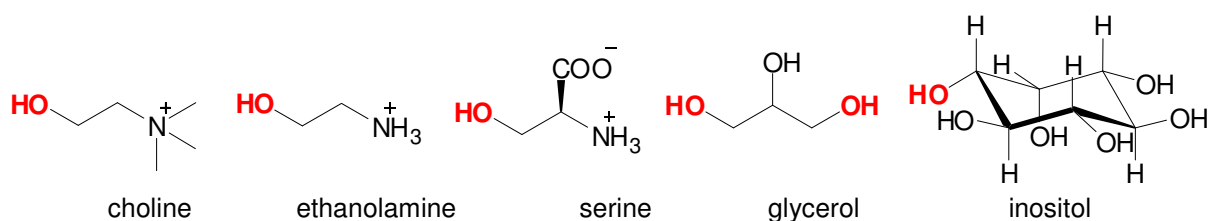


Figure 3: Structure of alcohol molecules found in membrane lipid. OH groups that bond phosphates are highlighted.

The fatty acid moieties vary from their chain length (number of carbon atoms, quoted C in Table 1), as well as the number and position of double bonds (unsaturation), quoted D. The majority of phospholipids have fatty acids chains typically made of 12 to 20 carbons, saturated at the sn1 position (e.g., palmitic or stearic acid), and mono- or poly-unsaturated at the sn2 position (e.g., oleic or arachidonic fatty acid chains). The double bond is often in conformer *cis* in bilayers, but *trans* forms can also be synthesized by dehydrogenation. Table 1 reports on the most common fatty acids found in biological membranes.

The fatty acid characteristics strongly affect lipid bilayer physical properties. The membrane thickness is directly correlated to chain length. Furthermore, the number of *cis*-unsaturations influences chain packing, and thus melting temperature T_m (i.e., transition temperature between gel and fluid phase, section 1.3.2). For example, at similar temperature, oleate chains having one *cis* double bond (18:1) exhibit larger lateral more disorganized space than stearate saturated chains (18:0). Therefore, T_m is lower in case of phospholipids containing oleate than stearate chains. Table 2 quotes the nomenclature of the common phospholipids; the first two letters refer to the fatty acids, whereas the other two refer to the head groups.

C:D	Common name	Structure	Melting point (°C)
10:0	Capric acid	$\text{CH}_3(\text{CH}_2)_8\text{COOH}$	31.6
12:0	Lauric acid	$\text{CH}_3(\text{CH}_2)_{10}\text{COOH}$	44
14:0	Myristic acid	$\text{CH}_3(\text{CH}_2)_{12}\text{COOH}$	54
16:0	Palmitic acid	$\text{CH}_3(\text{CH}_2)_{14}\text{COOH}$	63
18:0	Stearic acid	$\text{CH}_3(\text{CH}_2)_{16}\text{COOH}$	70
20:0	Arachidic acid	$\text{CH}_3(\text{CH}_2)_{18}\text{COOH}$	77
16:1	Palmitoleic acid	$\text{CH}_3(\text{CH}_2)_5\text{CH}=\text{CH}(\text{CH}_2)_7\text{COOH}$	-0.5
18:1	Oleic acid	$\text{CH}_3(\text{CH}_2)_7\text{CH}=\text{CH}(\text{CH}_2)_7\text{COOH}$	13.4
18:2	Linoleic acid	$\text{CH}_3(\text{CH}_2)_4\text{CH}=\text{CHCH}_2\text{CH}=\text{CH}(\text{CH}_2)_7\text{COOH}$	-5.0
20:4	Arachidonic acid	$\text{CH}_3(\text{CH}_2)_4(\text{CH}=\text{CHCH}_2)_4(\text{CH}_2)_2\text{COOH}$	-49.5

Table 1: Most common fatty acids found in membranes.



Abbreviation	Chemical name
DMPC	1,2-dimyristoyl- <i>sn</i> -glycero-3-phosphocholine
DPPC	1,2-dipalmitoyl- <i>sn</i> -glycero-3-phosphocholine
DSPC	1,2-distearoyl- <i>sn</i> -glycero-3-phosphocholine
POPC	1-palmitoyl-2-oleoyl- <i>sn</i> -glycero-3-phosphocholine
DOPC	1,2-dioleoyl- <i>sn</i> -glycero-3-phosphocholine
DLPC	1,2-dilinoleoyl- <i>sn</i> -glycero-3-phosphocholine
DOPE	1,2-dioleoyl- <i>sn</i> -glycero-3-phosphoethanolamine
POPS	1-palmitoyl-2-oleoyl- <i>sn</i> -glycero-3-phospho-L-serine
DPPG	1,2-dipalmitoyl- <i>sn</i> -glycero-3-phospho-(1'- <i>rac</i> -glycerol)
18:0 SM	N-stearoyl-D- <i>erythro</i> -sphingosylphosphorylcholine

Table 2: Abbreviations of the common phospholipids.

I.2.2. Sphingolipids

Another important class of membrane lipids is the sphingolipids. As phospholipids, sphingolipid molecules bear one polar head group and two lipid tails. Sphingolipids differ from phospholipids by the presence of one sphingosine tail, an unsaturated long-chain amino alcohol linked to a saturated and long (up to 24 carbon atoms) fatty acid chain (see Figure 2). A phosphorylated alcohol or a carbohydrate can attach to the terminus hydroxyl group of the sphingosine backbone to form sphingomyelin (SM) lipids and glycosphingolipids, respectively. SM is the only example of sphingolipids that can also be classified as a phospholipid, as they contain a phosphate group (Figure 2). The predominant fatty acid tails in SM are palmitic acid and oleic acid. Ceramide is a simple form of sphingolipids, composed of a sphingosine core linked to fatty acids via an amide bond (Figure 2). Sphingolipids are present in all membranes but they are abundant mainly in myelin and nervous tissue; SMs are important structural ingredients of nerve cell membranes. They are thought to participate in the formation of lipid domains, aggregating in cholesterol-enriched domains, with a potentially important role in membrane protein functions.



I.2.3. Sterols

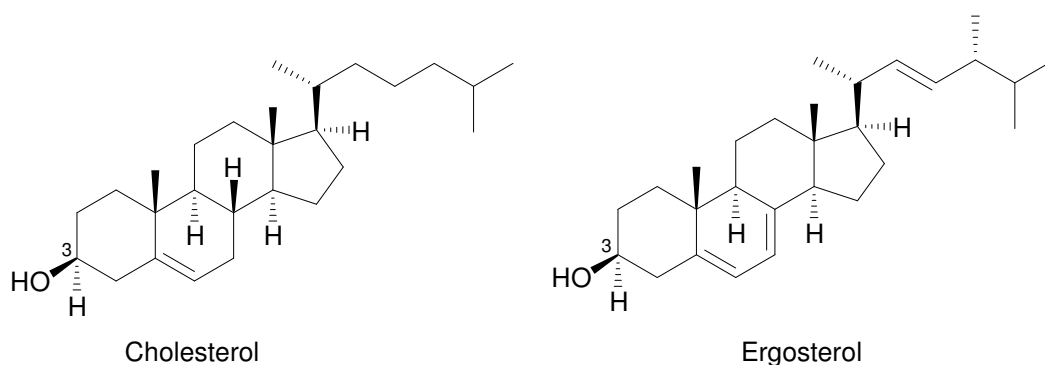


Figure 4: Chemical structures of sterols.

Sterols are a special class of lipids. They exhibit a polycyclic structure. Cholesterol, the major member of this class of compounds, is a constituent of membranes in mammalian cells (30-50 mol % of the total lipid fraction) but it is absent from most of prokaryotic cells [9]. The chemical structure of cholesterol differs from phospholipids and glycolipids. It consists of a fused cyclic four-ring structure containing a single polar hydroxyl group at position 3 and a short hydrocarbon side chain, the cyclic ring system being essentially rigid (Figure 4). The hydroxyl group provides cholesterol some amphiphilic character, which drives its orientation in membranes. Cholesterol strongly influences mechanical and structural properties of biological membranes [10] (for more details, the reader can refer to section III.7). Moreover, it serves as a signaling compound in cellular communication. Other sterols are also present in biological membranes; including ergosterol (Figure 4), which predominates in yeast and sitosterol in plants [11].

I.2.4. Carbohydrates

Carbohydrates are found in several biological membranes, as attached to lipids or to proteins, forming glycolipids and glycoproteins, respectively. Glycolipids are present in membranes in lower concentration than phospholipids and cholesterol. Carbohydrates, as glucose or galactose, are constituents of glycolipids, replacing the phosphate-containing head groups in phospholipids. Cerebrosides bear one sugar group (mostly galactose) attached to the terminus hydroxyl group of ceramides (Figure 2). They are mainly found in neuronal cell membranes. Gangliosides are more complex example of glycolipids, which are composed of additional carbohydrates in addition to sialic acid (N-acetylneuraminic acid, NANA) molecule in varying amounts. In animal cell membranes, most of glycolipids bear a sphingosine backbone, whereas in plant and bacterial cell membranes, glycolipids with a glycerol backbone are dominant. Lipopolysaccharides are major examples of glycolipids constituent of the outer membrane of Gram-negative bacteria. They consist of a complex lipid part (lipid A) and a long polysaccharide chain. Glycolipids contribute to membrane asymmetry, as they are present only in the outer layer of plasma membranes, their sugar moieties being oriented towards cell surface. Sphingolipids and glycolipids are involved in different recognition functions at the surface of cells. In human cells, glycolipids contribute to cell communication, which often results from interactions between glycolipids or glycoproteins at the surface of cells, with specific receptors, e.g., lectins.



I.2.5. Proteins

Although the lipid bilayer provides the core structure of biological membranes, membrane proteins (at the surface, anchored or transmembrane) control many specific biological functions of membranes [12]. They play important roles in: drug transport; transmission of signals from the outer compartment to the intracellular targets; enzymatic transformation; cell adhesion; or cell recognition by surface markers. The amounts and types of proteins highly depend on cell types. For instance, proteins represent approximately 50% of the plasma membrane weight and less than 25% of the myelin membrane weight. Specialized organelles such as internal membranes of mitochondria or chloroplasts contain the highest amount of proteins (up to 75%). Membrane proteins associate with the lipid bilayer in various ways. Either simply anchored or being fully transmembrane, they are attached to the lipid bilayer by hydrophobic regions that are embedded in the bilayer. Their hydrophilic regions are exposed to the interface or to bulk water. Other proteins lie on the bilayer surface by noncovalent interactions with the polar head group region and with other membrane proteins; these proteins are called peripheral membrane proteins [12].

I.3. Molecular shape and lipid phases

I.3.1. Lipid polymorphism

Due to their strong non-polar character, lipids dissolve readily in organic solvents (e.g., acetone, benzene) whereas their solubility is limited in water, in which they aggregate by hydrophobic effects. Lipid solubility is a key parameter to rationalize membrane properties, as xenobiotic permeation. The amphiphilic character obviously rationalizes self-association into bilayers in cellular (mainly aqueous) environments. The three common phases obtained by aggregation of these amphiphilic lipids are micelles, lamellar layers (bilayers mainly in biological systems) or hexagonal packing.

The packing parameter P is particularly useful to characterize intrinsic properties of a membrane lipid in terms of its capacity to associate into a specific arrangement:

$$P = \frac{v}{a l}$$

where v is the molecular volume; a the head group cross section area; and l the lipid length.

When $P < 1$, a conical lipid shape exists (e.g., lyso-PC). The latter is more likely found in micellar or normal hexagonal phases. This is due to the area in the lipid head group region, which becomes higher than that of the lipid tail region, thus inducing positive curvature. When $P = 1$, a cylindrical-shaped lipid exists (e.g., PC, PS). These are optimal conditions to form a lipid bilayer structure. When $P > 1$, the lipids are in inverted cone shape, which induces curved structure, as in the inverse hexagonal phase (e.g., PE). This is due to the area in the lipid tail region, which becomes higher than that of lipid head group region, thus inducing negative curvature (Figure 5).

Phospholipids and glycolipids have a packing parameter close to unity, and thus they tend to form flat bilayers in aqueous solutions. Cholesterol adopts conical shape that favors micelles. Membrane curvature reduces or favors lipid head group packing, thus facilitating or hindering drug penetration, respectively. It was shown that addition of free fatty acids (e.g., capric acid, palmitic acid, oleic acid and lysolipids) that adopt micellar or hexagonal structures, induce membrane curvature in the bilayer and lowers permeability barriers [13].



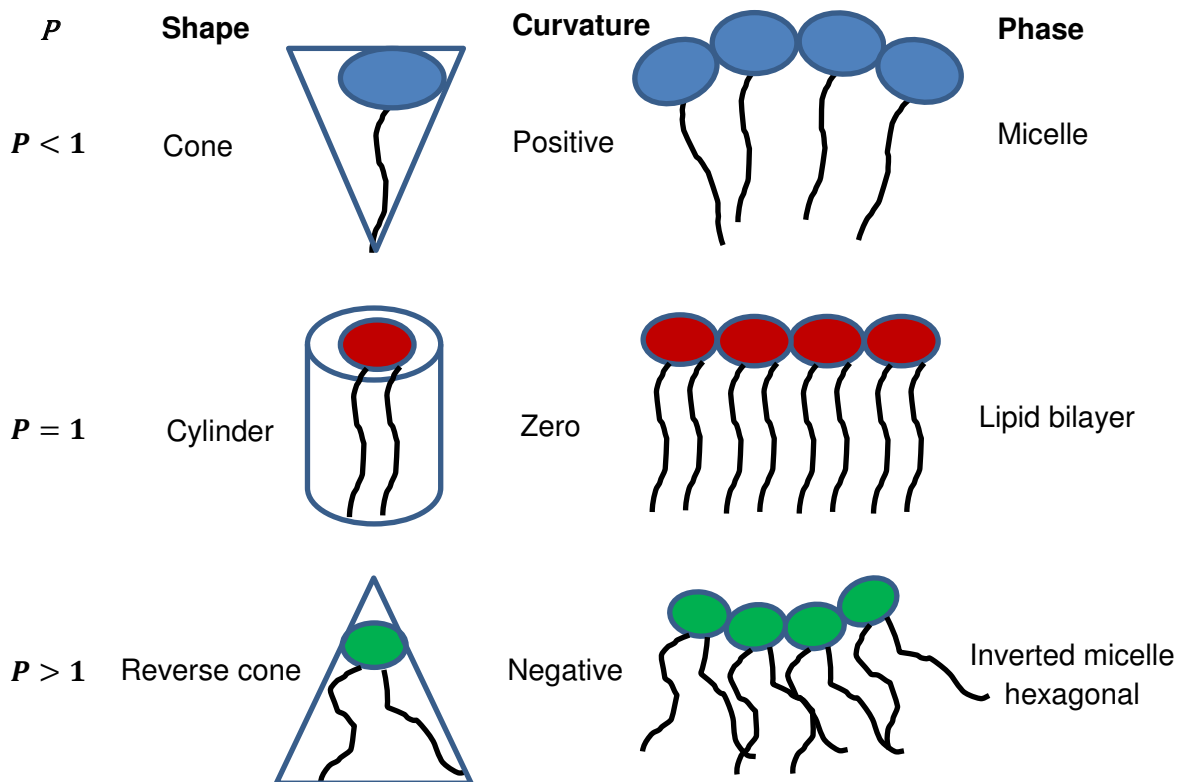


Figure 5: Lipid shapes and their influence on membrane structure.

I.3.2. Membrane fluidity and phase transitions

The supramolecular organization of lipid bilayers is a complex result of the high diversity in their composition (e.g., lipid types, amount of cholesterol, asymmetry) and the external physical conditions. Within an external aqueous environment, lipid bilayers can adopt different physical states or phases: 1) gel phase, which also refers to as solid crystalline phase, S_o or L_β , in which lipid tails are tightly packed and organized; 2) liquid disordered phase (L_d or L_α), also called fluid phase, and 3) liquid ordered phase (L_o) (Figure 6). The different phases are characterized by the spatial arrangements and thus the degrees of freedom of one lipid with respect to its neighboring lipids.

In general, biological membranes are highly dynamic. In L_d phase, lipids highly diffuse laterally within one leaflet of lipid bilayers, whereas this mobility is impeded in S_o phase. In plasma membrane, the lateral diffusion coefficient of lipids D_L is ranging from 10^{-7} to 10^{-8} $\text{cm}^2 \cdot \text{s}^{-1}$ for fluid phase membranes and from 10^{-8} to 10^{-9} $\text{cm}^2 \cdot \text{s}^{-1}$ for more ordered membranes (L_o) [14]. Moreover, lipids can diffuse transversally from one to another leaflet, so-called “flip-flop” processes. Due to the high energy barrier for polar head groups to cross the hydrophobic core of the bilayer, and the increasing of lateral tension followed by the addition of lipids in the “receiving” leaflet, this process is extremely slow 10^{-15} s^{-1} [15]. However it can be accelerated in the presence of membrane proteins [16]. Conversely, for cholesterol, the flip-flop process is fast (1 s^{-1}) [17]. As a comparison, proteins lateral diffusion is hundred times slower than lipids and no flip-flop is possible. Numerous studies on living cell membranes have shown that most of lipid bilayers adopt the L_d phase under physiologically conditions, which seems to be essential for normal cell growth and membrane function.



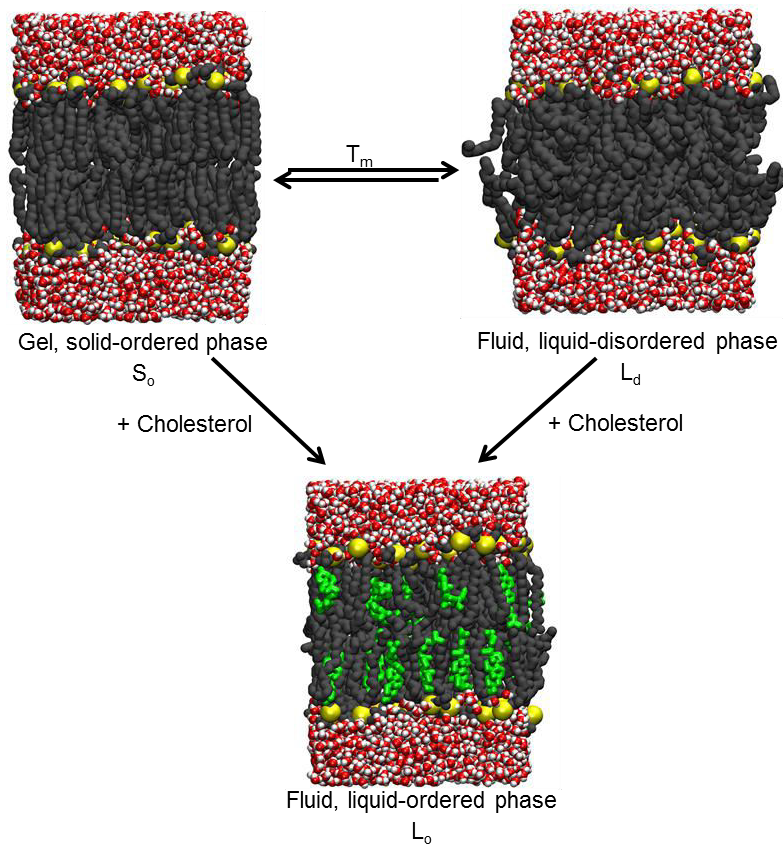


Figure 6: Scheme illustrating the different phases adopted by lipid bilayers in aqueous medium.

Lipid phase transitions induce strong changes in entropy of the system through reorganization of all components of the bilayers. Thus, the structure of lipid bilayers is dramatically affected by temperature. Below the transition temperature T_m (melting temperature), lipid bilayers adopt the S_o phase. Above T_m , lipid bilayers are in L_d phase. In other words, fluidity is increased vs. temperature. In some lipid mixtures, especially ternary mixtures containing cholesterol, the intermediate L_o phase can exist, at least in domains. Indeed depending on temperature but also lipid composition, different phases can coexist to form laterally segregated domains. Several intrinsic factors may affect membrane fluidity including chain length, unsaturation, sterols, and membrane protein concentration.

I.3.2.1 Chain length

In general, membrane fluidization temperature or T_m increases with the increase of fatty acid chain length. Longer fatty acid chains allow stronger van der Waals interactions in both the same and opposite monolayer, than the shorter chains. This favors packing, so in favor of gel phase formation. Therefore, the larger the carbon atom number, the higher the T_m . Hence, domains containing lipids with longer chains are stable at higher temperatures.

I.3.2.2 Unsaturation

The presence of *cis*-double bonds in lipid chains induces kinks which reduce van der Waals interactions between lipid chains. This decreases T_m , thus favoring the formation of the L_d phase at lower temperatures (Table 1). Furthermore, T_m is sensitive to the positioning of double bonds in the fatty acid chain. Lipids having a double bond close to the middle of the fatty acid chain exhibits a lower T_m compared to lipid having a double bond closer to the edge



of the chain. Indeed, in the former structure, kinks are located in the center of the leaflet, thus induce greater structural modifications. Moreover, as the fatty acid chains of unsaturated lipids are more folded and distant from each other, the corresponding bilayers are thinner than bilayers made of saturated lipids. In biological membranes, glycerophospholipids display mostly unsaturated lipid chains in position sn-2 and then, they adopt fluid phase. Conversely, sphingolipids have long saturated chains, adopting gel phase; they are fluidized by sterols.

I.3.2.3 Sterols

Sterols (e.g., cholesterol) exhibit particular effects on modulation of bilayer fluidity. In the absence of cholesterol, lipid bilayers can exist only in L_d or S_0 phases, whereas in the presence of cholesterol, L_o is also likely to be formed. When incorporated in S_0 phase, cholesterol reduces the well-ordered packing of lipids thus increasing membrane fluidity. Conversely, accumulation of cholesterol in L_d phase causes tighter packing with *trans* chain conformation of the lipid tails, thus reducing membrane permeability. The L_o phase is an intermediate between S_0 and L_d phases, with less lateral packing as in the former, however keeping relatively high rate of lateral diffusion. Coexistence of two phases within the membrane containing cholesterol has been observed. For more details see section III.7.

I.3.2.4 Supramolecular domains

Over the last 30 years, there have been growing evidences that plasma membrane is not uniform; instead membrane domains can be formed. These domains appear to be enriched in cholesterol and the sphingolipids (sphingomyelin and glycolipids). These clusters of sphingolipids and cholesterol are thought to form rafts, which bear somewhat L_o phase characteristic, surrounded by and coexisting with L_d phase. Rafts are thought to be highly dynamical, moving laterally within the plasma membrane with possible association to membrane proteins [17–19]. Even though the existence of such domains is still under debate, they could be involved in important cell processes such as endocytosis, signaling, protein organization, and lipid regulation [20–22]. Moreover, membrane proteins have also been observed to cluster through extracellular ligand binding sites or interaction between cells (cell-cell adhesion), which may drive phase separation [23].

I.4. Membrane composition of eukaryotic and prokaryotic cells

Biological cells consist of a cytoplasm, which is surrounded by the plasma membrane. There exist two major types of cells, namely i) eukaryotic cells, which are constituted of organelles and a nucleus (i.e., animal cells); and ii) prokaryotic cells, which consist of a single cell without internal organelles (e.g., bacteria). The review of van Meer et al. reports on synthesis, transport and distribution of lipids in eukaryotic mammalian cells and yeast [24]. Cell lipid composition shows great diversity among species but also within a same specie among cell types. For instance, in eukaryotic cells, plasma or intracellular membranes significantly differ in lipid composition (Figure 7).

The composition differs mainly from the types of constitutive lipids (e.g., phospholipids, sphingolipids, cholesterol, cardiolipin). Eukaryotic membranes are enriched in zwitterionic neutral lipids (e.g., PC, SM, and PE) and cholesterol. In contrast, prokaryotic cells are much more negatively charged; they are enriched in anionic lipids (e.g., PG, PS and CL). Cholesterol is absent in most of prokaryotic cells.



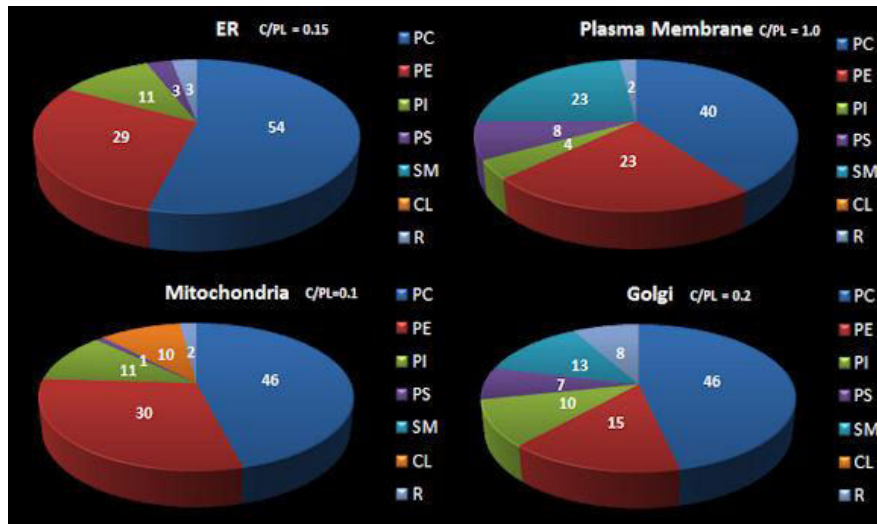


Figure 7: Phospholipid distribution in the different membranes in mammals. The cholesterol/ phospholipid ratio is also mentioned.

<http://employees.csbsju.edu/hjakubowski/classes/ch331/lipidstruct/PLCompositionCellOrganelles.jpg>

Moreover, lipids distribute asymmetrically between the two leaflets of eukaryotic and prokaryotic cells. For example, in human erythrocyte plasma membranes, PC and SM are more abundant in the outer leaflet whereas PE and PS are more concentrated on the inner leaflet. PI, a minor anionic lipid is also present in the inner leaflet (Figure 8) [25]. Due to its fast flip-flop capacity, cholesterol distributes equally in both leaflets and it preferentially interacts with sphingolipids.

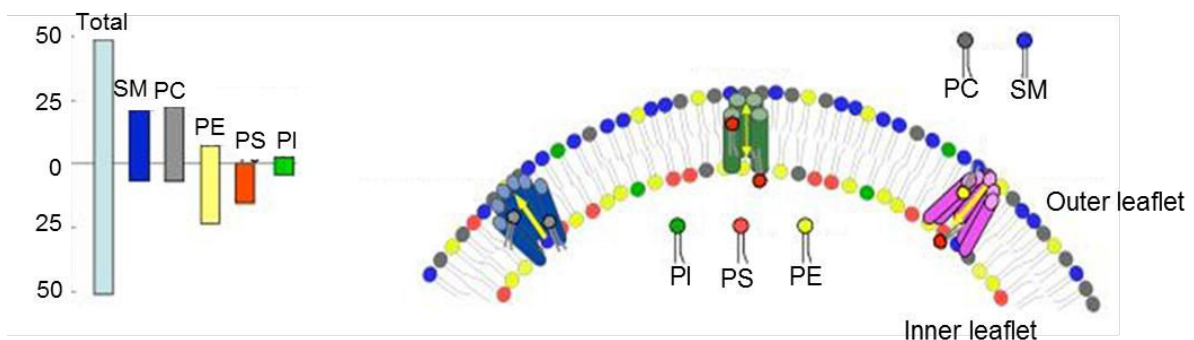


Figure 8: Plasma membrane of eukaryotic cells. The graph shows the distribution of phospholipids between the two leaflets of the human erythrocyte membrane. Adapted from [25].

The difference in composition and distribution of lipids between the two leaflets of both eukaryotic and prokaryotic cells contributes to the transmembrane potential, i.e., difference in charge distribution between both sides of membranes. The difference in potential between the extra and the intra-compartments is range from -90 to -110 mV and from -130 to 150 mV for mammals and bacterial cells, respectively [26]. The asymmetric distribution of neutral and charged lipids also induces membrane curvature. It also regulates several biological processes such as blood coagulation and vesicle fusion [25].

My next two sub-sections aim at better exemplifying the diversity of membrane lipid composition.



I.4.1. Human skin membrane

Skin protects the organism from physical, chemical and biological attacks. It also plays a vital role in thermoregulation. The skin consists of three major layers, morphologically different: the epidermis, the dermis and the hypodermis. Epidermis is the outermost layer of skin. It is subdivided into five layers called from the outer (superficial) to the innermost (deepest): stratum corneum (SC); stratum lucidum; stratum granulosum (SG); stratum spinosum; and stratum basale or basal layer. Dermis contains two layers: the dermal papillary layer; and the dermal reticular layer. There are no sub-layers that constitute hypodermis (Figure 9).

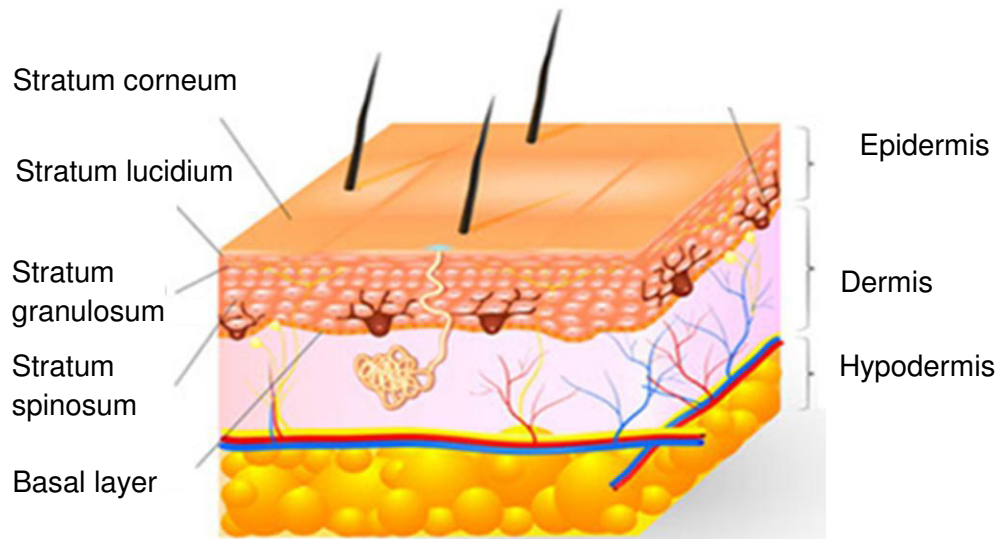


Figure 9: Human skin layers.

The living layers of human epidermis are composed of several classes of lipids, found in different proportions in the epidermal layers. The amount of phospholipids (i.e., PE, PC, PS, and SM) significantly decreases from the basal to the corneum layers. Namely, they present 45%, 25% and less than 5% of the total lipids presented in basal/spinosum, granular and corneum layers, respectively. Sphingolipids (mainly ceramides) and other neutral lipids (i.e., triglycerides, free fatty acids and cholesterol) are present in the epidermal layers. Conversely to phospholipids, their distribution increases from the basal to the corneum layer. Cholesterol sulfates are also present in the different layers in large SG proportions (Table 3) [27].

	Stratum Basal/Spinosum	Stratum Granular	Stratum corneum
Phospholipids	44.5	25.3	4.9
Cholesterol sulfate	2.4	5.5	1.5
Triglycerides	12.4	24.7	25.2
Free fatty acids	7.0	9.2	19.3
Cholesterol	11.2	11.5	14.0
Ceramides	7.3	11.7	18.1

Table 3: Lipid composition in human epidermis [27].



SC is believed to provide a physical barrier function to the skin. It consists of corneocytes embedded in lipid matrix. The extracellular lipid matrix is known to be the main penetration route of substances through the SC. This characteristic strongly depends on structural organization and physical state of the extracellular lipid matrix. The SC lipid composition markedly differs from that of classical biological membranes. A quantitative analysis of the SC lipids for different human skin regions (abdomen, leg, face and plantar) was assessed [28], showing the significant differences in lipid distribution were found at the four different regions.

The analysis of lipids at the skin surface revealed the presence of a wide variety of lipids. Ceramides are the predominant component of SC (up to 51%), then come cholesterol (up to 27%), and free fatty acids (up to 21%) [29]. Cholesterol sulfate (3%) and traces of phospholipids (0.4%) have also been found. Ceramides largely contribute to lipid matrix organization and therefore to skin barrier function. Free fatty acids are the key elements to form the SC lipid bilayer and to keep the SC surface under acidic conditions. Cholesterol has a stabilizing role with respect to temperature changes [30].

Fourteen subclasses of ceramides have been identified in human SC, differing from the molecular structure of both the sphingoid base and the acyl chain [31]. It is worth noting that the acyl-ceramides adopt a specific molecular structure, as they consist of long ω -hydroxyacids linked to a linoleic acid by an ester function, and long saturated lipid chains (24-34 carbons). These ceramides yield to more packed and ordered lipid bilayers, which provide the role of barrier to SC, as ordered bilayer are less permeable (two or three orders of magnitude from fluid to gel phase) [32,33].

Due to its specific lipid compositions, SC lipid organization showed the co-existing of two crystalline lamellar phases. Various studies showed the existence of a pH gradient through the epidermis from the inner to outer layers (pH 7.5 to pH 4.5). At the SC extracellular lipid matrix, the local pH is approximately ~6. At skin physiological temperatures (28°C - 32°C), two gel phases were observed at pH 5-6, made of ceramide/cholesterol and free fatty acids. At neutral pH, a single gel phase was observed. No fluid phase was observed at any pH [33].

I.4.2. Bacterial membranes

This section aims at providing a brief overview of bacterial membrane lipid composition. In 1884, Christian Gram developed a special technique (called Gram staining) to identify bacteria, allowing the classification of bacteria into two main groups based on the chemical and physical properties of their cell envelope; Gram positive (Gram+) and Gram negative (Gram-) bacteria (Figure 10).

The structure of the Gram+ bacteria cell envelope is composed of a single cell membrane, surrounded by thick layers of peptidoglycan (30 –100 nm thick) (Figure 10 (a)). The lipid content in Gram+ bacteria is generally low (2.6 % and 1.2% for *B.subtilis* and *M. lysodeiketikus*, respectively). The peptidoglycan structure is composed of polysaccharide chains cross-linked by peptide bridges; it provides structural rigidity to the cell envelope. Linked to the peptidoglycan, are teichoic acids, lipoteichoic acids and proteins.



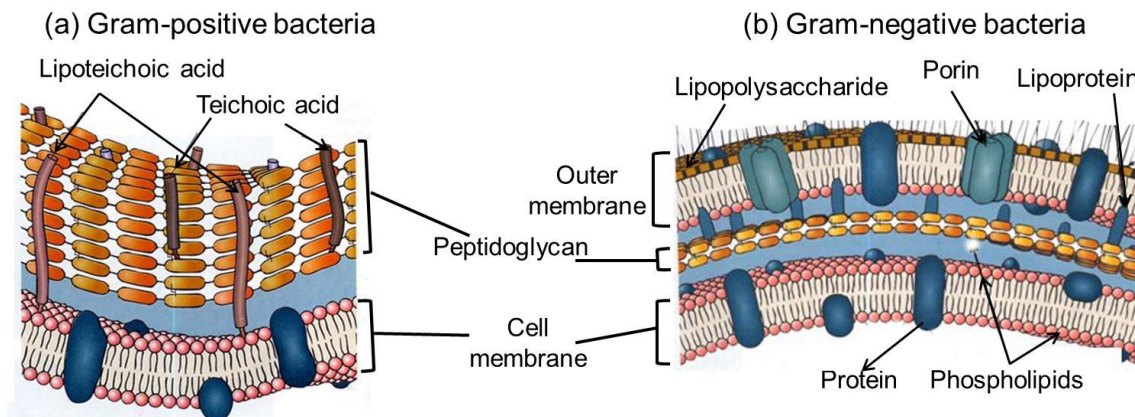


Figure 10: Structure of the Gram-positive bacteria (a) and Gram-negative bacteria (b). Adapted from http://images.slideplayer.fr/1/476607/slides/slide_20.jpg.

Teichoic acid is an anionic glycopolymer; it is composed of a disaccharide linkage unit and a chain polymer containing phosphodiester-linked polyol repeat units (e.g., glycerol phosphate, glycosyl phosphate, or ribitol phosphate repeats). Teichoic acids are covalently linked to the peptidoglycan and constitute up to 60% of the mass of cell wall. Lipoteichoic acids anchor peptidoglycan to the cell membrane via a glycolipid. These compounds largely contribute to the cell envelope shape and function [34,35].

The Gram- bacteria cell envelope is more complex. It contains an external membrane that surrounds the peptidoglycan and which is called the outer membrane (OM). As most of biological membranes, OM is a lipid bilayer that includes proteins (e.g., lipoproteins and porins) (Figure 10 (b)). It is asymmetric, phospholipids being predominant in the inner leaflet whereas the outer leaflet is mainly composed of glycolipids, particularly lipopolysaccharide (LPS), which is exclusively found in Gram- bacteria.

LPS is known to be crucial for the barrier function of OM. LPS structure is composed of lipid A and a branched sugar chain anchored to *O*-antigens that are highly immunogenic and frequently toxic in mammals. Lipid tails of LPS are generally saturated, leading to tight packing and ordered lipids thus limiting the diffusion of hydrophobic compounds. Moreover, the porin proteins found in the outer leaflet of OM serve as hydrophilic transmembrane channels, allowing passive diffusion of small hydrophilic compounds (e.g., amino acids, mono and di-saccharides) through OM. Hence, the presence of LPS and porins in OM is one of reasons that make Gram- bacteria highly resistant to hydrophobic antibiotics and toxic drugs in comparison with Gram+ bacteria. This also so participate to the selectivity of OM as permeability barrier [36].

The Gram- bacteria peptidoglycan is relatively thin (5-10% of the cell wall). Gram- bacteria are enriched in PE (up to 80%) whereas Gram+ bacteria contain large amount of PG (up to 70%). The inner leaflet of OM and the cell membrane is made of phospholipids, including PE, PG and in a extend PS and CL. For example, the inner leaflet of the OM of *Salmonella thyphimurium* and *E. coli* contains PE, PG, and CL in the ratio 81:17:2, whereas the ratio in the corresponding cell membrane is 60:33:7. The total lipid content for Gram- bacteria is relatively high (e.g., 22.6% and 19.0% for *E. coli* and *Salmonella pullorum* respectively). Cell membrane contains more than 10% of unsaturated acyl chains compared to OM.

Unlike animals, bacterial cell membrane does not contain sterols. Other lipids have been also found such as ornithine lipids, sulfolipids, glycolipids, pentacyclic triterpenoid lipids and



others, depending on the species. [37]. Proteins diversity present in cell membrane is quite high as compared to OM. The membrane diversity affects membrane organization and so membrane phase transitions [34].

I.5. Transport across cell membranes

One of the major functions of membrane is to regulate exchanges of small molecules including water, nutrients, ions, and xenobiotics including drugs. Cell membranes are selectively permeable (semipermeable) in that some substances can cross it freely whereas others are stuck at the membrane surface. There exist two major processes for drug transport, namely passive permeation and protein-mediated transport [38,39].

I.5.1. Passive permeation

Permeation is the net movement of solutes from a high- to a low-concentration region, as driven by the law of mass action (i.e., to reach equilibrium). As a consequence, increasing drug plasma concentration increases rate of transfer across membrane thus accelerating its action. Permeation through lipid bilayers is often described as the process of influx (drug entering into cells). This process occurs without any interactions with carrier membrane proteins and no additional energy is required. Fick's law of diffusion partially governs this process, which results Brownian movements of particles. According to this law, the permeability coefficient of a solute P is calculated as:

$$P = \frac{j}{A\Delta C}$$

where j is the solute flux, A is the interface area and ΔC is the concentration gradient across membrane.

Following this process, small hydrophobic compounds (i.e., carbon dioxide, dioxygen) diffuse somewhat rapidly through membranes, mainly because of the low energy barriers that must be crossed in this case. If too hydrophobic, the compounds can however be trapped in the lipid core of membranes. Conversely, ions require a very high energetic barrier to cross lipid bilayers, mainly due to their charges and hydration shells; they indeed usually exhibit low rates of diffusion.

For most of drugs, the rate of passive permeation is driven by a set of intrinsic descriptors (i.e., lipophilicity, hydrogen bonding capacity, molecular size, and ionization/charge) [40,41]. Membrane permeability studies are influenced by the Overton's rule, which positively correlates P to the lipophilicity of drugs expressed by the solute oil-water partition coefficient ($\log P$) [42]. Following these rules, the increase of the lipophilicity increases the passive permeation rate. However, a large lipophilicity may dramatically decrease the solubility on water of drugs and then affect their crossing capacity. Additionally, the increase of the hydrogen bond capacity decreases the capacity of drug to diffuse passively. Concerning the molecular size, usually the smaller the molecular size, the easier the drug absorption. Moreover, most of drugs are weak acids or bases and thus the uncharged/charged ratio depends on the pKa of drug as well as the pH of the environment. It might be important to note that the pH value differs in the intracellular environments and therefore drugs cannot diffuse out of cell via the same process [38]. For more details and recent developments, the reader can refer to Chapter V.



I.5.2. Protein-mediated transport

Xenobiotics that cannot cross membranes by passive permeation are usually transported through membranes by protein-mediated transport. Moreover, substrate flux against concentration gradients is sometimes required, both for influx and efflux. This process is achieved by special protein carriers e.g., the ABC, ATP-binding cassette transporters. However, transport of substrate against its gradient is energetically unfavorable, and therefore a source of energy is required. ABC transporters use the energy of ATP-hydrolysis; they are known as primary active transporters. Other transporters use the energy stored in the electrochemical gradient that may exist through the bilayer, i.e., the drug is transported together with the flux of ions (typically Na⁺ or H⁺); this transport usually refers to secondary active transport (for more details, the reader can refer to Chapter III). This process can also be considered as facilitated transport.

Facilitated transport is mainly known to carry electrolytes and small hydrophilic compounds (e.g. ions, amino acids, polar molecules) to cross membranes. The crossing occurs through proteins by 1) carrier proteins, to which substrates bind on one side of the membrane and is translocated to the other side by conformational changes supported by electrochemical gradient but also 2) channel proteins (pores). The latter type usually transports ions by following gradient concentration through the channel, whereas the former type is more dedicated to small organic compounds (e.g., glucose and amino acids), which are too large to pass in most of protein channels. Carrier and channel proteins are relatively selective and specific of a given class of compounds. Unlike passive permeation, the rate of transport through selective channels is saturable, which may occur at high concentration.

I.5.3. Endocytosis and exocytosis

Lipid bilayers can wrap around large molecules including nanoparticles, proteins or even bacterial cells; this process is called endocytosis. It produces vesicles, called endosome, which can be released inside the cell. Conversely, vesicles can fuse plasma membranes, to then release the large molecule outside cell (exocytosis). For instance, vitamin B12 crosses the gut wall by endocytosis process [43]. The size and shape of particles affect wrapping time and efficiency [44,45]. For example, spherocylindrical particles showed more efficient endocytosis than spherical particles, and endocytosis is unlikely in case of sharp edges [44]. The full wrapping of nanoparticles is related to the degree of rigidity and density of ligands as well as their length and hydrophilic/hydrophobic character [48,49].



Chapter II. Theory and methods

II.1. Molecular dynamics

Molecular dynamics (MD) have become a standard tool, used to study various biological events including crossing of biological membranes and interactions of drugs with their biological targets. This technique allows providing atomistic details along time of a given molecular system [48]. The underlying idea of MD simulations is to study the macroscopic behavior of a biological system simply by computing the natural time evolution of the underlying molecular system; this is achieved numerically, by integrating Newton's equations of motion over a sufficiently long time. The almost never-ending increase of computer power, allows sampling timescales going from hundreds of nanoseconds to several microseconds. MD numerically integrates Newton's equations by taking small and discrete time steps. At a given time, the evaluation of new positions and velocities of all atoms are given with respect to the properties of the previous time step [49]. This section will provide a brief introduction to the underlying formalism of MD, stressing the important methodological details to successfully run MD simulations.

II.1.1. Equation of motion

Let us consider a system of N atoms, the Newton equation (Second law) of motion is given on atom i as:

$$F_i = m_i \frac{d^2 x_i}{dt^2}, \quad i = 1, 2, \dots, N$$

where F_i is the force acting on the atom of mass m_i along the coordinate x_i . It is evaluated from all interactions occurring between atoms of the system. The force also corresponds to the derivative of the potential energy function V , which in turn is a function of the positions of all atoms:

$$F_i = -\frac{dV}{dx_i}$$

It is useful in molecular mechanics to subdivide the potential energy functions into two contributions, namely bonded and non-bonded interactions.

II.1.2. Bonded interactions

Bonded interactions describe all bonds (defined by two atoms), angles (defined by three atoms), and torsion (defined by four atoms):

$$V_{bonded} = V_{bond} + V_{angle} + V_{dihedral}$$

The first term, V_{bond} , represents the interaction between two atoms (i and j) linked by a covalent bond. As a first approximation, V_{bond} can be given by a simple harmonic spring potential, as a function of displacement from the equilibrium distance b_{ij} :

$$V_{bond}(r_{ij}) = \frac{1}{2} k_{ij}^b (r_{ij} - b_{ij})^2$$

where k_{ij}^b is the force constant that describes the bond strength and b_{ij} is the equilibrium distance. Noted that both k_{ij}^b and b_{ij} are specific of every atom pairs.



In a similar way, the angle θ_{ijk} formed by three atoms (i, j, k) linked by 2 covalent bonds is described by a harmonic potential V_{angle} as a function of the angle θ_{ijk} formed by three atoms (i, j, k):

$$V_{angle}(\theta_{ijk}) = \frac{1}{2} k_{ijk}^{\theta} (\theta_{ijk} - \theta_{ijk}^0)^2$$

where k_{ijk}^{θ} is the force constant and θ_{ijk}^0 is the equilibrium angle.

The equilibrium values of the bond and angle parameters are usually derived from structural databases, while force constants are derived from infrared spectroscopy or alternatively from high-level quantum calculations.

The third term, $V_{dihedral}$, describes the (steric) energetic barriers of four covalently linked atoms (i, j, k, l) to twist. These rotation barriers are particularly crucial to tackle 3D assemblies. It can be subdivided into two (i) proper dihedral and (ii) improper torsion potentials (V_{proper} and $V_{improper}$, respectively).

$$V_{dihedral} = V_{proper} + V_{improper}$$

Proper dihedral is used to constrain the torsion around a single bond (atoms j and k). Improper torsion describes out-of plane bending, which partially accounts for certain quantum effects not explicitly described in the molecular mechanics formalism and which strongly affect conformations (e.g., carbon or nitrogen hybridation). These two types of torsion may also differ from the potential function form.

Proper dihedral potential, V_{proper} , is assumed to be periodic. It is defined as a cosine function (so-called Ryckaert-Bellemans potential):

$$V_{proper}(\varphi_{ijkl}) = k_{\varphi} (1 + \cos(n\varphi - \varphi_s))$$

where k_{φ} is the force constant; n is the periodicity; and φ_s is the equilibrium dihedral angle between ijk and jkl planes.

Improper dihedrals are discontinuous (non-periodic). The corresponding potential is expressed by a harmonic potential:

$$V_{improper}(\xi_{ijkl}) = \frac{1}{2} k_{\xi} (\xi_{ijkl} - \xi_0)^2$$

k_{ξ} is the force constant and ξ_0 is the equilibrium angle.

II.1.3. Non-bonded interactions

Non-bonded interaction means interaction between non-covalently bonded atoms belonging to the same molecule or to two different molecules. They are mainly described by electrostatic and van der Waals interactions.

$$V_{non-bonded} = V_{electrostatic} + V_{van\ der\ Waals}$$

The first term describes the interactions between two charges on two atoms i and j (partial atomic charges). It is calculated for each pair according to the Coulomb's law:

$$V_{electrostatic}(r_{ij}) = \frac{1}{4\pi\epsilon_0} \frac{q_i q_j}{r_{ij}}$$



where q_i and q_j are the partial charges of the atoms i and j ; r_{ij} is the interatomic distance between i and j ; and ϵ_r is the relative dielectric constant.

The second term contains the attractive and repulsive contribution to the van der Waals interactions. It is usually given by the Lennard-Jones potential V_{LJ} :

$$V_{LJ}(r_{ij}) = \frac{C_{ij}^{(12)}}{r_{ij}^{12}} - \frac{C_{ij}^{(6)}}{r_{ij}^6}$$

where $C_{ij}^{(12)}$ and $C_{ij}^{(6)}$ are parameters related the collision diameter and the well depth for repulsion and dispersion, respectively. The repulsive contribution becomes predominant at short distances where electron-electron interactions are strong. The attractive forces are basically described by dipole-dipole interactions, which in the case of non-polar molecules come from the fluctuations in charge distribution in electron clouds. Fluctuations in electron distribution indeed produce instantaneous dipoles, which in turn induces another dipole in a second atom yielding attractive interaction (dispersion).

It is must be stressed that calculation of non-bonded intermolecular interactions is time consuming, as they evaluate pair interactions between all atoms in the system. For this reason, a cutoff distance is usually predefined as a setup of any MD simulations. It means that only interactions between atoms separated by a distance less than the cutoff distance are taken into account. Depending on the force field, this cutoff can be set from 0.9 to 1.4 nm for Coulomb and van der Waals interactions; the cutoff can be different for both types of interactions.

To improve accuracy of the simulations, small contributions to the potential energy of atoms $V_{LJ}(r_{ij})$ further than the cutoff should be taken into consideration. Indeed, a method to calculate long-range interactions (e.g., coulombic interactions) has to be applied. The best methods are based on Ewald summation; an efficient technique to calculate the interactions between a charge and its periodic copies. It is performed by splitting the calculation of the interaction potential into two parts: one short-ranged term that converges quickly in real space, and one long-ranged term that converges quickly in Fourier space. Particle Mesh Ewald (PME) method is commonly used.

II.1.4. Force field

The force field (FF) gathers all interaction potentials. It simply corresponds to the sum of potentials described above:

$$V_{total} = V_{bond} + V_{angle} + V_{dihedral} + V_{electrostatic} + V_{van\ der\ Waals}$$

Other terms can be added (e.g., specific terms for hydrogen bonding), as well as various mathematical forms can be used for the different contributions (e.g., Morse-type potential for V_{bond}). All parameters present in the different potentials are obtained either from experimental data or from high-level quantum chemical calculations. We again insist that quantum description is ignored in the molecular mechanics formalism, so MD is not suited to inherently describe reactivity. Different parameter sets and V_{total} equations are available, leading to several levels and versions of FFs. The choice of the FF is crucial to accurately describe all interactions in the molecular system. There are three main families FFs, namely: all-atom (AA); united-atom (UA); and coarse-grain (CG) (Figure 11).



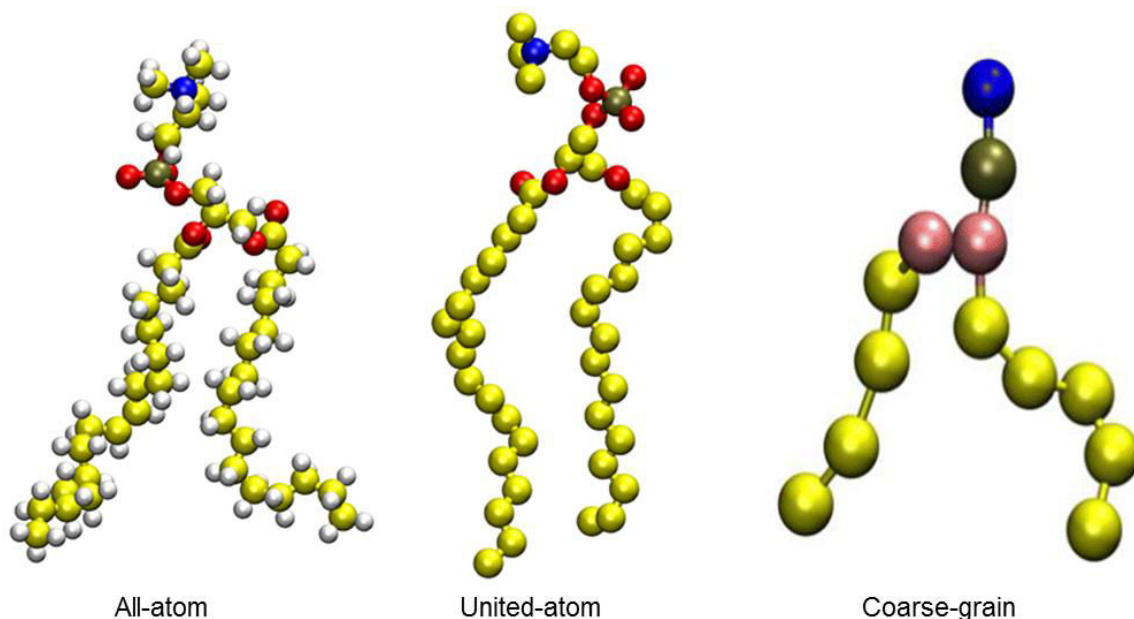


Figure 11: Different force field resolutions of a POPC molecule: AA-FF, UA-FF and CG-FF.

In AA-FFs, every type of atoms in the system is described explicitly, including hydrogen and therefore, all intra and intermolecular interactions are explicitly monitored.

To speed up calculations, UA-FFs have been developed, in which some atoms (mostly hydrogen atoms) are described as part of “pseudo-atoms”, describing a small group of atoms. For example, in lipid bilayer, the non-polar hydrogens of aliphatic chains are combined with the corresponding carbon atoms and formed a single CH_2 pseudo-atom. With this model, a smoother potential landscape can be produced, giving rise to faster re-orientation of hydrocarbon chains, which in turn increases the sampling rate of the conformational space. Gromos is one of the most popular UA-FFs.

To simulate larger systems (e.g., proteasomes, protein-DNA complexes, viruses) or longer processes (e.g., biological diffusion, protein movements), coarse-grained simulations can be used, which reduce the number of degrees of freedom of the system. The idea of CG is to represent a group of atoms or few united atoms as a single particle or “bead”. The popular models use a four-to-one mapping, i.e., a single interacting bead describes four heavy atoms (e.g., C, O, N...). This allows longer time steps of integration and increases the sampling time by about one order of magnitude. FFs adapted for CG contain a set of predefined bead types corresponding to different functional groups in different molecules. CG Martini FF has been widely used [50].

The choice of type of FF depends on the phenomena under studied as well as computational capacities. UA models have been widely used because of the adequate balance between accuracy and computational time. However, AA-FFs are sometimes mandatory when hydrogen atoms play crucial roles in the supramolecular assemblies. CG is recommended to study rare events, which occur in the order of the millisecond.

Nowadays, MD simulations can study a large variety of molecular systems. Several FFs have been developed, which may have certain specificity. For example, for organic liquids OPLS/AA FF appears to be well-adapted [51–53]. For proteins, the recent versions of AMBER, CHARMM and OPLS/AA FFs have showed reliable results [54,55]. Still now, the accurate description of DNA is a challenging issue and it is even more delicate for RNA [56].



The FFs for nucleic acids are still currently under improvements [57–60], even though recent modifications of AMBER FFs provide the most accurate results at the moment. Concerning lipid bilayers, several FFs at atomic resolution have been optimized, such as Berger lipids [61], AA Stockholm Lipids (SLipids) [62], UA Gromos family (e.g., 43A1-S3 [63] and 53A6 [64]), CHARMM36 [65,66], Lipid 14 [67] and CG Martini force fields [50].

II.1.5. Integration Algorithms

The evaluation of intramolecular and intermolecular forces between all atoms of the molecular system is assessed within the molecular mechanics formalism. Once a configuration of atoms is obtained at a given time t , a new one can be derived at time $t + \Delta t$, according to the differential equations of motion. To proceed time integration, many algorithms have been designed [68]. The leap-frog Verlet algorithm is probably the most commonly applied. It increments positions and velocities according to the following equations:

$$x(t + \Delta t) = x(t) + \Delta t v\left(t + \frac{1}{2}\Delta t\right)$$

$$v\left(t + \frac{1}{2}\Delta t\right) = v\left(t - \frac{1}{2}\Delta t\right) + \frac{\Delta t}{m} F(t)$$

The force $F(t)$ acting on each atom corresponds to the negative gradient of potential function. It is important to mention that the integration of these equations should be performed accurately by using time steps (Δt) less than the time scale of the fastest atomic motion in the molecular system. In principle those involving hydrogen atoms, namely ~ 13 fs being the vibrational frequency of bonds involving hydrogen; a 2 fs time step is usually used.

II.2. Environments

II.2.1. Ensembles

An ensemble is a collection of particles for a given system, which have an identical thermodynamic state, however bearing different microscopic parameters, such as positions and velocities. For instance, in the microcanonical ensemble (NVE), the volume V , the number of particles N and total energy E are constant. However, the evolution studied in MD simulation is generally defined under constant volume and temperature (NVT) called canonical ensemble, or under constant pressure and temperature (NPT), called isobaric-isothermal ensemble. Keeping E constant is in principle non relevant in MD simulations, while keeping volume constant does rarely correspond to experimental conditions. Therefore, NPT is usually more recommended as they correspond to typical real-life situations and most experiments. In order to keep the temperature and pressure constant, several methods have been developed, so-called thermostats and barostats, respectively.

II.2.1.1 Thermostat

Temperature results from the motion of molecules. It is computed from the kinetic energy of the system E_{kin} , in other words, the velocity of each particle v_i according to the following equation:

$$E_{kin} = \frac{1}{2} \sum_{i=1}^N m_i v_i^2 = \frac{3}{2} N_{df} kT$$



where m_i is the mass of particle i ; k is the Boltzmann's constant; and N_{df} is the number of degrees of freedom.

Thermostat methods couple the system to an external heat temperature bath. The coupling Berendsen thermostat method [69] either removes or adds energy to the system to maintain constant temperature. It scales the velocities of all atoms at each step directly using a weak coupling algorithm with respect to the target temperature T_0 . This algorithm slowly corrects the temperature deviation of the system according to:

$$\frac{dT}{dt} = \frac{T_0 - T}{\tau}$$

where T is the instantaneous temperature and τ is the decay coupling time constant. If $T > T_0$, the heat will be removed, but if $T < T_0$, the temperature will increase. However, Berendsen thermostat method is not capable of sampling a system in a proper thermodynamic ensemble as the kinetic energy fluctuations are neglected, so leading to suppress temperature fluctuations. Besides, the extended-ensemble Nose-Hoover thermostat is commonly used [70,71]. Roughly, it introduces an external "heat bath" potential that mimics a heat reservoir, by adding an extra degree of freedom to the equations of motion to lower temperature variations.

II.2.1.2 Barostats

Pressure coupling is controlled similarly to temperature coupling, i.e., by correcting the system volume with the so-called barostat algorithm. Temperature scales velocity while pressure scales dimension. The simulation box is scaled with a weak coupling algorithm to reach the target pressure. Since the pressure is derived from the forces normal to a surface, controlling the pressure implies box size scaling along the x -, y -, and z -directions. Compared to thermostat, in barostat approach, the external heat temperature bath is replaced by a pressure bath. Parrinello–Rahman barostat [72,73] maintains constant pressure using a similar approach as the Nosé–Hoover thermostat, i.e., by adding an external potential term in the equations of motion. It correctly describes fluctuations of the box volume.

Three pressure coupling schemes are available in GROMACS: isotropic, semiisotropic, and anisotropic. In isotropic coupling, all three components of the box vector are equally scaled, ensuring that the simulation box remains proportional. In semi-isotropic pressure coupling, two dimensions are coupled isotropically and the third scales independently. In anisotropic coupling, all components of the box vector are uncoupled, and as such, it imposes the least amount of constraint on the system. Lipid bilayers are usually simulated using semi-isotropic pressure coupling to maintain the size ratio of the bilayer constant and prevent the system elongation in one direction.

II.2.2. Water models

Several methods describe the effect of solvent molecules, mainly water as most of biological systems are immersed in aqueous environments. Several water models have been developed, which mainly differ from the number of interacting points, called sites, used to describe intermolecular interactions. The most popular water models are the Simple Point Charge (SPC) [74], the Extended SPC (SPC/E) [28] and the 3-point TIP3P [76] models. All of these models have three interacting sites, each atom being assigned to a point charge (



Figure 12 and Table 4). Water models with 3-sites are mostly used in MD simulations because of their simplicity and high computational efficiency. Other models exist, in which additional sites are added. In the four-site water model (e.g., TIP4P) a dummy atom is added along the bisector of HOH angle, near the oxygen atom. With this model, the electrostatic distribution around the water molecule is improved.

It is important to mention that the choice of water model should be suitable for the FF. In general, SPC and SPC/E are compatible with GROMOS, whereas TIP3P are compatible with AMBER and OPLS.

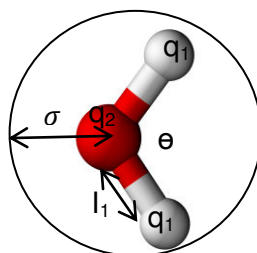


Figure 12: Water model having 3-sites of interactions.

Model	σ (Å)	ϵ (kJ.mol ⁻¹)	l_1 (Å)	q_1	q_2	θ (°)
SPC	3.166	0.650	1.0000	+0.410	-0.8200	109.47
SPC/E	3.166	0.650	1.0000	+0.4238	-0.8476	109.47
TIP3P	3.1506	0.6364	0.9572	+0.4170	-0.8340	104.52

Table 4: Parameters for some water models. l_1 are OH bond lengths, θ is the HOH bond angle, q_1 is the partial charge on the hydrogen atom, q_2 is the partial charge on the oxygen atom ($q_2 = -2 q_1$). σ and ϵ are Lennard-Jones parameters.

II.2.3. Periodic conditions

Periodic boundary conditions (PBC) are generally applied during MD simulations to minimize the edge effects of the box in which the molecular system is confined. Applying PBC allows mimic bulk properties (Figure 13). The periodicity is obtained by treating the simulation box as surrounded by its own image. Conceptually, when a particle leaves the simulation box through one face of the box, its image re-enters through the opposite face without any kind of interactions with the box boundary. Usually, a cubic or rectangular simulation box is used in membrane simulations. Technically, the simulation box should be large enough, so to prevent large compounds to directly interact with their mirror images in the neighboring boxes, i.e., when distance approaches cutoffs.





Figure 13: Periodic boundary conditions (PBC).

II.3. Potential of the mean force and related properties

Molecule partitioning, penetration, diffusion and permeation in biological membranes are of crucial pharmacological interest. Potential of the mean force (PMF), or free energy profile along a reaction coordinate may for instance evaluate the energetics cost required by a drug to be transported from one to another region (Figure 14). Biological membranes are highly inhomogeneous and complex systems; they constitute of several regions with different constitution and densities [77].

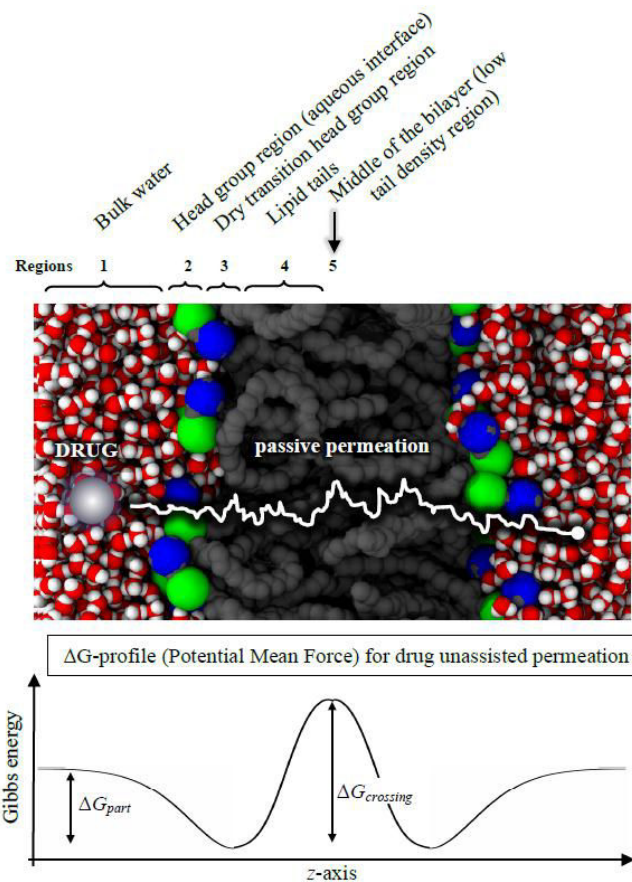


Figure 14: Pictorial description of unassisted (passive) permeation and energetic profile for drug crossing. ΔG_{part} is related to drug partitioning, whereas $\Delta G_{crossing}$ is the highest energetic barrier met by drugs through the bilayer (i.e., limiting step of crossing event) [78].



Experimental methods cannot provide detailed energy profiles, e.g., drug passive permeation through membrane. Computer simulations represent a powerful tool to explicitly describe membrane- anisotropy at an atomic resolution, and thus to monitor solute-membrane interactions.

PMF can be seen as an understanding of the average transition from a given state (A) to another state (B). The transition time between the two metastable states can be estimated from PMF. However, up to now, classical unbiased MD simulations are not suited to monitor phenomena longer than hundreds of microseconds, including diffusion and permeability processes. To drive these rare events, biased MD simulations can be employed. Among other techniques, *z*-constraint [79], umbrella sampling [80], and COSMOmic [81] allow PMF evaluation. The evaluation of diffusion coefficients and permeability coefficients can be obtained from the *z*-constraint method.

II.3.1. *z*-Constraint method

The first step of a *z*-constrained procedure is a slow pulling of the drug along *z*-axis perpendicular to the bilayer surface. The rate of drug pulling should be as slow as possible to allow both drug relaxation and prevention of any lipid bilayer deformations.

Once drug is pulled, a set of positions is generated at different (regularly separated) *z* values. At each position, a bias potential (*z*-constraint force) is applied to constrain the center-of-mass (COM) of drug. Eventually the constraining force $F(z, t)$ is determined.

At each position, movements are freely allowed in the *xy* plans of lipid bilayer. The derivative of PMF can be calculated by measuring the average force on a solute that is constrained in selected *z* positions after sufficient sampling.

The Gibbs energy of transfer from water to a *z*-depth, $\Delta G(z)$, can be calculated according to the following equation [77]:

$$\Delta G(z) = - \int_{water}^z \langle F(z) \rangle_t dz$$

where $\langle F(z) \rangle_t$ is the average constraint force at position *z* over the total simulation time. The partition coefficient $K(z)$ is calculated from $\Delta G(z)$ by:

$$K(z) = \exp[-\Delta G(z)/kT]$$

The permeability coefficient P and the resistance R to cross the entire bilayer can be calculated according to the following equation:

$$P = \frac{1}{R} = \frac{1}{\int_{z1}^{z2} R(z) dz} = \frac{1}{\int_{z1}^{z2} \frac{\exp[\Delta G(z)/kT]}{D(z)} dz}$$

where $R(z)$ is the local solute resistance. $D(z)$ is evaluated using the autocorrelation function discussed above. Once $\Delta G(z)$ and $D(z)$ are calculated, the integration can be performed numerically, giving the local permeability resistance and the permeability coefficient. For more details, the reader can see Chapter V.



II.3.2. Umbrella sampling

In Umbrella sampling [80], an artificial biased (restraint) potential $U(z)$, acting along z -axis perpendicular to the bilayer surface is added to the solute, forcing it to remain close to a reference position z_0 . The biased potential is expressed as a restraint harmonic potential:

$$U(z) = \frac{1}{2}K(z - z_0)^2$$

where K is the force constant of the restraint.

Similarly to z -constraint methods, PMF through the lipid bilayer can be obtained by defining a series of initial drug positions along z -axis. Each related atomic configuration is restrained using the biasing potential $U(z)$, within a sampling window. The biased probability distributions $P'(z)$ to find the system in a given state along the z -axis are measured. The Gibbs energy profile $G(z)$ along z -axis is given by:

$$G(z) = -k_B T \ln P'(z) - U(z) + F$$

To ensure sampling along the whole coordinate, the windows are chosen so that the harmonic biased potentials in each window overlap the nearby windows. F is shifted so as to obtain overlap in the common regions. It is specific for each window and depends on $U(z)$. As a biasing potential is used, an unbiasing procedure must be applied to calculate the correct Gibbs energy profiles. The weighted histogram analysis method (WHAM) [35] is usually used to extract the unbiased PMF by unweighting and combining the biased probabilities $P'(z)$ (also called histograms) of all windows, resulting in unbiased probability distributions which in turn, give the unbiased PMF.

II.3.3. COSMOmic

Conductor-like Screening Model for real solvent “COSMO-RS” software is used to calculate thermodynamics properties of homogeneous liquid systems. It is based on calculation of chemical potentials. Here the environment is described implicitly as a dielectric continuum; each molecule is described by its 3D charge density distribution $p(\sigma)$, so-called σ -profile. COSMOmic is an extension of COSMO-RS applied to micelles and lipid bilayers [81]. In this model, the bilayer is divided into layers along to z -axis (perpendicular to the bilayer surface), each layer being considered as an homogeneous liquid characterized by a specific σ -profile, $p_s(\sigma')$. Drug membrane crossing can thus be studied as crossing various regions of specific polarity. The PMF can be obtained by statistical thermodynamics in place of MD simulations [82]. The crossing events can be described by interacting σ -potential of both drug and membrane layers. σ -potential corresponds to the affinity of the solvent s to a solute surface having a polarity σ . The corresponding chemical potential (the partial Gibbs energy) of a drug in each layer $\mu_s^X(\sigma')$ can be evaluated for a large number of orientations, taking size effects and shape ratios of molecules in the system into consideration by adding combinatorial contribution μ_{comb}^X to the chemical potential [81]. The combinatorial contribution is based on the molecular volume and molecular area of the solute [82].

$$\mu_s^X(\sigma) = \mu_{comb}^X + \int p^X(\sigma) \mu_s d\sigma$$

For the special case of lipid bilayers, contributions of the elastic deformation energy of bilayer by a solute and the long-range electrostatic potential are also added [83].



The partition function of a solute X (Z_M^X) in a membrane M with respect to all n center positions and all m orientations is given by:

$$Z_M^X = \sum_{i=1}^n \sum_{j=1}^m \exp\left(-\frac{\mu_M^X(r_i, d_j)}{k_B T}\right)$$

where r_i is the solute position and d_j its orientation.

Subsequently, the probability to find solute X in layer i is given by:

$$p_M^X(r_i) = \frac{Z_M^X(r_i)}{Z_M^X}$$

and the Gibbs energy profile of the solute throughout the solvent (lipid bilayer) is calculated as:

$$G_M^X(r_i) = -k_B T \ln p_M^X(r_i)$$

To summarize, COSMOmic analyses allow conformational sampling of drugs in bilayers together with evaluation of PMF through the bilayer, with reasonable accuracy. Indeed, high correlation was observed between COSMOmic and experimental partition coefficients ($\log P$) for a series of small molecules (glycerol, methanol, acetone, 1-butanol, benzylalcohol, aniline, 2-nitrotoluene, p-xylene, 4-chloro-3-methylphenol, 2,4,5-trichloroaniline, hexachlorobenzene) inserting in dimyristoylphosphatidylcholine (DMPC) membrane bilayer [84]. The accuracy of this method was particularly good with respect to various AA-FF and UA-FF, keeping in mind the dramatic gain of computational time with the COSMOmic formalism.

II.4. Diffusion coefficient and autocorrelation function

The diffusion coefficient $D(z)$ of compounds in lipid bilayers can be measured by several methods. Theoretically, the easiest way is from the mean square displacement (MSD) using Einstein relation. For diffusion in the z direction, the equation is:

$$D(z) = \lim_{t \rightarrow \infty} \frac{1}{2t} \langle |z(t) - z(t=0)|^2 \rangle$$

where $\langle |z(t) - z(t=0)|^2 \rangle$ is the MSD. The time origin ($t=0$) can be shifted to enhance statistics. The slope of the MSD curve is proportional to the diffusion coefficient.

Another approach is widely used to calculate local diffusion coefficient $D(z)$ over free energy barriers based on the fluctuation-dissipation theorem. In this latter, the autocorrelation function of the random forces applied to the compound is related to the friction coefficient $\xi(z, t)$ via the following equation:

$$\xi(z, t) = \frac{\langle \Delta F(z, t) \cdot \Delta F(z, t=0) \rangle}{kT}$$

where k is the Boltzmann constant; T is the temperature; and $\Delta F(z, t)$ represents the random force.

$\Delta F(z, t)$ corresponds to the fluctuations of the instantaneous force from the average force acting on the molecule: $\Delta F(z, t) = F(z, t) - \langle F(z) \rangle$. It can be calculated from the forces on the constrained position compound using z -constraint method.



Time integration of this equation gives the local static friction coefficient. Once the static friction coefficient is calculated, the local diffusion coefficient $D(z)$ can be calculated as follows:

$$D(z) = \frac{kT}{\xi(z, t)} = \frac{(kT)^2}{\int \langle \Delta F(z, t) \cdot \Delta F(z, 0) \rangle dt}$$

The challenge is to calculate the force autocorrelation function corresponding to (ACF) $\langle \Delta F(z, t) \cdot \Delta F(z, t = 0) \rangle$.

ACF can be defined as a “memory function”; it calculates how parameters can have a time dependent effect on itself. ACF is a powerful tool to evaluate various properties of the system.

For a property f , the ACF is defined as:

$$C_f(t) = \langle f(t) \cdot f(t = 0) \rangle$$

where t is the time. The correlation time τ gives the time needed for the property f to be uncorrelated with itself.

Technically, the calculations of the force fluctuation autocorrelation functions require a set of properties of interest, taken at time intervals Δt much shorter than correlation time τ [49].

$$C_f(j\Delta t) = \frac{1}{M} \sum_{i=0}^{N-1-M} f(i\Delta t) f((i+j)\Delta t)$$

where N is the time frame for the calculation. M should be $M \leq N/2$ to compute all points with the same statistical accuracy. The simulation length should be significantly longer than τ to calculate correlation function and to improve the accuracy.

ACF roughly decays exponentially. The force fluctuation time autocorrelation function can be estimated through a fit to double, triple or several exponentials.

$$C_f(\Delta t) = \sum_i^{N=2,3} C_i e^{-\frac{\Delta t}{\tau_i}}$$

In practice, $D(z)$ is highly sensitive to the convergence of the system and the length of sampling. Several nanoseconds of simulations are required to calculate well-converged ACF. For more details, the reader can see section V.2.2.

II.5. Analysis of simulation results

Equilibrium properties and dynamics processes of lipid bilayers can be evaluated from sufficiently sampled MD simulations. From such calculations, atomic positions and velocities are obtained vs. time (trajectories), together with potential energies. The analyses are performed when the system is converged and reach equilibrium in terms of location and potential energy. There exist several parameters that are characteristics of structural lipid bilayer properties [85].



II.5.1. Lipid order parameter

Lipid order parameter (S_{CD}) determines the relative order of the lipid chain. It mainly reflects order and orientation of lipid tails with respect to the normal of the bilayer surface. Lipid order parameter is calculated for each acyl group by:

$$S_{CD} = \frac{3}{2} \langle \cos^2 \theta \rangle - \frac{1}{2}$$

where the angular brackets denotes the average over all sampled molecular orientations, and θ is the angle between carbon-deuterium (C-D) bond vector and the bilayer normal axis.

Negative value of S_{CD} indicates a perpendicular alignment of lipid chain with respect to the normal of bilayer (-0.5 is the minimum). A value of 1 is the highest; it corresponds to a perfect alignment along the bilayer normal. A value of S_{CD} close to 0 corresponds to fully disordered systems. However, in special case, $S_{CD} = 0$ may also indicate a highly ordered system when the C-H vector is titled at angle of 54.7, so-called the magic angle. In general, the order decreases from the interface region to the middle of the membrane. Local orientational order parameters can be measured experimentally from solid-state deuterium NMR spectra by calculation of quadrupole splitting Δ_{vq} according to:

$$\Delta_{vq} = \frac{3}{2} S \frac{e^2 q Q}{h}$$

where $\frac{e^2 q Q}{h}$ is the quadrupolar coupling constant. It equals 168 kHz for a C-D bond in lipid acyl chain.

II.5.2. Area per lipid

The average area per lipid (APL) is calculated by dividing the xy area of the box by the number of lipids per leaflet. It is often used to follow membrane equilibration. The APL strongly depends on FF details and simulations parameter (e.g., composition, temperature). For instance, Slipids FF showed a high capacity to reproduce the APL close to experimental data for large number of lipid bilayers and temperatures [86–88]. APL shows a high sensitivity to hydrophilic effects in the polar head group region and between lipid chains. It decreases with increasing the length of lipid chains [89]. Experimentally, several techniques can determine the APL including X-ray scattering, and NMR spectroscopy [90–92]. The APLs obtained from experimental data for various lipids found in nature are represented in Table 5.

II.5.3. Bilayer thickness

The thickness can be measured from the calculated highest electron density across the bilayer [91,93,94]. The peak-to-peak distance in this distribution, along the bilayer normal, corresponds to the distance between the polar head group regions of both leaflets, thus correctly picturing bilayer thickness. In phospholipid bilayer, the peak-to-peak distance corresponds to the layer between phosphate groups of both leaflets.

Another calculation can be used, called Luzzati thickness D_B . It is computed from volume per lipid (V_L) and APL:

$$D_B = 2 \frac{V_L}{APL}$$

Practically, D_B is computed as a function of the box volume (V_B) and water phase volume:



$$D_B = 2 \frac{(V_B - n_W V_{1W})}{APL}$$

where n_W is the number of water molecules and V_{1W} is the volume of one water molecule. Experimentally, bilayer thickness can be measured using X-ray and neutron diffraction, respectively [92–94]. D_B values of several fluid bilayers at different temperatures are given in Table 5.

	20 (°C)		30 (°C)		50 (°C)		60 (°C)	
	APL (Å)	D_B (Å)						
POPC	62.7	39.8	64.3	39.1	67.3	37.9	68.1	37.7
DLPC	59.6	33.0	60.8	32.6	64.8	31.0	65.9	30.7
DMPC	-	-	59.9	36.7	63.3	35.2	65.7	34.2
DPPC	-	-	-	-	63.1	39.0	65.0	38.1

Table 5: Lipid area (APL) and Luzzati bilayer thickness (D_B) of several fluid bilayers at different temperatures [92].

II.5.4. Distribution

The analysis of spatial distribution of certain properties over time (including angles, positions, H-bonds or distances between atoms and molecules) is of great importance to visualize the behavior of a system along simulation time. It enables better investigation of local atomic and molecular structural variations. The analysis is performed over the equilibrated portion of the MD-trajectory, which should be sufficiently representative of the real behavior under study. The distance along the z-axis of COM of molecule or characteristic chemical groups with respect to the center of lipid bilayer is used to determine its spatial distribution in the membranes. The averaged value must be given with its standard deviation, which is representative of fluctuations occurring within the time scale of the simulation. The number of H-bonds can also be followed, e.g., described as all distances between H-bond donor and acceptor below a threshold value of 3.0 Å.

II.5.5. Radial distribution function

The Radial Distribution Function (RDF) is a useful tool to predict the atom position and molecular structure of a system. It gives the probability to find a particle at a given distance r from another particle. The concept is to construct a spherical shell of radius r and thickness dr around a chosen molecule or atom type and it calculates the pair distribution $g(r)$ of molecular pairs at this radius. For a single molecule or atom, $g(r)$ is defined as:

$$g(r) = \frac{n(r)}{\rho 4\pi r^2 dr}$$

where $n(r)$ is the number of atoms in this spherical shell, ρ is the mean particle density; it is given by N/V where N is the number of atoms in volume V . Then, the total number in the shell is $\rho 4\pi r^2 dr$ and the number of atoms in the volume elements varies as r^2 .

This analysis allows us to evaluate the probability of water molecules around a given drug and their hydration number. This latter is given by integrating the above equation up to (r) the first minimum in the RDF curves:



$$n = \int_{r=0}^r n(r) = \int_{r=0}^r \rho 4\pi r^2 dr g(r)$$

where $n(r)$ is the number of water molecules in the first shell with a thickness of dr at a distance r from the COM of the drug molecule.



Chapter III. *In silico* pharmacology: drug membrane partitioning and crossing

Authors:

Florent Di Meo,^a Gabin Fabre,^b Karel Berka,^c Tahani Ossman,^a Benjamin Chantemargue,^{a,c} Markéta Paloncýová,^c Pierre Marquet,^a Michal Otyepka^c and Patrick Trouillas^{a,c,*}

^a INSERM UMR 850, Univ. Limoges, Faculty of Pharmacy, 2 rue du Dr Marcland, F-87025, Limoges, France

^b LCSN, Univ. Limoges, Faculty of Pharmacy, 2 rue du Dr Marcland, F-87025, Limoges, France

^c Regional Centre for Advanced Technologies and Materials, Department of Physical Chemistry, Faculty of Science, Palacký University, Olomouc, Czech Republic

Reference:

F. Di Meo et al. *Pharmacol. Res.* 111 (2016) 471–486. doi:10.1016/j.phrs.2016.06.030 [78].

This review assesses how theoretical methods can now be considered as a new pharmacological tool, supporting or predicting experimental evidence, explicitly addressing: i) lipid bilayer insertion (Section III.3); ii) passive membrane permeation (Section III.4.1); iii) facilitated transport by membrane proteins (Section III.4.2); iv) biotransformation by membrane proteins (Section III.5); and v) efflux by active membrane transporters (Section III.6). The strengths of different *in silico* methodologies will be discussed, emphasizing on the importance of lipid bilayer composition (Section III.7).

As an important part of my thesis is focusing on the interactions between pharmacological drugs and membrane, I have contributed to review MD studies of the interactions between i) antiviral drugs (section III.3.5), ii) antimicrobial peptide drugs (section III.3.6) and membranes, as well the influence of membrane composition on the lipids phases formation (III.7).

III.1. Introduction

Drug-membrane interaction is a crucial pharmacological step that directly affects ADME (absorption, distribution, metabolism and excretion) of drugs, and subsequently drug action or toxicity [95,96]. Biological membranes are complex dynamical systems composed of a huge number of different lipids and proteins, with mass ratio ranging from 1:3 to 3:1 [97]. According to the fluid mosaic model proposed by Singer and Nicholson in 1972, the plasma membrane forms "islands" of proteins immersed in the "two-dimensional sea" of lipids [98]. This model is still a valid description of most biological membranes with some significant exceptions, e.g., skin membrane [99].

In this review, we will mainly focus on drug interactions with the lipid bilayer and with membrane proteins. Although only about 30 % of human genes encode for membrane proteins [100], more than 60 % of molecular targets of commonly used drugs are membrane proteins (Figure 15) [101]. Drug-protein interactions, related mechanism of a drug action, have been under close consideration [102], which is often better documented than drug-lipid interactions and membrane crossing. Drug-lipid interactions are pharmacologically significant as i) drug partitioning to membranes is more common than nonspecific protein binding [103];



ii) nonpolar xenobiotics can accumulate in lipid bilayers [104]; and passive transport contributes to drug disposition [105].

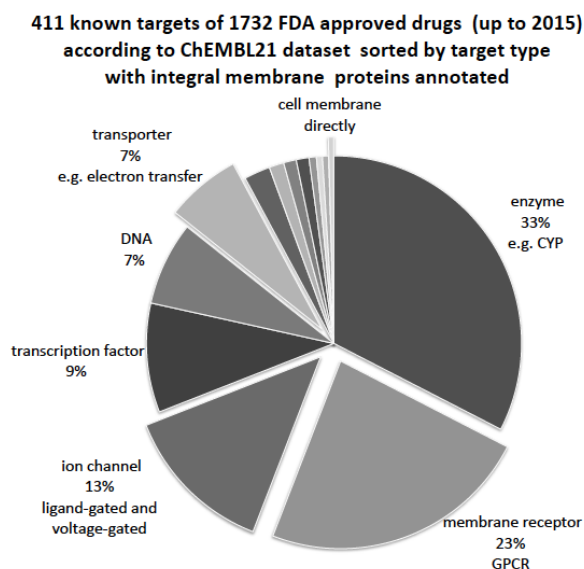


Figure 15: 411 known targets of 1732 FDA approved drugs (up to 2015) according to ChEMBL21 dataset sorted by target type. Membrane bound targets consist about 62.4 % are annotated by expansion of triangle.

The biophysical techniques used to investigate drug-membrane interactions provide meaningful but fragmented information on: drug insertion; average location in the inner or outer parts of lipid bilayers; conformational and orientational behaviors; diffusion coefficients; partition coefficients; and membrane (passive) permeation. The mentioned biophysical methods are rather expensive, time consuming and cannot be employed easily in high-throughput screening. Alternatively, *in silico* molecular modeling has gained substantial attention and maturity over the past decade. Since their conceptualization [106–108], the *in silico* membrane models have witnessed an extensive development [109–111]. The exponential growth of computing resources also drives the development in accuracy at reasonable time. Molecular dynamics (MD) simulations of lipid bilayer membranes evaluate drug-membrane interaction at both atomic and femtosecond resolutions, which is hardly reached simultaneously by experimental methods.

III.2. Glossary of *in silico* terms

The aim of this section is only to guide non-experts in the specialized vocabulary, so as to facilitate and focus on understanding of the physical-chemical picture of drug-membrane crossing.

Molecular Mechanics: Methods to calculate the potential energy of a given molecular system as a function of position of the atoms in the system. The calculation is based on the classical (Newtonian) mechanics and empirical noncovalent terms as described by a force field.

Force field: Empirical formula of the potential energy together with tabulated empirical atomic parameters. Formula usually includes the bond deformation energy, the angle deformation energy, the energy associated with changes in dihedrals, the energy due to electrostatic (Coulomb) interactions, and the energy associated with van der Waals



interactions. Some force fields also include specific terms such as H-bonding, or an energetic term describing polarization effects.

All atom force field: All atoms are explicitly treated as partially charged van der Waals balls on springs. Van der Waals interactions between distant atoms (e.g., above 1 nm) are usually neglected, so to reduce the computational costs.

United atom force field: All atoms are treated as in all atom force fields, except nonpolar hydrogens that are united with the carbon they are attached to. United atom force fields are known to overestimate diffusion coefficients due to smaller friction.

Coarse-grained (CG) force field: The number of degrees of freedom (e.g., atoms) is decreased (with respect to all atom force field description) by associating some atoms into atomic (super)-groups, called beads. These beads are treated as interacting polar, non-polar, apolar, or charged moieties.

Classical, free or unbiased MD simulations: The evolution (trajectory) of a molecular system in time by integration of Newtonian equations of motion at given conditions (e.g., pressure, temperature, ionic strength, etc.). Currently, we achieve timescales from hundreds of nanoseconds to a few microseconds depending on system size and available computational power.

Biased MD simulations: Dedicated MD algorithms designed to speed up the exploration of potential energy either by constraining or focusing on geometrical variables of interest, e.g., steered MD; constrained MD; targeted MD, metadynamics, replica exchange MD.

Homology modeling: A theoretical approach, which provides structural models of proteins based on sequence homology (similarity). Assuming that two similar protein sequences should adopt remarkably close 3D structures, an unknown structure can be built by aligning its amino acid sequence onto a known structure of a reference (homologue) protein.

III.3. Drug insertion and partitioning into lipid bilayers

One of the main advantages of MD simulations is the ability to describe the preferred location and orientation of drugs in membranes at atomic resolution. Locations and orientations have been successfully predicted for a wide variety of drugs, in agreement with experimental data obtained on biomimetic membrane models [112]. In addition to providing locations and orientations, biased MD simulations enable evaluation of Gibbs energy (ΔG)-profiles along a chosen direction, e.g., the membrane normal (z -axis) to picture membrane crossing and estimate membrane partitioning (Figure 16). This energetic profile reflects the selective drug affinity to the different membrane regions. Along the z -axis, a bilayer can conceptually be divided into five regions: region 1) bulk water ($z > \sim 2.5$ nm); region 2) the aqueous interface between water and phosphate groups ($\sim 2.0 < z < \sim 2.5$ nm); region 3) the dry transition region between phosphate groups and acyl chains ($\sim 1.5 < z < \sim 2.0$ nm); region 4) the hydrophobic region of the bilayer ($\sim 0.5 < z < \sim 1.5$ nm); and region 5) the middle of the bilayer with low tail density ($z < \sim 0.5$ nm).¹ The difference in Gibbs energies between the bulk water and the potential well in the membrane (ΔG_{part} , see Figure 16) provides a much more complex view on drug-membrane partitioning than the commonly used 1-octanol/water partition coefficients $\log P$ [113,114], which cannot catch complexity of membrane bilayer

¹ Although the boundaries, given in bracket for a neat 1,2-dioleoyl-sn-glycero-3-phosphocholine (DOPC) bilayer, may differ with membrane composition, they are pertinent to the present analysis.



structure [115]. Here a non-exhaustive list is given, in which we exemplify the success of MD studies at predicting or confirming membrane insertion of a number of drugs, sorted by therapeutic classes.

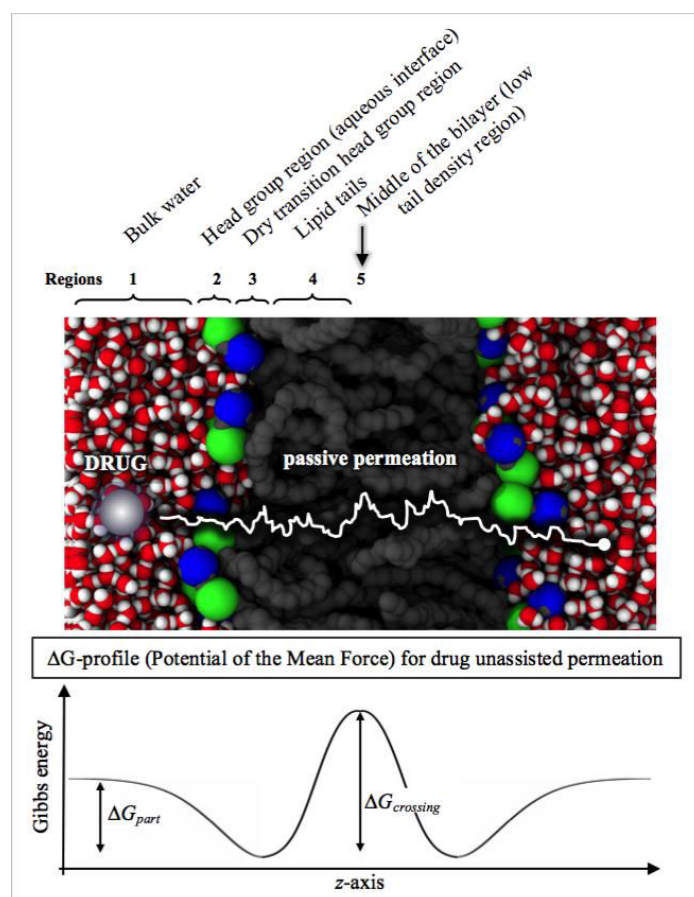


Figure 16: Pictorial description of unassisted (passive) permeation and energetic profile for drug crossing. ΔG_{part} is related to drug partitioning, whereas $\Delta G_{crossing}$ is the highest energetic barrier met by drugs through the bilayer (i.e., limiting step of crossing event). The potential well and the $\Delta G_{crossing}$ may be localized in different regions; this very scheme reflects the behavior of a polar or an amphiphilic compound (high barrier in the lipid tail region).

III.3.1. Anesthetics

Local anesthetics (LAs), including articaine, lidocaine, prilocaine, tetracaine and phenytoin bear titratable amino groups and may exist in both charged and uncharged states at physiological pH. MD simulations predict that all charged forms partition in the polar head group region in contact with water molecules (region 2), whereas uncharged forms insert deeper into the bilayers (regions 3-5) and cross membrane by passive permeation [116–126]. MD simulations help to decide whether LAs directly inhibit voltage-sensitive sodium and potassium channels [127–129], or as suggested by their location in membranes, increase lipid bilayer fluidity hence decreasing lipid order [116,121,123,125,126]. Membrane modifications associated with LA insertion in lipid bilayer most likely occur in the surrounding of ion channels, thus affecting ion exchanges.

The general anesthetics (GAs)' family includes: small gases such as neon and NO; fluorinated molecules (e.g., halothane, desflurane); amphiphilic compounds (e.g.,



benzodiazepines, propofol, ketamine); and 1-alkanols. Two main mechanisms of action have been considered, namely via receptors [130] or via membrane disruption. MD simulations confirmed X-ray diffraction studies showing that, at therapeutic concentration, ketamine inserts in membranes at the lipid/water interface affecting neither membrane thickness nor area per lipid, however inducing significant changes in lateral pressure profile that could affect ion channels [131]. Additionally, several MD studies addressed the relationship between lateral pressure and pressure reversal (cessation of anesthesia by hyperbaric pressure) [132]. Molecular descriptors rationalizing pressure reversal were identified, e.g., location of some GAs' moieties; orientation of lipid head groups or tails [133]; and intra-membrane GA aggregation [134,135].

III.3.2. β -blockers

Beside their β -adrenergic blocking activities, β -blockers can also affect lipid bilayer properties, especially the non-selective β -blockers such as alprenolol, oxprenolol and propranolol. This mechanism of action is known as the non-specific membrane effect; it results in anesthetic [136] and cardioprotective effects [137]. Non-selective β -blockers were reported to fluidize 1,2-dipalmitoylphosphatidylcholine (DPPC) lipid bilayer membranes [138], whereas they significantly rigidified liposomes made of 1-palmitoyl,2-oleoyl-sn-glycero-3-phosphocholine (POPC) [139]. MD simulations were recently carried out to describe the interactions between propranolol and POPC bilayer. Propranolol was shown to specifically bind the carbonyl and phosphate groups, resulting in an increase and decrease of packing in the polar head group and the lipid tail regions, respectively [139]. This result agrees with the modification of lateral pressure observed for LAs, and may explain the anesthetic effects of β -blockers. However, to confirm this mechanism a particular attention has to be paid to specificity of β -blockers and membrane composition.

III.3.3. Non-steroidal anti-inflammatory drugs

Non-steroidal anti-inflammatory drugs (NSAIDs) are widely used as inhibitors of cyclooxygenases (COX). The most common drugs in this family are ibuprofen, aspirin and naproxen. Several studies highlighted that the related gastro-intestinal toxicity could result from intercalation of NSAIDs in-between phospholipids and subsequent perturbations of the bilayer structure [140], including membrane thinning and fluidizing effects [141–143]. Interaction between NSAIDs and lipid bilayers is mainly driven by the fact that they all bear a carboxylic acid moiety that can be deprotonated at relatively low pH values (e.g., pK_a values of ibuprofen, aspirin and naproxen are 4.5-5.2, 3.5 and 4.2, respectively). It means that at physiological pH, the negatively charged forms predominate and can locate just below the polar head groups of lipid bilayers (regions 2 to 3), as seen theoretically and experimentally [142,144]. When MD simulations are carried out on the neutral form, NSAIDs are predicted to be much deeper in bilayers, lying between lipid chains close to the middle of membrane (regions 4-5) [142,143,145,146]. Membrane alteration may increase membrane permeability to H^+ , which may participate in rationalizing gastro-intestinal toxicity [141].

III.3.4. Antioxidants

Antioxidants have been extensively studied for their beneficial effects on human health, despite the fact that from a medical viewpoint, only a few applications exist, e.g., usage in organ conservation [147,148]. Among other processes, antioxidants are capable of inhibiting lipid peroxidation, which requires location sufficiently deep inside lipid bilayer membranes,



where oxidation occurs (propagation and termination stages). Several MD-based studies have rationalized the insertion of polyphenol antioxidants in lipid bilayers, with a preferred location in contact with the polar head group region (region 3), in agreement with experimental studies [149–152]. Structure-property relationships were thoroughly established, showing, e.g., the role of OH groups at orienting the molecules towards membrane surface [153–156]. Methylation or hydrophobic moieties drive antioxidants deeper in membranes, increasing lipid peroxidation inhibition, as clearly confirmed theoretically for α -tocopherol (having one phenolic OH group, adjacent methyl groups and a long lipid tail) that penetrates deeper into lipid bilayers (regions 3-5) than most of polyphenols [157]. Additionally, it is capable of 'flip-flop' from one to the other leaflet, increasing contact with lipid chains [157]. Ascorbic acid (or vitamin C) is also a very common antioxidant that partitions outside lipid bilayer, in contact with the water phase (region 2) [157]. Membrane complexity can also be taken into consideration, e.g., the depth of penetration for α -tocopherol in bilayer strongly depends on lipid composition [158–160]. Also synergy effects between antioxidants were shown, by MD simulations [157], to occur inside lipid bilayer due to the formation of noncovalent complexes (Figure 17), which may increase their total antioxidant activity [161,162].

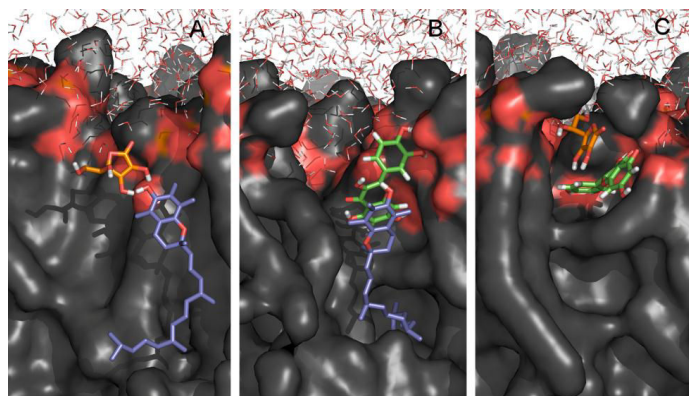


Figure 17: Location of α -tocopherol, ascorbic acid and a prototypical polyphenol (quercetin) in a DOPC lipid bilayer.

III.3.5. Antiviral drugs

Adamantane derivatives such as amantadine, rimantadine and memantine are antiviral drugs widely used against influenza A. They are suggested to block the so-called M2 ion channel [163]. This process is partially attributed to the interactions of these drugs with the lipid bilayer surrounding the channel. MD simulations showed that both the protonated and deprotonated forms of adamantane derivatives preferentially locate in lipid bilayers, in contact with the polar head groups (region 3) [164,165]. MD simulations showed that at such a location, these antiviral compounds disrupt the intramolecular interactions between choline and carbonyl groups in lipids, subsequently distorting significantly their conformations.

The photoactivated antiviral activities of hypericin and its brominated derivatives were shown to dramatically affect membrane cell by causing lipid peroxidation [166,167]. MD simulations were carried out for hypericin, mono- and tetra-brominated hypericin, showing a preferred location close to the polar head group region at the lipid/water interface (region 2) in a pure DPPC bilayer [167]. Such location was favored by the existence of several hydrogen bonds between the drugs and water molecules. The depth of penetration increased with the level of bromination of hypericin. Higher concentration of cholesterol also drove the drugs slightly



deeper in the bilayer, suggesting a better capacity to cross membranes [166]. At high concentrations, hypericin molecules could also self-assemble to form strong noncovalent aggregates in both the water phase and the bilayer [166].

MD simulations showed that the oleuropein aglycone antiviral agent (from virgin olive oil) preferentially locates in the hydrophobic core of different lipid bilayers, i.e., POPC/cholesterol and POPC/POPG/cholesterol [168]. This compound located deeper in the latter model due to stronger effects of the negatively charged lipids on the order parameters compared to zwitterionic ones. This antiviral agent affected the thickness of the bilayers as well as locations of phosphate atoms in the membrane, mainly for POPG-containing membranes.

III.3.6. Antimicrobial peptides

Due to their structural properties (amino acid composition, amphiphilic properties, cationic charges and small size) antimicrobial peptides (AMPs) are ideal candidates to penetrate or cross cell membranes of microbes, either to affect them or to reach intracellular targets, respectively [169]. There are several mechanisms for AMPs to kill cells and four of which involve membrane interactions: i) disruption of the bacterial membrane structure; ii) pore formation; iii) membrane thinning; iv) translocation of the peptide across membrane; v) receptor inhibition; and vi) inhibition of nucleic acid synthesis [169–172]. MD simulations showed a high ability to picture what can be considered here as the first step of the mechanism for AMP antimicrobial action, namely the binding mode with membrane. Various AMPs (CM15, cyclo(RRWRF), piscidins, β -hairpin tachyplesins, bacteriocins such as plantaricin EF) were indeed theoretically confirmed to efficiently insert in lipid bilayers [172–177]. The role of hydrophobic effects, H-bonding and electrostatic interactions rationalize the peptide positioning. Due to the molecular weight of these peptide drugs, the physical chemical properties of membranes are much influenced, including fluidity, order parameter and Gibbs energy barrier of water penetration. Atomistic models revealed conformational flexibility of AMPs in lipid bilayers [173] but also the formation of aggregates that may influence lateral diffusion and membrane integrity [172,174,177].

III.4. Drug entrance into cytoplasmic media

III.4.1. Drug passive diffusion and permeation

Even though pores, vesicle formation or protein transporters may control influx, in particular for charge species or essential elements such as sugars and amino acids, unassisted (spontaneous) passive permeation through the lipid bilayers is the major drug influx process. Permeation could in principle be observed with fully sampled free MD simulations. As far as sufficient sampling is reached, free (unbiased) MD simulations allow prediction of permeability in terms of simple models, according to number of crossing events. Crossing events and permeability through both pores and lipid bilayers were thereby predicted [178]. To improve statistics, these authors have counted the semipermeation events (crossing over one membrane leaflet). However, most of drugs passively permeate within at least several milliseconds [179], while the time scale that is accessible by unbiased MD simulation with nowadays-regular computational power is somewhat not more than several microseconds. It means that, for most of drugs, permeation is a rare event within the microsecond-time-scale, as reached by MD simulations. CG calculations allow accessing longer simulation time scale, as well as biased MD simulations (e.g., z-constrained, Umbrella-sampling or metadynamics)



that somehow "force" membrane-crossing events. The accurate computation of all aspects of passive permeation turned out to be a theoretical challenge [180], in which all-dynamical aspects of local solute-environment interactions have to be thoroughly described.

The "homogeneous solubility-diffusion" model can partially depict permeation. Here the process is decomposed into three stages, namely dissolution into the lipid bilayer, diffusion through membrane interior, and dissolution back to the surrounding environment (water) [181]. To make the description more realistic, the "inhomogeneous solubility-diffusion" model account for inhomogeneity (defects) in the membrane interior. Ideally any defect (even rare) should be taken into consideration, e.g., transient pores favoring drug permeation. These formalisms are likely to provide a picture of the dominant mechanism for passive permeation through biological membranes. An elegant alternative approach, borrowed from polymer science, is to consider hopping transport via free volumes. This approach highlights the importance of evaluating all free volumes in membranes, a task for which MD is ideally suited. This is particularly relevant to rationalize permeation of small molecules.

The evaluation of permeability coefficients should consider the Gibbs energy barriers required to cross the different sections of the lipid bilayer $\Delta G(z)$ profile along the z -axis (perpendicular to membrane surface), as well as the local diffusion coefficients $D(z)$. The global permeation then combines both $\Delta G(z)$ and $D(z)$ expressions within a single expression of the local resistance to membrane crossing:

$$R = \int_{z_1}^{z_2} R(z) dz = \int_{z_1}^{z_2} \frac{\exp[\Delta G(z)/kT]}{D(z)} dz = \frac{1}{P} = \frac{\Delta c}{J}$$

where P is the predicted membrane permeability coefficient; Δc is the concentration difference between z_1 and z_2 ; and J is the flux of solute from z_1 to z_2 , i.e., through membrane.

The Gibbs energy profile provides the $\Delta G(z)$ values (Scheme 2). Although it is inaccessible to the experimental techniques in an atomistic detail, several theoretical methods are available. Gibbs energy profile is alternatively called potential of mean force (PMF), as the main objective is to calculate the energetic cost required by the drug to follow its way through the membrane. Some methods indeed evaluate the average force exerted on a drug to be constrained at a given depth, specifically z -constraint method.

Concerning the diffusion coefficients $D(z)$, it is highly dependent on drug location and it strongly changes through membrane crossing. Again, if correctly employed, (biased or unbiased) MD simulations are the way, how to depict the local effects driving $D(z)$. During the z -constraint simulations, the forces applied to drug are monitored. The force autocorrelation function then allows calculation of the friction coefficient $\xi(z, t)$, obtained from the difference $\Delta F(z, t)$ between the instantaneous force and the averaged force acting on the drug:

$$\xi(z, t) = \frac{\langle \Delta F(z, t) \cdot \Delta F(z, t = 0) \rangle}{kT}$$

The local diffusion coefficient is then given by:

$$D(z) = \frac{kT}{\xi} = \frac{(kT)^2}{\int \langle \Delta F(z, t) \cdot \Delta F(z, t = 0) \rangle dt}$$

The atomic-level simulations intrinsically account for all intermolecular interactions, as far as sufficient sampling is reached.



The permeation of eight small organic compounds with various polarities (acetamide, acetic acid, benzene, ethane, methanol, methyl acetate, methylamine, and water) was evaluated using the equations above and MD simulations [181,182]. The Gibbs energy profiles confirmed high-energy barriers in the middle of the membrane for polar (hydrophilic) compounds, whereas more apolar (hydrophobic) compounds showed barrier only in the polar head group region (Figure 18A).

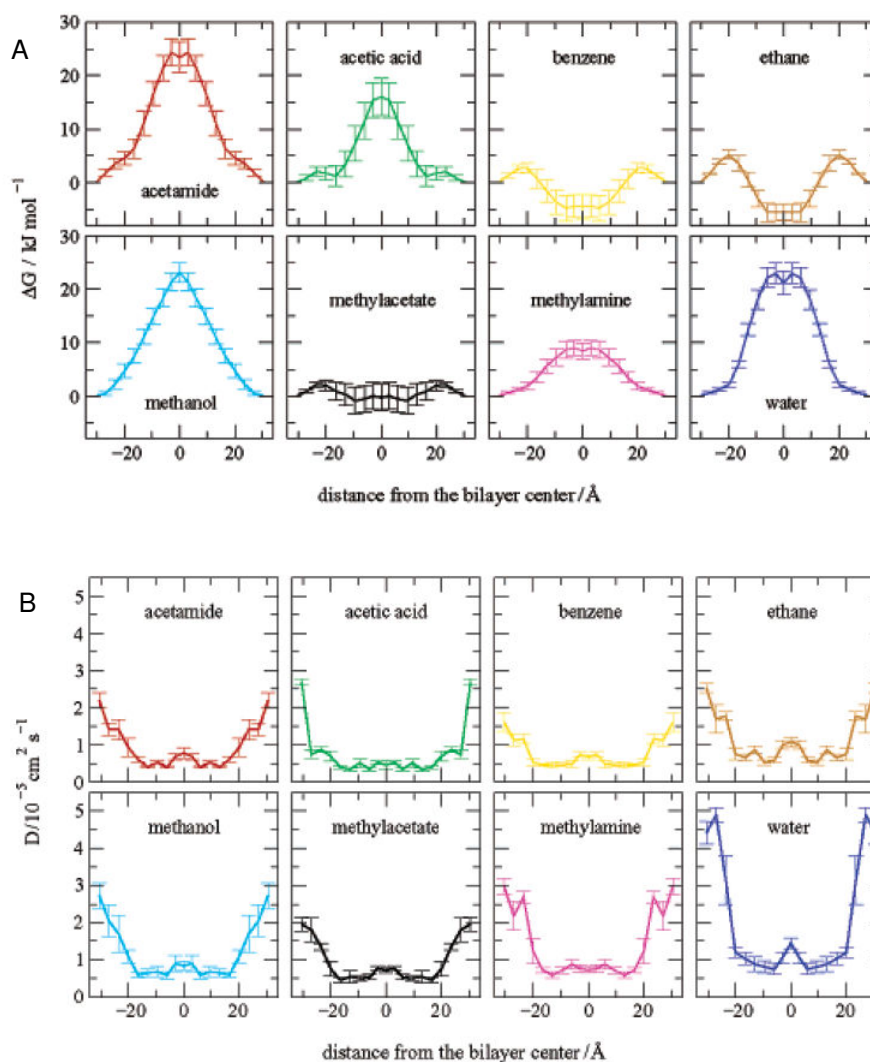


Figure 18: Predicted (A) Gibbs energy profiles and (B) diffusion coefficients of eight derivatives. Adapted from [182].

The same trend was confirmed for resistance to permeation. The diffusion coefficient was shown to be sensitive to membrane crossing, namely: i) decreasing in the polar head group region; ii) being uniform in between lipid chains; and iii) increasing when reaching the middle of the membrane as a result of the presence of free space (Figure 18B). Interestingly, diffusion coefficients turned out to be somewhat isotropic, as seen when comparing the predicted lateral and normal (z -axis) diffusion coefficients of water molecules in a DPPC bilayer [181]; this isotropy should however be considered with care for larger molecular-weight systems. Although the general trend for the predicted permeabilities was correct, their predicted values were roughly higher by 1 order of magnitude with respect to experimental values [181,182].



Biased MD simulations were also used to predict passive permeability of various drugs [183], e.g., a nifedipine analogue (an early attempt performed by a 4-ns MD simulation in DMPC bilayer) [184]; valproic acid [185]; β -blockers [186]; psoralen derivatives [187]; hypericin [188]. It must be stressed that to reach similar estimations from both theoretical simulations and experimental measurements is still a delicate issue, even more complex because different systems and different conditions are often used. However, relative permeability seems to be fairly predicted, which is particularly useful when dealing with families of drugs obtained from a lead compound [183,189].

More recently, a multiscale approach was proposed, in which compatible (mainly in terms of electrostatics) CG and atomic-level force fields were used on a 1,2-dimyristoyl-sn-glycero-3-phosphocholine (DMPC) lipid bilayer model [190]. Here the same list of eight organic solutes as used in Ref. [191] was considered. Within inhomogeneous solubility-diffusion formalism, the permeability values were within two orders of magnitude from the experimental values. However, this approach has appeared particularly promising as it allows working on larger membranes (thus minimizing artifacts induced by the boundary conditions), while at the same time ensuring better sampling. With this approach, the diffusion coefficients in the middle of the bilayer were higher than in the water phase, contrary to what was obtained with the standard atomic-level MD simulations [191]. However this can be an inherent artifact of CG simulations, as in this case a CG bead is represented by four water molecules. The transmembrane permeations of two steroid hormones (progesterone and testosterone) were evaluated using the same methodology [192]. The proposed limiting step for membrane crossing was that related to the highest Gibbs energy barrier required to cross the membrane, the transversal diffusion coefficient being roughly constant along the bilayer. The estimated lateral coefficients were lower than those along the normal z -axis. This study also highlighted the contribution of other membrane perturbation occurring during drug crossing, in particular intrusion of water molecules rather deep in the bilayer, in interaction with the drug. Regarding the size of the two steroid hormones, a particular attention was also paid to orientational effects.

Along this line, a recent work evaluated permeability coefficients using bias-exchange metadynamics [193]. To ensure better sampling of the whole hypersurface (including conformational and orientational variability of the drug), four collective variables were considered to benchmark the permeation of ethanol through a POPC bilayer. Among these variables was the position of the center of mass of ethanol along the z -axis, but also distances between specific moieties of both molecules. A permeability coefficient of 6×10^{-2} cm/s was obtained in a reasonable concord with performed unbiased MD simulations using 60 ethanol molecules in a POPC bilayer made of 128 lipids, corresponding to 8 permeation events, i.e., a mean permeation time estimation of $2.3 \pm 1.1 \mu\text{s}$ [193].

III.4.2. Facilitated diffusion mediated by membrane transport protein

An alternative way for drugs to influx is by facilitated diffusion, which is mediated by a superfamily of membrane transport proteins named solute carrier (SLC) [194,195]. This influx is a secondary active transport, which means that it only uses the energy stored in electrochemical gradients. More than 380 different SLC proteins, divided into 52 families, have been annotated in the human genome [196–201]. Most of the SLC transporters can be grouped into two large structural folds in membrane transporters, namely major facilitator superfamily (MFS) and neurotransmitter:sodium symporter (NSS) or LeuT-like fold [199]. Here a particular attention is paid to the MFS superfamily since only those influx transporters



are described as being of "emerging clinical importance" in drug discovery [195] by the International Transporter Consortium [202].

In silico studies on human MFS transporters are rather limited, mainly due to the absence of X-ray crystallographic structures. However, homologous models (mostly bacterial) have provided substantial insights in SLC transporter functions [200,203–205]. It is important to note that the surrounding membrane is not necessarily involved directly in the large-scale events; however, it naturally restrains protein movements to some extents. The use of protein models embedded in lipid bilayers is thus mandatory to simulate the transport cycle. In this section, we will only focus on *in silico* studies in which the membrane is explicitly included.

MFS transporters all adopt similar secondary structure consisting of twelve transmembrane helices (TM) organized into two N-terminal (TM1-TM6) and C-terminal domain (TM7-TM12) substructures (Figure 19A). The X-ray crystallographic structures supported by computational studies described two main conformations, namely inward- or outward-facing (IF and OF, respectively, see Figure 19B). The drug/substrate transport across the membrane is thus driven by large-scale conformation changes from one to the other state, following a "clamp-and-switch" model of function [206]. This suggests the existence of intermediate occluded conformations in IF- and/or OF-states, later confirmed by the X-ray structure of the Xylose:H⁺ symporter (Xyle) [207,208]. Such mechanical pathway was also suggested by means of steered and targeted (biased)-MD simulations in several transporters (namely, xylose Xyle [209], glucose² GLUT1 [211] and lactose LacY [212–214] transporters). It is worth noting that the "clamp-and-switch" model is actually a recent enhancement of the "rocker-switch" model [206]. Particular attention should be paid to a recent computational study on the glycerol-3-phosphate:phosphate transporter (GlpT) [215]. Although this transporter drives efflux, this study provides useful insights in the deep understanding of influx since all MFS transporters are very likely to share the "clamp-and-switch" mechanical pathway. The complete potential energy surface of the transport process was elucidated using a MD iterative protocol including biased-MD simulations and string method with swarm of trajectories.

The complete Gibbs energy landscape of transport cycle was then calculated with and without substrate underlining the "catalytic" role of the substrate. The existence of occluded-IF and -OF states was also confirmed to be thermodynamically stable states if and only if the substrate is bound to the transporter. This should explain why occluded states are so challenging to observe experimentally, since the substrate is not always present in crystal structures. Furthermore, details about the role of specific TMs along the transport cycle were investigated to correlate local and global conformational changes. The role of TM1 and TM7 to the periplasmic gating process was stressed as observed in GLUT1 influx transporter [211], whereas TM4, TM5, TM10 and TM11 were shown to be involved in the cytoplasmic gating. Such observations have strengthened the hypothesis of the asymmetrical global conformational changes along the transport cycle of MFS.

Joint experimental and computational studies are likely to elucidate more local events. For example in H⁺-cotransporters (e.g., LacY and Xyle), the H⁺-conduction (electrochemical gradient) from the periplasmic to cytoplasmic side is shown to provide the energy required to

² It must be stressed that this model was built by homology modeling using Xyle as reference [209]. The theoretical results agreed with the recently crystallized human GLUT1 in the IF-state [210].



the transport cycle. Such conduction along amino acid side chains (mainly Glu, Asp and His) proceeds by proton transfer reactions that locally change charge states of protonatable residues, leading to salt-bridge breaking/formation that trigger the IF-to-OF transition [209,213,214,216,217].

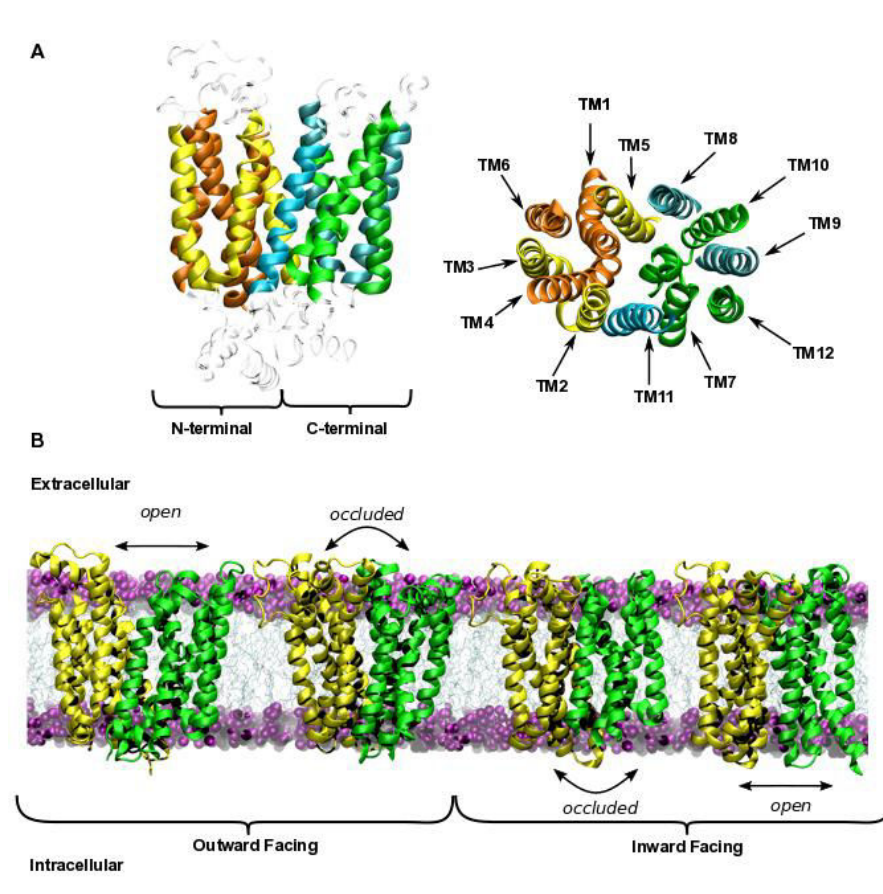


Figure 19: (A) X-ray structure of Glucose transporter type 3 (PDB-ID: 4ZW9 - GLUT3 [218], a detailed structural description is also available in Ref. [206]). (B) Examples of the several conformations detailed in the “clamp-and-switch” model from X-ray structures. Occluded-OF and occluded/open-IF structures were taken from X-ray structures of Xyle transporters (PDB-ID: 4GBY [208], 4JA3 [207] and 4JA4 [207], respectively); open-OF structure was taken from the GLUT3 transporter. N- and C-terminal domains are depicted in yellow and green, respectively.

Although MFS transport cycles have been extensively investigated theoretically, only a few studies have tackled the direct influence of the surrounding membrane. Yet, studying lipid-protein supramolecular assemblies [214,219] as well as considering membrane composition [214] have repeatedly been suggested to be of crucial importance. Another currently missing aspect is the direct study of human transporters of clinical interest. Only three human MFS transporter structures have been elucidated so far [210,220]. To the best of our knowledge, either homolog (e.g., with PEPT-1/2, see [221]) or homology-modeling-made (e.g., with PEPT-1 and OAT1, see Refs. [222,223]) transporters were used so far. Interestingly, the dynamic of the overall mechanism of PEPT-1 was found to be very close to that of LacY although they belong to two different distant SLC families. This supports the hypothesis that MFS transporters exhibit large-scale conformational transitions during transport cycle regardless substrates. MFS transporters mainly differ in local binding events that govern their substrate selectivity [221].



III.5. Membrane proteins for biotransformations

Drug-membrane interactions can be altered via biotransformation processes. Usually we distinguish two phases (I and II) of biotransformation of drugs [224]. In both phases, membrane-bound proteins are involved, e.g., cytochrome P450 (CYP) in phase I, uridine 5'-diphospho-glucuronosyltransferase (UGT) in phase II, or multidrug-resistance proteins later in excretion.

Phase I biotransformation of majority of drugs, is executed by CYP enzymes [225]. CYP enzymes are found in a majority of living organisms [226], but while bacterial CYPs are soluble enzymes, eukaryotic ones are attached to the membrane of either endoplasmic reticulum or mitochondria, and to the a much lower extent in the Golgi apparatus, peroxisomes or plasma membranes [227]. The sequence length of mammalian CYPs is around 500 amino acids including a ~20-25 amino acid long N-terminal transmembrane helix attached to a catalytic domain encompassing heme prosthetic group.

The important role of membrane topology in action of mammalian CYP was shown first by molecular simulations connecting together fragmental pieces of experimental evidences. The first atomistic membrane models of human CYP2C9 anchored to phosphatidylcholine bilayers [146,228] were constructed using homology modeling of the human CYP2C9 sequence over available crystal structures of catalytic domain [229,230] with added N-terminal helix. Those preliminary models were then positioned in different orientations into a lipid bilayer model; the whole molecular assembly was further equilibrated with 100 ns+ long MD simulations. Equilibrated consensus orientation showed that not only transmembrane N-terminal helix but also F/G loop of the catalytic domain was immersed into the membrane as it was confirmed by experimental evidence from epitope labeling, tryptophan fluorescence scanning and others [231–233]. CYP membrane orientation was later supported by additional MD simulations of other CYP family members [234–239], and recent experiments [240–242], including whole *Saccharomyces cerevisiae* CYP51 structures [241]. Importantly, CYP positioning and orientation allow drugs to pass from the membrane into the active site of CYP via a membrane-facing active site access channel, whereas more polar drugs and metabolites can access to, or egress, the active site via the cytosol-facing channel (Figure 20), which was recently supported by evaluation of the free energy of passage of metabolite from the active site by several channels with metadynamics MD simulations [243]. The role of membrane on function of P450 enzyme in drug biotransformation was recently overviewed by Backes et al [244].

Metabolites from CYP biotransformations are usually more polar than the parent substrates. A statistical analysis carried out over the phase I metabolites showed that CYP products of hydroxylation and dealkylation reactions prevail. As a result, phase I products tend to have lower average molecular weight by 20–25 Da and tend to reduce lipophilicity; only a minority of metabolites (4 – 8%) being more lipophilic than their parents due to some dealkylation reactions [252]. It was indeed shown by theoretical calculations that those metabolites are not as deeply immersed in lipid bilayer as their parent compounds. Moreover, affinity of metabolites towards lipid bilayer is lower whereas the barriers for passive membrane crossing are higher than for substrates [234,253].



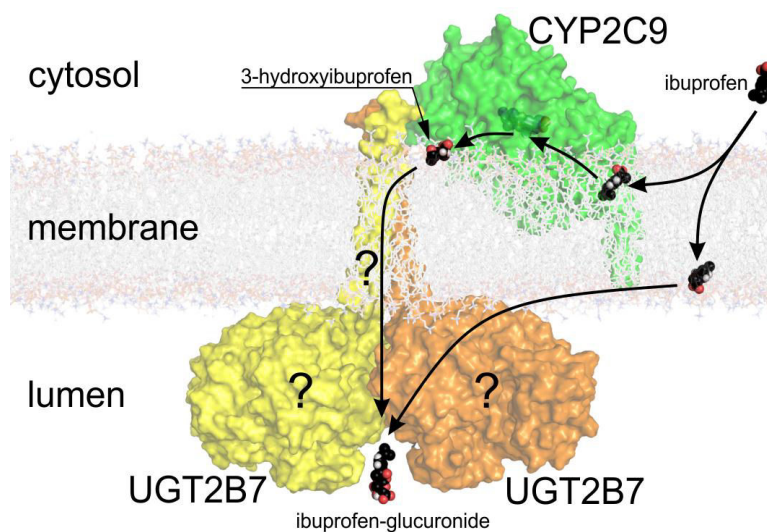


Figure 20: Scheme of biotransformation of ibuprofen with membrane-bound CYP2C9 and UGT2B7 enzymes. Ibuprofen is transformed by cytochromes P450 (CYP2C9, CYP2C8, CYP2C19, CYP3A4) or UDP-glucuronosyltransferases (UGT2B7, UGT2B4, UGT1A1, UGT1A3, UGT1A9) [245] to hydroxyibuprofens or ibuprofen-glucuronides, respectively. CYP2C9 model was modelled in DOPC membrane according to Berka et al. [146]. UGT2B7 was modeled according to Laakonen et al. [246] from UGT2B7 CTD domain [247] using I-TASSER server [248] and Modeller 9.14 software [249]. Membrane topology and proposed dimeric organization of UGT2B7 are depicted as an arbitrary illustration of known experimental data from [250]. Also the transfer route of glucuronidation of hydroxyibuprofens is unknown. Ibuprofen biotransformation pathway was taken from Drugbank (www.drugbank.ca) [251]. CYP structure was modelled according to Ref. [146].

The most important enzymes catalyzing phase II reactions are UGTs, glutathione S-transferases (GSTs), N-acetyltransferases (NATs), and sulfotransferases (SULTs)[254]. Of those, the major drug metabolizing enzymes are from UGT1 and UGT2 subfamilies. UGT enzymes transfer a glucuronic acid to the drug forming a glycosidic bond [255,256]. The complete human UGT crystal structure is not available, but the crystal structure of the UGT2B7 C-terminal domain was published [247]. This structure together with templates for the missing N-terminal domain from various sources (plant UGT enzymes, bacterial glycosyltransferases and macrolide transferases) have served for construction of several atomistic UGT models [246,254,257–259]. Albeit none of the models was built as cast in a membrane, they were used to identify the effects of amino acids in UGT1A1, whose mutations are known to play a role in the Crigler-Najjar type I or II syndromes or the Gilbert syndrome [246], or to assess substrate specificity between UGT1A9 and UGT1A10 [258]. The full atomistic membrane model of UGTs is however still missing.

Statistical analysis over the phase II metabolites showed rather systematic modifications of the physicochemical properties of biotransformed drugs and drug-like molecules. Conversely to phase I reactions, phase II conjugation reactions lead to a substantial gain in molecular weight (145 amu on average). Furthermore, phase II reactions lower *logP* values of drugs by 1.4 log units on average [252]. This agrees with previous analysis of membrane positioning of quercetin metabolites by means of MD simulations [260]. The conjugated substituent groups pulled quercetin moiety toward membrane surface. Overall, biotransformation reactions usually weaken drug-membrane interactions, leading to the excretion of drug in a final phase.



III.6. Efflux transport toward drug resistance

Drug extrusion (efflux) mainly occurs through membrane protein transporters. To the best of our knowledge, human efflux transporters are from the SLC and ATP-binding cassette (ABC) families.

MFS are a major class of SLC transporters in drug disposition. As said above (Section 4.2) they work following the "clamp-and-switch" mechanism that is actually not a unidirectional process; it means that this process can drive both influx (see Section 4.2) or efflux (e.g., GlpT transporter [215,261–263]). MD simulations may however support some discriminations between both processes, e.g., highlighting asymmetry in the influx or efflux substrate binding cavity that is likely to modulate drug transport specificity [264].³ A particular attention should also be paid to the MATE (multi-antimicrobial extrusion protein) transporter, which represents the only efflux SLC-type transporters considered of emerging clinical importance by the International Transporter Consortium [195]. Although a few theoretical investigations have been achieved [265], they can hardly be transposed to the human homolog functions (MATE-1 and MATE-K). This is complicated by the fact that no X-ray crystallographic structure is available for these human transporters so far. The rest of this section will review the computational efforts made to rationalize the main efflux process, namely through the ABC transporters.

Human ABC transporters are active exporters [266–268] that share a common architecture including two transmembrane domains (TMDs) and two cytoplasmic nucleotide-binding domains (NBDs, see Figure 21A). TMDs are mainly responsible for binding of drugs and their release into the periplasmic (extracellular) compartment. NBDs bind ATP molecules and catalyze their hydrolysis. As observed for MFS transporters (Section 4.2), ABC-transporters were also crystallized in both their IF and OF-states.

The IF-to-OF transition is the actual drug efflux mechanism; it has also been theoretically studied to reach a comprehensive atomic-scale understanding. NBDs have been suggested to be more than a simple energy provider (ATP hydrolysis). Starting from IF-conformation, the two NBDs proceed to a rigid body motion that keeps the TMDs' alignment [271]. This leads to the NBD-NBD noncovalent dimerization [203,272], which was predicted to trigger the further large-scale conformational changes [273]. The computational picture of the NBD-NBD supramolecular assembly shows the major role of dispersive and electrostatic interactions [274,275]. The further steps lead to OF-state, which are still a computational challenge due to coupling to the ATP-hydrolysis reaction. This would ideally require highly demanding computational effort, e.g., hybrid QM/MM calculations to accurately describe kinetics of ATP-hydrolysis. Another approach (MD-based only) to describe the impact of ATP-hydrolysis is to simulate a two-step mechanism: (i) ATP binding; then (ii) replace ATP by ADP and prolong the simulation [276,277]. Nevertheless, the complete supramolecular movement of both the protein and the membrane has not been described yet.

A relevant example of the computational contribution to the understanding of overall large-scale OF-to-IF transitions has recently been achieved on a bacterial ABC lipid flippase model (Msba) by biased-MD simulations [270,278]. In this very case (i.e., OF-to-IF transition), no ATP hydrolysis is required, making the use of MD simulations particularly adapted as only

³ It must be stressed that drug-protein binding affinities can be assessed by Molecular Mechanics / Poisson-Boltzmann or Generalized Born Surface Area (MM/PBSA or MM/GBSA); however these methods are not described here as drug-protein binding is out of the scope of this review.



conformational changes have to be figured out. A plausible sequential pathway has been proposed: i) increase of the inter- NBD-NBD distance; ii) TMD β -opening; iii) NBD γ -twisting; and iv) TMD α -opening (see Figure 21B, for definition of α , β , γ angles). The key role of NBDs was thus pointed out since their dissociation was predicted to trigger the OF-to-IF transition. Also the third step (NBD γ -twisting), so-called the "doorknob" model, requires a careful description. It increases electrostatic repulsive interactions at the NBD-NBD interface leading to the NBD dissociation by opening TMD (α -opening), required to reach the IF-state [270].

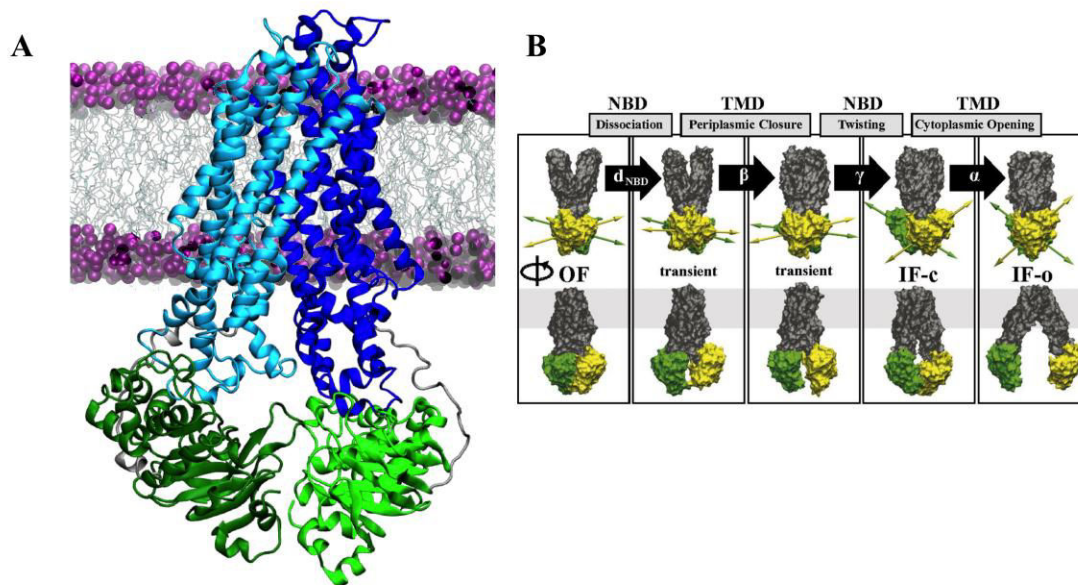


Figure 21: (A) X-ray structure of a ABC-transporter (PDB-ID: 3G5U, P-glycoprotein [269]). TMDs and NBDs are depicted in bluish and greenish colors, respectively. (B) Proposed sequential OF-to-IF pathway of the MsbA transporter (reproduced from [270] ©2013 by National Academy of Sciences).

MD simulations have also described some other key features of ABC-transporters. The high flexibility of the TMD within the IF-state has been suggested to allow drug inclusion into the transporter binding site directly from the inner membrane [279]. The MD framework is also currently the only tool capable of describing the role of atomic lipid-protein interactions as also shown for SLC transporters. Even though much work remains to be done, lipids have been shown to allow the reorientation of aromatic side chains and stabilize the protein in the membrane [279–281].

III.7. Membrane composition

The composition of cells and organelles' membranes is much more complex than simple bilayers made of a single phospholipid type; its composition and the related structure are pharmacologically crucial. It has been shown both experimentally [282] and theoretically [188,283,284] that the composition and especially lipid phase significantly affect drug membrane permeability or partitioning. The permeability through a fluid membrane is significantly higher than the permeability through an ordered membrane [282]. MD simulations can provide a correct description of the lipid bilayer phases, reproducing the phase transition temperature (T_m) [20,22], as well as order parameters obtained by NMR static splitting quadrupole [285]. Further, the lipid membrane composition was shown to affect the activity [286] or the orientation [287] of the membrane proteins.



Cholesterol is a particularly determinant ingredient; in animal cells it represents up to 20-50% of the bilayer and may control e.g., fluidity, rigidity. Theoretical chemistry studies have extensively investigated its role. MD simulations enable some general conclusions to be drawn, i.e., cholesterol addition: i) increases both thickness and rigidity of bilayers and decreases fluctuations [20,288,289]; ii) modify lateral packing [289,290]; iii) increases the order of initially disordered phase, whereas it is known to decrease order of ordered phases [291,292]; iv) decreases area per lipid [290,293]; v) drives, together with temperature, the formation of the liquid ordered (L_o) phase [290]; vi) induces phase separation [20] and the formation of (nano)-domains of lipids [21], also as suggested by lateral pressure heterogeneities [288,289]. It is unclear whether cholesterol is homogeneously distributed in the membranes, but it partitions better in between saturated lipids because the double bond precludes tight packing due to curved shape of lipids. There is no influence of cholesterol in the middle of the membrane. The lateral organization of cholesterol molecules is driven by repulsive interactions between them, which are of entropic origin mainly (as enthalpy decreases when packing increases) [294]. Packing that is related to free volumes and van der Waals contact can elegantly and efficiently be described by V_{tail} [283], i.e., the potential interaction energy between the lipid atoms in the lipid tail region (Lennard-Jones and short-range Coulomb potentials between all pairs of atoms). In the presence of cholesterol, V_{tail} decreases, thus increasing van der Waals contacts and packing [283].

Cholesterol is usually described to reduce the permeability. However, a thorough understanding at the atomic-level has appeared crucial. When cholesterol concentration increases, the energetic barriers increase in the lipid tail region [283], due to an increase in van der Waals contacts between lipid tails and cholesterol molecules. In other words, inside the bilayer, cholesterol increases packing, so it decreases both the amount of free volumes and area per lipid. It means that those van der Waals contacts must be broken to enable penetration of a given drug, which leads to a permeability decrease in this region [294,295]; the effect is even stronger for large solutes. Conversely, in the head group region, cholesterol addition increases distances between polar head groups, thus facilitating deeper insertion (increase permeation). These opposite effects of cholesterol in the different regions of the bilayer (bell-shape of the permeability-dependence according to the region of the bilayer) make that cholesterol influence depends on drug polarity, i.e., it may facilitate permeation for compounds for which the barrier is localized in the head group region [295]. In other words, cholesterol addition induces: i) permeability decrease for polar compounds; and conversely ii) permeability increase for hydrophobic compounds. The size of the head group is also important (i.e., permeability is more sensitive to cholesterol addition to lipid bilayers with small head groups) [283].

Small molecules and drugs are also known to affect membrane lateral organization, thus reshaping membrane domains. Even though no general trend based on chemical-physical properties has been elucidated so far, it has been recently shown in DPPC / dilinoeoyl-phosphatidylcholine (DLiPC) / cholesterol membrane with simple hydrophobic compounds that: i) aromaticity of compounds significantly affects membrane organization and cholesterol repartition; and ii) remodeling depend neither on size nor on cyclic nature of compounds [296]. Such observations agree with the crucial role of van der Waals interactions on the shape of membrane domains.

Sphingolipids (including sphingomyelin) are also important ingredients of lipid bilayers. Sphingomyelin/cholesterol mixtures appeared to be more packed than DOPC/cholesterol [289]. In ternary lipid mixtures (DPPC/DLPC/cholesterol) containing saturated and



polyunsaturated lipids, the coexistence of L_o/L_d phases was observed below T_m [293]. As expected, L_o and L_d domains were composed of saturated lipids / cholesterol and unsaturated lipids, respectively. In this case, cholesterol appeared to drive the lateral separation of the lipid phase domains [293]. Inhomogeneity in L_o regions was theoretically confirmed in other lipid ternary mixtures, in which the sub-structures were composed of saturated lipid chains, oriented parallel to the lipid bilayer normal with locally hexagonal order [297]. Saturated acyl chain indeed showed more ordering and less flexibility with respect to unsaturated chains [298].

To access larger systems and longer time scales, biased-MD and CG simulations can be used, in particular to better rationalize phase separation and coexistence of L_o/L_d but also gel/ L_o or phases. By doing so, a micro-emulsion-type state (formed with nanometer-sized L_o domains in an L_d environment) was shown to be probable [299]. Domains could be stabilized by the mismatch of curvatures between both L_o and L_d phase monolayers, generating elastic tensions that decrease the line tension between the two phases. In CG simulations, symmetric leaflets of ternary mixtures exhibited L_o/L_d phase separation [300]. The inter-leaflet association of nano-domains was investigated by CG simulations, and key intermolecular interactions were identified [184,186,191,192]. In order to model realistic membranes, symmetric and asymmetric bilayer models were constructed using CG simulations. These models consisted of seven different lipids including GM3 glycolipids in the outer leaflet and an anionic lipid (PIP2) in the inner leaflet [302]. In the outer leaflet, GM3 glycolipids were strongly arranged together, leading to order clustering and nano-domain formation. The lateral distribution of lipids in the inner leaflet appeared more random with small domains composed of PIP2. A slow (lateral) diffusion was observed for most lipids, especially for GM3, together with flip-flops of cholesterol. A study of the glycosphingolipid GM1 and the palmitoyl sphingomyelin PSM in ternary and quaternary lipid bilayers also showed spontaneous phase separation (Figure 22) [303]. Umbrella sampling simulations and CG simulations also predicted that cholesterol flip-flop was faster in polyunsaturated than in saturated bilayers [304]. Lipid composition and the degree of unsaturation of the lipids indeed modified local membrane curvature [305,306]. Finally, salt concentrations (NaCl) and water showed a significant impact on dynamic and structural properties of binary mixtures and stabilization of nano-domains [302,307].



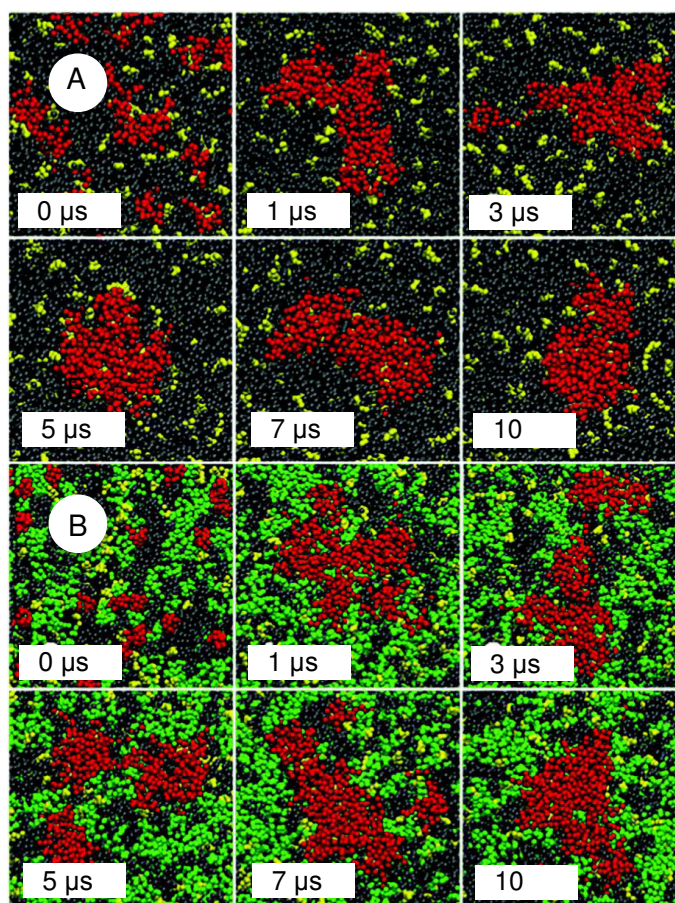


Figure 22: Formation of nano-domains in (A) ternary and (B) quaternary mixtures. GM1, POPC, PSM and cholesterol are represented in red, grey, green and yellow, respectively. Adapted from [303].

III.8. Conclusion

In conclusion, standard atomic-level, biased and CG-MD simulations are sets of theoretical tools that are now capable of predicting drug passages through (increasingly realistic) biological membranes. The recent developments and achievements have paved the way towards *in silico* pharmacology. Although, benchmarking and comparison to experiments are still mandatory to reach a predictive usage in real-life applications (i.e., to support clinical decisions), this is no longer science fiction. The pharmacological processes are described in an increasingly realistic way. Moreover, atomic-level MD simulations are building a picture of insertion, interaction, crossing, inhomogeneities with an atomic resolution, which usually allows identification of forces driving the processes with a remarkable accuracy. The reader should bear in mind the computational resources required for the different simulations, which can be exemplified by providing estimation of computational time for a series of representative systems (Table 6).

Still membrane organization vs. lipid composition has to be improved from the point of view of intermolecular interactions. Up to now, only CG simulation succeeded in visualizing phase separation or lipid segregation. However, the use of CG beads naturally overestimates some specific intermolecular interactions (e.g., between lipids, with solvent), most probably lowering some enthalpic contributions with respect to entropic contribution. In this context, joint CG and all-atom MD approaches has appeared promising.



	Lipid bilayer made of 128 POPC + box of water	Protein (ca. 65 kDa) embedded in lipid bilayer + box of water
All-atom MD simulations	10	1
United-atom MD simulations	20	2
CG simulations	2000	200

Table 6: Simulation time (in ns) for two representative molecular systems with three types of force field with regular computational facilities (8 CPUs) achievable within a day.

Also, the atomic-scale description of large conformational changes is still a major challenge. This includes description of membrane curvature, which can be partially caught by CG simulations, which, e.g., can simulate the spontaneous endocytosis and provide crucial information of nanoparticle shape and size that enable an efficient wrapping by membrane [308–310]. Other large conformational changes in pharmacological processes are those occurring in membrane proteins, for which biased MD simulations are highly promising techniques.



Chapter IV. Molecule insertion

IV.1. Preliminary theoretical insights on molecule insertion

The affinity of drugs to biological membrane is crucial for numerous biological processes. The physical chemical driving forces of drug-membrane interactions is still not fully pictured for many drugs. A full characterization at the atomic level of these interactions should support understanding of the critical role of lipid membranes in pharmacology and toxicity. In the beginning of this chapter, we have focused on several drugs used in renal transplantation (antivirals, immunosuppressants and antibiotics), for which some key steps of drug delivery and release is still under debate (Figure 23). The passage through membranes is one of these non-elucidated processes. Unbiased MD simulations on a DOPC lipid bilayer model have predicted drug insertion. These drugs cover a broad range of properties e.g., various pK_a , $\log P$ and molecular size. This study is a preliminary study which opens many questions to be tackled in Chapter V.

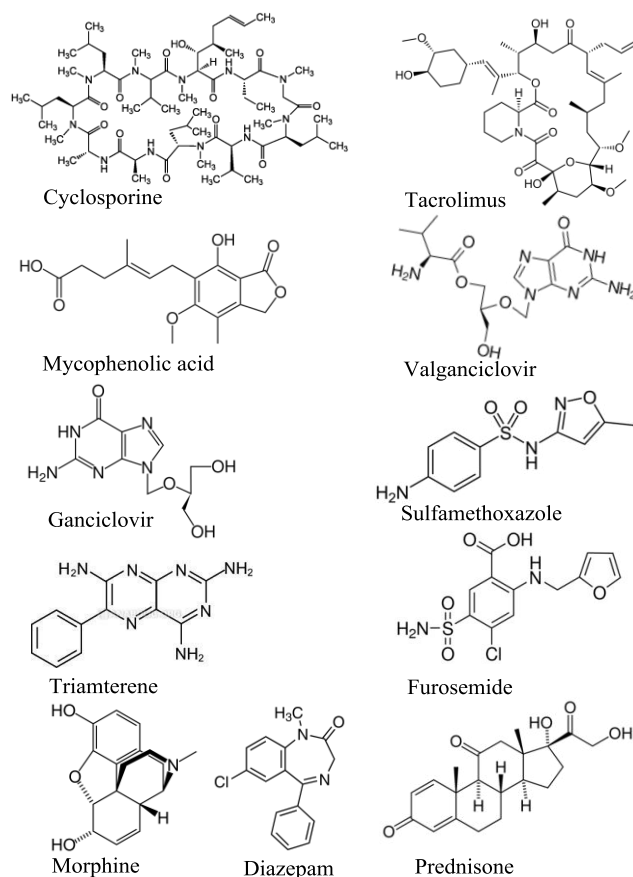


Figure 23: Chemical structures of studied drugs.

The behaviour of these drugs was evaluated by placing four molecules of each compound at different initial positions of membrane (inside & outside the bilayer), then unbiased 1 μ s-long MD simulations were performed according to the methodology described in section IV.3.2.1. For weak acids (e.g., mycophenolic acid, sulfamethoxazole) or weak bases (e.g., morphine) drugs, the charged forms were also studied, to evaluate pH effects on drug insertion.

The drug distance along the z-axis (perpendicular to membrane surface described by the P-atom layer) was followed with respect to membrane center. A sufficiently long sampling



(made after 300ns when the favored location was converged) has enabled providing spatial distribution of drugs through bilayer. Analyses of the drug center of mass (COM) and COM of various characteristic groups (OH groups, COOH groups, CO groups, NH₂ groups, phenyl groups...) were assessed. The angle between the z-axis and different vectors or planes was defined to describe drug orientation. The number of H-bonds was also analyzed.

Due to their amphiphilic character, when starting in the water phase, most of tested drugs quickly insert bilayer, within 50 to 80 ns. The COM of the majority of studied drugs was located below membrane surface in the dry transition region between phosphate groups and acyl chains ($1.5 < z < 2.0$ nm), in interaction with the polar head group region (Table 7).

Classes of compounds	Compound	d_{MD} COM (nm) ^a	logP	α (°)
Immunosuppressants	Cyclosporine	1.6 ± 0.2 0.6 ± 0.2	4.12	
	Tacrolimus	0.6 ± 0.3	3.19	
	Mycophenolic acid	1.6 ± 0.3	2.8	150 ± 20
	Mycophenolate	1.8 ± 0.2	-	150 ± 20
Antibiotics	Valganciclovir	1.5 ± 0.3	-1.28	150 ± 13
	Ganciclovir	1.5 ± 0.3	-1.65	150 ± 15
	Sulfamethoxazole	1.3 ± 0.1	0.89	
	Sulfamethoxazole	2.3 ± 0.2 1.8 ± 0.1	-	
Diuretics	Triamterene	1.2 ± 0.3	0.98	
	Furosemide	1.5 ± 0.1	2.03	
Analgesic	Morphine	1.3 ± 0.2	0.89	
	N-protonated morphine	1.8 ± 0.2	-	
others	Diazepam	1.2 ± 0.2	2.82	150 ± 20
	Prednisone	2.4 ± 0.2 1.5 ± 0.2	1.46	150 ± 15

^a Standard deviation

Table 7: Location, orientation of drugs studied. d is the average distance from the membrane center for COM or characteristic groups obtained via MD simulations (d_{MD}).

As expected, the hydrophobic groups (e.g., phenyl groups in case of triamterene and diazepam) orient towards the center of bilayer while polar groups (i.e., COOH, NH₂, SO₂, CO and OH groups) interact with the polar head group region (Figure 24). As a proof of MD convergence and sufficient sampling, when starting inside the lipid bilayer (center of bilayer), the drugs relax to the same location within less than 500 ns.



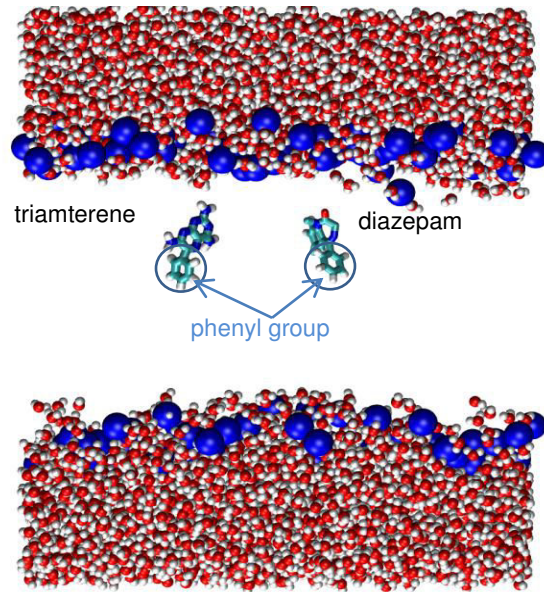


Figure 24: Characteristic snapshot of triamterene and diazepam at their preferred location in DOPC lipid bilayer.

The charged forms i.e., deprotonated forms of sulfamethoxazole and mycophenolate, and N-protonated form of morphine were shown to locate outside the bilayer at the lipid/water interface. For both charged states, a preferred location was observed in the dry transition region between phosphate groups and acyl chains, at ~ 1.8 nm from membrane center, in interaction with both the lipid polar head group and water molecules (Table 7 and Figure 25). For the anionic form (e.g., sulfamethoxazole), a density peak was observed in the aqueous interface between water and choline groups, at ~ 2.3 nm from membrane center. The MD simulations have clearly showed that the depth of penetration and orientation of drugs in membranes are driven by the number and position of polar groups, which in turn drive the different contributions of noncovalent intermolecular interactions (electrostatic, H-bonding and in a less extend van der Waals) between the polar groups of drug and lipids. The negative charge favors Coulomb (electrostatic) and H-bond interactions with choline moieties. The positive charge favors electrostatic interactions with phosphate groups.

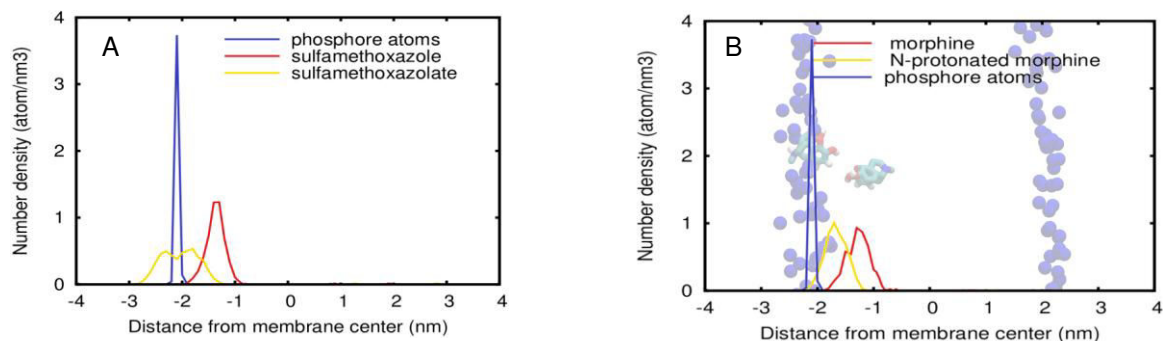


Figure 25: A) Location of sulfamethoxazole and its anionic form, sulfamethoxazolate, in the lipid bilayer; and B) Location of morphine and its cationic form, N-protonated morphine, in the lipid bilayer.

For all compounds containing a *keto* group, the distributions of the α -angle (defined between the C=O vector and the z-axis perpendicular to membrane surface) exhibit a maximum at around 150° , indicating a preferred orientation of the *keto* group towards the polar head groups, confirming importance of electrostatic interactions (Table 7).



Interestingly, prednisone ($\log P = 1.46$) has showed its inability to cross the polar head group region. When starting outside of the bilayer (i.e., in the water phase) the molecule approaches the polar head groups and it remains in the aqueous interface between water and choline groups at $d = 2.4 \pm 0.2$ nm from bilayer center. When starting inside bilayer, prednisone reaches the polar head groups, and it lies at $d = 1.6 \pm 0.2$ nm from bilayer center, in a parallel orientation to bilayer surface (Figure 26). Again, the keto group is oriented towards the polar head groups.

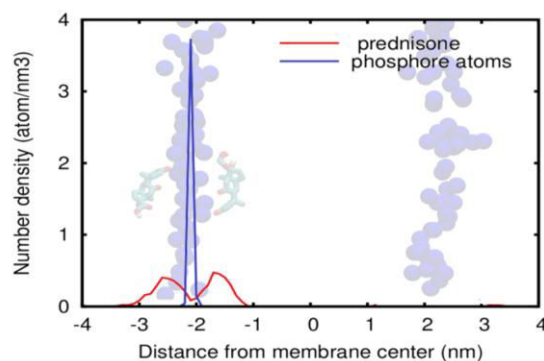


Figure 26: Location of prednisone in the lipid bilayer membrane.

Regarding the molecular size, both tacrolimus and cyclosporine (Cs), are relatively larger and complex structures. Interestingly, MD simulations have showed that their insertion from the water phase is quick. However, 1 μ s fully sufficient to allow all reorganizations in between lipid chains, as the system was not fully converged. This suggests that large molecules dramatically affect relaxation time, and may influence diffusion (see section V.3.4). In the time scale of MD simulations, both compounds showed rather deep location inside lipid bilayer, close to membrane center (~ 0.6 nm from the membrane center) (Table 7 and Figure 27A). These results positively correlate with the great lipophilicity of these compounds.

In case of Cs a second location has been observed, namely below the polar head groups at $d = 1.6 \pm 0.2$ nm from membrane center (Table 7 and Figure 27B). The favorable location of Cs below the polar head groups agrees with penetration experiments, which have proved its capacity to insert and interact with lipid membranes, affecting the part of acyl chains close to the head group region [311]. Cs has a hydrophobic cyclic undecapeptide structure, which may adopt various conformations and so to precede many conformational re-arrangements, which can rationalize the deeper insertion, here observed. A recent 3D structure analysis study highlighted the crucial role of conformational flexibility and intramolecular hydrogen bonding in passive permeation of Cs [312]. This study showed that Cs permeation requires a particular conformation, in which the hydrophilic groups are buried by locking them into a intramolecular hydrogen bond network. This enhances the lipophilic character of Cs, allowing reaching the hydrophobic core of the bilayer, thus rationalizing the second (deeper) location close to membrane center. Additionally, experimental studies reveal that depending on concentration, Cs disorganizes the acyl region, possibly inducing phase separation in some lipid models (Cs-rich phase). Cs was also shown to increase fluidity in gel phase, but to increase order in fluid phase [313]. Here unbiased 1 μ s-long MD simulations have proved accuracy at predicting location in lipid bilayer. However, to evaluate Cs-induced membrane reorganization, longer-time simulations, possibly with several Cs, are required.



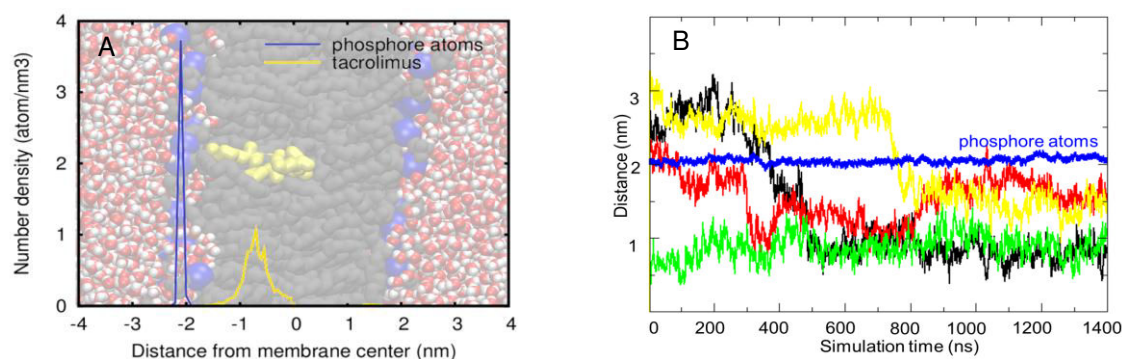


Figure 27: A) location distribution of tacrolimus in lipid bilayer membrane and B) evolution along trajectory of location for several Cs molecules starting from different positions.

These simulations provide a correct picture of insertion/positioning at the atomic and microsecond time scales. Neutral forms insert below the polar head groups whereas charged forms anchor the polar surface, interacting with polar head groups and water molecules. The molecular size has shown little effect on molecule insertion but it largely affects relaxation time. In addition to hydrophobic effects, the crucial role of noncovalent (electrostatic and H-bonding) interactions in molecule insertion is highlighted here. Finally, it is worth mentioning that no correlation is obtained between $\log P$ and the depth of penetration on this series of eleven drugs. Although, this series is too small to draw complete conclusions, this no-correlation observation highlights the limitation of the $\log P$ parameter (Figure 28).

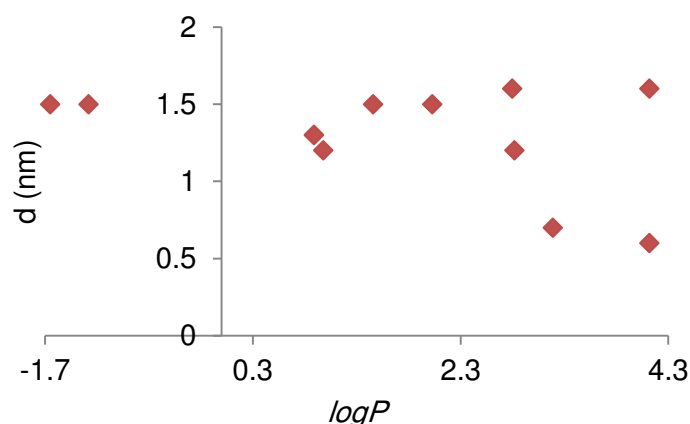


Figure 28: Predicted depth of drug penetration vs. $\log P$ for a series of eleven drugs.

In Chapter IV, we list the publications dealing with drug insertion, which I have co-authored during my Ph.D. I have only worked on the theoretical part. The first publication, (section IV.2) deals with ganciclovir (GCV), an antiviral drug widely used to prevent cytomegalovirus diseases in renal transplantation. GCV is used as a probe drug, before extrapolating to a series of drugs clinically used, owing to a few characteristics that make it an ideal candidate: our team has been working on the pharmacokinetics of this drug for a while; it is excreted in urine without catabolism; it crosses biological membranes passively, and it is excreted actively by an efflux transporter; in intra-cells, GCV is phosphorylated into GCV monophosphate, diphosphate and triphosphate. However, GCV and its metabolites showed an intracellular accumulation, leading to hematological toxicity such as neutropenia. The contribution of polymorphisms in membrane transporters to GCV neutrophil toxicity has been suggested. Therefore, to elucidate the factors associated to this toxicity is of crucial



importance, and as a first step it requires a better understanding of the exchange between the inner/outer membrane of the drug itself and of its metabolites (i.e. influx and efflux). Concerning GCV influx, it has been clearly shown that the molecule crosses biological membranes, as there exist experimental evidence that intracellular GCV concentrations are correlated with the effects of the drug. Passive permeation, after or before drug accumulation in the membrane, has been suggested. In this paper, we studied the compartment of GCV and its metabolites through membrane and their capacity to diffuse passively using unbiased MD simulations. *In silico* model of pure phospholipids (DOPC) was used. MD simulations suggest that GCV has a tendency to accumulate in lipid bilayers. This accumulation in both bilayer leaflets may facilitate drug delivery inside cells through passive permeation. Moreover, the particular GCV location close to the lipid bilayer surface supports its great capacity to be actively transported by ABC/MRP transporters. It is important to mention that after phosphorylation, the metabolites cannot penetrate back to the lipid bilayers and the metabolites either act or accumulate in cells.

The following publication (section IV.3) has studied the behavior of a series of antioxidants (anthocyanin derivatives) in interaction with lipid bilayers. Antioxidants are used in organ preservation to scavenge the reactive oxygen species that are produced during the ischemia-reperfusion process, occurring at different stages of organ transplantation, namely from collection and preservation to transplantation. In particular, this may induce lipid peroxidation and it may be carefully controlled and contained. To efficiently inhibit lipid peroxidation, antioxidants have to incorporate in lipid bilayers. MD simulations have appeared a valuable tool to describe all intermolecular interactions driving penetration and orientation of these compounds, here in a model of DOPC lipid bilayer.



IV.2. Multidrug Resistance-Associated Protein 4 (MRP4) controls ganciclovir intracellular accumulation and contributes to ganciclovir-induced neutropenia in renal transplant patients

Authors:

BILLAT Pierre-André^{a,b}, OSSMAN Tahani^{a,b}, SAINT-MARCOUX Franck^{a,b,c}, ESSIG Marie^{a,b,d}, REROLLE Jean-Philippe^{b,d}, KAMAR Nassim^{e,f}, ROSTAING Lionel^{e,f}, KAMINSKI Hannah^g, FABRE Gabin^h, OTYEPKA Michalⁱ, WOILLARD Jean-Baptiste^{a,b,c}, MARQUET Pierre^{a,b,c}, TROUILLAS Patrick^{a,b,i}, PICARD Nicolas^{a,b,c}.

^aUniv. Limoges, UMR 850, F-87000 Limoges, France;

^bINSERM, UMR 850, F-87000 Limoges, France;

^c CHU Limoges, Service de pharmacologie, toxicologie et pharmacovigilance, F-87000 Limoges, France;

^dCHU Limoges, Service de néphrologie, dialyse et transplantation, F-87000 Limoges, France;

^eCHU Toulouse Rangueil, Service de néphrologie, Dialyse et transplantation d'organes, F-31000 Toulouse, France ;

^fINSERM, U1043, IFR-BMT, CHU Purpan, F-31000 Toulouse, France; Univ. Toulouse Paul Sabatier, F-31000 Toulouse, France ;

^gCHU Bordeaux, F-33000 Bordeaux, France;

^hUniv. Limoges, LCSN, Faculté de Pharmacie, F-87025 Limoges, France;

ⁱRegional Centre of Advanced Technologies and Materials, Department of Physical Chemistry, Faculty of Science, Palacký University of Olomouc, Olomouc, Czech Republic.

Reference:

P.-A. Billat, T. Ossman et al. *Pharmacol. Res.* 111 (2016) 501–508. doi:10.1016/j.phrs.2016.07.012 [314].

IV.2.1. Introduction

Infection or reactivation of cytomegalovirus (CMV) is one of the major complications in immunosuppressed patients and is a major cause of morbidity and mortality. As the risk of infection is significantly higher in the first months post-transplantation, a universal prophylaxis or a preemptive strategy using ganciclovir (GCV, Figure 29A) or its oral prodrug valganciclovir (VGCV) is recommended. VGCV is rapidly hydrolyzed into GCV in blood. GCV is eliminated in its unchanged chemical form, through renal filtration and secretion. GCV action relies on phosphorylation into GCV monophosphate by the host and viral (pUL97) kinases. GCV diphosphate and triphosphate are further produced by non-specific cellular kinases [315–317].

GCV induces several adverse hematological effects, in particular, neutropenia [318]. Such toxicity leads to treatment being discontinued prematurely or to decrease doses. However, systemic exposure to the drug might not necessarily be a critical matter of concern. Indeed, a weak relationship between the plasma area under the curve of GCV and hematological toxicity has been reported [319–321]. In a group of 22 renal transplant patients, we found no relationship between GCV plasma exposure (evaluated as area under the GCV concentration vs. time curve; AUC_{0-5h}) and evolution of neutrophil concentration (p=0.44). In



contrast, the AUC_{0-5h} of intracellular GCV-triphosphate (the terminal active GCV metabolite) was significantly related to the decrease in neutrophil count over the first 3 months of treatment ($\beta = -0.0019 \pm 5.10^{-4}$, $p < 0.01$) [322]. This has clearly supported the hypothesis that the driving mechanisms of GCV or GCV phosphorylated metabolites intracellular accumulation play a role in GCV toxicity.

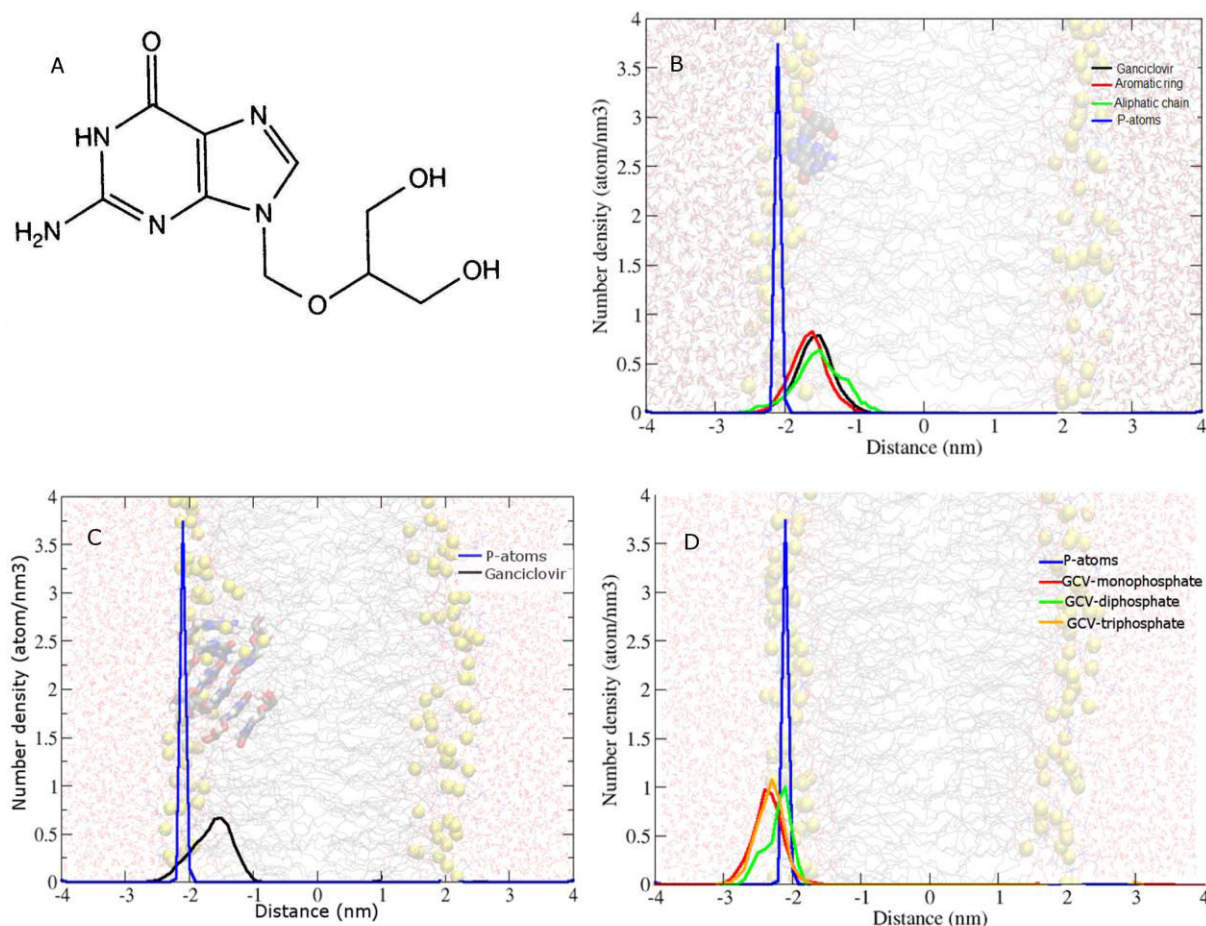


Figure 29: (A) Chemical structure of ganciclovir (GCV). (B) Average location of COM (center of mass) of GCV (black profile), the aromatic rings (red profile) and the aliphatic chain (green profile); the blue profile describes the P-atom distribution. (C) Average location of COM (center of mass) of GCV (black profile); the blue profile describes the P-atom distribution. (D) Average location of COM (center of mass) of GCV- monophosphate (red profile), GCV-diphosphate (green profile) and GCV-triphosphate (orange profile); the blue profile describes the P-atom distribution. (For interpretation of the references to color in this figure legend, the reader is referred to the web version of this article).

GCV membrane crossing has only rarely been documented up until now. Purine nucleobase carriers and nucleoside transporters were found to be involved in GCV permeation into human erythrocytes [323]. These transporters belong to the solute carriers (SLC) superfamily and mediate the movement of naturally occurring nucleosides as well as nucleoside analogs across membranes.

Specifically, the concentrative nucleoside transporter (CNT) 2 transports purine-nucleosides and CNT3 transports both pyrimidine and purine nucleosides, and equilibrative nucleoside transporters (ENTs; SLC29 family) have broad substrate specificity to purine and pyrimidine nucleosides [324,325]. On the other hand, efflux transporters of the ABC superfamily



expressed in blood cells (*ABCB1*, *ABCC4*, *ABCG2*) were found to carry purine analogs or GCV specifically.

Based on the hypothesis that genetic variability in GCV membrane transporters could play a role in intracellular drug accumulation, which might in turn contributes to GCV hematological toxicity, we investigated the association between functional polymorphisms in a selected panel of candidate transporters and the risk of GCV-induced neutrophil toxicity in renal transplant recipients. In order to further understand the mechanism of GCV membrane penetration in lipid membranes, molecular dynamics (MD) simulations were carried out.

IV.2.2. Materials and Methods

IV.2.2.1 Clinical pharmacogenetic study

IV.2.2.1.1. Selection of candidate genes and polymorphisms

Nine transporters previously found to carry analogues of puric bases and ideally GCV were selected. Among these, only 7 transporters expressed in blood cells were finally retained. Seventeen candidate gene polymorphisms were carefully selected from the literature and the SOPHIE (Study of Pharmacogenetics in Ethnically Diverse Populations) database (<http://pharmacogenetics.ucsf.edu/index.html>) based on reported evidences of clinical or *in vitro* functional effects and a Minor Allele Frequency (MAF) threshold of 2.5 % in Caucasians.

IV.2.2.1.2. Population studies

A first population of 174 renal transplant patients derived from a French multicenter cohort of 444 patients, enrolled between October 2007 and October 2011, constituted the exploratory group (EPIGREN; DGS (French Health General Direction) registration: 060566). A second group of 96 renal transplant patients included since February 2013 in an independent French multicenter served as the replication group (EPHEGREN; Clinical Trial Registry No. NCT 01989832). A vast majority of patients in these two studies were of European descent (given patient skin color). All the patients provided written informed consent for pharmacogenetic investigations. The patients included from the two cohorts received VGCV for the treatment or the prophylaxis of CMV infections. This study was approved by local ethic committees. Patient characteristics are given in Table 8.

	Exploratory group (EPIGREN) n=174	Confirmation group (EPHEGREN) n=96
Median age (range), years	59 (25-83)	57 (23-80)
Gender (male/female)	103/73	63/33
Median weight (range), kg	70 (38-159)	73 (45-117)
Median (range) of average creatinine clearance over the follow-up, mL/min	44.0 (8.95-115)	52.6 (15.1-149)
Median antiviral treatment duration, weeks	16 (1-235)	5.3 (1-71)
Proportion of CMV seropositivity in Recipients (R+)	0.57	0.56
Proportion of CMV seropositivity in graft donors (D+)	0.61	0.75
Proportion of patients receiving a VGCV dose > 450mg	0.16	0.24
Proportion of recipients treated with cotrimoxazole	0.32	NA

Table 8: patient characteristics.



IV.2.2.1.3. Identification of genotypes

Patients' DNA were isolated from EDTA-treated whole blood tubes using the Qiagen DNA blood minikit or from saliva collected with the ORAGENE OG-500 DNA kit (DNA Genotek inc. Ottawa, Canada). Genomic DNA extraction was performed following the manufacturer protocols.

Genotyping was performed using TaqMan® Real Time Polymerase Chain Reaction (PCR) allelic discrimination assays (Life Technologies, Saint-Aubin, France) using the Type-it Fast Probe PCR Master Mix (Qiagen, Courtaboeuf, France) and the Rotor-Gene Q PCR instrument (Qiagen). Assays were ordered from Life Technologies as validated assays (rs11568658 and rs2274407) or custom assays for rs2229109, rs1128503 rs2032582, rs1045642, rs2231137, rs12208357, rs35167514, rs2413775, rs10868138. The deletion in SLC22A1 gene (referred as rs202220802, rs34305973, rs35191146) was explored by direct sequencing on a 3130-XL instrument (Applied Biosystems, Life Technologies) as previously described [326].

IV.2.2.1.4. Statistical analysis

The following variables were analyzed: dose of VGCV (considered as low if all treatment doses were ≤ 450 mg per day), duration of VGCV treatment (in weeks, from VGCV introduction, up to 46 months), evolution of creatinine clearance (estimated using the Cockcroft-Gault formula), co-treatments associated with a particular risk of neutropenia (mycophenolate mofetil dose and cotrimoxazole intake: yes/no), CMV donor and recipient serologies. Statistical analysis of associations between genotypes, and the evolution of neutrophil counts from drug introduction, considered as baseline, up to 46 months was performed using generalized estimating equation (gee) multiple linear regression with an autoregressive correlation matrix. This method takes into account the correlation between the visits (including all visits with available data since treatment initiation) for a given subject [327] (R package geepack ; <http://www.r-project.org>). All available data over the follow-up concerning continuous variables (creatinine clearance, neutrophil count) were considered. In the exploratory group, variables with a $p \leq 0.10$ in the univariate analysis were included in the multivariate analysis and only factors with a Bonferroni-corrected p value of ≤ 0.05 were considered as significant in the final model (corrected $p = \alpha \times$ number of variables selected in the final model). In the replication group, a corrected p value ≤ 0.05 for an association discovered in the exploratory cohort (at the univariate or multivariate step) was the criteria for proceeding to study in the replication cohort. In both cohorts, the final model was selected by a backward stepwise strategy based on the likelihood ratio test. Corrected p -values ≤ 0.05 were considered as significant. β represents the effect of the covariate on the slope of neutrophil count for the treatment length.

IV.2.2.2 Cellular assays

Human Embryonic Kidney 293T/17 (HEK293T) cells (CRL-11268™, American Type Culture Collection, Manassas, VA) and Jurkat cells (TIB-152™, ATCC) were routinely cultured at 37°C with 5 % CO₂ and 95 % humidity in Dulbecco's modified Eagle's medium (Life technologies, Cergy-Pontoise, France) and RPMI 1640 medium (Life technologies), respectively. Media contained 10 % heat-inactivated fetal bovine serum, 100 U.mL⁻¹ penicillin, and 100 µg.mL⁻¹ streptomycin.



ABCC4-pcDNA5/FRT plasmid containing the reference sequence of the MRP4 gene was a generous gift from Prof. Deanna Kroetz, department of Biopharmaceutical Sciences and Pharmaceutical Chemistry, University of California, San Francisco (CA). A variant (rs11568658) construct was obtained by site-directed mutagenesis, using the Quick change II XL Site-Directed Mutagenesis Kit (Agilent Technologies®, Massy, France) and the following primers:

5'-ttagtaacatggccatgtggaagacaaccacaggc-3' (reverse)

5'-gcctgtggtgtctccacatggccatgttactaa-3' (forward)

Plasmid sequences were verified by sequencing.

Transient transfection of HEK293T cells was performed with 10 µg of pDNA (or empty vector) and transport activities were analyzed through measuring intra-cellular accumulation of GCV (10 mg.L⁻¹) after 30 minutes of incubation at 37 °C, as described previously [328].

Jurkat cells were chosen for inhibition experiments because they derive from blood cells and express MRP4, BCRP and the P-gp [329]. 500 µL of cells suspension (1×10⁶ cells/mL) was transferred into 1 mL microtubes. The cells were washed twice with 1 mL of Dulbecco's Phosphate-Buffered Saline (DPBS, Life technologies) and incubated at 37 °C during 30, 60 and 90 seconds with 500 µL of prewarmed DPBS containing GCV at 20 mg.L⁻¹ (corresponding to usual plasma peak concentration), with or without MK-571 (50 µmol.L⁻¹). The tubes were then transferred on ice and the cells were pelleted down (200 g; 1 minute at 4 °C), washed twice with 1 mL of DPBS, desiccated and lysed with 200 µL of 1 % pentadecafluorooctanoic acid. Cell lysates were stored at -20 °C until analysis.

Intracellular amounts of GCV were determined using a validated LC-MS/MS method [330] and results normalized to per-well protein content as measured using the bicinchoninic acid protein assay (BCA, Thermo Scientific, Rockford, IL).

IV.2.2.3 Methods of calculation

MD simulations were performed using a system constituted of 128 molecules of DOPC (1, 2-dioleoyl-sn-glycero-3-phosphocholine) arranged in a bilayer, which was surrounded by an explicit SPC/E (extended single point charge) water model (4511 molecules of water) and ions (18 Na⁺, 18 Cl⁻).

The topology was generated with the PRODRG program after B3LYP/6-31+G(d,p) optimization. The partial atomic charges were generated using the RESP method.

The lipid bilayer model relaxation and all MD simulation were conducted according to the methodology described previously [331]. We should note that the Gromos43a1-S3 force field was preferred over Berger for MD simulation, as the latter is known to overestimate lipophilicity of compounds [332].

To assess analysis, membrane surface was defined by the averaged location of P-atoms of phosphatidylcholine head groups; the z-axis is defined as being perpendicular to this surface. The distribution of GCV location in membrane was defined as the number density of center of mass, the aromatic ring, and the aliphatic moieties of GCV. Averaging was obtained from the last 300 ns of MD simulations (representative of equilibrium location). The α-angle between the z-axis and the C=O vector was also monitored over the last 300 ns of the simulations was monitored over the simulation to describe the GCV orientation. To calculate the free-energy profile of GCV membrane penetration and crossing, TurBOMOLE in the



Tmolex package and COSMOmic from the COSMOthermX package were used. Twenty different conformations of GCV obtained using CONFAB were optimized using DFT/cosmo with TURBOMOLE at the functional b-p and basis set TZVP. Then, the free energy profiles for all geometries were calculated at 310 K using the COSMOmic software. In this implicit methodology, the DOPC bilayer was separated into 50 slices. About 162 orientations of GCV were used in DOPC membrane to estimate their free energy profiles. The final free energy profiles of all conformations were averaged over the individual free energy profile, which allowed evaluating partition coefficients.

IV.2.3. Results

IV.2.3.1 Association of membrane transporter polymorphisms with GCV neutrophil toxicity

Genotype distributions and allele frequencies in the exploratory group are shown in Table 9. As previously described, *ABCB1* SNPs were in strong linkage disequilibrium (D' rs1128503 - rs2229109 = 0.996; D' rs1128503 - rs1045642 = 0.726; D' rs2229109 - rs1045642 = 0.786) [333].

The factors associated with neutrophil count decrease in the exploratory group are reported in Table 10. The dose of VGCV (>450 mg/d) was found to be significant in univariate, but not multivariate analysis. Among the 22 tested covariates, 7 SNPs were included in the multivariate model. Two of them exhibited a significant association with neutrophil count, namely rs2229109 in *ABCB1* and rs11568658 in *ABCC4*. These 2 SNPs and the VGCV dose were next investigated in the replication cohort. No significant association between the dose or *ABCB1* rs2229109 and the evolution of neutrophil counts was found but *ABCC4* rs11568658 was significantly related to neutrophil count after multivariate analysis.

Gene	Variant	Genotype (n)			Minor allele frequency
		wt/wt	wt/vt	vt/vt	
<i>SLC29A1</i>	rs747199	129/206	68/206	9/206	21 %
<i>SLC28A3</i>	rs10868138	168/206	37/206	1/206	9 %
<i>SLC28A2</i>	rs2413775	101/203	79/203	23/203	31 %
<i>SLC22A1</i>	rs12208357	144/205	51/205	10/205	17 %
	rs34059508	198/206	8/206	0/206	2.0 %
	420 DEL	133/199	62/199	4/199	18 %
	rs628031	87/199	94/199	18/199	33 %
<i>ABCG2</i>	rs2231137	170/206	35/206	1/206	9.0 %
<i>ABCC4</i>	rs2274407	176/206	30/206	0/206	7.0 %
	rs3742106	70/186	89/186	27/186	38 %
	rs11568658	197/205	8/205	0/205	2.0 %
<i>ABCB1</i>	rs1045642	63/206	103/206	40/206	44 %
	rs2032582	77/206	92/206	37/206	40 %
	rs1128503	70/206	96/206	40/206	43 %
	rs2229109	188/205	17/205	0/205	4.0 %

wt : wild type; vt : variant

Table 9: Variant genotype distributions and allele frequencies in the exploratory group.



Covariates	Genotype	Univariate analysis			Multivariate analysis		
		β	S.D	p value	β	S.D	p value
Dose > 450mg/d	-	-0.4366	0.044	0.049			
Treatment length (weeks)	-	0.00147	0.0021	0.480			
Mycophenolate mofetil dose (mg)	-	-0.3989	0.3452	0.250			
Cotrimoxazole intake (Yes/No)	-	-0.1494	0.1842	0.420			
CMV R+	-	-0.0305	0.1892	0.870			
CMV D+	-	-0.026	0.1856	0.890			
<i>ABCB1</i> -rs2229109	G/A vs G/G	0.6924	0.2714	0.011	0.8801	0.2531	0.00051
<i>ABCB1</i> -rs1128503	G/A vs A/A	-0.2197	0.02221	0.320			
<i>ABCB1</i> -rs1128503	G/G vs A/A	-0.2292	0.2322	0.320			
<i>ABCB1</i> -rs2032582	G/T vs G/G	0.1073	0.1865	0.570			
<i>ABCB1</i> -rs2032582	T/T vs G/G	-0.1846	0.2353	0.598			
<i>ABCB1</i> -rs1045642	T/C vs C/C	0.2766	0.1966	0.160			
<i>ABCB1</i> -rs1045642	T/T vs C/C	0.3721	0.2422	0.120			
<i>ABCC4</i> -rs11568658	G/T vs G/G	-0.638	0.322	0.048	-0.6854	0.2804	0.0145
<i>ABCC4</i> -rs3742106	A/C vs A/A	0.1044	0.1858	0.570			
<i>ABCC4</i> -rs3742106	C/C vs A/A	0.3575	0.336	0.280			
<i>ABCC4</i> -rs2274407	G/T vs G/G	-0.1603	0.162	0.32			
<i>ABCG2</i> -rs2231137	A/G vs A/A	-1.236	0.208	2.80.10 ⁻⁰⁹	-1.2393	0.2123	5.3.10 ⁻⁹
<i>ABCG2</i> -rs2231137	G/G vs A/A	-1.3669	0.0853	< 2.10 ⁻¹⁶	-1.3732	0.0981	< 2.10 ⁻¹⁶
<i>SLC22A1</i> -rs34059508	G/A vs G/G	-1.1352	0.6133	0.064			
<i>SLC22A1</i> -rs12208357	C/T vs C/C	-0.1404	0.1634	0.390			
<i>SLC22A1</i> -rs12208357	T/T vs C/C	-0.1669	0.2272	0.460			
<i>SLC22A1</i> -420deletion	-	0.3287	0.179	0.066			
<i>SLC22A1</i> -rs628031	G/A vs A/A	0.1337	0.265	0.610			
<i>SLC22A1</i> -rs628031	G/G vs A/A	0.0204	0.2624	0.440			
<i>SLC28A2</i> -rs2413775	A/T vs A/A	0.0217	0.1806	0.900			
<i>SLC28A2</i> -rs2413775	T/T vs A/A	0.2063	0.3313	0.530			
<i>SLC28A3</i> -rs10868138	G/A vs A/A	-0.0557	0.2223	0.800	-0.1156	0.2079	0.58
<i>SLC28A3</i> -rs10868138	G/G vs A/A	-1.8346	0.1623	<2.10 ⁻¹⁶	-2.594	0.2861	< 2.10 ⁻¹⁶
<i>SLC29A1</i> -rs747199	C/G vs C/C	0.3878	0.2528	0.130			
<i>SLC29A1</i> -rs747199	G/G vs C/C	0.3101	0.2301	0.180			

Table 10: Association of clinical and genetic covariates with neutrophil count evolution in the exploratory group.

IV.2.3.2 Transport of GCV in Jurkat and MRP4-expressing cells

The accumulation GCV (20 mg.L⁻¹) in Jurkat cells was significantly enhanced in the presence of MK-571 (Tebu-bio[®], Le Perray-en-Yvelines, France), a selective inhibitor of MRP-transporters [334] (+22.7 % after 90 seconds incubation; Figure 30A).

In order to investigate the specific role of MRP4 in GCV efflux and the consequence of the rs11568658 variant, GCV (10 mg.L⁻¹) was incubated with HEK293T cells transfected with *ABCC4* reference and variant (rs11568658) sequences. After 30 minutes of incubation, GCV concentration was significantly higher in cells expressing MRP4 variant than in those expressing the MRP4 of reference (+290%, p<0.0001, Figure 30B). The accumulation of GCV in MRP4 variant transfected cells was similar to that observed in cells transfected with an empty vector (p=0.18) thus demonstrating a complete loss of transport activity.



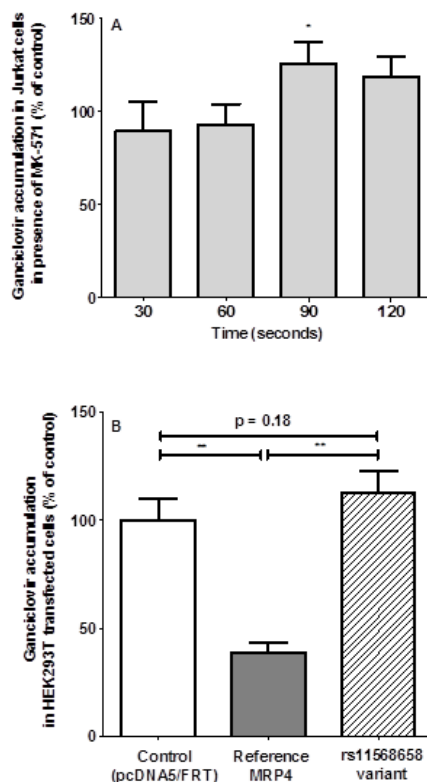


Figure 30: Ganciclovir intracellular accumulation into (A) Jurkat cells in presence of 50 $\mu\text{mol.L}^{-1}$ of the MRP inhibitor MK-571 and (B) HEK293T cells transiently transfected with *ABCC4* (MRP4) reference and variant (rs15868658) sequences or with an empty vector (pcDNA5/FRT). Data are expressed as mean values \pm SD of three independent experiments, each performed in duplicate (A) or at least triplicate (B). * $p < 0.001$ or ** $p < 1.10^{-4}$ on comparison with control conditions.

IV.2.3.3 Mechanisms of the insertion of GCV and metabolites in lipid bilayers

MD simulations have repeatedly succeeded in the evaluation of partition coefficients and the location of a number of xenobiotics in pure lipid bilayer membranes. This technique provides an accurate molecular picture of drug insertion and preferred location, independently of the presence of any transport protein. Three independent free MD simulations systematically show rather fast GCV insertion in lipid bilayers (within less than 100 ns). Thanks to intermolecular (Coulomb and H-bonding) interactions between GCV and the highly polar surface, the drug is preferentially located at 1.5 ± 0.3 nm from the center of the membrane that is just beneath the polar head group region (Figure 29B). The drug is roughly parallel to the bilayer surface but with many fluctuations. COSMOmic calculation allowed evaluating a 98%:2% ratio, i.e. partitioning mainly in the lipid bilayer. Drug accumulation is likely because of the formation of noncovalent n-mer aggregates, which are transiently stabilized by π -stacking interactions between aromatic rings, with interatomic distance of ca. 3.9 Å, typical of DNA nucleobase stacking. The standard deviation, highlighting fluctuation, is slightly higher pointing out that in such aggregates some compounds are somehow pushed deeper into the bilayer, whereas other remain stuck to the membrane surface (Figure 29C).

As expected, GCV-mono, di and triphosphate metabolites are located in the outer part of lipid bilayer, close to the head polar region at $d=2.4\pm 0.3$ nm from membrane center (Figure 29D). This is attributed to the negative charge, which anchor the metabolites to the (positively



charged) choline moieties and prevents deeper insertion of the metabolites in between lipid chains.

IV.2.4. Discussion

Hematological toxicity is a major concern during VGCV therapy. It can cause marrow toxicity, notably neutropenia which could consequently expose immunosuppressed patients to life-threatening infections. Identifying the risk factors for neutropenia in patients treated with GCV or VGCV is expected to lower the incidence of toxicity and would help to design alternative strategies in high-risk patients. In this study, twelve patients in the exploratory study (7%) and six in the confirmation study (6%) experienced at least one episode of neutropenia defined as an absolute neutrophil count $< 1.10^6$ cells/mL, which is in the lower range of the incidence reported in previous reports regarding solid organ transplantation (7–68%) [335–337]. Only 5 patients received colony-stimulating factors in the replication study population, while no such treatment was reported in the exploratory study. We chose to study the evolution of the neutrophil count rather than neutropenia incidence to evaluate VGCV toxicity because of the low incidence of acute neutropenia and the absence of any international consensus defining a neutrophil concentration threshold value reflecting neutropenia in renal transplant patients. Thrombocytopenia ($< 150.10^6$ /mL) is another important hematologic adverse event whose incidence is similar to that of neutropenia [335,337,338]. Since it is considered to be a less relevant issue than neutropenia in renal transplant patients, it has not been consistently reported in patient clinical files in the exploratory study and it has not been taken into consideration in this study.

Renal function state is a major feature in GCV pharmacokinetics, thought to be important for its toxicity. VGCV dose is thus generally adapted according to the creatinine clearance estimation using the Cockcroft-Gault formula [339].

Until now, no clear relationships have been established between drug dose and neutrophil toxicity. Some studies have suggested that high VGCV doses lead to a high risk of neutropenia but no formal toxic threshold has been proposed [321,335]. Other studies showed no or only poor relationships between the occurrence of adverse events and GCV exposure, or trough concentration [319,340]. In the exploratory study, an association was found between the use of high VGCV dose (>450 mg/day) and a decrease in neutrophil count in univariate but not in multivariate analysis. This association was not found either in the replication group ($p=0.45$). This result suggests that doses had been adapted according to renal function, as recommended, and presumably explains the low occurrence of neutropenia in these patients.

On the other hand, treatments with mycophenolate mofetil or cotrimoxazole are known to increase the risk of neutropenia. They were not associated with neutrophil evolution in the exploratory group. There is, however, a limitation because potential changes in the dose of VGCV or of the co-treatments were not systematically reported in the first cohort.

Our hypothesis is that active transport processes of GCV could substantially limit the toxicity by decreasing GCV intracellular accumulation in blood cells. Among the numerous techniques used to probe drug-membrane interactions, MD simulations are carried out more and more successfully. When using proper models and methodologies, the behavior of drug-membrane systems can be accurately evaluated. Regarding GCV, MD simulations suggest that the drug is likely to accumulate in lipid bilayers. This concurs with the rather high polarity of GCV ($\log P = -1.65$), but also with its amphiphilic character. Accumulation in both



bilayer leaflets may constitute a reservoir of drug prior to delivery inside cells through passive diffusion, which does not preclude GCV transport by CNTs/ENTs. Also, in this accumulating region, close to the membrane surface, GCV appears particularly well located in order to be actively flushed out by ABC transporters. After phosphorylation, the metabolites penetration back to the lipid bilayers is prevented and the metabolites either act or accumulate in cells.

To perform a relevant pharmacogenetic study, we selected genes that may be involved in GCV transport (efflux or influx) in blood cells. As GCV is an analogue of puric bases, transporters expressed in neutrophils capable of carrying puric bases were retained. Our hypothesis was that individual or combinations of polymorphisms in these genes could influence GCV intracellular accumulation and thus the likelihood of neutrophil toxicity, independently of VGCV dose and other confounding factors (e.g. cotreatments, creatinine clearance ...). We thus performed a stepwise multivariate procedure which allowed us to investigate the additional value of a given gene polymorphism by adjusting the model on other polymorphisms or non-genetic factors. Although a stepwise procedure decreases the number of tests performed as compared to univariate testing of each variable on the phenotype, it still leads to multiple testing. Consequently, we applied a Bonferroni correction on final multivariate models. This cannot totally exclude that false positive findings occurred here but the replication in an independent dataset of patients is a strong argument against chance findings. Moreover, genetic polymorphisms in these transporters were selected only if clear evidences for clinical or *in vitro* functional effects had been reported in the literature, and if their MAF was above 2.5% in Caucasians (to ensure sufficient statistical power). Other polymorphisms were excluded which has to be considered as a limit of the study although it ensures consistency.

Regarding efflux transporters, *ABCC4* rs11568658 genotype appeared to be related to the decrease in neutrophil count in the exploratory cohort. Although this variant has a low frequency (approx. 2%), the effect size was important which makes the statistical power of the replication study adequate (power of 0.922; R 'pwr' package). A similar effect was found in this replication study and experiments with transfected HEK293T cells confirmed that this variant decreases MRP4-mediated efflux of GCV. This result concords with a previous study carried out on two other substrates, namely 3'-azido-2',3'-dideoxythymidine (AZT) and 9-(2-phosphonylmethoxyethyl)adenine (PMEA) [341]. MRP4 is expressed in blood cells; it mediates the efflux of a number of antiviral drugs and endogenous compounds from cells [342,343]. It has been previously described that GCV is a substrate of MRP4. Adachi et al. indeed showed *in vitro* using MCF-7 cells that overexpression of MRP4 decreases the intracellular accumulation of GCV and confers resistance to the cytotoxic effects of the drug. In addition, they showed that the efflux of intracellular GCV was faster in MRP4-transfected cells than in the vector cells (half-lives of 16 and 32 min, respectively) [344].

This SNP leads to an amino acid substitution (p.Gly¹⁸⁷Trp) in the transmembrane domain of MRP4. Two other variants in *ABCC4* were studied: rs3742106 and rs2274407. The rs3742106 is located in the 3' UTR region and it has previously been associated with an elevation of lamivudine-triphosphate concentrations (approx. + 20%) in variant carriers [345]. This variant was however not found to be related to increased concentrations of tenofovir diphosphate in human peripheral blood mononuclear cells 24h post-dose [346]. The latter variant, rs2274407 (p.Lys⁴⁰³Asn), located in exon 8, was found to be associated with higher incidence of high-grade thrombocytopenia in methotrexate-treated patients [347]. Gradhand et al. found that this variant allele was associated with a reduction in MRP4 liver expression



(-46%) [348]; this was however not confirmed by Ansari et al. [347]. None of these two still controversial SNPs were related to a decrease in neutrophil count in the present study.

Regarding *ABCB1* (the gene coding the P-gp), rs2229109 SNP (leading to the Ser⁴⁰⁰Asn substitution) had contradictory impacts on neutrophil evolution in the exploratory and replication cohorts.

This SNP was found to enhance the trans-epithelial permeability of vinblastine and vincristine, by increasing the cellular efflux of these drugs [349]. More recently, a comprehensive *in vitro* study demonstrated that the SNP effect is substrate-dependent [350]. The authors confirmed that the variant protein (rs229109-A allele) transports vinblastine more efficiently than the wild-type protein. They showed conversely that the variant has a drastically reduced ability to transport tacrolimus, while it transports cyclosporine, rhodamine 123 and doxorubicin in a similar extent to the wild-type protein [350]. Here we found in the exploratory cohort that the variant had a protective effect on neutrophil toxicity ($\beta=0.88\pm0.25$ $p=0.00102$), which might suggest a more efficient efflux of GCV. This finding is consistent with the literature suggesting that the variant could contribute to the resistance to several chemotherapeutic agents (presumably through increased transport activity) [351–353]. Conversely, in the replication cohort, the carriers of this variant showed a trend toward a more pronounced decrease of neutrophil count ($\beta=-0.82\pm0.39$ $p=0.068$) suggesting increased intracellular accumulation of GCV. We have no explanation for these opposite results. Since the effect of the SNP can differ depending on the substrate, the expected effect regarding GCV cannot be predicted. Among all the other SNPs or haplotypes in *ABCB1*, none was associated with a significant variation in neutrophils toxicity which suggests that the P-gp polymorphism is unlikely to contribute substantially to VGCV toxicity.

IV.2.5. Conclusion

This study provides direct evidence that GCV is a substrate of the efflux transporter MRP4 and suggests that the intracellular fate of GCV is significantly influenced by *ABCC4* rs11568658 variant in renal transplant recipients receiving GCV. This variant may accentuate the risk of severe neutrophil decrease. MRP4 has many other substrates; one can suggest that drug interactions could occur and result in decreased efflux of GCV.



IV.3. Interaction of wine anthocyanin derivatives with lipid bilayer membranes

Authors:

Tahani Ossman^a, Gabin Fabre^{b, c}, Patrick Trouillas^{a, c},

^a UMR 850 INSERM, Univ. Limoges, Faculté de Pharmacie, 2 rue du Docteur Marcland, 87025 Limoges, France

^b LCSN – EA1069, Faculté de Pharmacie, Université de Limoges, 2 rue du Dr. Marcland, 87025 Limoges, France

^c Regional Center of Advanced Technologies and Materials, Department of Physical Chemistry, Faculty of Science, Palacký University, 17. listopadu 1192/12, 77146 Olomouc, Czech Republic

Reference:

T. Ossman et al., *Comput. Theor. Chem.* 1077 (2016) 80–86. doi:10.1016/j.comptc.2015.10.034 [314].

IV.3.1. Introduction

The antioxidant properties related to wine are mainly attributed to the presence of polyphenols, particularly flavonoid derivatives. Anthocyanins are a subclass of flavonoid largely distributed in red wine. They are known to participate in red, purple, and blue colors of grapes and wine [354], but also various berries, other fruits, vegetables and flowers.

The general chemical structure of anthocyanins is formed of three cyclic carbon rings C6-C3-C6 denoted as A, B and C (Figure 31). The structure is usually written as a flavylium cation, which bears a positive charge. Most of anthocyanins occur in nature as glycosides, mainly 3-*O*-glucosides. The structural diversity of anthocyanins stems from the number and position of hydroxyl and methoxy groups in the aglycone, as well as from the nature, size and position of the sugar moiety. Stability, reactivity and chemical activity of anthocyanins depend on all the aforementioned structural parameters [355].

Anthocyanins are very sensitive to pH, providing various chemical forms and colors in aqueous solution depending on pH values. The (red) flavylium cation (AH^+ , Figure 31) predominates at pH values ranging from 1 to 3. When the pH value increases deprotonation from C7, C4' and C5 occurs successively to form three (purple) quinonoidal basic forms (A_7 , $A_{4'}$, and A_5 , respectively, Figure 31). Increasing again the pH values above 7 allows a second deprotonation yielding (blue) quinonoidal anions (e.g., $A_{4',7}^-$, Figure 31) [356,357]. Alternatively, above pH values of 2-3, hydration reactions produce (colorless) hemiketals, which tautomerises through ring opening into (yellow-ish) chalcones (Figure 31). Anthocyanins also react with other phenolic compounds to produce various derivatives, for example pyranoanthocyanins that are produced during wine aging.

In vivo, anthocyanins are extensively degraded. They can be deglycosylated and transformed into phenolic acids, aldehydes and other phenolic derivatives [358]. In plants and beverages such as wine, they can combine with other phenolic compounds to form pyranoanthocyanins [359,360]. Although anthocyanins are usually unstable as isolated compounds in solution, they can be partially stabilized by intra and intermolecular noncovalent interactions either with cofactors such as other phenolic compounds (co-pigmentation) or with themselves (self-association). These interactions are favored by the



capacity of polyphenols to interact by π - π stacking and van der Waals interactions [355,361,362].

Anthocyanins have been extensively studied *in vitro* and *in vivo* for their biological and pharmacological activities such as antioxidant activities [363–367] possibly related to their role in the prevention of cardiovascular disease [368,369]; anti-inflammatory; anti-tumor [370]; anti-diabetic [371]; and their capacity to control oxidative stress during pregnancies [372]. Here, we focused on the antioxidant activities of certain wine anthocyanin derivatives. As antioxidants and scavengers of reactive oxygen species (ROS), phenolic compounds are efficient electron and hydrogen atom donor from their OH groups towards free radicals [373,374]. This capacity is largely attributed to their capacity to delocalize spin in the rather extended π -conjugated system. As antioxidants, they have also been shown to inhibit lipid peroxidation in biological membranes [363,367,375,376]. It should be noted that several polyphenols having structures similar to anthocyanins exhibited the capacity to partition into the lipophilic core of membrane, even affecting membrane fluidity [377,378]. However, there is a lack of information about the molecular mechanisms of this inhibition; mainly because the incorporation of anthocyanins in lipid bilayers and their capacity to cross cell membrane is not fully elucidated at the molecular level. This work presents a theoretical evaluation of interactions between anthocyanins derivatives and lipid bilayer membranes. A series of representative wine anthocyanin derivatives have been selected for this study, based on the malvidin structure, the major anthocyanin structure found in wine. To cover a wide range of physical-chemical properties, molecular dynamics (MD) simulation were carried out for (i) the different charge forms of malvidin-3-*O*-glucoside (AH^+ , A_7 , A_4^+ , A_5 and $A_{4,7}^-$); the aglycone form, malvidin; and the corresponding chalcone, hemiketal and pyranoanthocyanin.



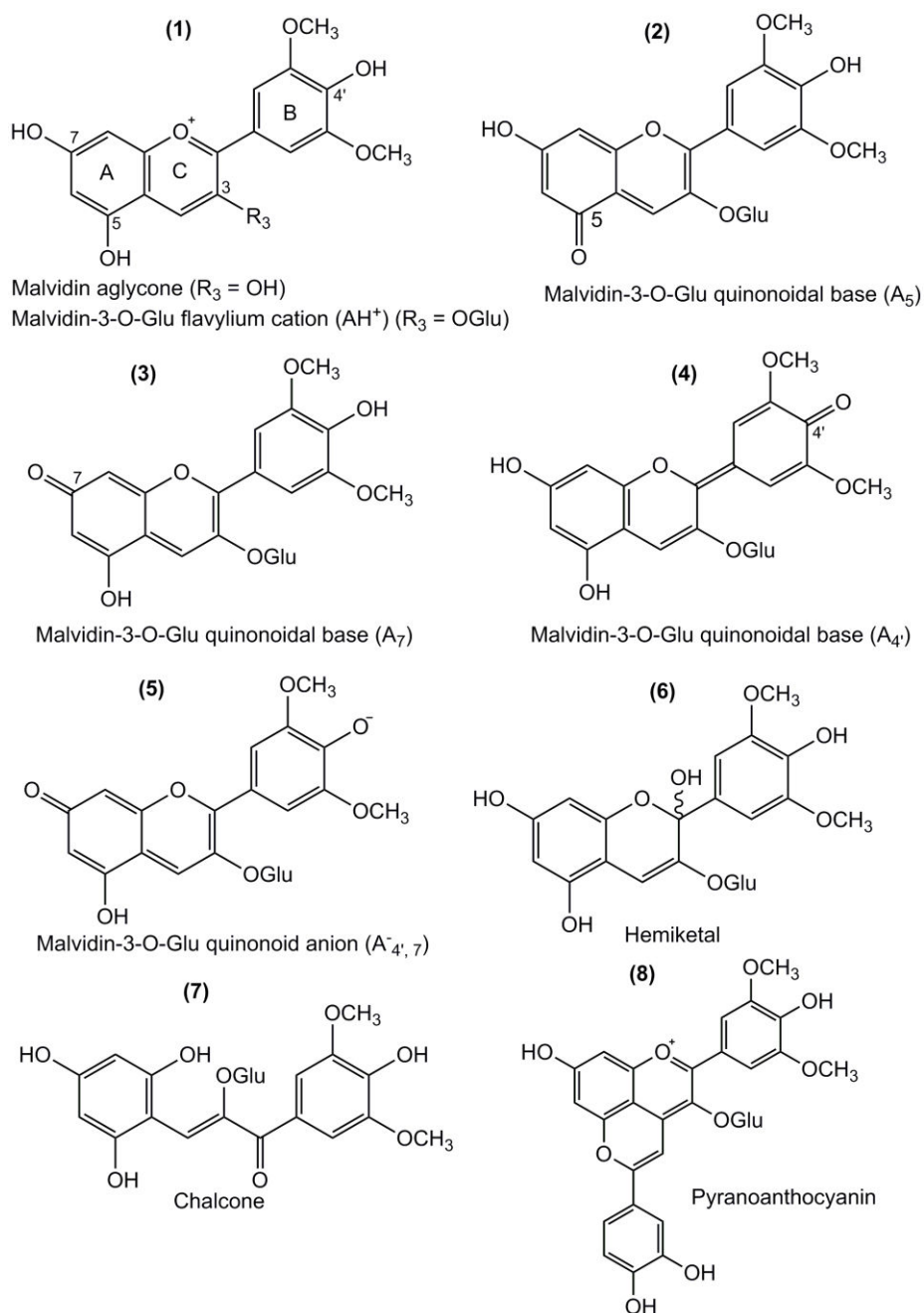


Figure 31: Chemical structures of a series of anthocyanin derivatives, based on the malvidin moiety.

IV.3.2. Material and methods

IV.3.2.1 Free MD simulations

MD simulations were carried out using a bilayer constituted of 128 molecules of DOPC (1,2-dioleoyl-*sn*-glycero-3-phosphocholine). An explicit SPC (single point charge) water model was used to model the water molecules surrounding the membrane. Ions (Na^+ and Cl^-) were added at physiological ionic concentration (0.9%). An 8 nm thick box was used with periodic boundary conditions in all dimensions. The z-axis was defined as the vector normal to membrane surface. The lipid model was minimized without flavonoid presence during 100 ns. All MD simulations were performed with the GROMACS package version 5.0.4 [379].



Conformations were optimized using density functional theory (DFT) at the B3LYP/6-31+G(d,p) level. The topology was built using the online server PRODRG [380]. Partial atomic charges of molecules play a crucial role to estimate their physical and chemical properties, and PRODRG was shown to underestimate the absolute values of partial charges [381]. Thus in this work, partial atomic charges of all compounds were refined with quantum mechanics calculations using Gaussian09 [382], RESP and R.E.D. III softwares [383]. Two different models were used, differing on the level of theory. The method reported by Duan et al. (B3LYP/cc-pVDZ in an implicit PCM type solvation with $\epsilon = 4$, [384]) was used for all compounds. To compare the influence of charge method on the interaction of anthocyanins with membranes, Cornell et al. method (HF/6-31G(d) in gas phase, [385]) was also used for AH^+ , $A_{4,7}^-$ and A_4 . Unless stated, the analyses are given for the Duan et al. charge method. Partial charges were averaged over several conformers generated using confab, which applies a torsion driving approach to systematically explore the conformation space and to create several low-energy conformers (a series of local minima) [386]. Dipole moments were obtained from calculations with Gaussian software [382] of ESP charges with methods corresponding either to Duan et al. or Cornell et al. charge models, averaged over different conformers.

The anthocyanin derivatives were initially placed in the water phase surrounding the membrane. For each compound, a MD simulation was performed using multiple non-interacting molecules in order to enhance sampling. MD simulations were 400 ns long. They were carried out using Gromos43A1-s3 force field [387] and the NPT ensemble. Temperature was regulated at 310 K by the Nose–Hoover thermostat [70] and pressure was kept constant semi-isotropically (x - y and z axis independently) at 1 atm by the Parrinello–Rahman barostat [72] with coupling constants of 0.5 ps and 5.0 ps, respectively. Cut-off for short-range van der Waals and Coulomb interactions was set to 1.4 nm. Particle Mesh Ewald [388] was used for long-range non-bonding interactions. VMD [389] was used to visualize trajectories and to produce Figures. Analyses of position and orientation were performed on the last 150 ns of MD simulations, after the anthocyanins reached their equilibrium positions.

The global orientation of molecules was assessed by the angle α defined between the z -axis and the longest molecular axis of the flavonoid (aglycone) moiety, namely vector \vec{V} . Because this moiety is somewhat planar, \vec{V} partially documents on the orientation of the π -system. This vector is defined by the hydrogen atom at carbon C6 and oxygen atom at carbon C4' in the A and B-rings, respectively (Figure 32). When α equals 0° or 180° , the global orientation of molecules is perpendicular to membrane surface, that is the π -system is perpendicular to the surface; when α equals 90° , the molecule lies parallel to membrane surface. Averaging was obtained from the time when the representative equilibrium location was reached to the end of the simulation.

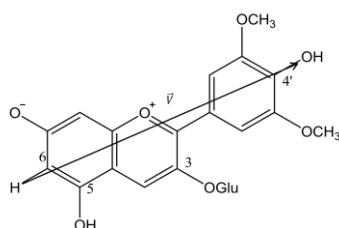


Figure 32: Definition of the vector \vec{V} used to determine the orientation of flavonoid moiety in membranes.



IV.3.2.2 Free energy profiles

COSMOmic [83,390] was used to calculate the free energy profile of membrane penetration and crossing. Different conformations of each anthocyanin compounds were also generated using confab [386]. COSMOmic is based on the evaluation of σ -profiles, which is defined as the distributions of charge density on the molecular surface. σ -Profiles were obtained for all conformers, DOPC and water molecules using DFT/COSMO with TURBOMOLE at the default and recommended functional in TURBOMOLE (i.e., B-P86) [391] and TZVP basis set. Then, free energy profiles for all geometries were calculated at 310 K using the COSMOmic software. In this implicit methodology, the DOPC bilayer was separated into 50 slices. About 162 orientations of each compound were used in DOPC membrane to estimate their free energy profiles; the final free energy profiles were the average of all individual profiles.

IV.3.3. Results and discussions

IV.3.3.1 Positioning of malvidin-3-O-glucoside in lipid bilayer: neutral vs charged forms

The center of mass (COM) of three neutral quinonoidal forms of malvidin-3-O-glucoside (A_7 , A_4 or A_5) was located at 1.6 ± 0.2 , 2.3 ± 0.2 or 1.2 ± 0.3 nm distances from membrane center, respectively (Table 11). Equilibrium positions A_5 and A_7 were located below the polar head groups of lipids, in interaction with lipid tails. A_5 penetrated deeper in the hydrophobic core of lipids than A_7 . It should be noted that these two forms showed a greater affinity to the lipid chains than any other charged forms. Conversely, the A_4 form remained in the water phase (Figure 33). The locations of free energy minima calculated by COSMOmic were similar to those obtained with MD simulations (Table 11). These results show the significant effect of deprotonation sites on the position of quinonoidal basic forms in membrane. The predominant form A_7 is ideally located in the lipid bilayer to inhibit both the initiation and propagation steps of lipid peroxidation, partially explaining the good antioxidant activity of malvidin-3-O-glucoside in membranes.

Interestingly the charged forms of malvidin-3-O-glucoside penetrated the lipid bilayer. The COM of the flavylum cation AH^+ was located at 1.8 ± 0.2 nm from membrane center (Table 11). This equilibrium location was supported by the minimum of the free energy profile, located at 1.6 nm from membrane center (Figure 34). This suggests that AH^+ is stabilized close to the polar head groups due to its positive charge that favors electrostatic interactions with the phosphate groups of the phospholipids. Additionally, H-bonding, electrostatic and van der interactions between the sugar moiety and polar head groups anchor AH^+ . By contrast, the double-deprotonated anionic form $A_{4,7}^-$ is located outside the membrane, but still in contact with the head group region at the interface with water, namely COM at 2.5 ± 0.2 nm from membrane center (Table 11). This equilibrated location is driven by the negative charge, which favors Coulomb and H-bond interactions with phospholipid choline moieties.



	ΔG_{part} (kcal mol ⁻¹) ^a	ΔG_{pen} (kcal mol ⁻¹) ^a	d_{COSMOmic} (nm) ^a	d_{MD} COM (nm) ^b	d_{MD} Sugar group (nm)	d_{MD} B-ring (nm)	d_{MD} O- (nm)	μ (Debye)	α (°)
(A ⁻ _{4,7})	-7.5 ± 0.5	32.7 ± 0.5	2.3	2.5 ± 0.2 ^c 2.3 ± 0.2 ^d	2.5 ± 0.2 ^c 2.5 ± 0.2 ^d	2.5 ± 0.2 ^c 2.1 ± 0.3 ^d	-	16.4 ^c 18.1 ^d	78 ± 18
AH ⁺	-12.7 ± 1	16.1 ± 1.5	1.6	1.8 ± 0.2 ^c 1.8 ± 0.4 ^d	2.1 ± 0.2 ^c 2.2 ± 0.3 ^d	1.6 ± 0.2 ^c 1.7 ± 0.3 ^d	-	29.2 ^c 28.9 ^d	90 ± 14 ^c 87 ± 16 ^d
A ₄	-7.3 ± 0.2	20.0 ± 0.5	2.1	2.3 ± 0.2 ^c 1.8 ± 0.2 ^d	2.3 ± 0.2 ^c 2.0 ± 0.4 ^d	2.5 ± 0.2 ^c 1.8 ± 0.2 ^d	2.6 ± 0.2	13.3 ^c 9.6 ^d	40 ± 30 ^c 88 ± 17 ^d
A ₅	-6.1 ± 1	15.5 ± 1	1.7	1.2 ± 0.3	1.4 ± 0.3	0.9 ± 0.3	1.6 ± 0.2	10.4	150 ± 13
A ₇	-7.9 ± 0.2	16.2 ± 1	1.8	1.6 ± 0.2	1.6 ± 0.2	1.3 ± 0.2	2.0 ± 0.3	7.9	162 ± 15
Aglycone	-2.1 ± 0.4	3.4 ± 0.5	2.0	1.2 ± 0.1	-	0.9 ± 0.2	-	12.6	153 ± 12
Pyranocyanin	-9.3 ± 0.5	19.9 ± 2	2.0	1.8 ± 0.2	1.7 ± 0.1	1.3 ± 0.2	-	7.6	128 ± 13
Hemiketal	-7.4 ± 0.2	15.8 ± 1	1.7	1.5 ± 0.3	1.7 ± 0.3	1.2 ± 0.3	-	6.1	No preferred orientation
Chalcone	-7.1 ± 0.3	12.3 ± 2	2.0	1.6 ± 0.2	1.7 ± 0.6	1.3 ± 0.5	-	8.5	99 ± 35

^a Standard error

^b Standard deviation

^c using Duan et al. charge method

^d using Cornell et al. charge method

Table 11: Location, orientation, free energy barriers and dipole moments of malvidin derivatives studied. d is the average distance from the membrane center for COM or characteristic groups (B-ring and sugar), obtained either via MD simulations (d_{MD}) or COSMOmic (d_{COSMOmic}).



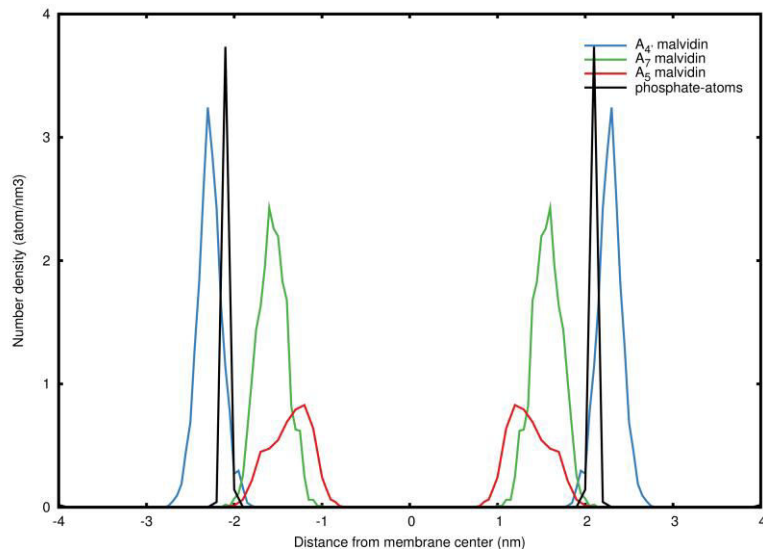


Figure 33: Location of the quinonoidal forms of malvidin-3-*O*-glucoside (A_4 , A_7 , and A_5) in the lipid bilayer membrane.

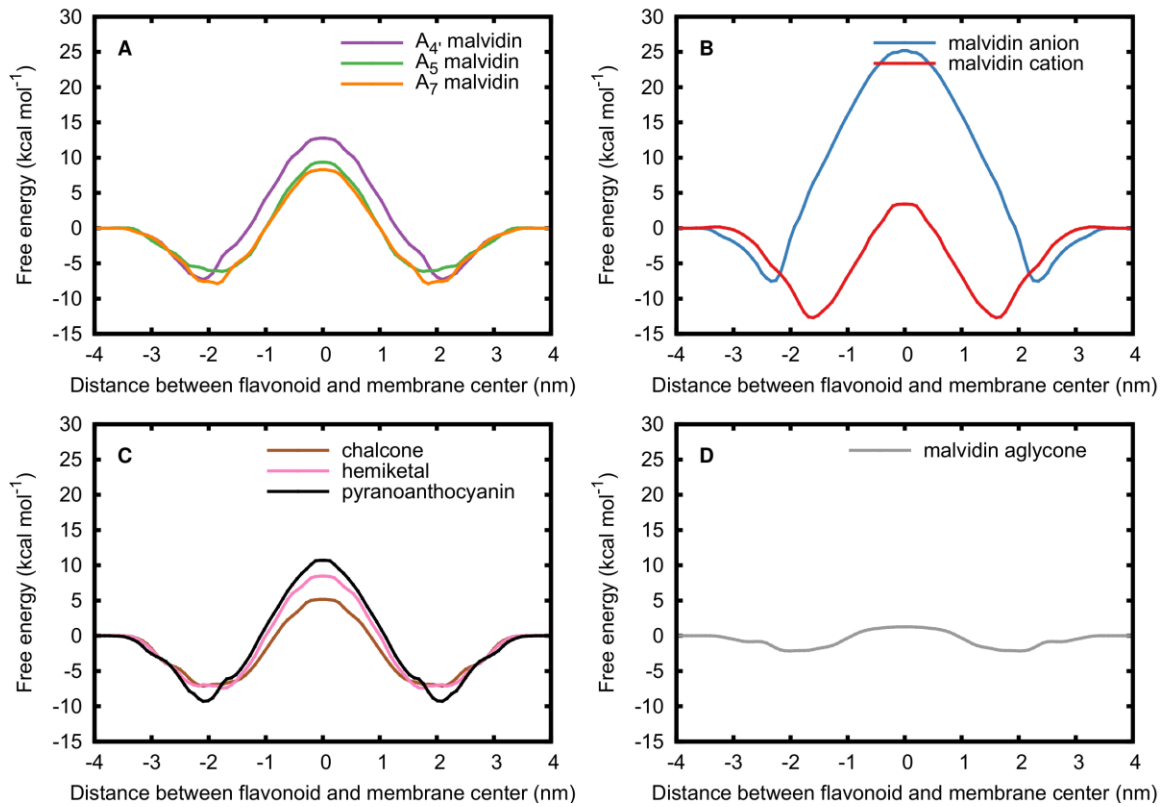


Figure 34: Free energy profiles of penetration in the lipid bilayer for (A) malvidin-3-*O*-glucoside deprotonated forms A_4 , A_7 , and A_5 ; (B) malvidin-3-*O*-glucoside anionic ($A_{4,7}^-$) and cationic (AH^+) forms; (C) chalcone, hemiketal and pyranoanthocyanin forms; and (D) malvidin aglycone.



The orientation of malvidin-3-*O*-glucoside was evaluated by two parameters. First, the position of B-ring (see Figure 31) was compared to the one of the COM. B-rings of A₅ and A₇ were 3 Å deeper in the membrane than the corresponding COM, confirming the rather hydrophobic character of B-ring as substituted by methoxy groups. Second, the orientation of the aglycone moiety in the membrane was evaluated by the angle α as defined in section IV.3.2 (Figure 32 and Table 11). The α angle values were $150^\circ \pm 13^\circ$ and $162^\circ \pm 15^\circ$ for A₅ and A₇, respectively. This indicated that the aglycone moiety was almost perpendicular to the surface. Significant differences in orientation were observed when the B-ring is deprotonated at C4'-OH, namely A_{4'} and A_{4',7}⁻. In this case, the B-ring is polar and appeared to be located at the same z-distance to membrane center as the COM, confirming that the molecule is roughly parallel to membrane surface (Table 11). This correlated with α angle values, indicating a near parallel orientation of the aglycone moiety of A_{4'} with respect to membrane surface (Table 11). These results reflect i) the relative hydrophobic character of B-ring, thus enhancing penetration into the lipophilic core of membrane; and ii) the significant effect of deprotonation site on the penetration.

Free energy profiles were also evaluated for all malvidin-3-*O*-glucoside forms to tackle the capacity of membrane crossing. As said above the equilibrium positions predicted by COMOmic were roughly similar to those predicted by free MD simulations, except a slight shift of 0.2 nm towards the surface with COSMOmic. The free energy profiles enabled calculation of free energy barriers of partition (ΔG_{part}) and penetration (ΔG_{pen}). ΔG_{part} is the difference in free energy between water and equilibrium location, and ΔG_{pen} is the difference in free energy between the energy maximum (mainly at the center of the bilayer) and minimum (equilibrium location). ΔG_{part} values were ranging from -7.3 ± 0.2 to -12.7 ± 1 kcal mol⁻¹ (Table 11), indicating a 100% partition in the membrane rather than in water. ΔG_{pen} was huge for the anionic form A_{4',7}⁻ 32.7 ± 0.5 kcal mol⁻¹, making impossible DOPC bilayer crossing by the anionic form. Conversely, AH⁺, A₇, A_{4'}, and A₅ exhibited much lower ΔG_{pen} values of 16.1 ± 1.5 , 16.2 ± 1 , 20.0 ± 0.5 , and 15.5 ± 1 kcal mol⁻¹ respectively. This roughly corresponds to one crossing event every few hours if one considers a 1 μ M concentration and second-order kinetics (Table 11 and Figure 34 A&B).

IV.3.3.2 Impact of the sugar moiety on malvidin-3-*O*-glucoside partitioning and penetration

To evaluate the effect of glycosylation, A₇ was compared to its aglycone form of malvidin-3-*O*-glucoside (i.e. malvidin). The equilibrated location of the COM of the aglycone, as obtained by free MD simulation, was ca. 0.4 nm deeper in the lipid bilayer than its glycosylated counterpart (Figure 35). This means that malvidin lies rather deep in the bilayer embedded in between lipid chains, confirming the better affinity of aglycones to membrane, because the sugar moiety pull the compounds towards the surface, anchoring in head group region.

The free energy profile of the aglycone malvidin was dramatically different from that of its glycoside counterpart A₇ (Figure 34). ΔG_{part} and ΔG_{pen} were much lower, being 2.1 ± 0.4 kcal mol⁻¹ and 3.4 ± 0.5 kcal mol⁻¹, respectively. Even though about 97% of malvidin molecules partition in the membrane rather than in water, the aglycone can easily diffuse passively through membrane, that is to say much more easily than its corresponding glycosylated form. One can estimate one crossing event every 5 μ s for a 1 μ M concentration. This result stresses the impact of deglycosylation that usually occur in vivo for most of polyphenols. The better contact with the lipid chains in both leaflets explains that malvidin is more efficient than malvidin-3-*O*-glucoside at inhibiting lipid peroxidation in liposomes [392].



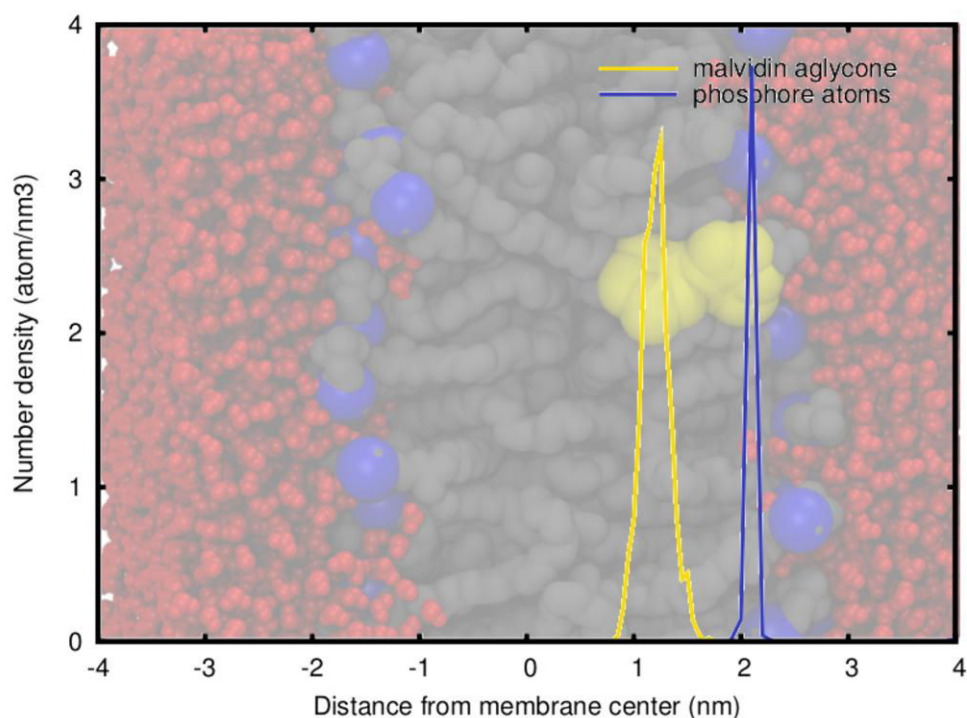


Figure 35: Location of the aglycone malvidin in membrane.

IV.3.3.3 Positioning of chalcone, hemiketal and pyranoanthocyanin forms in membrane.

Chalcone, hemiketal and pyranoanthocyanin were located between the hydrophobic and hydrophilic regions of the membrane at 1.5 to 1.8 nm from membrane center (Table 11). For these three compounds, the sugar moiety was always located at 1.7 nm from membrane center, confirming its role as anchor in polar head regions. By contrast, B-ring was located deeper than the COM, at around 1.2 nm from membrane center (Table 11). This is confirmed by α -angle values for chalcone and pyranoanthocyanin, which were greater than 90° . Such locations allow these compounds to be efficient as lipid peroxidation inhibitor.

The free energy profiles were comparable to those of quinoidal forms (A_5 , A_7 and A_4' , see Figure 34 A&C). ΔG_{part} were -7.1 ± 0.3 , -7.4 ± 0.2 and -9.3 ± 0.5 kcal mol $^{-1}$ for chalcone, hemiketal and pyranoanthocyanin, respectively (Table 11). The minimum position corresponding to the stable location of these molecules is at 1.9 ± 0.3 nm from membrane center, in polar head groups (Figure 36). Therefore, all these compounds have a better affinity to the lipid bilayer than to water. The differences in ΔG_{pen} between the three compounds were more pronounced; ΔG_{pen} was significantly lower for chalcone than for hemiketal or pyranoanthocyanin (i.e. 12.3 ± 2 , 15.8 ± 1 and 19.9 ± 2 kcal mol $^{-1}$, respectively). Therefore, chalcone exhibits the greatest passive diffusion capacity (average membrane crossing time of 5 s vs. 6 h for chalcone and hemiketal, respectively, assuming a 1 μ M concentration and second-order kinetics).

IV.3.3.4 Influence of methods of charge calculation

The charge description is a critical issue to predict the capacity of a compound to penetrate lipid bilayers. It is particularly sensitive for charge species. The charge distribution of three different forms of malvidin-3-*O*-glucoside (AH^+ , $A_{4,7}^-$ and A_4') were calculated using two



methods as described by Duan et al. [384] and Cornell et al. [385] (see Section IV.3.2 for details). The values of partial charges are plotted in Figure 36 as spheres. The charge methods have only a slight impact on the average location of both AH^+ and $A_{4,7}^-$. Indeed, the positions of their COM, B-ring or sugar moiety were similar with both methods (Table 11). Surprisingly for neutral form A_4 , a significant difference was observed in terms of location and orientation in membrane with both methods of charge calculation. With the Duan et al. method, the molecule was located outside the membrane, in the water phase, at 2.3 ± 0.2 nm from the center of membrane whereas the Cornell et al. method led to a location inside the bilayer, in close contact with the surface, at 1.8 ± 0.4 nm from the membrane center. The sum of partial charges on B-ring of A_4 were -0.3534 and -0.2595 with both methods, respectively. This difference explains the equilibrated location outside the membrane with the former method. Indeed in this case, the more negative charge of B-ring favors its interaction with choline groups outside the membrane therefore impeding penetration. As an important conclusion, which should be systematically properly evaluated, the results obtained by free MD simulations can be affected by partial charge evaluation, which also depend on the quantum mechanics method used to derive them. The lack of experimental results for malvidin positioning in membrane prevents ranking of charge methods.

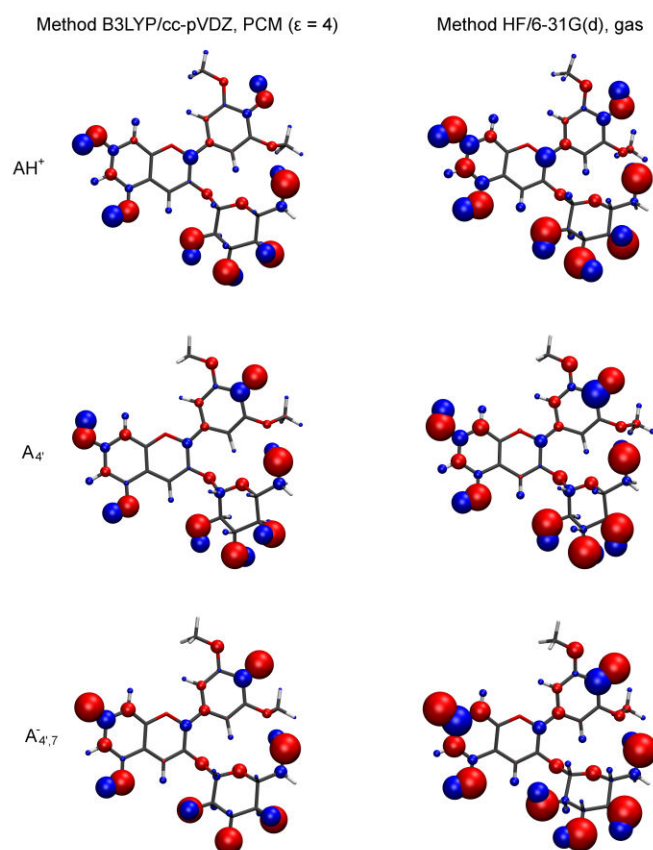


Figure 36: Charge distribution in the flavylium cation (AH^+), quinonoidal base (A_4) and quinonoid anion ($A_{4,7}^-$) as obtained by two different methods of calculation. The atomic charge value is related to the sphere diameter. Red and blue sphere colors represent negative and positive charge, respectively. (For interpretation of the references to color in this figure legend, the reader is referred to the web version of this article.)



IV.3.4. Conclusion

In this paper, we have predicted the position and orientation of several phenolic compounds found in wine in lipid bilayers, as well as their capacity to passively diffuse. All these compounds mainly partition inside the lipid chains rather than water, although the depth of penetration depends on (i) total charge; (ii) deprotonation sites; and (iii) presence or absence of sugar moiety. As expected, glycosylation pulls the compound towards the polar head region, impeding crossing. Hence, the anthocyanin aglycones are better candidate to inhibit lipid peroxidation with respect to their glycosylated forms. Regarding the different pK_a of anthocyanins, one can expect that only the anionic quinonoid bases or the hydration products circulate in water environment and then approach membranes. However, close to the membrane surface and inside the lipid bilayer, large pH variations may occur and re-protonations are expected (i.e., presence at least of the neutral quinonoid bases). From a methodological point of view, the method used to compute partial charges for the force field of anthocyanins could also influence prediction of membrane interaction/penetration. This is a critical issue that should systematically and thoroughly be benchmarked.



Chapter V. Drug permeation: towards the semi-quantitative elucidation of structure permeation relationship

V.1. Introduction

The finding of novel therapeutic drugs has become not only a matter of pharmacodynamics (PD) at its target but also a matter of pharmacokinetics (PK). Indeed it has become clear that comprehensive understanding of every ingredient of ADME (Absorption, Distribution, Metabolism and Elimination) is required to enhance the balance between efficacy and toxicity. In this context, drug-membrane interaction and crossing is an event of utmost importance in the study of ADME. Two major processes have been identified for small drugs to cross membrane, namely passive (unassisted) permeation or crossing through proteins, mainly channels [178] and transporters [40]. In other words, the efficacy of a drug is strongly dependent on the capacity/effectiveness for membrane crossing event, i.e., the time it takes to reach its pharmacological target. The cell permeability coefficient evaluates the kinetics of this process, which can be assessed experimentally. For instance, many cell permeability coefficients are available in the literature, as measured on the Caco-2 cell line[393]. However, it must be stressed that the exact contribution of passive permeation to the global cell permeability cannot be obtained from the Caco-2 permeability assay, as in this case active transport is not precluded. A few alternative assays have been designed in this purpose including the use of artificial membranes (e.g., PAMPA permeation assays) or unilamellar vesicle liposomes [40,77].

In case of small and medium-size molecules, passive permeation is the most common routes for cell drug intake [40,41,394]. The occurrence of passive permeation events is related to a number of physical chemical descriptors (e.g., lipophilicity, pKa, molecular weight, hydrogen-bonding capacity). It has long been correlated to the octanol/water partition coefficient ($\log P$). Besides, cellular drug transport events have been challenged over the past year and are still on debate. Two models have been proposed, namely the 'coexistence' and 'transporter-only' models [40,41,395]. The former considers that both passive permeation and protein-carried transport exist while, alternatively, the 'transporter-only' model in some extend stipulates that membrane transport is exclusively mediated by one or more protein transporters. Although none have been strongly refuted nor confirmed, Matsson et al. have recently suggested that the 'transporter-only' is unlikely to fully explain concentration dependent transport rate suggesting a significant contribution of passive permeation [395].

Molecular computer simulations thus appear as a relevant tool to bring its contribution up to the drug transport debate. The likelihood of passive permeation for a given drug can indeed be estimated by providing an atomic-scale and dynamic view of such events. Molecular dynamics (MD) simulations have more recently proved to be promising in prediction of permeability coefficients of small molecules (e.g., water, ethanol and benzene), in agreement with experimental values [1,396,397]. MD simulations have the advantage to provide a description of intermolecular driving forces of crossing events. Until now, most of benchmarking studies have focused on small-size molecules (i.e., molar mass lower than 100 g/mol), in other words, there have been only few MD-based studies to evaluate permeability coefficients for drugs so far [398].

Most of drugs are expected to achieve passive permeation within at least several microseconds. It thus means that for most of drugs, a proper sampling of many crossing



events is beyond the reach of conventional atomistic MD simulations. However, over the past decade, several theoretical models have been successfully applied on prototypical compounds to overcome such limitations assigned to too low achievable timescale. These models focus on a selected set of geometrical parameters related to the crossing events, i.e., biased-MD simulations. A powerful approach is to decompose membrane-crossing events into three steps: i) drug dissolution into the lipid bilayer; ii) diffusion through membrane interior; and iii) dissolution back to the surrounding environment [181]. This so-called “homogeneous solubility-diffusion” model have been refined by splitting membrane into different regions so to account for inhomogeneity (see Section V.2.1) [181]. It is worth noting that another formalism has recently been proposed, in which permeability is calculated by: i) defining several microstates within the membrane interior by means of metadynamics; and ii) assessing the transition between them [193].

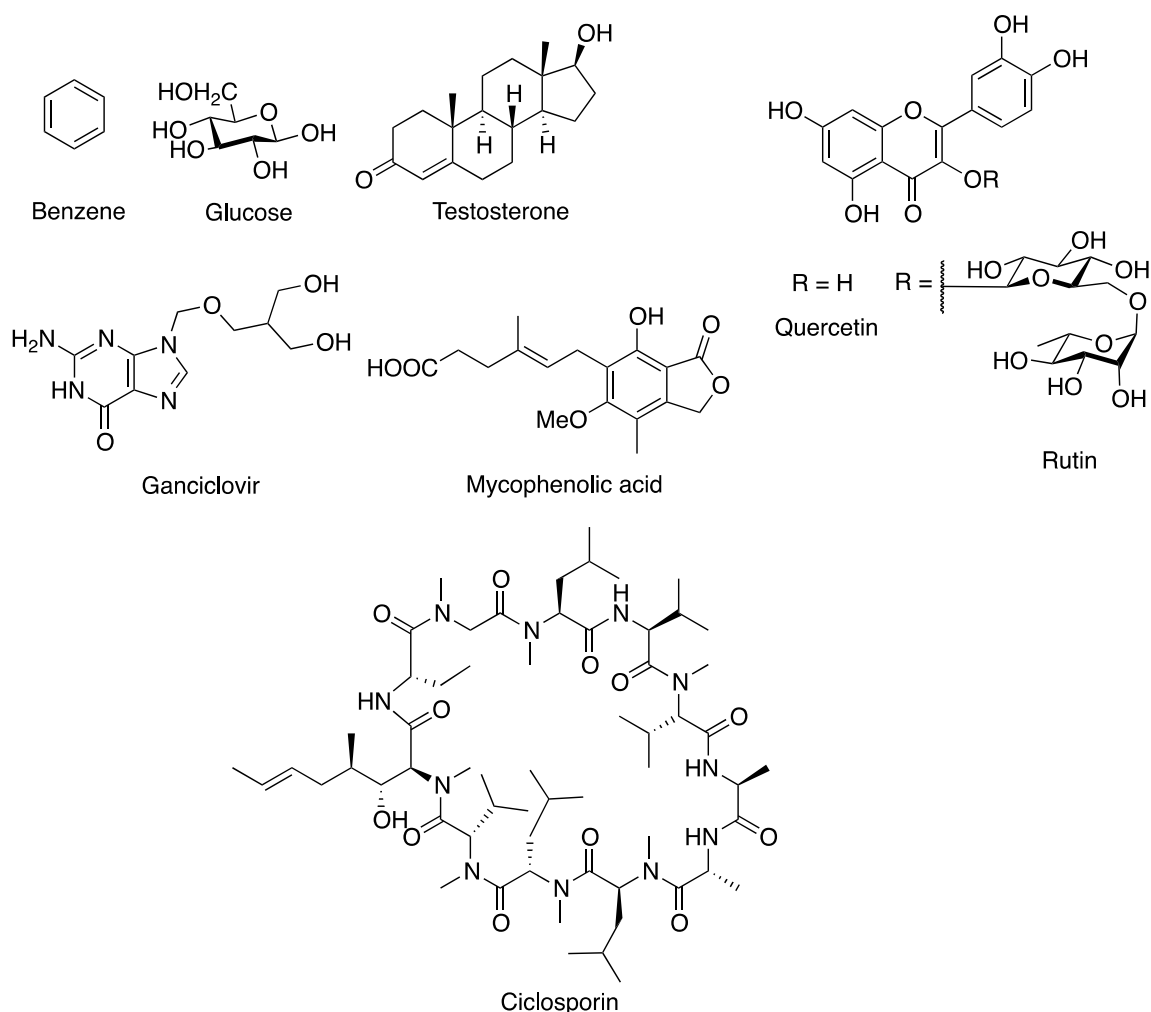


Figure 37: Chemical structures of the 8-member set of compounds studied in this work.

The present study aims at applying the “inhomogeneous solubility-diffusion” model to calculate the permeability coefficients of a series of drugs, then to establish structure-permeation relationships (SPR) and to highlight atomistic features responsible for passive permeation. A series of eight molecules including six drugs (testosterone, ganciclovir, mycophenolic acid, ciclosporin, quercetin and rutin) and two reference compounds (glucose and benzene), see Figure 37; mycophenolic acid was studied in both its neutral and charged states. These eight compounds have been chosen due to their broad and characteristic



physical chemical features, i.e., polar/apolar, aglycone/glycoside, neutral/charged and small/large. The permeability coefficients will then be discussed in terms of their relative values, as well as the driving forces elucidated here at the atomic scale. Comparison to available experimental data will be discussed.

V.2. Theoretical methodologies

V.2.1. Inhomogeneous solubility-diffusion model by z-constraint MD simulations

The overall permeability coefficient P , or alternatively the resistance R equal to the inverse of P , quantifies the capacity of a drug to cross the lipid bilayer without any assistance (originated by biomolecules or by any external modification) but the gradient between the outer and the inner compartments. The crossing events are followed along the z -axis, normal to the bilayer surface, as defined by polar head groups. Within the solubility-diffusion model formalism, the permeability coefficient is expressed as [1]:

$$P = \frac{1}{R} = \frac{J}{\Delta c} = \left(\int_{z_1}^{z_2} \frac{dz}{K(z)D(z)} \right)^{-1}$$

where J and Δc are the flux and the concentration gradient of the drug from z_1 to z_2 , respectively; $K(z)$ and $D(z)$ are the depth-dependent partition and diffusion profiles, respectively. The flux and concentration gradient are virtually inaccessible by MD simulations, as the molecular systems (membrane + solute) are too small, including a few (if not only one) solutes in the lipid bilayer. Conversely, partitioning and diffusion profiles can be calculated from the intermolecular forces required to move along the z -axis; this can be obtained by various biased formalisms, including z -constraint MD simulations [77,396,399,400]. In these methods, the lipid bilayer is split into several windows centered at a given z -value; the forces required to maintain the drug at a given depth (in a given window) is evaluated and they are converted in terms of Gibbs energy (see details in Sections V.2.2 and V.2.3).

V.2.2. Technical details on MD simulations

A lipid bilayer made of 1-palmitoyl-2-oleoyl-sn-glycero-3-phosphocholine (POPC) was used, as a prototypical example of phospholipids, widely distributed in mammal cells. Lipids, water, ions and the eight tested compounds were modeled using the GROMOS 43a1 force field [401]. Force field parameters of the nine tested compounds (the eight compounds displayed in Figure 37 and the deprotonated form of mycophenolic acid) were derived from the GROMOS 43a1 forcefield and quantum-based calculations. Indeed, all molecules were first optimized at the B3LYP/6-31+G(d,p) density functional theory (DFT) level using the Gaussian09 package [402]. The optimized geometries were then used to calculate RESP atomic charges by fitting the electrostatic potential obtained from Duan et al. formalism [383].

The NPT ensemble was considered for all MD simulations, which were carried out under semi-isotropic pressure coupling and using periodic boundary conditions independently in the xy and z directions. A time step of 2 fs was used for all simulations. The temperature was kept at 310 K by Nose-Hoover thermostat [403,404], with a coupling constant of 0.5 ps. The pressure was kept at 1 bar using Parrinello–Rahman barostat [405], with a coupling constant of 5.0 ps. Coulomb and van der Waals interactions were explicitly calculated considering a cut-off of 1.2 nm. Longer range electrostatic interactions were computed using Particle-



Mesh-Ewald (PME) method [406]. All calculations were carried out using the GROMACS package.

The initial lipid bilayer was consisting of 128 molecules of POPC (i.e., 2 x 64 lipids), solvated by 5440 water molecules, i.e., roughly 40 water per lipid. Counterions (Na^+ and Cl^-) were included, according to physiological concentrations (i.e., $[\text{NaCl}] = 0.154 \text{ M}$). Lipid bilayers were built using memgen server [407]. The pure lipid bilayer was equilibrated prior to drug insertion during 600 ns to ensure structural POPC membrane properties.

To set up z-constraint MD simulations, drug was manually inserted in the upper water layer at ca. 3.6 nm distance from the center-of-mass (COM) of the lipid bilayer. After a short MD relaxation (200 ps), 80 ns steered MD simulations were performed, in which the drug was pulled towards the center of the lipid bilayer along z-axis with a pulling force set up at 0.05 nm/ns with a linear force constraint of $1000 \text{ kJ.mol}^{-1}.\text{nm}^{-2}$. z-Constraint initial structures were then selected to define windows every 0.2 nm. For each window, MD simulations were performed in which the drug center-of-mass was constrained at a given depth (defined by a z-value) using the PMF method with a linear constraining force of $2000 \text{ kJ.mol}^{-1}.\text{nm}^{-2}$ along the z-axis. The z-constrained simulations were run for at least 30 ns per window, however they were extended until 150 ns per window in case of slow convergence in Gibbs energy and diffusion profiles. Constraint force and z-positions of drug COM were extracted every 2 fs and 20 fs, respectively.

V.2.3. Partitioning and free energy profiles

The partitioning profile $K(z)$ is directly derived from the Gibbs energy profile $\Delta G(z)$, as follows:

$$K(z) = \exp\left(\frac{-\Delta G(z)}{kT}\right)$$

In z-constraint MD simulations, the Gibbs energy profile is accessible by integrating the average constraint forces $f(z,t)$ over the window along the z-axis. The z-Constraint approach has been shown reliable at predicting: i) location; ii) orientation; and iii) partition of drugs in lipid bilayer membranes, with respect to experimental data. z-Constraint MD simulations enable evaluation of the two major thermodynamic events in drug-membrane crossing, namely drug insertion ΔG_{ins} and drug-leaflet crossing ΔG_{cross} . The former is pictured by the difference in Gibbs energy difference between bulk water and the local energetic minimum in membrane interior; the latter reflects the difference in Gibbs energy between the center of the membrane and the local energetic minimum in membrane interior, in other words, the energy required to pass from one to the other leaflet.

V.2.4. Diffusion profiles

The diffusion profile $D(z)$ reflects the variation of the diffusion coefficient along the z-axis. The diffusion coefficient reflects the dynamical aspects of interactions between a drug and its surrounding environment. Along the z-constraint MD simulations, a local diffusion coefficient is calculated for each window by assessing the static friction coefficient ξ . Assuming that ξ is large and that it decays rapidly with respect to other timescales in the system, including thermal fluctuations (i.e., RT per mole) [181,182,408,409], friction and diffusion coefficients are calculated as follows:



$$D(z) = \frac{RT}{\xi} = \frac{(RT)^2}{\int_0^\infty \langle \Delta f(z, t) \cdot \Delta f(z, t = 0) \rangle dt}$$

where force fluctuation $\Delta f(z, t)$ at a given depth z is:

$$\Delta f(z, t) = f(z, t) - \langle f(z, t) \rangle$$

To integrate the force fluctuation autocorrelation function (ACF) over time, ACF was fitted to double or triple exponential functions:

$$\langle \Delta f(z, t) \cdot \Delta f(z, t = 0) \rangle \approx \sum_{i=1}^{2,3} c_i \exp(-t/\tau_i)$$

The use of double or triple exponential functions to describe ACF comes from the physically meaningful decomposition of solute motion into two or three distinct regimes, respectively. In case of small compounds, the existence of two regimes was clearly identified, namely fast- and long- regimes before a few tens of femtoseconds and a few tens of picoseconds, respectively. The former regime corresponds to the response of the solute to the immediate environmental effects, the solute being somehow temporarily trapped in “local cages”. The latter regime was shown to be more region-dependent and it pictures the correlation in movements of solute when hopping from one to another local cage. A systematic particular attention should be paid to the fitting procedure, owing to the complex profile of ACF [182]. In this work, the first two regimes were observed as expected, however due to the relatively large size of the drugs (see Figure 38a), a third “very long” regime was observed, namely timescale ranging from tenths to a few nanoseconds. This regime pictures the long-term reminiscence of solute-lipid interactions. This might be assigned to the time required to reorganize lipids after the drug has proceeded to several hopping events; the bigger the drug, the longer the effect of lipid reorganization on drug random motion and so drug diffusion. As here the third regime clearly appeared and could not be ignored, a triple exponential fitting was used, which in addition has prevented the manual adjustments required with double exponential fitting [182]. It must be stressed that both double and triple exponential fitting have provided the same qualitative profile in low-density lipid chain region where reorganization is fast (Figure 38b). However, double exponential fitting overestimates drug diffusion in high-density regions.

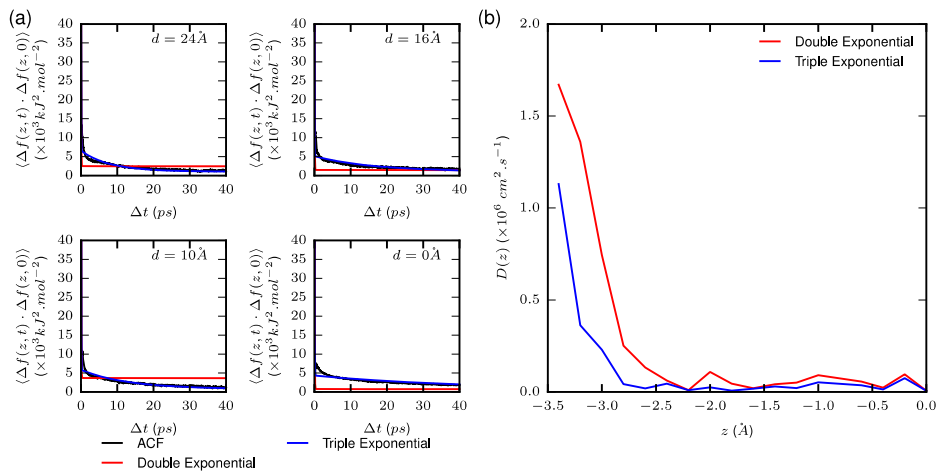


Figure 38: (a) Force fluctuation autocorrelation function and double/triple exponential fit in four different z -constraint windows and (b) z -dependent diffusion profiles according to fitting procedure. Ganciclovir profile is shown as example.

We must stress that the use of static friction coefficients to calculate diffusion coefficients is valid only in a region where the Gibbs energy is constant, while allowing the variability attributed to thermal fluctuations (i.e., RT) [182,409]. The largest Gibbs energy differences $\Delta\Delta G$ observed along the z -axis (Table 12) are within this framework (maximum $\Delta\Delta G$ reaching the upper limit of this approximation, e.g., $6.0 \times RT$ in case of rutin).

Molecules	$\Delta\Delta G_{\max}$	
Benzene	0.81	(1.3xRT)
Ganciclovir	3.66	(5.9xRT)
Glucose	2.76	(4.5xRT)
Quercetin	3.35	(5.4xRT)
Rutin	3.72	(6.0xRT)
Testosterone	0.86	(1.4xRT)
Mycophenolic acid	2.10	(3.4xRT)
Mycophenolate	2.73	(4.4xRT)
Ciclosporin	2.28	(3.7xRT)

Table 12: Calculated maximum Gibbs energy differences ($\Delta\Delta G$, kcal.mol⁻¹) along z -constraint windows.

V.2.5. Resistance and permeation coefficients

The global resistance R for the drug to cross the different sections of the bilayer can be obtained by reformulation the equation discussed in section V.2.1, i.e., by integration of the local resistance $R(z)$, as obtained in each window of the constrained MD simulation:

$$R = 2x \int_{outside}^0 R(z) dz = 2x \int_{outside}^0 \frac{1}{K(z)D(z)} dz$$

The permeability coefficient is then calculated as the inverse of R . Here, benzene and glucose were selected for the sake of comparison both to experimental evidences and to other theoretical studies. Concerning benzene, P was 4.7 cm.s⁻¹, which is similar to that obtained theoretically by similar methodology in DPPC at 50 °C (P was 9.91 cm.s⁻¹) [396]. This is consistent with fast passive permeation, as expected for this type of compounds (e.g., benzoic and *p*-toluic acid permeabilities being respectively 0.57 and 1.1 cm.s⁻¹ in egg lecithin bilayer membrane à 25 °C) [410]. Conversely, and as expected, glucose exhibited a much higher permeation coefficient (P was 1.8x10⁻⁵ cm.s⁻¹). It must be stressed that most of experimental permeation coefficients are often obtained with membrane systems more complex than simple lipid bilayers. For instance, in the Caco-2 cells, active transport is not precluded, as, e.g., they contain influx and efflux transporters. Therefore the robustness of the theoretical methodology can only be tested against a few compounds (e.g., benzene or glucose). To establish correct SPR on a series of compounds with sufficient chemical variability can also contribute to check the robustness of the theoretical methodology.

V.3. Structure-Permeation Relationship

The passive permeation coefficients of testosterone, ganciclovir, mycophenolic acid, ciclosporin, quercetin and rutin were evaluated according to the methodology described in section 2. Considering that this model of passive permeation has provided a correct qualitative description, here we aim at establishment of a SPR on real-world series of compounds, i.e., drugs clinically used. Here the SPR is discussed in terms of simple physical



chemical features of drugs (e.g., role of polarity, sugar moiety, charge state and size), but also in terms of intermolecular interactions. To picture the inhomogeneous character of membrane along the membrane z-axis, the four region model [181,182] will be used in the following discussion:

Region 0. Bulk water ($z > \sim 2.7$ nm)

Region 1. The low density polar head region corresponding to the aqueous interface between water and phosphate groups ($2.0 < z < 2.7$ nm).

Region 2. The high density polar head region is the dry transition region between phosphate groups and acyl chains ($1.3 \text{ nm} < z < 2.0$ nm).

Region 3. The high density lipid tail region consists in the hydrophobic region of the bilayer including double bond ($0.6 \text{ nm} < z < 1.3$ nm).

Region 4. The low density lipid tail region corresponds to the middle of the bilayer with low tail density owing to the high flexibility of lipid tails ($z < 0.6$ nm).

For sake of clarity, numbering of regions is only used in figures.

Molecules	ΔG_{ins}	ΔG_{cross}	$\log P$	R_{MD}	P_{MD}
Benzene	-5.0	0.5	2.1	2.1×10^{-1}	4.7
Glucose	-1.3	8.2	-3.3	5.6×10^4	1.8×10^{-5}
Testosterone	-2.3	2.7	3.3	7.7	1.3×10^{-1}
Quercetin	-11.8	14.0	1.6	8.9×10^1	1.1×10^{-2}
Rutin	-6.6	25.2	-0.5	1.7×10^{13}	5.8×10^{-14}
Mycophenolic acid	-9.5	7.2	2.9	4.5×10^{-1}	2.2
Mycophenolate	-5.3	11.2	-	1.6×10^4	6.5×10^{-5}
Ganciclovir	-6.2	12.5	11.7	9.0×10^4	1.1×10^{-5}
Ciclosporin	-7.4	6.1	4.12	1.9	5.2×10^{-1}

Table 13: Calculated maximum Gibbs energy differences ($\Delta\Delta G$, kcal.mol⁻¹) along z-constraint windows. Insertion and crossing Gibbs free energy transfer (ΔG_{ins} and ΔG_{cross} , kcal.mol⁻¹), octanol/water partition coefficient ($\log P$), overall membrane resistance (R , in s.cm⁻¹), calculated permeability coefficients (P_{theo} in cm.s⁻¹).

V.3.1. Role of polarity

Polarity is the most important driving forces of membrane passive permeation, namely, the lower the polarity, the higher the affinity to the lipid bilayer, and so the higher the penetration into the membrane. The role of polarity has long been described by $\log P$. This descriptor is indeed roughly correlated to partitioning, however it does not describe: i) the specificity of the lipid bilayer composition; and ii) the dynamical aspects of membrane passive permeation. In this section, we compare passive permeation of glucose, benzene and testosterone; glucose is polar ($\log P = -3.3$) whereas the other two are typical apolar compounds ($\log P = 2.1$ and 3.3 for benzene and testosterone, respectively). In testosterone the apolar feature is owing to its aliphatic character contrary to benzene (see Figure 37).



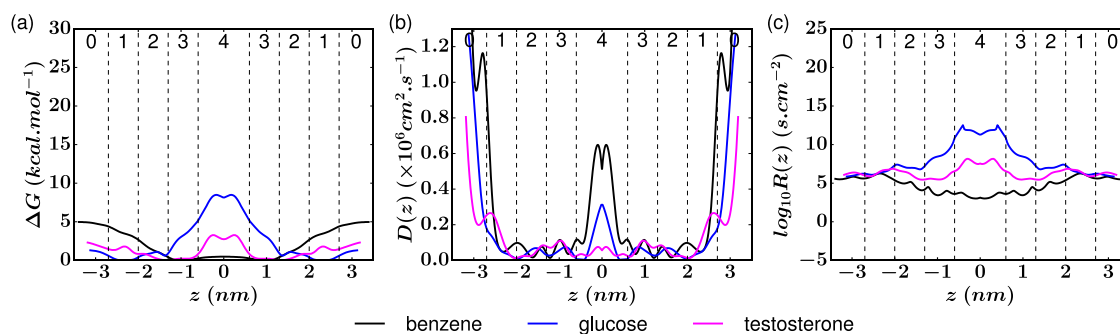


Figure 39: Profiles of (a) Gibbs energy profiles, (b) diffusion coefficient, and (c) resistance to membrane crossing of benzene (black), glucose (blue) and testosterone (magenta).

Gibbs energy profile. Both benzene and testosterone exhibit preferential locations in the high-density lipid tail region, i.e., at 1-1.3 nm from the center of lipid bilayer with rather low (in absolute value) Gibbs energy of insertion ($\Delta G_{ins} = -5.0$ and -2.3 kcal.mol⁻¹, for benzene and testosterone, respectively). The difference between both compounds qualitatively agrees with $\log P$ values (2.1 and 3.3, respectively). The ΔG_{cross} values are low for both compounds, with however a slight but significant difference between both ($\Delta G_{cross} = 0.5$ and 2.7 kcal.mol⁻¹, respectively). Interestingly, this difference does not agree with $\log P$ values. This can at least partially be rationalized by the smaller size of benzene leading to less steric hindrance, thus lowering energetic reorganization requirements to cross the center of the membrane with respect to testosterone.

Glucose exhibits little partitioning in membrane ($\Delta G_{ins} = -1.3$ kcal.mol⁻¹), in full agreement with its high polarity. It locates in the low-density polar headgroup region, i.e., at 2.1 nm from the lipid bilayer center. Electrostatic and H-bonding interactions between the sugar hydroxyl groups on one side and both phosphate moieties and water molecules on the other side are the driving forces to anchor glucose in this region. The Gibbs energy profile of glucose exhibits another local minimum in the high-density headgroup region (1.3 nm, see Figure 39 a) confirming the important role played by H-bonding interactions between sugar hydroxyl groups and phosphate moieties. Although we describe a favored location of glucose inside the membrane, this should be tempered by the low ΔG_{ins} value, which is close to the chemical accuracy. In other words, glucose can easily and superficially exchange from bulk water to high-density polar head regions and vice versa. Expectedly, the Gibbs energy profile exhibits a rapid increase in the apolar regions (i.e., below 1.3 nm distance from center of lipid bilayer membrane), eventually reaching a maximum in the membrane center ($\Delta G_{cross} = 8.2$ kcal.mol⁻¹).

Diffusion coefficients. Benzene diffusion profile is in agreement with previous theoretical studies, exhibiting fast diffusion outside the membrane (2.7×10^{-6} cm².s⁻¹ at 2.7 nm) and in between membrane leaflets (0.5×10^{-6} at 0.0 nm, see Figure 39 b). Diffusion in high-density polar head and lipid tail regions is significantly slower (ca. ranging from ca. 0.01 to 0.1×10^{-6} cm².s⁻¹). These values are one order of magnitude lower than those obtained previously in lipid bilayer MD simulations [411]. However, such calculations were performed at higher temperature (i.e., 50°C), partially explaining the difference. However, present results are still within the physical accuracy threshold of the z-constraint method [182,411,412]. Interestingly, glucose globally diffuses 4-fold slower than benzene while testosterone diffuses one order of magnitude slower than benzene. This suggests that polarity does not play a



crucial role in diffusion in lipid bilayers. This agrees with previous observations that have shown strong relation of diffusion profiles in membrane interior to both the molecular volume and the particle density at a given region [411,412]. The influence of molecular volume is thoroughly discussed further in Section V.3.4.

Resistance and permeability. Benzene, glucose and testosterone resistance profiles roughly adopt the shape of Gibbs energy profiles, confirming the predominant role of intermolecular potential energy to drive passive permeation of these three compounds, which are covering a broad range of polarity. In other words, diffusion has little influence on the global permeation, with however a secondary role in specific regions. For instance, benzene does not exhibit local resistance in the center of the lipid bilayer, as the low ΔG_{cross} value compensates the relatively high diffusion coefficient. Another effect of diffusion is seen with testosterone, which exhibits a higher resistance in the high-density polar head region compare to the other regions. This is due to slow diffusion and unfavorable partitioning. Diffusion has virtually no effect on glucose resistance, mainly due to the high ΔG_{cross} values. Here we confirm that for polar drugs, polarity plays a key role in passive permeation by mostly affecting partitioning throughout the different regions of the lipid bilayers. For apolar drugs, partitioning is relatively low; thereby, passive permeation relies more on both diffusion and partitioning contributions.

Expectedly, the following sequence in terms of calculated permeability is obtained: $P_{benzene} > P_{testosterone} > P_{glucose}$. It is worth noting that the permeability coefficient of benzene suggest a fast passive permeation, in agreement with previous studies ($P = 4.7 \text{ cm}\cdot\text{s}^{-1}$) [181,182,397]. Glucose permeability is slower by five orders of magnitude with respect to benzene, meaning that passive permeation of glucose is expected to be a rare event. This is indirectly confirmed by the existence of glucose transporters (GLUT) [413] that are dedicated to glucose transport through membranes in most living organisms. Calculated testosterone permeability coefficient is $1.3 \times 10^{-1} \text{ cm}\cdot\text{s}^{-1}$ suggesting that, as usually proposed, steroid hormones efficiently cross membrane by passive permeation [40,414]. This is also indirectly confirmed by the absence of known transporter for sexual hormones as well as nuclear location of testosterone receptors in human cells.

V.3.2. Role of sugar moieties

Flavonoids are a large class of natural polyphenols. They are powerful antioxidants that are largely found in human diets (e.g., fruit, spices and beverages) [415]. As other xenobiotics, they need to reach their biological targets (e.g., to prevent oxidative stress) by crossing cell membranes [151,416]. Quercetin is one of the most used antioxidant polyphenol prototypes *in silico*, *in vitro* and *in vivo* [149,150,152,152,417]. Quercetin is usually naturally synthesized in plants in its glycoside form, e.g., rutin (Figure 37). Quercetin/rutin is a particularly adequate prototypical couple to evaluate how sugar substitution may affect passive permeation.



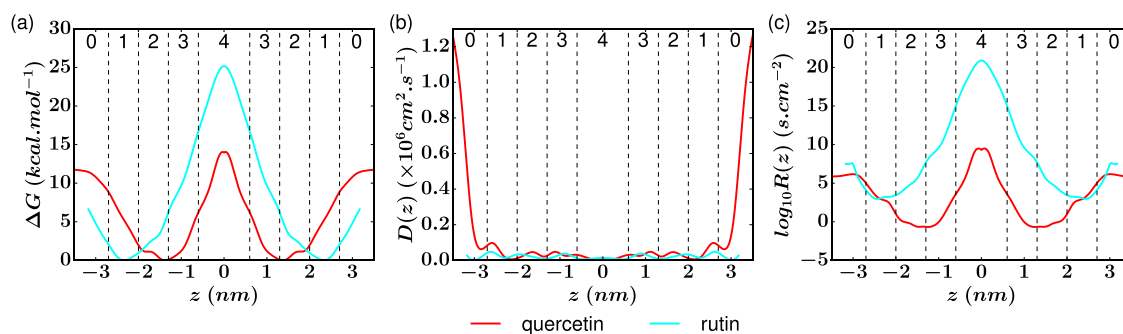


Figure 40: Profiles of (a) Gibbs energy profiles, (b) diffusion coefficient, and (c) resistance to membrane crossing of quercetin (red) and rutin (cyan).

Gibbs energy profiles. Quercetin is amphiphilic as owing to its polyaromatic skeleton substituted by several OH groups. As already confirmed theoretically and experimentally [149–152,417], quercetin better partition inside the bilayer ($\Delta G_{ins} = -11.8$ kcal.mol⁻¹), see Figure 40a. It preferentially locates in the high density polar headgroup region (ca. at 1.3 nm from lipid bilayer center) allowing H-bonding to polar head groups as well as weak dispersive interactions between lipid double-bonds and quercetin aromatic rings. The ΔG_{cross} value is relatively high ($\Delta G_{cross} = 14.0$ kcal.mol⁻¹) since it requires the breaking of the noncovalent bonding network with the polar head group region. The presence of the sugar moiety in rutin dramatically increases polarity, thus decreasing ΔG_{ins} (-6.6 kcal.mol⁻¹) and increasing ΔG_{cross} (25.2 kcal.mol⁻¹) with respect to the aglycone derivative (quercetin), see Figure 40a. Rutin preferentially locates in the low-density polar head region, meaning almost outside the membrane (i.e., at 2.4 nm from the lipid bilayer center). Rutin orients its sugar moiety towards the outer membrane, whereas the aglycone moiety locates just beneath polar head group region. Rutin is thus tightly anchored to this region by noncovalent interactions (mainly H-bonding), which also strongly drive orientation.

Diffusion. Diffusion of rutin and quercetin is relatively fast in water-rich regions. The diffusion profile then exhibits a dramatic decrease in membrane interior by two orders of magnitude ($D(z)$ equals 1.4×10^{-6} cm².s⁻¹ and 0.01×10^{-6} cm².s⁻¹ at 3.4 and 0.2 nm from the lipid bilayer center, respectively for quercetin, see Figure 40b). Surprisingly, in between lipid chains, rutin diffuses only 3-fold slower than quercetin although molecular volume of rutin is much bigger than that of quercetin. The flexibility between the flavonoid and sugar moieties allows stretching and conformational arrangements of rutin, which facilitate its motion in membrane interior; its molecular volume is adopting an ellipsoid rather than a globular shape.

Resistance and permeability. Partitioning is again the driving force for passive permeation of polyphenols. Indeed the R profiles of both quercetin and rutin clearly adopt the shape of the Gibbs energy profiles (Figure 40), suggesting little contribution of local diffusion effects when comparing both systems. Interestingly, quercetin exhibits a low local resistance in both the lipid-tail and polar head high-density regions (i.e., from 2.4 to 0.6 nm from the lipid bilayer center). This is rationalized by the planar conformation of this highly π -conjugated system, which does not require extensive lipid reorganization. The passive permeability coefficient (Table 13) suggests that passive permeation is likely to occur in spite of relatively high ΔG_{cross} value. This indicates that diffusion does not play a qualitative role in permeation of amphiphilic molecules (similar profiles of D and ΔG), however it does play a significant quantitative role (R value). Addition of highly polar sugar moiety (rutin) definitely precludes



passive permeation ($P = 1.1 \times 10^{-2}$ and 5.8×10^{-14} $\text{cm} \cdot \text{s}^{-1}$ for quercetin and rutin, respectively) due to a strong extra anchoring to membrane surface and water molecules attributed to the sugar moiety, which cannot be compensated by diffusion.

V.3.3. Role of pH

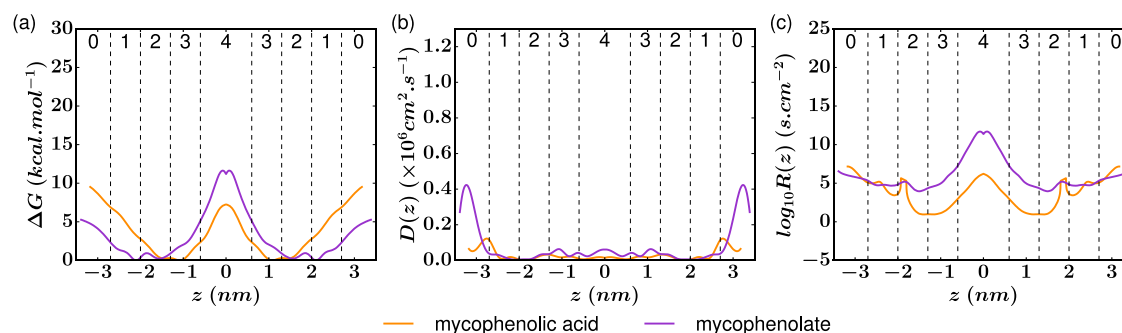


Figure 41: Profiles of (a) Gibbs energy profiles, (b) diffusion coefficient, and (c) resistance to membrane crossing of MPA (orange) and mycophenolate (purple).

Under physiological conditions, a large number of drugs are involved in acid base reactions. The environmental pH value thus plays a crucial role in passive permeation, as it drives the charge state of drugs, which may strongly affect drug insertion and crossing. Mycophenolic acid (MPA, see Figure 37) is an immunosuppressant drug commonly used in transplantation to prevent organ transplant rejection [333]. The pKa of MPA is 4.5 leading to the predominance of its deprotonated form under physiological conditions, namely mycophenolate. [418]

Gibbs energy profiles. Mycophenolate expectedly exhibits a much less favorable Gibbs energy profile with respect to MPA. The presence of negative charge in mycophenolate significantly increases ΔG_{ins} with respect to MPA (-9.5 and -5.3 $\text{kcal} \cdot \text{mol}^{-1}$ for both forms, respectively, see Table 13). The preferred location of both forms differs by 1 nm (2.1 and 1.1 nm from lipid bilayer center for mycophenolate and MPA, respectively), the mycophenolate being shifted towards the polar head group region. Interestingly, in spite of its negative global charge, the partitioning of mycophenolate inside bilayer is higher for mycophenolate than for glucose. Mycophenolate is amphiphilic owing to both its apolar aromatic and the (charged) carboxylate moiety, separated by a short C5-chain. The ΔG_{cross} value of mycophenolate is 5 $\text{kcal} \cdot \text{mol}^{-1}$ higher than MPA ($\Delta G_{cross} = 7.2$ and 11.2 , respectively). This difference appears lower than expected, which is partly attributed to the strong delocalization of the negative charge. This effect is assigned to the close electron withdrawing groups.

Diffusion. Both forms diffuse relatively slowly in the membrane interior and the two diffusion coefficients are of the same order of magnitude. This indicates that neither partial nor total atomic charges do play a significant role in diffusion properties.

Permeability. As for the other xenobiotics, partitioning drives passive permeation, crossing event being again the limiting step for both MPA and mycophenolate. Mycophenolate permeability is five orders of magnitude higher than MPA ($P = 6.5 \times 10^{-5}$ $\text{cm} \cdot \text{s}^{-1}$ and 2.2 , respectively). These values suggest that MPA is prone to fast passive permeation while mycophenolate would permeate much slower. Having in mind that MPA occurs mainly in its deprotonated form under physiological pH, two conclusions can be drawn: i) this drug could cross in its charged state (mycophenolate) however with a slow kinetics; or ii) acid-base



balance could be shifted at the membrane surface (local modifications of pH and pK_a values) favoring the re-protonation of mycophenolate, then facilitating membrane crossing in the acid form. Both processes are likely to occur and could lead to a double-regime of absorption. It is worth noting that the permeability coefficient of mycophenolate is roughly ranging within the same order of magnitude than those experimentally obtained for a number of drugs exhibiting similar molecular weight and chemical features (e.g., piroxicam, acebutolol and labetalol) [419].

V.3.4. Role of molecular size

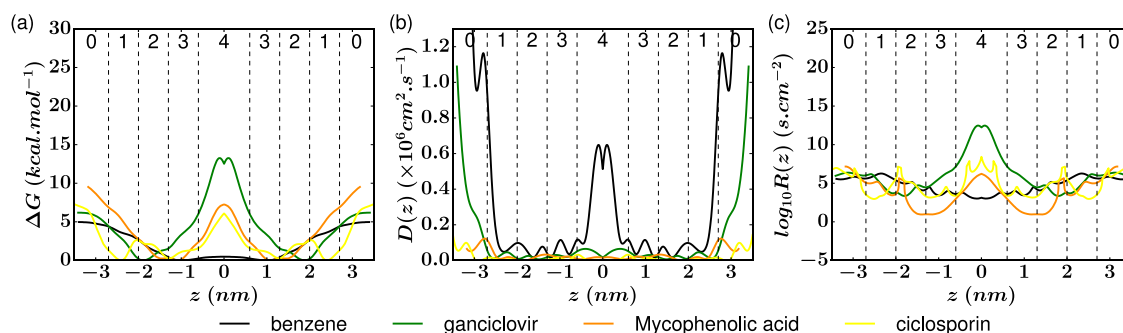


Figure 42: Profiles of (a) Gibbs energy profiles, (b) diffusion coefficient, and (c) resistance to membrane crossing of benzene (black), ganciclovir (green) and mycophenolic acid (orange).

The size of the xenobiotics is expected to play a crucial role in its permeation, as particle density along membrane crossing is a determinant parameter of the resistance to crossing. Solubility-diffusion model has been shown to be reliable in case of spherical and ellipsoidal particles [399] and small drugs [411]. In the present study, its use is extended to larger compounds with high degree of flexibility. A particular attention has been paid to sufficiently sample conformational arrangements and adaptation to the surrounding environment. To evaluate the influence of molecular size, benzene, ganciclovir, MPA and ciclosporin profiles have been compared (Figure 42). Interestingly, the Gibbs energy profile of ciclosporin exhibits a ΔG_{cross} value slightly lower than MPA ($\Delta G_{cross} = 6.1$ and 7.2 kcal.mol⁻¹, respectively, see Table 13). The corresponding permeability coefficients are also somewhat similar between both compounds ($P = 0.5$ and 2.2 cm.s⁻¹, respectively). It is worth noting that z -dependent profiles of large molecules as ciclosporin should be carefully considered. Indeed, in the z -constrained process, only the COM of drug is constrained, meaning that other parts of the (large) drug may lie in significantly different locations (with a significantly different environment).

As a general trend for all four membrane regions, the larger the molecule, the lower the diffusion coefficient (Figure 43). However the non-linear evolution of $\log D$ vs. molecular volume underlines the importance of flexibility in passive permeation.



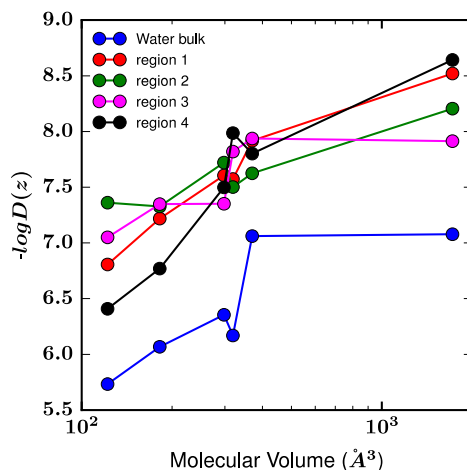


Figure 43: Diffusion coefficient per region vs. molecular volume in the 5 membrane regions. Low-density polar head, high-density polar head, high-density lipid tail and low-density lipid tail regions are quoted 1, 2, 3 and 4, respectively.

V.4. Conclusion

The interaction of drugs with membranes is an area of high importance for the pharmaceutical industry when considering the efficacy and safety of their products. The cell membrane is often overlooked in drug development programmes as it is generally the receptors and enzymes contained within it that are the targets of the drug molecule. Biased MD simulations have appeared relevant to evaluate permeability coefficients and to establish qualitative SPR. The evaluation of ΔG and D profiles along the z -axis has allowed rationalization of driving forces responsible for resistance to membrane crossing. Polarity, charge state, substituents and molecular size are important descriptors to predict membrane permeation. MD simulations should support the knowledge on drug influx and unravel the contribution of passive permeation with respect to active transport. In further developments a particular care should be paid to membrane composition, which should strongly modify permeation profiles. According to membrane ingredients, order in membranes could be significantly affected, so should be the ΔG , D and R profiles.



Conclusion

MD simulations of membrane insertion and permeation have enabled establishment of SPR. Hydrophobic (apolar) drugs insert quickly in lipid bilayers, with relatively favorable partitioning; these compounds have virtually no interaction with the polar head group region. The transfer energy required to go from one to the other leaflet is relatively low. For such drugs, passive permeation is described by both the contribution of partitioning (ΔG -profiles) and diffusion. As expected, hydrophilic (polar) drugs exhibit rather unfavorable partitioning coefficients (here, relative concentration in between lipid bilayer with respect to water phase). These drugs preferentially anchor to the aqueous interface between water and phosphate groups. Passive permeation of polar drugs is slow and it is mainly driven by the ΔG -profile, exhibiting rather high barriers to cross the center of the bilayer. Amphiphilic drugs quickly interact with the lipid bilayer surface (when starting from water), and further insert inside the bilayer, just below the interface in close contact to the polar head group region, hydrophobic moieties being oriented towards center of membrane whereas its polar moieties interact with the polar head group region.

MD simulations have systematically confirmed that anchoring and orientation of drugs in membranes are driven by intermolecular noncovalent (electrostatic and H-bonding) interactions. Both insertion and permeation of anionic forms of drugs are precluded, due to strong anchoring to the aqueous interface between water and phosphate groups, and to high energetic barriers to go from one to the other leaflet. In this case, we believe that the anionic form of the drug sufficiently approach membrane interface, where acid-base balance is most probably highly modified, thus favoring insertion and permeation of the drug in its neutral form, for which the preferred location is deeper in the bilayer and ΔG_{cross} is lower. The latter result is particularly important as many drugs exhibit pK_a in the physiological pH range, thus existing in various charge states. Interestingly, molecular size poorly influences ΔG -profiles, which highlights the fluidity of the membrane that allow great conformational reorganization in the presence of drugs. This however does not prevent structural modifications of the bilayer (e.g., modification of area per lipid, thickness, packing). Diffusion coefficients are more sensitive to molecular size, which depends on the membrane region exhibiting different particle densities.

Our work, as well as current theoretical studies, on drug-membrane interaction/insertion/positioning/permeation is particularly promising for near-future biological applications. Such *in silico* prediction should contribute to rational design of novel drugs, paying a particular attention to drug-delivery strategies. Benchmarking studies are still required to show the robustness of MD methodologies, supported by well-thought joint experimental/theoretical studies. However, we are fully convinced that MD-based SPR and later quantitative (Q) SPR studies will pave the way towards *in silico* pharmacology with a real clinical interest.

It must be stressed that real biological membranes are much more complex than simple lipid bilayers; membrane ingredients (e.g., cholesterol) have shown to strongly affect membrane properties and thus drug permeation. The use of more and more complex lipid bilayer models is thus mandatory to better reproduce realistic conditions and predict drug pharmacology.

Among the other near-future challenges of theoretical chemistry of drug-membrane interactions is to increase simulation time and system size. The constant and rapid increase of computation power, following Moore's law, has appeared promising to address these two



issues. Also the simulation methodologies are constantly evolving towards accuracy, e.g., the use of coarse-grained simulations allow simulating very large molecular systems along real-world simulation time.



References

- [1] E. Awoonor-Williams, C. Rowley, Molecular Simulation of Nonfacilitated Membrane Permeation, *bioRxiv*. (2015) 29140. doi:10.1101/029140.
- [2] Book Review: *Lehninger Principles of Biochemistry* - David L. Nelson, Michael M. Cox, (n.d.). <http://www.organic-chemistry.org/books/reviews/1429208929.shtm> (accessed October 9, 2016).
- [3] C.R.H. Raetz, Z. Guan, B.O. Ingram, D.A. Six, F. Song, X. Wang, J. Zhao, Discovery of new biosynthetic pathways: the lipid A story, *J. Lipid Res.* 50 (2009) S103–S108. doi:10.1194/jlr.R800060-JLR200.
- [4] M. Schlame, S. Brody, K.Y. Hostetler, Mitochondrial cardiolipin in diverse eukaryotes, *Eur. J. Biochem.* 212 (1993) 727–733. doi:10.1111/j.1432-1033.1993.tb17711.x.
- [5] M. Nowicki, F. Müller, M. Frentzen, Cardiolipin synthase of *Arabidopsis thaliana*, *FEBS Lett.* 579 (2005) 2161–2165. doi:10.1016/j.febslet.2005.03.007.
- [6] E. Goormaghtigh, P. Chatelain, J. Caspers, J.M. Ruyschaert, Evidence of a specific complex between adriamycin and negatively-charged phospholipids, *Biochim. Biophys. Acta BBA - Biomembr.* 597 (1980) 1–14. doi:10.1016/0005-2736(80)90145-5.
- [7] T.M. Fong, M.G. McNamee, Stabilization of acetylcholine receptor secondary structure by cholesterol and negatively charged phospholipids in membranes, *Biochemistry (Mosc.)*. 26 (1987) 3871–3880. doi:10.1021/bi00387a020.
- [8] P.W. van Dijck, Negatively charged phospholipids and their position in the cholesterol affinity sequence, *Biochim. Biophys. Acta.* 555 (1979) 89–101.
- [9] R. Lipowsky, E. Sackmann, *Structure and Dynamics of Membranes: I. From Cells to Vesicles / II. Generic and Specific Interactions*, Elsevier, 1995.
- [10] T. Róg, M. Pasenkiewicz-Gierula, I. Vattulainen, M. Karttunen, Ordering effects of cholesterol and its analogues, *Biochim. Biophys. Acta BBA - Biomembr.* 1788 (2009) 97–121. doi:10.1016/j.bbamem.2008.08.022.
- [11] E.J. Behrman, V. Gopalan, Cholesterol and Plants, *J. Chem. Educ.* 82 (2005) 1791. doi:10.1021/ed082p1791.
- [12] B. Alberts, A. Johnson, J. Lewis, M. Raff, K. Roberts, P. Walter, *Molecular Biology of the Cell*, 4th ed., Garland Science, 2002.
- [13] H. Jespersen, J.H. Andersen, H.J. Ditzel, O.G. Mouritsen, Lipids, curvature stress, and the action of lipid prodrugs: Free fatty acids and lysolipid enhancement of drug transport across liposomal membranes, *Biochimie.* 94 (2012) 2–10. doi:10.1016/j.biochi.2011.07.029.
- [14] G. Lindblom, G. Orädd, Lipid lateral diffusion and membrane heterogeneity, *Biochim. Biophys. Acta BBA - Biomembr.* 1788 (2009) 234–244. doi:10.1016/j.bbamem.2008.08.016.
- [15] F.-X. Contreras, L. Sánchez-Magraner, A. Alonso, F.M. Goñi, Transbilayer (flip-flop) lipid motion and lipid scrambling in membranes, *FEBS Lett.* 584 (2010) 1779–1786. doi:10.1016/j.febslet.2009.12.049.



- [16] N. Sapay, W.F.D. Bennett, D.P. Tieleman, Molecular simulations of lipid flip-flop in the presence of model transmembrane helices, *Biochemistry (Mosc.)*. 49 (2010) 7665–7673. doi:10.1021/bi100878q.
- [17] M. Eeman, M. Deleu, From biological membranes to biomimetic model membranes, *Base*. (2010). <http://popups.ulg.ac.be/1780-4507/index.php?id=6568> (accessed August 31, 2016).
- [18] D. Lingwood, K. Simons, Lipid rafts as a membrane-organizing principle, *Science*. 327 (2010) 46–50. doi:10.1126/science.1174621.
- [19] K. Simons, W.L.C. Vaz, Model Systems, Lipid Rafts, and Cell Membranes1, *Annu. Rev. Biophys. Biomol. Struct.* 33 (2004) 269–295. doi:10.1146/annurev.biophys.32.110601.141803.
- [20] W.F.D. Bennett, D.P. Tieleman, Computer simulations of lipid membrane domains, *Biochim. Biophys. Acta*. 1828 (2013) 1765–1776. doi:10.1016/j.bbamem.2013.03.004.
- [21] M.L. Berkowitz, Detailed molecular dynamics simulations of model biological membranes containing cholesterol, *Biochim. Biophys. Acta BBA - Biomembr.* 1788 (2009) 86–96. doi:10.1016/j.bbamem.2008.09.009.
- [22] R.N.A.H.L. Todd P. W. McMullen, Cholesterol–phospholipid interactions, the liquid-ordered phase and lipid rafts in model and biological membranes, *Curr. Opin. Colloid Amp Interface Sci.* 8 (2004) 459–468. doi:10.1016/j.cocis.2004.01.007.
- [23] S. Banjade, M.K. Rosen, Phase transitions of multivalent proteins can promote clustering of membrane receptors, *eLife*. 3 (2014) e04123. doi:10.7554/eLife.04123.
- [24] G. van Meer, D.R. Voelker, G.W. Feigenson, Membrane lipids: where they are and how they behave, *Nat. Rev. Mol. Cell Biol.* 9 (2008) 112–124. doi:10.1038/nrm2330.
- [25] B. Fadeel, D. Xue, The ins and outs of phospholipid asymmetry in the plasma membrane: roles in health and disease, *Crit. Rev. Biochem. Mol. Biol.* 44 (2009) 264–277. doi:10.1080/10409230903193307.
- [26] M.R. Yeaman, N.Y. Yount, Mechanisms of Antimicrobial Peptide Action and Resistance, *Pharmacol. Rev.* 55 (2003) 27–55. doi:10.1124/pr.55.1.2.
- [27] M.A. Lampe, M.L. Williams, P.M. Elias, Human epidermal lipids: characterization and modulations during differentiation, *J. Lipid Res.* 24 (1983) 131–140.
- [28] M.A. Lampe, A.L. Burlingame, J. Whitney, M.L. Williams, B.E. Brown, E. Roitman, P.M. Elias, Human stratum corneum lipids: characterization and regional variations, *J. Lipid Res.* 24 (1983) 120–130.
- [29] Comparison of rat epidermal keratinocyte organotypic culture (ROC) with intact human skin: Lipid composition and thermal phase behavior of the stratum corneum, (n.d.). <http://www.sciencedirect.com/science/article/pii/S0005273607004786> (accessed August 24, 2016).
- [30] J.M. Jungersted, L.I. Hellgren, T. Drachmann, G.B.E. Jemec, T. Agner, Validation of cyanoacrylate method for collection of stratum corneum in human skin for lipid analysis, *Skin Pharmacol. Physiol.* 23 (2010) 62–67. doi:10.1159/000265676.
- [31] E.H. Mojumdar, G.S. Gooris, D. Groen, D.J. Barlow, M.J. Lawrence, B. Demé, J.A. Bouwstra, Stratum corneum lipid matrix: Location of acyl ceramide and cholesterol in the unit



cell of the long periodicity phase, *Biochim. Biophys. Acta BBA - Biomembr.* 1858 (2016) 1926–1934. doi:10.1016/j.bbamem.2016.05.006.

[32] G.K. Menon, G.W. Cleary, M.E. Lane, The structure and function of the stratum corneum, *Int. J. Pharm.* 435 (2012) 3–9. doi:10.1016/j.ijpharm.2012.06.005.

[33] I. Plasencia, L. Norlén, L.A. Bagatolli, Direct Visualization of Lipid Domains in Human Skin Stratum Corneum's Lipid Membranes: Effect of pH and Temperature, *Biophys. J.* 93 (2007) 3142–3155. doi:10.1529/biophysj.106.096164.

[34] T.J. Silhavy, D. Kahne, S. Walker, *The Bacterial Cell Envelope*, Cold Spring Harb. Perspect. Biol. 2 (2010). doi:10.1101/cshperspect.a000414.

[35] S. Brown, J.P. Santa Maria, S. Walker, Wall Teichoic Acids of Gram-Positive Bacteria, *Annu. Rev. Microbiol.* 67 (2013). doi:10.1146/annurev-micro-092412-155620.

[36] F. Nazzaro, F. Fratianni, L. De Martino, R. Coppola, V. De Feo, Effect of Essential Oils on Pathogenic Bacteria, *Pharmaceuticals.* 6 (2013) 1451–1474. doi:10.3390/ph6121451.

[37] C. Sohlenkamp, O. Geiger, Bacterial membrane lipids: diversity in structures and pathways, *FEMS Microbiol. Rev.* 40 (2016) 133–159. doi:10.1093/femsre/fuv008.

[38] A.M. Seddon, D. Casey, R.V. Law, A. Gee, R.H. Templer, O. Ces, Drug interactions with lipid membranes, *Chem. Soc. Rev.* 38 (2009) 2509. doi:10.1039/b813853m.

[39] Biology, (n.d.). <http://highered.mheducation.com/sites/0073031208/index.html> (accessed August 30, 2016).

[40] K. Sugano, M. Kansy, P. Artursson, A. Avdeef, S. Bendels, L. Di, G.F. Ecker, B. Faller, H. Fischer, G. Gerebtzoff, H. Lennernaes, F. Senner, Coexistence of passive and carrier-mediated processes in drug transport, *Nat. Rev. Drug Discov.* 9 (2010) 597–614. doi:10.1038/nrd3187.

[41] D. Smith, P. Artursson, A. Avdeef, L. Di, G.F. Ecker, B. Faller, J.B. Houston, M. Kansy, E.H. Kerns, S.D. Krämer, H. Lennernäs, H. van de Waterbeemd, K. Sugano, B. Testa, Passive Lipoidal Diffusion and Carrier-Mediated Cell Uptake Are Both Important Mechanisms of Membrane Permeation in Drug Disposition, *Mol. Pharm.* 11 (2014) 1727–1738. doi:10.1021/mp400713v.

[42] Q. Al-Awqati, One hundred years of membrane permeability: does Overton still rule?, *Nat. Cell Biol.* 1 (1999) E201–E202. doi:10.1038/70230.

[43] D. Sholefield, A. Sebt, A. Harris, *Pharmacology Case Studies for Nurse Prescribers*, M&K Update Ltd, 2015.

[44] R. Vácha, F.J. Martinez-Veracochea, D. Frenkel, Receptor-Mediated Endocytosis of Nanoparticles of Various Shapes, *Nano Lett.* 11 (2011) 5391–5395. doi:10.1021/nl2030213.

[45] H. Ding, Y. Ma, Theoretical and Computational Investigations of Nanoparticle–Biomembrane Interactions in Cellular Delivery, *Small.* 11 (2015) 1055–1071. doi:10.1002/smll.201401943.

[46] H. Ding, Y. Ma, Role of physicochemical properties of coating ligands in receptor-mediated endocytosis of nanoparticles, *Biomaterials.* 33 (2012) 5798–5802. doi:10.1016/j.biomaterials.2012.04.055.



- [47] E.L. da Rocha, G.F. Caramori, C.R. Rambo, Nanoparticle translocation through a lipid bilayer tuned by surface chemistry, *Phys. Chem. Chem. Phys.* 15 (2013) 2282–2290. doi:10.1039/C2CP44035K.
- [48] D.W. Borhani, D.E. Shaw, The future of molecular dynamics simulations in drug discovery, *J. Comput. Aided Mol. Des.* 26 (2011) 15–26. doi:10.1007/s10822-011-9517-y.
- [49] A.R. Leach, *Molecular Modelling: Principles and Applications*, Pearson Education, 2001.
- [50] S.J. Marrink, H.J. Risselada, S. Yefimov, D.P. Tieleman, A.H. de Vries, The MARTINI Force Field: Coarse Grained Model for Biomolecular Simulations, *J. Phys. Chem. B.* 111 (2007) 7812–7824. doi:10.1021/jp071097f.
- [51] W.L. Jorgensen, J. Tirado-Rives, Potential energy functions for atomic-level simulations of water and organic and biomolecular systems, *Proc. Natl. Acad. Sci. U. S. A.* 102 (2005) 6665–6670. doi:10.1073/pnas.0408037102.
- [52] C. Caleman, P.J. van Maaren, M. Hong, J.S. Hub, L.T. Costa, D. van der Spoel, Force Field Benchmark of Organic Liquids: Density, Enthalpy of Vaporization, Heat Capacities, Surface Tension, Isothermal Compressibility, Volumetric Expansion Coefficient, and Dielectric Constant, *J. Chem. Theory Comput.* 8 (2012) 61–74. doi:10.1021/ct200731v.
- [53] G.A. Kaminski, R.A. Friesner, J. Tirado-Rives, W.L. Jorgensen, Evaluation and Reparametrization of the OPLS-AA Force Field for Proteins via Comparison with Accurate Quantum Chemical Calculations on Peptides†, *J. Phys. Chem. B.* 105 (2001) 6474–6487. doi:10.1021/jp003919d.
- [54] J.W. Ponder, D.A. Case, Force Fields for Protein Simulations, in: V. Daggett (Ed.), *Adv. Protein Chem., Academic Press*, 2003: pp. 27–85. <http://www.sciencedirect.com/science/article/pii/S006532330366002X> (accessed May 7, 2015).
- [55] K.A. Beauchamp, Y.-S. Lin, R. Das, V.S. Pande, Are Protein Force Fields Getting Better? A Systematic Benchmark on 524 Diverse NMR Measurements, *J. Chem. Theory Comput.* 8 (2012) 1409–1414. doi:10.1021/ct2007814.
- [56] T.E. Cheatham, D.A. Case, Twenty-five years of nucleic acid simulations, *Biopolymers.* 99 (2013) 969–977. doi:10.1002/bip.22331.
- [57] J. Šponer, X. Cang, T.E. Cheatham III, Molecular dynamics simulations of G-DNA and perspectives on the simulation of nucleic acid structures, *Methods.* 57 (2012) 25–39. doi:10.1016/j.ymeth.2012.04.005.
- [58] D.E. Condon, I. Yildirim, S.D. Kennedy, B.C. Mort, R. Kierzek, D.H. Turner, Optimization of an AMBER Force Field for the Artificial Nucleic Acid, LNA, and Benchmarking with NMR of L(CAAU), *J. Phys. Chem. B.* 118 (2014) 1216–1228. doi:10.1021/jp408909t.
- [59] M. Krepl, M. Zgarbová, P. Stadlbauer, M. Otyepka, P. Banáš, J. Koča, T.E. Cheatham, P. Jurečka, J. Šponer, Reference Simulations of Noncanonical Nucleic Acids with Different χ Variants of the AMBER Force Field: Quadruplex DNA, Quadruplex RNA, and Z-DNA, *J. Chem. Theory Comput.* 8 (2012) 2506–2520. doi:10.1021/ct300275s.



- [60] M. Krepl, M. Havrila, P. Stadlbauer, P. Banas, M. Otyepka, J. Pasulka, R. Stefl, J. Sponer, Can We Execute Stable Microsecond-Scale Atomistic Simulations of Protein–RNA Complexes?, *J. Chem. Theory Comput.* 11 (2015) 1220–1243. doi:10.1021/ct5008108.
- [61] O. Berger, O. Edholm, F. Jähnig, Molecular dynamics simulations of a fluid bilayer of dipalmitoylphosphatidylcholine at full hydration, constant pressure, and constant temperature., *Biophys. J.* 72 (1997) 2002–2013.
- [62] J.P.M. Jämbeck, A.P. Lyubartsev, Derivation and Systematic Validation of a Refined All-Atom Force Field for Phosphatidylcholine Lipids, *J. Phys. Chem. B.* 116 (2012) 3164–3179. doi:10.1021/jp212503e.
- [63] S.-W. Chiu, S.A. Pandit, H.L. Scott, E. Jakobsson, An improved united atom force field for simulation of mixed lipid bilayers, *J. Phys. Chem. B.* 113 (2009) 2748–2763. doi:10.1021/jp807056c.
- [64] C. Oostenbrink, T.A. Soares, N.F.A. Vegt, W.F. Gunsteren, Validation of the 53A6 GROMOS force field, *Eur. Biophys. J.* 34 (2005) 273–284. doi:10.1007/s00249-004-0448-6.
- [65] J.B. Klauda, R.M. Venable, J.A. Freites, J.W. O'Connor, D.J. Tobias, C. Mondragon-Ramirez, I. Vorobyov, A.D.J. MacKerell, R.W. Pastor, Update of the CHARMM all-atom additive force field for lipids: validation on six lipid types, *J. Phys. Chem. B.* 114 (2010) 7830–7843. doi:10.1021/jp101759q.
- [66] R.W. Pastor, A.D. MacKerell, Development of the CHARMM Force Field for Lipids, *J. Phys. Chem. Lett.* 2 (2011) 1526–1532. doi:10.1021/jz200167q.
- [67] C.J. Dickson, B.D. Madej, Å.A. Skjevik, R.M. Betz, K. Teigen, I.R. Gould, R.C. Walker, Lipid14: The Amber Lipid Force Field, *J. Chem. Theory Comput.* 10 (2014) 865–879. doi:10.1021/ct4010307.
- [68] J.L. Klepeis, K. Lindorff-Larsen, R.O. Dror, D.E. Shaw, Long-timescale molecular dynamics simulations of protein structure and function, *Curr. Opin. Struct. Biol.* 19 (2009) 120–127. doi:10.1016/j.sbi.2009.03.004.
- [69] H.J.C. Berendsen, Transport Properties Computed by Linear Response through Weak Coupling to a Bath, in: M. Meyer, V. Pontikis (Eds.), *Comput. Simul. Mater. Sci.*, Springer Netherlands, 1991: pp. 139–155. http://link.springer.com/chapter/10.1007/978-94-011-3546-7_7 (accessed May 12, 2015).
- [70] S. Nosé, A molecular dynamics method for simulations in the canonical ensemble, *Mol. Phys.* 52 (1984) 255–268. doi:10.1080/00268978400101201.
- [71] W.G. Hoover, Canonical dynamics: Equilibrium phase-space distributions, *Phys. Rev. A.* 31 (1985) 1695–1697. doi:10.1103/PhysRevA.31.1695.
- [72] M. Parrinello, A. Rahman, Polymorphic transitions in single crystals: A new molecular dynamics method, *J. Appl. Phys.* 52 (1981) 7182–7190.
- [73] S. Nosé, M.L. Klein, Constant pressure molecular dynamics for molecular systems, *Mol. Phys.* 50 (1983) 1055–1076. doi:10.1080/00268978300102851.
- [74] H.J.C. Berendsen, J.P.M. Postma, W.F. van Gunsteren, J. Hermans, Interaction Models for Water in Relation to Protein Hydration, in: B. Pullman (Ed.), *Intermolecular Forces*, Springer Netherlands, 1981: pp. 331–342. http://link.springer.com/chapter/10.1007/978-94-015-7658-1_21 (accessed May 11, 2015).



- [75] H.J.C. Berendsen, J.R. Grigera, T.P. Straatsma, The missing term in effective pair potentials, *J. Phys. Chem.* 91 (1987) 6269–6271. doi:10.1021/j100308a038.
- [76] W.L. Jorgensen, J. Chandrasekhar, J.D. Madura, R.W. Impey, M.L. Klein, Comparison of simple potential functions for simulating liquid water, *J. Chem. Phys.* 79 (1983) 926–935. doi:10.1063/1.445869.
- [77] M. Orsi, J.W. Essex, Chapter 4. Passive Permeation Across Lipid Bilayers: a Literature Review, in: M.S.P. Sansom, P.C. Biggin (Eds.), *Mol. Simul. Biomembr.*, Royal Society of Chemistry, Cambridge, 2010: pp. 76–90. <http://ebook.rsc.org/?DOI=10.1039/9781849732154-00076> (accessed July 13, 2016).
- [78] F. Di Meo, G. Fabre, K. Berka, T. Ossman, B. Chantemargue, M. Palonciová, P. Marquet, M. Otyepka, P. Trouillas, In silico pharmacology: Drug membrane partitioning and crossing, *Pharmacol. Res.* 111 (2016) 471–486. doi:10.1016/j.phrs.2016.06.030.
- [79] S.J. Marrink, H.J.C. Berendsen, Permeation Process of Small Molecules across Lipid Membranes Studied by Molecular Dynamics Simulations, *J. Phys. Chem.* 100 (1996) 16729–16738. doi:10.1021/jp952956f.
- [80] J. Kästner, Umbrella sampling, *Wiley Interdiscip. Rev. Comput. Mol. Sci.* 1 (2011) 932–942. doi:10.1002/wcms.66.
- [81] A. Klamt, U. Huniar, S. Spycher, J. Keldenich, COSMOmic: A Mechanistic Approach to the Calculation of Membrane–Water Partition Coefficients and Internal Distributions within Membranes and Micelles, *J. Phys. Chem. B.* 112 (2008) 12148–12157. doi:10.1021/jp801736k.
- [82] A. Klamt, F. Eckert, W. Arlt, COSMO-RS: An Alternative to Simulation for Calculating Thermodynamic Properties of Liquid Mixtures, *Annu. Rev. Chem. Biomol. Eng.* 1 (2010) 101–122. doi:10.1146/annurev-chembioeng-073009-100903.
- [83] A. Klamt, U. Huniar, S. Spycher, J. Keldenich, COSMOmic: A Mechanistic Approach to the Calculation of Membrane–Water Partition Coefficients and Internal Distributions within Membranes and Micelles, *J. Phys. Chem. B.* 112 (2008) 12148–12157. doi:10.1021/jp801736k.
- [84] M. Palonciová, G. Fabre, R.H. DeVane, P. Trouillas, K. Berka, M. Otyepka, Benchmarking of Force Fields for Molecule–Membrane Interactions, *J. Chem. Theory Comput.* 10 (2014) 4143–4151. doi:10.1021/ct500419b.
- [85] M. Deleu, J.-M. Crowet, M.N. Nasir, L. Lins, Complementary biophysical tools to investigate lipid specificity in the interaction between bioactive molecules and the plasma membrane: A review, *Biochim. Biophys. Acta BBA - Biomembr.* 1838 (2014) 3171–3190. doi:10.1016/j.bbamem.2014.08.023.
- [86] J.P.M. Jämbeck, A.P. Lyubartsev, Derivation and Systematic Validation of a Refined All-Atom Force Field for Phosphatidylcholine Lipids, *J. Phys. Chem. B.* 116 (2012) 3164–3179. doi:10.1021/jp212503e.
- [87] J.P.M. Jämbeck, A.P. Lyubartsev, An Extension and Further Validation of an All-Atomistic Force Field for Biological Membranes, *J. Chem. Theory Comput.* 8 (2012) 2938–2948. doi:10.1021/ct300342n.



- [88] J.P.M. Jämbeck, A.P. Lyubartsev, Another Piece of the Membrane Puzzle: Extending Slipids Further, *J. Chem. Theory Comput.* 9 (2013) 774–784. doi:10.1021/ct300777p.
- [89] H.I. Petrache, S.W. Dodd, M.F. Brown, Area per Lipid and Acyl Length Distributions in Fluid Phosphatidylcholines Determined by ²H NMR Spectroscopy, *Biophys. J.* 79 (2000) 3172–3192. doi:10.1016/S0006-3495(00)76551-9.
- [90] J.F. Nagle, R. Zhang, S. Tristram-Nagle, W. Sun, H.I. Petrache, R.M. Suter, X-ray structure determination of fully hydrated L alpha phase dipalmitoylphosphatidylcholine bilayers., *Biophys. J.* 70 (1996) 1419–1431.
- [91] N. Kučerka, S. Tristram-Nagle, J.F. Nagle, Structure of Fully Hydrated Fluid Phase Lipid Bilayers with Monounsaturated Chains, *J. Membr. Biol.* 208 (2006) 193–202. doi:10.1007/s00232-005-7006-8.
- [92] N. Kučerka, M.-P. Nieh, J. Katsaras, Fluid phase lipid areas and bilayer thicknesses of commonly used phosphatidylcholines as a function of temperature, *Biochim. Biophys. Acta BBA - Biomembr.* 1808 (2011) 2761–2771. doi:10.1016/j.bbamem.2011.07.022.
- [93] J.F. Nagle, S. Tristram-Nagle, Structure of lipid bilayers, *Biochim. Biophys. Acta BBA - Rev. Biomembr.* 1469 (2000) 159–195. doi:10.1016/S0304-4157(00)00016-2.
- [94] N. Kučerka, J.F. Nagle, J.N. Sachs, S.E. Feller, J. Pencer, A. Jackson, J. Katsaras, Lipid Bilayer Structure Determined by the Simultaneous Analysis of Neutron and X-Ray Scattering Data, *Biophys. J.* 95 (2008) 2356–2367. doi:10.1529/biophysj.108.132662.
- [95] Wiley: Drug-Membrane Interactions: Analysis, Drug Distribution, Modeling, Volume 15 - Joachim K. Seydel, Michael Wiese, Raimund Mannhold, et al, (n.d.). <http://eu.wiley.com/WileyCDA/WileyTitle/productCd-3527616497.html> (accessed March 18, 2016).
- [96] S. Balaz, Modeling Kinetics of Subcellular Disposition of Chemicals, *Chem. Rev.* 109 (2009) 1793–1899. doi:10.1021/cr030440j.
- [97] G.M. Cooper, *The Cell*, 2nd edition. A Molecular Approach, 2nd ed., Sinauer Associates, Sunderland, MA, USA, 2000.
- [98] S.J. Singer, G.L. Nicolson, The fluid mosaic model of the structure of cell membranes., *Science.* 175 (1972) 720–31.
- [99] I. Iwai, H. Han, L. den Hollander, S. Svensson, L.-G. Ofverstedt, J. Anwar, J. Brewer, M. Bloksgaard, A. Laloef, D. Nosek, S. Masich, L. a Bagatolli, U. Skoglund, L. Norlén, L. Den Hollander, S. Svensson, L.-G. Ofverstedt, J. Anwar, J. Brewer, M. Bloksgaard, A. Laloef, D. Nosek, S. Masich, L. a Bagatolli, U. Skoglund, L. Norlén, The Human Skin Barrier Is Organized as Stacked Bilayers of Fully Extended Ceramides with Cholesterol Molecules Associated with the Ceramide Sphingoid Moiety., *J. Invest. Dermatol.* 132 (2012) 2215–2225. doi:10.1038/jid.2012.43.
- [100] Y. Arinaminpathy, E. Khurana, D.M. Engelman, M.B. Gerstein, Computational analysis of membrane proteins: the largest class of drug targets., *Drug Discov. Today.* 14 (2009) 1130–5. doi:10.1016/j.drudis.2009.08.006.
- [101] J.P. Overington, B. Al-Lazikani, A.L. Hopkins, How many drug targets are there?, *Nat. Rev. Drug Discov.* 5 (2006) 993–996. doi:10.1038/nrd2199.



- [102] F.R. Salsbury, Molecular Dynamics Simulations of Protein Dynamics and their relevance to drug discovery, *Curr. Opin. Pharmacol.* 10 (2010) 738–744. doi:10.1016/j.coph.2010.09.016.
- [103] S. Nagar, K. Korzekwa, Commentary: Nonspecific Protein Binding versus Membrane Partitioning: It Is Not Just Semantics, *Drug Metab. Dispos.* 40 (2012) 1649–1652. doi:10.1124/dmd.112.046599.
- [104] S. Endo, B.I. Escher, K.-U. Goss, Capacities of Membrane Lipids to Accumulate Neutral Organic Chemicals, *Environ. Sci. Technol.* 45 (2011) 5912–5921. doi:10.1021/es200855w.
- [105] D. Smith, P. Artursson, A. Avdeef, L. Di, G.F. Ecker, B. Faller, J.B. Houston, M. Kansy, E.H. Kerns, S.D. Krämer, H. Lennernäs, H. van de Waterbeemd, K. Sugano, B. Testa, Passive Lipoidal Diffusion and Carrier-Mediated Cell Uptake Are Both Important Mechanisms of Membrane Permeation in Drug Disposition, *Mol. Pharm.* 11 (2014) 1727–1738. doi:10.1021/mp400713v.
- [106] D. Bassolino-Klimas, H.E. Alper, T.R. Stouch, Solute diffusion in lipid bilayer membranes: An atomic level study by molecular dynamics simulation, *Biochemistry (Mosc.)* 32 (1993) 12624–12637. doi:10.1021/bi00210a010.
- [107] D. Bassolino-Klimas, H.E. Alper, T.R. Stouch, Mechanism of Solute Diffusion through Lipid Bilayer Membranes by Molecular Dynamics Simulation, *J. Am. Chem. Soc.* 117 (1995) 4118–4129. doi:10.1021/ja00119a028.
- [108] S.J. Marrink, H.J.C. Berendsen, Permeation Process of Small Molecules across Lipid Membranes Studied by Molecular Dynamics Simulations, *J. Phys. Chem.* 100 (1996) 16729–16738. doi:10.1021/jp952956f.
- [109] R.O. Dror, R.M. Dirks, J.P. Grossman, H. Xu, D.E. Shaw, Biomolecular Simulation: A Computational Microscope for Molecular Biology, *Annu. Rev. Biophys.* 41 (2012) 429–452. doi:10.1146/annurev-biophys-042910-155245.
- [110] M. Karplus, J.A. McCammon, Molecular dynamics simulations of biomolecules, *Nat. Struct. Mol. Biol.* 9 (2002) 646–652. doi:10.1038/nsb0902-646.
- [111] M. Karplus, J. Kuriyan, Molecular dynamics and protein function, *Proc. Natl. Acad. Sci. U. S. A.* 102 (2005) 6679–6685. doi:10.1073/pnas.0408930102.
- [112] W. Kopeć, J. Telenius, H. Khandelia, Molecular dynamics simulations of the interactions of medicinal plant extracts and drugs with lipid bilayer membranes, *FEBS J.* 280 (2013) 2785–2805. doi:10.1111/febs.12286.
- [113] D.A. Smith, Discovery and ADMET: Where are We Now, *Curr. Top. Med. Chem.* 11 (2011) 467–481.
- [114] J.-M. Alakoskela, P. Vitovic, P.K.J. Kinnunen, Screening for the drug-phospholipid interaction: correlation to phospholipidosis., *ChemMedChem.* 4 (2009) 1224–51. doi:10.1002/cmdc.200900052.
- [115] S. Natesan, V. Lukacova, M. Peng, R. Subramaniam, S. Lynch, Z. Wang, R. Tandlich, S. Balaz, Structure-Based Prediction of Drug Distribution Across the Headgroup and Core Strata of a Phospholipid Bilayer Using Surrogate Phases, *Mol. Pharm.* 11 (2014) 3577–3595. doi:10.1021/mp5003366.



- [116] S. Amjad-Iranagh, A. Yousefpour, P. Haghighi, H. Modarress, Effects of protein binding on a lipid bilayer containing local anesthetic articaine, and the potential of mean force calculation: a molecular dynamics simulation approach, *J. Mol. Model.* 19 (2013) 3831–3842. doi:10.1007/s00894-013-1917-6.
- [117] R.C. Bernardi, D.E.B. Gomes, R. Gobato, C.A. Taft, A.T. Ota, P.G. Pascutti, Molecular dynamics study of biomembrane/local anesthetics interactions, *Mol. Phys.* 107 (2009) 1437–1443. doi:10.1080/00268970902926238.
- [118] J.J.L. Cascales, S.D.O. Costa, R.D. Porasso, Thermodynamic study of benzocaine insertion into different lipid bilayers, *J. Chem. Phys.* 135 (2011) 135103. doi:10.1063/1.3643496.
- [119] C.-J. Högberg, A. Maliniak, A.P. Lyubartsev, Dynamical and structural properties of charged and uncharged lidocaine in a lipid bilayer, *Biophys. Chem.* 125 (2007) 416–424. doi:10.1016/j.bpc.2006.10.005.
- [120] L.J. Martin, R. Chao, B. Corry, Molecular dynamics simulation of the partitioning of benzocaine and phenytoin into a lipid bilayer, *Biophys. Chem.* 185 (2014) 98–107. doi:10.1016/j.bpc.2013.12.003.
- [121] M.F. Martini, M. Pickholz, Molecular dynamics study of uncharged bupivacaine enantiomers in phospholipid bilayers, *Int. J. Quantum Chem.* 112 (2012) 3341–3345. doi:10.1002/qua.24208.
- [122] M. Pickholz, L. Fernandes Fraceto, E. de Paula, Distribution of neutral prilocaine in a phospholipid bilayer: Insights from molecular dynamics simulations, *Int. J. Quantum Chem.* 108 (2008) 2386–2391. doi:10.1002/qua.21767.
- [123] R.D. Porasso, W.F. Drew Bennett, S.D. Oliveira-Costa, J.J. López Cascales, Study of the Benzocaine Transfer from Aqueous Solution to the Interior of a Biological Membrane, *J. Phys. Chem. B.* 113 (2009) 9988–9994. doi:10.1021/jp902931s.
- [124] Å.A. Skjevik, B.E. Haug, H. Lygre, K. Teigen, Intramolecular hydrogen bonding in articaine can be related to superior bone tissue penetration: A molecular dynamics study, *Biophys. Chem.* 154 (2011) 18–25. doi:10.1016/j.bpc.2010.12.002.
- [125] P. a Zapata-Morin, F.J. Sierra-Valdez, J.C. Ruiz-Suárez, The interaction of local anesthetics with lipid membranes., *J. Mol. Graph. Model.* 53C (2014) 200–205. doi:10.1016/j.jmglm.2014.08.001.
- [126] E.H. Mojumdar, A.P. Lyubartsev, Molecular dynamics simulations of local anesthetic articaine in a lipid bilayer, *Biophys. Chem.* 153 (2010) 27–35. doi:10.1016/j.bpc.2010.10.001.
- [127] D.S. Ragsdale, J.C. McPhee, T. Scheuer, W.A. Catterall, Molecular determinants of state-dependent block of Na⁺ channels by local anesthetics, *Science.* 265 (1994) 1724–1728.
- [128] G.M. Lipkind, H.A. Fozzard, Molecular Modeling of Local Anesthetic Drug Binding by Voltage-Gated Sodium Channels, *Mol. Pharmacol.* 68 (2005) 1611–1622. doi:10.1124/mol.105.014803.
- [129] M.F. Sheets, D.A. Hanck, Molecular Action of Lidocaine on the Voltage Sensors of Sodium Channels, *J. Gen. Physiol.* 121 (2003) 163–175. doi:10.1085/jgp.20028651.



- [130] P.-L. Chau, New insights into the molecular mechanisms of general anaesthetics, *Br. J. Pharmacol.* 161 (2010) 288–307. doi:10.1111/j.1476-5381.2010.00891.x.
- [131] H. Jerabek, G. Pabst, M. Rappolt, T. Stockner, Membrane-mediated effect on ion channels induced by the anesthetic drug ketamine., *J. Am. Chem. Soc.* 132 (2010) 7990–7997. doi:10.1021/ja910843d.
- [132] E. Yamamoto, T. Akimoto, H. Shimizu, Y. Hirano, M. Yasui, K. Yasuoka, Diffusive Nature of Xenon Anesthetic Changes Properties of a Lipid Bilayer: Molecular Dynamics Simulations, *J. Phys. Chem. B.* 116 (2012) 8989–8995. doi:10.1021/jp303330c.
- [133] B. Fábíán, M. Darvas, S. Picaud, M. Sega, P. Jedlovszky, The effect of anaesthetics on the properties of a lipid membrane in the biologically relevant phase: a computer simulation study, *Phys. Chem. Chem. Phys.* 17 (2015) 14750–14760. doi:10.1039/C5CP00851D.
- [134] P.-L. Chau, K.M. Tu, K.K. Liang, I.T. Todorov, S.J. Roser, R. Barker, N. Matubayasi, The effect of pressure on halothane binding to hydrated DMPC bilayers, *Mol. Phys.* 110 (2012) 1461–1467. doi:10.1080/00268976.2012.659682.
- [135] K.M. Tu, N. Matubayasi, K.K. Liang, I.T. Todorov, S.L. Chan, P.-L. Chau, A possible molecular mechanism for the pressure reversal of general anaesthetics: Aggregation of halothane in POPC bilayers at high pressure, *Chem. Phys. Lett.* 543 (2012) 148–154. doi:10.1016/j.cplett.2012.06.044.
- [136] J. V. Levy, Myocardial and local anesthetic actions of β -adrenergic receptor blocking drugs: Relationship to physicochemical properties, *Eur. J. Pharmacol.* 2 (1968) 250–257. doi:10.1016/0014-2999(68)90074-5.
- [137] A.D. Auerbach, L. Goldman, beta-Blockers and reduction of cardiac events in noncardiac surgery: scientific review, *JAMA.* 287 (2002) 1435–1444.
- [138] M. Mizogami, K. Takakura, H. Tsuchiya, The interactivities with lipid membranes differentially characterize selective and nonselective β 1-blockers, *Eur. J. Anaesthesiol.* 27 (2010) 829–834. doi:10.1097/EJA.0b013e32833bf5e4.
- [139] G. Först, L. Cwiklik, P. Jurkiewicz, R. Schubert, M. Hof, Interactions of beta-blockers with model lipid membranes: Molecular view of the interaction of acebutolol, oxprenolol, and propranolol with phosphatidylcholine vesicles by time-dependent fluorescence shift and molecular dynamics simulations, *Eur. J. Pharm. Biopharm.* 87 (2014) 559–569. doi:10.1016/j.ejpb.2014.03.013.
- [140] L.M. Lichtenberger, Where is the evidence that cyclooxygenase inhibition is the primary cause of nonsteroidal anti-inflammatory drug (NSAID)-induced gastrointestinal injury?: Topical injury revisited, *Biochem. Pharmacol.* 61 (2001) 631–637. doi:10.1016/S0006-2952(00)00576-1.
- [141] L.M. Lichtenberger, Y. Zhou, V. Jayaraman, J.R. Doyen, R.G. O’Neil, E.J. Dial, D.E. Volk, D.G. Gorenstein, M.B. Boggara, R. Krishnamoorti, Insight into NSAID-induced membrane alterations, pathogenesis and therapeutics: characterization of interaction of NSAIDs with phosphatidylcholine., *Biochim. Biophys. Acta.* 1821 (2012) 994–1002. doi:10.1016/j.bbailip.2012.04.002.



- [142] M.B. Boggara, M. Mihailescu, R. Krishnamoorti, Structural Association of Nonsteroidal Anti-Inflammatory Drugs with Lipid Membranes, *J. Am. Chem. Soc.* 134 (2012) 19669–19676. doi:10.1021/ja3064342.
- [143] H. Khandelia, S. Witzke, O.G. Mouritsen, Interaction of Salicylate and a Terpenoid Plant Extract with Model Membranes: Reconciling Experiments and Simulations, *Biophys. J.* 99 (2010) 3887–3894. doi:10.1016/j.bpj.2010.11.009.
- [144] C.B. Fox, R.A. Horton, J.M. Harris, Detection of Drug–Membrane Interactions in Individual Phospholipid Vesicles by Confocal Raman Microscopy, *Anal. Chem.* 78 (2006) 4918–4924. doi:10.1021/ac0605290.
- [145] M.B. Boggara, R. Krishnamoorti, Partitioning of nonsteroidal antiinflammatory drugs in lipid membranes: a molecular dynamics simulation study., *Biophys J.* 98 (2010) 586–95. doi:10.1016/j.bpj.2009.10.046.
- [146] K. Berka, T. Hendrychová, P. Anzenbacher, M. Otyepka, Membrane Position of Ibuprofen Agrees with Suggested Access Path Entrance to Cytochrome P450 2C9 Active Site, *J. Phys. Chem. A.* 115 (2011) 11248–11255. doi:10.1021/jp204488j.
- [147] D. Morin, T. Hauet, M. Spedding, J. Tillement, Mitochondria as target for antiischemic drugs, *Adv. Drug Deliv. Rev.* 49 (2001) 151–174.
- [148] R. Thuillier, G. Allain, S. Giraud, T. Saintyves, P.O. Delpech, P. Couturier, C. Billault, E. Marchand, L. Vaahtera, J. Parkkinen, T. Hauet, Cyclodextrin curcumin formulation improves outcome in a preclinical pig model of marginal kidney transplantation, *Am. J. Transplant. Off. J. Am. Soc. Transplant. Am. Soc. Transpl. Surg.* 14 (2014) 1073–1083. doi:10.1111/ajt.12661.
- [149] K. Ioku, T. Tsushida, Y. Takei, N. Nakatani, J. Terao, Antioxidative activity of quercetin and quercetin monoglucosides in solution and phospholipid bilayers, *Biochim. Biophys. Acta BBA - Biomembr.* 1234 (1995) 99–104. doi:10.1016/0005-2736(94)00262-N.
- [150] L. Movileanu, I. Neagoe, M.L. Flonta, Interaction of the antioxidant flavonoid quercetin with planar lipid bilayers, *Int. J. Pharm.* 205 (2000) 135–146. doi:10.1016/S0378-5173(00)00503-2.
- [151] A. Arora, M.G. Nair, G.M. Strasburg, Structure–Activity Relationships for Antioxidant Activities of a Series of Flavonoids in a Liposomal System, *Free Radic. Biol. Med.* 24 (1998) 1355–1363. doi:10.1016/S0891-5849(97)00458-9.
- [152] J. Terao, M. Piskula, Q. Yao, Protective effect of epicatechin, epicatechin gallate, and quercetin on lipid peroxidation in phospholipid bilayers, *Arch. Biochem. Biophys.* 308 (1994) 278–284. doi:10.1006/abbi.1994.1039.
- [153] G. Fabre, A. Hänchen, C.-A. Calliste, K. Berka, S. Banala, M. Otyepka, R.D. Süßmuth, P. Trouillas, Lipocarbazole, an efficient lipid peroxidation inhibitor anchored in the membrane, *Bioorg. Med. Chem.* 23 (2015) 4866–4870. doi:10.1016/j.bmc.2015.05.031.
- [154] P. Podloucká, K. Berka, G. Fabre, M. Paloncýová, J.-L. Duroux, M. Otyepka, P. Trouillas, Lipid Bilayer Membrane Affinity Rationalizes Inhibition of Lipid Peroxidation by a Natural Lignan Antioxidant, *J. Phys. Chem. B.* 117 (2013) 5043–5049. doi:10.1021/jp3127829.



- [155] T.W. Sirk, E.F. Brown, A.K. Sum, M. Friedman, Molecular Dynamics Study on the Biophysical Interactions of Seven Green Tea Catechins with Lipid Bilayers of Cell Membranes, *J. Agric. Food Chem.* 56 (2008) 7750–7758. doi:10.1021/jf8013298.
- [156] T.W. Sirk, E.F. Brown, M. Friedman, A.K. Sum, Molecular Binding of Catechins to Biomembranes: Relationship to Biological Activity, *J. Agric. Food Chem.* 57 (2009) 6720–6728. doi:10.1021/jf900951w.
- [157] G. Fabre, I. Bayach, K. Berka, M. Palonciová, M. Starok, C. Rossi, J.-L. Duroux, M. Otyepka, P. Trouillas, Synergism of antioxidant action of vitamins E, C and quercetin is related to formation of molecular associations in biomembranes, *Chem. Commun.* 51 (2015) 7713–7716. doi:10.1039/C5CC00636H.
- [158] J. Atkinson, T. Harroun, S.R. Wassall, W. Stillwell, J. Katsaras, The location and behavior of α -tocopherol in membranes, *Mol. Nutr. Food Res.* 54 (2010) 641–651. doi:10.1002/mnfr.200900439.
- [159] D. Marquardt, J.A. Williams, N. Kučerka, J. Atkinson, S.R. Wassall, J. Katsaras, T.A. Harroun, Tocopherol activity correlates with its location in a membrane: a new perspective on the antioxidant vitamin E, *J. Am. Chem. Soc.* 135 (2013) 7523–7533. doi:10.1021/ja312665r.
- [160] D. Marquardt, J.A. Williams, J.J. Kinnun, N. Kučerka, J. Atkinson, S.R. Wassall, J. Katsaras, T.A. Harroun, Dimyristoyl phosphatidylcholine: a remarkable exception to α -tocopherol's membrane presence, *J. Am. Chem. Soc.* 136 (2014) 203–210. doi:10.1021/ja408288f.
- [161] P. Lambelet, F. Saucy, J. Löliger, Chemical evidence for interactions between vitamins E and C, *Experientia.* 41 (1985) 1384–1388.
- [162] A. Nègre-Salvayre, A. Affany, C. Hariton, R. Salvayre, Additional antilipoperoxidant activities of alpha-tocopherol and ascorbic acid on membrane-like systems are potentiated by rutin, *Pharmacology.* 42 (1991) 262–272.
- [163] L.H. Pinto, L.J. Holsinger, R.A. Lamb, Influenza virus M2 protein has ion channel activity, *Cell.* 69 (1992) 517–528.
- [164] C.F. Chew, A. Guy, P.C. Biggin, Distribution and dynamics of adamantanes in a lipid bilayer., *Biophys J.* 95 (2008) 5627–5636. doi:10.1529/biophysj.108.139477.
- [165] C. Li, M. Yi, J. Hu, H.-X. Zhou, T.A. Cross, Solid-State NMR and MD Simulations of the Antiviral Drug Amantadine Solubilized in DMPC Bilayers, *Biophys. J.* 94 (2008) 1295–1302. doi:10.1529/biophysj.107.112482.
- [166] E.S.E. Eriksson, L.A. Eriksson, The influence of cholesterol on the properties and permeability of hypericin derivatives in lipid membranes, *J. Chem. Theory Comput.* 7 (2011) 560–574. doi:10.1021/ct100528u.
- [167] E.S.E. Eriksson, D.J.V.A. dos Santos, R.C. Guedes, L.A. Eriksson, Properties and Permeability of Hypericin and Brominated Hypericin in Lipid Membranes, *J. Chem. Theory Comput.* 5 (2009) 3139–3149. doi:10.1021/ct9002702.
- [168] V. Galiano, J. Villalaín, Oleuropein aglycone in lipid bilayer membranes. A molecular dynamics study, *Biochim. Biophys. Acta BBA - Biomembr.* 1848 (2015) 2849–2858. doi:10.1016/j.bbamem.2015.08.007.



- [169] A.A. Bahar, D. Ren, Antimicrobial Peptides, *Pharmaceuticals*. 6 (2013) 1543–1575. doi:10.3390/ph6121543.
- [170] K.V.R. Reddy, R.D. Yedery, C. Aranha, Antimicrobial peptides: premises and promises, *Int. J. Antimicrob. Agents*. 24 (2004) 536–547. doi:10.1016/j.ijantimicag.2004.09.005.
- [171] K.A. Brogden, Antimicrobial peptides: pore formers or metabolic inhibitors in bacteria?, *Nat. Rev. Microbiol.* 3 (2005) 238–250. doi:10.1038/nrmicro1098.
- [172] P.K. Kyriakou, B. Ekblad, P.E. Kristiansen, Y.N. Kaznessis, Interactions of a class IIb bacteriocin with a model lipid bilayer, investigated through molecular dynamics simulations, *Biochim. Biophys. Acta BBA - Biomembr.* (2016). doi:10.1016/j.bbamem.2016.01.005.
- [173] Y. Wang, D.E. Schlamadinger, J.E. Kim, J.A. McCammon, Comparative Molecular Dynamics Simulations of the Antimicrobial Peptide CM15 in Model Lipid Bilayers, *Biochim. Biophys. Acta*. 1818 (2012) 1402–1409. doi:10.1016/j.bbamem.2012.02.017.
- [174] C. Appelt, F. Eisenmenger, R. Kühne, P. Schmieder, J.A. Söderhäll, Interaction of the Antimicrobial Peptide Cyclo(RRWRF) with Membranes by Molecular Dynamics Simulations, *Biophys. J.* 89 (2005) 2296–2306. doi:10.1529/biophysj.105.063040.
- [175] B.S. Perrin, Y. Tian, R. Fu, C.V. Grant, E.Y. Chekmenev, W.E. Wieczorek, A.E. Dao, R.M. Hayden, C.M. Burzynski, R.M. Venable, M. Sharma, S.J. Opella, R.W. Pastor, M.L. Cotten, High-Resolution Structures and Orientations of Antimicrobial Peptides Piscidin 1 and Piscidin 3 in Fluid Bilayers Reveal Tilting, Kinking, and Bilayer Immersion, *J. Am. Chem. Soc.* 136 (2014) 3491–3504. doi:10.1021/ja411119m.
- [176] T. Yuan, X. Zhang, Z. Hu, F. Wang, M. Lei, Molecular dynamics studies of the antimicrobial peptides piscidin 1 and its mutants with a DOPC lipid bilayer, *Biopolymers*. 97 (2012) 998–1009. doi:10.1002/bip.22116.
- [177] E. Han, H. Lee, Structural effects of tachyplesin I and its linear derivative on their aggregation and mobility in lipid bilayers, *J. Mol. Graph. Model.* 59 (2015) 123–128. doi:10.1016/j.jmgm.2015.04.007.
- [178] J.S. Hub, F.K. Winkler, M. Merrick, B.L. de Groot, Potentials of Mean Force and Permeabilities for Carbon Dioxide, Ammonia, and Water Flux across a Rhesus Protein Channel and Lipid Membranes, *J. Am. Chem. Soc.* 132 (2010) 13251–13263. doi:10.1021/ja102133x.
- [179] M. Orsi, J.W. Essex, Permeability of drugs and hormones through a lipid bilayer: insights from dual-resolution molecular dynamics, *Soft Matter*. 6 (2010) 3797–3808. doi:10.1039/C0SM00136H.
- [180] D. Bochicchio, E. Panizon, R. Ferrando, L. Monticelli, G. Rossi, Calculating the free energy of transfer of small solutes into a model lipid membrane: Comparison between metadynamics and umbrella sampling, *J. Chem. Phys.* 143 (2015) 144108. doi:10.1063/1.4932159.
- [181] S.-J. Marrink, H.J. Berendsen, Simulation of water transport through a lipid membrane, *J. Phys. Chem.* 98 (1994) 4155–4168.



- [182] D. Bemporad, J.W. Essex, C. Luttmann, Permeation of Small Molecules through a Lipid Bilayer: A Computer Simulation Study, *J. Phys. Chem. B.* 108 (2004) 4875–4884. doi:10.1021/jp035260s.
- [183] M. Orsi, J.W. Essex, Chapter 4:Passive Permeation Across Lipid Bilayers: a Literature Review, in: Chapter 4Passive Permeat. *Lipid Bilayers Lit. Rev.*, 2010: pp. 76–90. <http://pubs.rsc.org/en/content/chapter/bk9780854041893-00076/978-0-85404-189-3> (accessed May 10, 2016).
- [184] H.E. Alper, T.R. Stouch, Orientation and Diffusion of a Drug Analog in Biomembranes: Molecular Dynamics Simulations, *J. Phys. Chem.* 99 (1995) 5724–5731. doi:10.1021/j100015a065.
- [185] J. Ulander, A.D.J. Haymet, Permeation Across Hydrated DPPC Lipid Bilayers: Simulation of the Titrable Amphiphilic Drug Valproic Acid, *Biophys. J.* 85 (2003) 3475–3484. doi:10.1016/S0006-3495(03)74768-7.
- [186] D. Bemporad, C. Luttmann, J.W. Essex, Behaviour of small solutes and large drugs in a lipid bilayer from computer simulations, *Biochim. Biophys. Acta BBA - Biomembr.* 1718 (2005) 1–21. doi:10.1016/j.bbamem.2005.07.009.
- [187] D.J.V.A. dos Santos, L.A. Eriksson, Permeability of Psoralen Derivatives in Lipid Membranes, *Biophys. J.* 91 (2006) 2464–2474. doi:10.1529/biophysj.105.077156.
- [188] E.S.E. Eriksson, L.A. Eriksson, The Influence of Cholesterol on the Properties and Permeability of Hypericin Derivatives in Lipid Membranes, *J. Chem. Theory Comput.* 7 (2011) 560–574. doi:10.1021/ct100528u.
- [189] M. Palonciová, K. Vávrová, Ž. Sovová, R. DeVane, M. Otyepka, K. Berka, Structural Changes in Ceramide Bilayers Rationalize Increased Permeation through Stratum Corneum Models with Shorter Acyl Tails, *J. Phys. Chem. B.* 119 (2015) 9811–9819. doi:10.1021/acs.jpcc.5b05522.
- [190] M. Orsi, W.E. Sanderson, J.W. Essex, Permeability of Small Molecules through a Lipid Bilayer: A Multiscale Simulation Study, *J. Phys. Chem. B.* 113 (2009) 12019–12029. doi:10.1021/jp903248s.
- [191] D. Bemporad, J.W. Essex, C. Luttmann, Permeation of Small Molecules through a Lipid Bilayer: A Computer Simulation Study, *J. Phys. Chem. B.* 108 (2004) 4875–4884. doi:10.1021/jp035260s.
- [192] M. Orsi, J.W. Essex, Permeability of drugs and hormones through a lipid bilayer: insights from dual-resolution molecular dynamics, *Soft Matter.* 6 (2010) 3797. doi:10.1039/c0sm00136h.
- [193] Z. Ghaemi, M. Minozzi, P. Carloni, A. Laio, A Novel Approach to the Investigation of Passive Molecular Permeation through Lipid Bilayers from Atomistic Simulations, *J. Phys. Chem. B.* 116 (2012) 8714–8721. doi:10.1021/jp301083h.
- [194] K.M. Giacomini, S.-M. Huang, Transporters in Drug Development and Clinical Pharmacology, *Clin. Pharmacol. Ther.* 94 (2013) 3–9. doi:10.1038/clpt.2013.86.
- [195] K.M. Giacomini, S.-M. Huang, D.J. Tweedie, L.Z. Benet, K.L.R. Brouwer, X. Chu, A. Dahlin, R. Evers, V. Fischer, K.M. Hillgren, K.A. Hoffmaster, T. Ishikawa, D. Keppler, R.B. Kim, C.A. Lee, M. Niemi, J.W. Polli, Y. Sugiyama, P.W. Swaan, J.A. Ware, S.H. Wright, S.W.



Yee, M.J. Zamek-Gliszczynski, L. Zhang, Membrane transporters in drug development, *Nat. Rev. Drug Discov.* 9 (2010) 215–236. doi:10.1038/nrd3028.

[196] M.H. Saier, C.V. Tran, R.D. Barabote, TCDB: the Transporter Classification Database for membrane transport protein analyses and information, *Nucleic Acids Res.* 34 (2006) D181–D186. doi:10.1093/nar/gkj001.

[197] M.H. Saier, V.S. Reddy, D.G. Tamang, Å. Västermark, The Transporter Classification Database, *Nucleic Acids Res.* 42 (2014) D251–D258. doi:10.1093/nar/gkt1097.

[198] A. Schlessinger, S.W. Yee, A. Sali, K.M. Giacomini, SLC classification: an update, *Clin. Pharmacol. Ther.* 94 (2013) 19–23. doi:10.1038/clpt.2013.73.

[199] A. Schlessinger, P. Matsson, J.E. Shima, U. Pieper, S.W. Yee, L. Kelly, L. Apeltsin, R.M. Stroud, T.E. Ferrin, K.M. Giacomini, A. Sali, Comparison of human solute carriers, *Protein Sci. Publ. Protein Soc.* 19 (2010) 412–428. doi:10.1002/pro.320.

[200] A. Schlessinger, N. Khuri, K.M. Giacomini, A. Sali, Molecular modeling and ligand docking for solute carrier (SLC) transporters, *Curr. Top. Med. Chem.* 13 (2013) 843–856.

[201] M.A. Hediger, B. Cléménçon, R.E. Burrier, E.A. Bruford, The ABCs of membrane transporters in health and disease (SLC series): introduction, *Mol. Aspects Med.* 34 (2013) 95–107. doi:10.1016/j.mam.2012.12.009.

[202] S.-M. Huang, L. Zhang, K.M. Giacomini, The International Transporter Consortium: A Collaborative Group of Scientists From Academia, Industry, and the FDA, *Clin. Pharmacol. Ther.* 87 (2010) 32–36. doi:10.1038/clpt.2009.236.

[203] J. Li, P.-C. Wen, M. Moradi, E. Tajkhorshid, Computational characterization of structural dynamics underlying function in active membrane transporters, *Curr. Opin. Struct. Biol.* 31 (2015) 96–105. doi:10.1016/j.sbi.2015.04.001.

[204] D. Dwyer, Molecular Modeling and Molecular Dynamics Simulations of Membrane Transporter Proteins, in: Q. Yan, Q.Y. MD (Eds.), *Membr. Transp.*, Humana Press, 2003: pp. 335–350. <http://dx.doi.org/10.1385/1-59259-387-9%3A335> (accessed February 15, 2016).

[205] F. Khalili-Araghi, J. Gumbart, P.-C. Wen, M. Sotomayor, E. Tajkhorshid, K. Schulten, Molecular dynamics simulations of membrane channels and transporters, *Curr. Opin. Struct. Biol.* 19 (2009) 128–137. doi:10.1016/j.sbi.2009.02.011.

[206] E.M. Quistgaard, C. Löw, F. Guettou, P. Nordlund, Understanding transport by the major facilitator superfamily (MFS): structures pave the way, *Nat. Rev. Mol. Cell Biol.* 17 (2016) 123–132. doi:10.1038/nrm.2015.25.

[207] E.M. Quistgaard, C. Löw, P. Moberg, L. Trésaugues, P. Nordlund, Structural basis for substrate transport in the GLUT-homology family of monosaccharide transporters, *Nat. Struct. Mol. Biol.* 20 (2013) 766–768. doi:10.1038/nsmb.2569.

[208] L. Sun, X. Zeng, C. Yan, X. Sun, X. Gong, Y. Rao, N. Yan, Crystal structure of a bacterial homologue of glucose transporters GLUT1-4, *Nature.* 490 (2012) 361–366. doi:10.1038/nature11524.

[209] G. Wisedchaisri, M.-S. Park, M.G. Iadanza, H. Zheng, T. Gonen, Proton-coupled sugar transport in the prototypical major facilitator superfamily protein XylE, *Nat. Commun.* 5 (2014) 4521. doi:10.1038/ncomms5521.



- [210] D. Deng, C. Xu, P. Sun, J. Wu, C. Yan, M. Hu, N. Yan, Crystal structure of the human glucose transporter GLUT1, *Nature*. 510 (2014) 121–125. doi:10.1038/nature13306.
- [211] M.-S. Park, Molecular Dynamics Simulations of the Human Glucose Transporter GLUT1, *PLoS ONE*. 10 (2015) e0125361. doi:10.1371/journal.pone.0125361.
- [212] M.Ø. Jensen, Y. Yin, E. Tajkhorshid, K. Schulten, Sugar transport across lactose permease probed by steered molecular dynamics, *Biophys. J.* 93 (2007) 92–102. doi:10.1529/biophysj.107.103994.
- [213] Y. Yin, M.Ø. Jensen, E. Tajkhorshid, K. Schulten, Sugar binding and protein conformational changes in lactose permease, *Biophys. J.* 91 (2006) 3972–3985. doi:10.1529/biophysj.106.085993.
- [214] M. Andersson, A.-N. Bondar, J.A. Freites, D.J. Tobias, H.R. Kaback, S.H. White, Proton-coupled dynamics in lactose permease, *Struct. Lond. Engl.* 1993. 20 (2012) 1893–1904. doi:10.1016/j.str.2012.08.021.
- [215] M. Moradi, G. Enkavi, E. Tajkhorshid, Atomic-level characterization of transport cycle thermodynamics in the glycerol-3-phosphate:phosphate antiporter, *Nat. Commun.* 6 (2015) 8393. doi:10.1038/ncomms9393.
- [216] J. Holyoake, M.S.P. Sansom, Conformational change in an MFS protein: MD simulations of LacY, *Struct. Lond. Engl.* 1993. 15 (2007) 873–884. doi:10.1016/j.str.2007.06.004.
- [217] D. Wang, G.A. Voth, Proton Transport Pathway in the CIC Cl⁻/H⁺ Antiporter, *Biophys. J.* 97 (2009) 121–131. doi:10.1016/j.bpj.2009.04.038.
- [218] D. Deng, P. Sun, C. Yan, M. Ke, X. Jiang, L. Xiong, W. Ren, K. Hirata, M. Yamamoto, S. Fan, N. Yan, Molecular basis of ligand recognition and transport by glucose transporters, *Nature*. 526 (2015) 391–396. doi:10.1038/nature14655.
- [219] A.-N. Bondar, C. del Val, S.H. White, Rhomboid protease dynamics and lipid interactions, *Struct. Lond. Engl.* 1993. 17 (2009) 395–405. doi:10.1016/j.str.2008.12.017.
- [220] F. Gruswitz, S. Chaudhary, J.D. Ho, A. Schlessinger, B. Pezeshki, C.-M. Ho, A. Sali, C.M. Westhoff, R.M. Stroud, Function of human Rh based on structure of RhCG at 2.1 Å, *Proc. Natl. Acad. Sci.* 107 (2010) 9638–9643. doi:10.1073/pnas.1003587107.
- [221] S. Doki, H.E. Kato, N. Solcan, M. Iwaki, M. Koyama, M. Hattori, N. Iwase, T. Tsukazaki, Y. Sugita, H. Kandori, S. Newstead, R. Ishitani, O. Nureki, Structural basis for dynamic mechanism of proton-coupled symport by the peptide transporter POT, *Proc. Natl. Acad. Sci.* 110 (2013) 11343–11348. doi:10.1073/pnas.1301079110.
- [222] I.F. Tsigelny, D. Kovalskyy, V.L. Kouznetsova, O. Balinskyi, Y. Sharikov, V. Bhatnagar, S.K. Nigam, Conformational Changes of the Multispecific Transporter Organic Anion Transporter 1 (OAT1/SLC22A6) Suggests a Molecular Mechanism for Initial Stages of Drug and Metabolite Transport, *Cell Biochem. Biophys.* 61 (2011) 251–259. doi:10.1007/s12013-011-9191-7.
- [223] D. Meredith, R.A. Price, Molecular Modeling of PepT1 — Towards a Structure, *J. Membr. Biol.* 213 (2007) 79–88. doi:10.1007/s00232-006-0876-6.
- [224] P. Anzenbacher, U.M. Zanger, *Metabolism of Drugs and Other Xenobiotics*, Wiley-VCH Verlag GmbH & Co. KGaA, Weinheim, Germany, 2012. doi:10.1002/9783527630905.



- [225] F.P. Guengerich, Human Cytochrome P450 Enzymes, in: *Cytochrome P450*, 2005: pp. 377–530.
- [226] D.R. Nelson, Cytochrome P450 Nomenclature, 2004, in: I.R. Phillips, E.A. Shephard (Eds.), *Methods Mol. Biol. Vol 320 Cytochrome P450 Protoc. Second Ed.*, Humana Press Inc., Totowa, NJ, n.d.
- [227] M. Seliskar, D. Rozman, Mammalian cytochromes P450--importance of tissue specificity., *Biochim. Biophys. Acta.* 1770 (2007) 458–66. doi:10.1016/j.bbagen.2006.09.016.
- [228] V. Cojocar, K. Balali-Mood, M.S.P. Sansom, R.C. Wade, Structure and dynamics of the membrane-bound cytochrome P450 2C9., *PLoS Comput. Biol.* 7 (2011) e1002152. doi:10.1371/journal.pcbi.1002152.
- [229] M.R. Wester, J.K. Yano, G. Schoch, C. Yang, K.J. Griffin, C.D. Stout, E.F. Johnson, The structure of human cytochrome P450 2C9 complexed with flurbiprofen at 2.0-Å resolution., *J. Biol. Chem.* 279 (2004) 35630–35637. doi:10.1074/jbc.M405427200.
- [230] P.A. Williams, J. Cosme, A. Ward, H.C. Angove, D. Matak Vinković, H. Jhoti, Crystal structure of human cytochrome P450 2C9 with bound warfarin., *Nature.* 424 (2003) 464–8. doi:10.1038/nature01862.
- [231] C.A. Brown, S.D. Black, Membrane topology of mammalian cytochromes P-450 from liver endoplasmic reticulum. Determination by trypsinolysis of phenobarbital-treated microsomes., *J. Biol. Chem.* 264 (1989) 4442–9.
- [232] E. Szczesna-Skorupa, B. Mallah, B. Kemper, Fluorescence resonance energy transfer analysis of cytochromes P450 2C2 and 2E1 molecular interactions in living cells., *J. Biol. Chem.* 278 (2003) 31269–31276. doi:10.1074/jbc.M301489200.
- [233] G.A. Schoch, J.K. Yano, M.R. Wester, K.J. Griffin, C.D. Stout, E.F. Johnson, Structure of Human Microsomal Cytochrome P450 2C8, 279 (2004) 9497–9503. doi:10.1074/jbc.M312516200.
- [234] K. Berka, M. Paloncýová, P. Anzenbacher, M. Otyepka, Behavior of Human Cytochromes P450 on Lipid Membranes., *J. Phys. Chem. B.* 117 (2013) 11556–11564. doi:10.1021/jp4059559.
- [235] J.L. Baylon, I.L. Lenov, S.G. Sligar, E. Tajkhorshid, Characterizing the Membrane-Bound State of Cytochrome P450 3A4: Structure, Depth of Insertion and Orientation, *J. Am. Chem. Soc.* 135 (2013) 8542–8551. doi:10.1021/ja4003525.
- [236] I.G. Denisov, A.Y. Shih, S.G. Sligar, Structural differences between soluble and membrane bound cytochrome P450s, *J. Inorg. Biochem.* 108 (2012) 150–158. doi:10.1016/j.jinorgbio.2011.11.026.
- [237] Y.-L. Cui, Q. Xue, Q.-C. Zheng, J.-L. Zhang, C.-P. Kong, J.-R. Fan, H.-X. Zhang, Structural features and dynamic investigations of the membrane-bound cytochrome P450 17A1, *Biochim. Biophys. Acta BBA - Biomembr.* 1848 (2015) 2013–2021. doi:10.1016/j.bbamem.2015.05.017.
- [238] J. Park, L. Czapla, R.E. Amaro, Molecular simulations of aromatase reveal new insights into the mechanism of ligand binding., *J. Chem. Inf. Model.* 53 (2013) 2047–56. doi:10.1021/ci400225w.



- [239] J. Sgrignani, A. Magistrato, Influence of the membrane lipophilic environment on the structure and on the substrate access/egress routes of the human aromatase enzyme. A computational study., *J. Chem. Inf. Model.* 52 (2012) 1595–1606. doi:10.1021/ci300151h.
- [240] D.R. McDougale, J.L. Baylon, D.D. Meling, A. Kambalyal, Y. V. Grinkova, J. Hammernik, E. Tajkhorshid, A. Das, Incorporation of charged residues in the CYP2J2 F-G loop disrupts CYP2J2–lipid bilayer interactions, *Biochim. Biophys. Acta BBA - Biomembr.* 1848 (2015) 2460–2470. doi:10.1016/j.bbamem.2015.07.015.
- [241] B.C. Monk, T.M. Tomasiak, M. V Keniya, F.U. Huschmann, J.D.A. Tyndall, J.D. O'Connell, R.D. Cannon, J.G. McDonald, A. Rodriguez, J.S. Finer-Moore, R.M. Stroud, Architecture of a single membrane spanning cytochrome P450 suggests constraints that orient the catalytic domain relative to a bilayer, *Proc. Natl. Acad. Sci.* 111 (2014) 3865–3870. doi:10.1073/pnas.1324245111.
- [242] A.A. Sagatova, M. V. Keniya, R.K. Wilson, B.C. Monk, J.D.A. Tyndall, Structural Insights into Binding of the Antifungal Drug Fluconazole to *Saccharomyces cerevisiae* Lanosterol 14 α -Demethylase, *Antimicrob. Agents Chemother.* 59 (2015) 4982–4989. doi:10.1128/AAC.00925-15.
- [243] M. Palonciová, V. Navrátilová, K. Berka, A. Laio, M. Otyepka, Role of Enzyme Flexibility in Ligand Access and Egress to Active Site: Bias-Exchange Metadynamics Study of 1,3,7-Trimethyluric Acid in Cytochrome P450 3A4, *J. Chem. Theory Comput.* 12 (2016) 2101–2109. doi:10.1021/acs.jctc.6b00075.
- [244] E.E. Scott, C.R. Wolf, M. Otyepka, S.C. Humphreys, J.R. Reed, C.J. Henderson, L.A. McLaughlin, M. Palonciová, V. Navratilova, K. Berka, P. Anzenbacher, U.P. Dahal, C. Barnaba, J.A. Brozik, J.P. Jones, F. Estrada, J.S. Laurence, J.W. Park, W.L. Backes, The Role of Protein-Protein and Protein-Membrane Interactions on P450 Function, *Drug Metab. Dispos.* (2016) dmd.115.068569. doi:10.1124/dmd.115.068569.
- [245] S.-F. Zhou, Z.-W. Zhou, L.-P. Yang, J.-P. Cai, Substrates, inducers, inhibitors and structure-activity relationships of human Cytochrome P450 2C9 and implications in drug development, *Curr. Med. Chem.* 16 (2009) 3480–3675.
- [246] L. Laakkonen, M. Finel, A Molecular Model of the Human UDP-Glucuronosyltransferase 1A1, Its Membrane Orientation, and the Interactions between Different Parts of the Enzyme, *Mol. Pharmacol.* 77 (2010) 931–939. doi:10.1124/mol.109.063289.
- [247] M.J. Miley, A.K. Zielinska, J.E. Keenan, S.M. Bratton, A. Radomska-Pandya, M.R. Redinbo, Crystal Structure of the Cofactor-Binding Domain of the Human Phase II Drug-Metabolism Enzyme UDP-Glucuronosyltransferase 2B7, *J. Mol. Biol.* 369 (2007) 498–511. doi:10.1016/j.jmb.2007.03.066.
- [248] A. Roy, A. Kucukural, Y. Zhang, I-TASSER: a unified platform for automated protein structure and function prediction, *Nat. Protoc.* 5 (2010) 725–738. doi:10.1038/nprot.2010.5.
- [249] N. Eswar, B. Webb, M.A. Marti-Renom, M. s. Madhusudhan, D. Eramian, M. Shen, U. Pieper, A. Sali, Comparative Protein Structure Modeling Using MODELLER, in: *Curr. Protoc. Protein Sci.*, John Wiley & Sons, Inc., 2001. <http://onlinelibrary.wiley.com/doi/10.1002/0471140864.ps0209s50/abstract> (accessed March 14, 2016).



- [250] K.W. Bock, C. Köhle, Topological aspects of oligomeric UDP-glucuronosyltransferases in endoplasmic reticulum membranes: Advances and open questions, *Biochem. Pharmacol.* 77 (2009) 1458–1465. doi:10.1016/j.bcp.2008.12.004.
- [251] D.S. Wishart, C. Knox, A.C. Guo, S. Shrivastava, M. Hassanali, P. Stothard, Z. Chang, J. Woolsey, DrugBank: a comprehensive resource for in silico drug discovery and exploration, *Nucleic Acids Res.* 34 (2006) D668–D672. doi:10.1093/nar/gkj067.
- [252] J. Kirchmair, A. Howlett, J.E. Peironcelly, D.S. Murrell, M.J. Williamson, S.E. Adams, T. Hankemeier, L. Van Buren, G. Duchateau, W. Klaffke, R.C. Glen, How do metabolites differ from their parent molecules and how are they excreted?, *J. Chem. Inf. Model.* 53 (2013) 354–367. doi:10.1021/ci300487z.
- [253] M. Palonciová, K. Berka, M. Otyepka, Molecular Insight into Affinities of Drugs and Their Metabolites to Lipid Bilayers., *J. Phys. Chem. B.* 117 (2013) 2403–10. doi:10.1021/jp311802x.
- [254] S.P. Tripathi, A. Bhadauriya, A. Patil, A.T. Sangamwar, Substrate selectivity of human intestinal UDP-glucuronosyltransferases (UGTs): in silico and in vitro insights., *Drug Metab. Rev.* 45 (2013) 231–52. doi:10.3109/03602532.2013.767345.
- [255] P.I. Mackenzie, K. Walter Bock, B. Burchell, C. Guillemette, S. Ikushiro, T. Iyanagi, J.O. Miners, I.S. Owens, D.W. Nebert, Nomenclature update for the mammalian UDP glycosyltransferase (UGT) gene superfamily, *Pharmacogenet. Genomics.* 15 (2005) 677–685. doi:10.1097/01.fpc.0000173483.13689.56.
- [256] Y. Ishii, A. Nurrochmad, H. Yamada, Modulation of UDP-Glucuronosyltransferase Activity by Endogenous Compounds, *Drug Metab. Pharmacokinet.* 25 (2010) 134–148. doi:10.2133/dmpk.25.134.
- [257] F. R., M. Nakajima, T. Yamamoto, H. Nagao, T. Yokoi, In silico and in vitro Approaches to Elucidate the Thermal Stability of Human UDP-glucuronosyltransferase UGT 1A9, *Drug Metab. Pharmacokinet.* 24 (2009) 235–244. doi:10.2133/dmpk.24.235.
- [258] S.P. Tripathi, R. Prajapati, N. Verma, A.T. Sangamwar, Predicting substrate selectivity between UGT1A9 and UGT1A10 using molecular modelling and molecular dynamics approach, *Mol. Simul.* 0 (2015) 1–19. doi:10.1080/08927022.2015.1044451.
- [259] C.W. Locuson, T.S. Tracy, Comparative modelling of the human UDP-glucuronosyltransferases: insights into structure and mechanism., *Xenobiotica Fate Foreign Compd. Biol. Syst.* 37 (2007) 155–168. doi:10.1080/00498250601129109.
- [260] P. Košinová, K. Berka, M. Wykes, M. Otyepka, P. Trouillas, P. Kosinova, P. Ko, Positioning of antioxidant quercetin and its metabolites in lipid bilayer membranes: implication for their lipid-peroxidation inhibition., *J Phys Chem B.* 116 (2012) 1309–18. doi:10.1021/jp208731g.
- [261] Y. Huang, M.J. Lemieux, J. Song, M. Auer, D.-N. Wang, Structure and Mechanism of the Glycerol-3-Phosphate Transporter from *Escherichia coli*, *Science.* 301 (2003) 616–620. doi:10.1126/science.1087619.
- [262] G. Enkavi, E. Tajkhorshid, Simulation of spontaneous substrate binding revealing the binding pathway and mechanism and initial conformational response of GlpT, *Biochemistry (Mosc.).* 49 (2010) 1105–1114. doi:10.1021/bi901412a.



- [263] C.J. Law, G. Enkavi, D.-N. Wang, E. Tajkhorshid, Structural Basis of Substrate Selectivity in the Glycerol-3-Phosphate: Phosphate Antiporter GlpT, *Biophys. J.* 97 (2009) 1346–1353. doi:10.1016/j.bpj.2009.06.026.
- [264] J. Baker, S.H. Wright, F. Tama, Simulations of substrate transport in the multidrug transporter EmrD, *Proteins Struct. Funct. Bioinforma.* 80 (2012) 1620–1632. doi:10.1002/prot.24056.
- [265] Y.M. Leung, D.A. Holdbrook, T.J. Piggot, S. Khalid, The NorM MATE transporter from *N. gonorrhoeae*: insights into drug and ion binding from atomistic molecular dynamics simulations, *Biophys. J.* 107 (2014) 460–468. doi:10.1016/j.bpj.2014.06.005.
- [266] D.C. Rees, E. Johnson, O. Lewinson, ABC transporters: the power to change, *Nat. Rev. Mol. Cell Biol.* 10 (2009) 218–227. doi:10.1038/nrm2646.
- [267] J. ter Beek, A. Guskov, D.J. Slotboom, Structural diversity of ABC transporters, *J. Gen. Physiol.* 143 (2014) 419–435. doi:10.1085/jgp.201411164.
- [268] I.B. Holland, M.A. Blight, ABC-ATPases, adaptable energy generators fuelling transmembrane movement of a variety of molecules in organisms from bacteria to humans, *J. Mol. Biol.* 293 (1999) 381–399. doi:10.1006/jmbi.1999.2993.
- [269] S.G. Aller, J. Yu, A. Ward, Y. Weng, S. Chittaboina, R. Zhuo, P.M. Harrell, Y.T. Trinh, Q. Zhang, I.L. Urbatsch, G. Chang, Structure of P-glycoprotein reveals a molecular basis for poly-specific drug binding, *Science.* 323 (2009) 1718–1722. doi:10.1126/science.1168750.
- [270] M. Moradi, E. Tajkhorshid, Mechanistic picture for conformational transition of a membrane transporter at atomic resolution, *Proc. Natl. Acad. Sci.* 110 (2013) 18916–18921. doi:10.1073/pnas.1313202110.
- [271] S.-Y. Chang, F.-F. Liu, X.-Y. Dong, Y. Sun, Molecular insight into conformational transmission of human P-glycoprotein, *J. Chem. Phys.* 139 (2013) 225102. doi:10.1063/1.4832740.
- [272] H. Liu, D. Li, Y. Li, T. Hou, Atomistic molecular dynamics simulations of ATP-binding cassette transporters, *Wiley Interdiscip. Rev. Comput. Mol. Sci.* (2016) n/a-n/a. doi:10.1002/wcms.1247.
- [273] B.J. Grant, A.A. Gorfe, J.A. McCammon, Large conformational changes in proteins: signaling and other functions, *Curr. Opin. Struct. Biol.* 20 (2010) 142–147. doi:10.1016/j.sbi.2009.12.004.
- [274] C.F. Higgins, K.J. Linton, The ATP switch model for ABC transporters, *Nat. Struct. Mol. Biol.* 11 (2004) 918–926. doi:10.1038/nsmb836.
- [275] P.M. Jones, A.M. George, Opening of the ADP-bound active site in the ABC transporter ATPase dimer: evidence for a constant contact, alternating sites model for the catalytic cycle, *Proteins.* 75 (2009) 387–396. doi:10.1002/prot.22250.
- [276] G. Gyimesi, S. Ramachandran, P. Kota, N.V. Dokholyan, B. Sarkadi, T. Hegedűs, ATP hydrolysis at one of the two sites in ABC transporters initiates transport related conformational transitions, *Biochim. Biophys. Acta BBA - Biomembr.* 1808 (2011) 2954–2964. doi:10.1016/j.bbamem.2011.07.038.
- [277] G. Gyimesi, S. Ramachandran, P. Kota, N.V. Dokholyan, B. Sarkadi, T. Hegedűs, Corrigendum to “ATP hydrolysis at one of the two sites in ABC transporters initiates transport



related conformational transitions" [Biochim. Biophys. Acta 1808 (2011) 2954–2964], Biochim. Biophys. Acta BBA - Biomembr. 1818 (2012) 1435. doi:10.1016/j.bbamem.2012.01.004.

[278] M. Moradi, E. Tajkhorshid, Computational Recipe for Efficient Description of Large-Scale Conformational Changes in Biomolecular Systems, J. Chem. Theory Comput. 10 (2014) 2866–2880. doi:10.1021/ct5002285.

[279] P.-C. Wen, B. Verhalen, S. Wilkens, H.S. Mchaourab, E. Tajkhorshid, On the origin of large flexibility of P-glycoprotein in the inward-facing state., J. Biol. Chem. 288 (2013) 19211–20. doi:10.1074/jbc.M113.450114.

[280] J.-F. St-Pierre, A. Bunker, T. Róg, M. Karttunen, N. Mousseau, Molecular dynamics simulations of the bacterial ABC transporter SAV1866 in the closed form, J. Phys. Chem. B. 116 (2012) 2934–2942. doi:10.1021/jp209126c.

[281] M.L. O'Mara, A.E. Mark, The Effect of Environment on the Structure of a Membrane Protein: P-Glycoprotein under Physiological Conditions, J. Chem. Theory Comput. 8 (2012) 3964–3976. doi:10.1021/ct300254y.

[282] T.X. Xiang, B.D. Anderson, Permeability of acetic acid across gel and liquid-crystalline lipid bilayers conforms to free-surface-area theory, Biophys. J. 72 (1997) 223–237. doi:10.1016/S0006-3495(97)78661-2.

[283] C.L. Wennberg, D. van der Spoel, J.S. Hub, Large Influence of Cholesterol on Solute Partitioning into Lipid Membranes, J. Am. Chem. Soc. 134 (2012) 5351–5361. doi:10.1021/ja211929h.

[284] M. Paloncýová, R.H. DeVane, B.P. Murch, K. Berka, M. Otyepka, Rationalization of Reduced Penetration of Drugs through Ceramide Gel Phase Membrane, Langmuir. 30 (2014) 13942–13948. doi:10.1021/la503289v.

[285] A. Botan, F. Favela-Rosales, P.F.J. Fuchs, M. Javanainen, M. Kanduč, W. Kulig, A. Lamberg, C. Loison, A. Lyubartsev, M.S. Miettinen, L. Monticelli, J. Määttä, O.H.S. Ollila, M. Retegan, T. Róg, H. Santuz, J. Tynkkynen, Toward Atomistic Resolution Structure of Phosphatidylcholine Headgroup and Glycerol Backbone at Different Ambient Conditions, J. Phys. Chem. B. 119 (2015) 15075–15088. doi:10.1021/acs.jpcc.5b04878.

[286] A.G. Lee, How lipids affect the activities of integral membrane proteins, Biochim. Biophys. Acta. 1666 (2004) 62–87. doi:10.1016/j.bbamem.2004.05.012.

[287] V. Navrátilová, M. Paloncýová, M. Kajšová, K. Berka, M. Otyepka, Effect of Cholesterol on the Structure of Membrane-Attached Cytochrome P450 3A4, J. Chem. Inf. Model. 55 (2015) 628–635. doi:10.1021/ci500645k.

[288] P.S. Niemelä, S. Ollila, M.T. Hyvönen, M. Karttunen, I. Vattulainen, Assessing the Nature of Lipid Raft Membranes, PLoS Comput Biol. 3 (2007) e34. doi:10.1371/journal.pcbi.0030034.

[289] P.S. Niemelä, M.T. Hyvönen, I. Vattulainen, Atom-scale molecular interactions in lipid raft mixtures, Biochim. Biophys. Acta. 1788 (2009) 122–135. doi:10.1016/j.bbamem.2008.08.018.



- [290] Y. Zhang, A. Lervik, J. Seddon, F. Bresme, A coarse-grained molecular dynamics investigation of the phase behavior of DPPC/cholesterol mixtures, *Chem. Phys. Lipids*. 185 (2015) 88–98. doi:10.1016/j.chemphyslip.2014.07.011.
- [291] H. Ohvo-Rekilä, B. Ramstedt, P. Leppimäki, J.P. Slotte, Cholesterol interactions with phospholipids in membranes, *Prog. Lipid Res.* 41 (2002) 66–97.
- [292] T. Róg, M. Pasenkiewicz-Gierula, I. Vattulainen, M. Karttunen, Ordering effects of cholesterol and its analogues, *Biochim. Biophys. Acta*. 1788 (2009) 97–121. doi:10.1016/j.bbamem.2008.08.022.
- [293] H.J. Risselada, S.J. Marrink, The molecular face of lipid rafts in model membranes, *Proc. Natl. Acad. Sci.* 105 (2008) 17367–17372. doi:10.1073/pnas.0807527105.
- [294] C. Díaz-Tejada, I. Ariz-Extreme, N. Awasthi, J.S. Hub, Quantifying Lateral Inhomogeneity of Cholesterol-Containing Membranes, *J. Phys. Chem. Lett.* 6 (2015) 4799–4803. doi:10.1021/acs.jpcclett.5b02414.
- [295] F. Zocher, D. van der Spoel, P. Pohl, J.S. Hub, Local Partition Coefficients Govern Solute Permeability of Cholesterol-Containing Membranes, *Biophys. J.* 105 (2013) 2760–2770. doi:10.1016/j.bpj.2013.11.003.
- [296] J. Barnoud, G. Rossi, S.J. Marrink, L. Monticelli, Hydrophobic Compounds Reshape Membrane Domains, *PLOS Comput Biol.* 10 (2014) e1003873. doi:10.1371/journal.pcbi.1003873.
- [297] A.J. Sodt, M.L. Sandar, K. Gawrisch, R.W. Pastor, E. Lyman, The Molecular Structure of the Liquid-Ordered Phase of Lipid Bilayers, *J. Am. Chem. Soc.* 136 (2014) 725–732. doi:10.1021/ja4105667.
- [298] S. Capponi, J.A. Freites, D.J. Tobias, S.H. White, Interleaflet mixing and coupling in liquid-disordered phospholipid bilayers, *Biochim. Biophys. Acta BBA - Biomembr.* 1858 (2016) 354–362. doi:10.1016/j.bbamem.2015.11.024.
- [299] S. Meinhardt, R.L.C. Vink, F. Schmid, Monolayer curvature stabilizes nanoscale raft domains in mixed lipid bilayers, *Proc. Natl. Acad. Sci.* 110 (2013) 4476–4481. doi:10.1073/pnas.1221075110.
- [300] J.D. Perlmutter, J.N. Sachs, Interleaflet Interaction and Asymmetry in Phase Separated Lipid Bilayers: Molecular Dynamics Simulations, *J. Am. Chem. Soc.* 133 (2011) 6563–6577. doi:10.1021/ja106626r.
- [301] T. Róg, A. Orłowski, A. Llorente, T. Skotland, T. Sylvänne, D. Kauhanen, K. Ekroos, K. Sandvig, I. Vattulainen, Interdigitation of long-chain sphingomyelin induces coupling of membrane leaflets in a cholesterol dependent manner, *Biochim. Biophys. Acta BBA - Biomembr.* 1858 (2016) 281–288. doi:10.1016/j.bbamem.2015.12.003.
- [302] H. Koldsø, D. Shorthouse, J. Hélie, M.S.P. Sansom, Lipid Clustering Correlates with Membrane Curvature as Revealed by Molecular Simulations of Complex Lipid Bilayers, *PLoS Comput Biol.* 10 (2014) e1003911. doi:10.1371/journal.pcbi.1003911.
- [303] I. Basu, C. Mukhopadhyay, In silico phase separation in the presence of GM1 in ternary and quaternary lipid bilayers, *Phys. Chem. Chem. Phys.* 17 (2015) 17130–17139. doi:10.1039/C5CP01970B.



- [304] S. Jo, H. Rui, J.B. Lim, J.B. Klauda, W. Im, Cholesterol Flip-Flop: Insights from Free Energy Simulation Studies, *J. Phys. Chem. B.* 114 (2010) 13342–13348. doi:10.1021/jp108166k.
- [305] W.F.D. Bennett, J.L. MacCallum, M.J. Hinner, S.J. Marrink, D.P. Tieleman, Molecular View of Cholesterol Flip-Flop and Chemical Potential in Different Membrane Environments, *J. Am. Chem. Soc.* 131 (2009) 12714–12720. doi:10.1021/ja903529f.
- [306] G. Parisio, A. Ferrarini, M.M. Sperotto, Model studies of lipid flip-flop in membranes, *Int. J. Adv. Eng. Sci. Appl. Math.* (2016) 1–13. doi:10.1007/s12572-015-0155-9.
- [307] C. Hong, D.P. Tieleman, Y. Wang, Microsecond Molecular Dynamics Simulations of Lipid Mixing, *Langmuir.* 30 (2014) 11993–12001. doi:10.1021/la502363b.
- [308] H. Ding, Y. Ma, Theoretical and Computational Investigations of Nanoparticle–Biomembrane Interactions in Cellular Delivery, *Small.* 11 (2015) 1055–1071. doi:10.1002/smll.201401943.
- [309] R. Vácha, F.J. Martinez-Veracoechea, D. Frenkel, Receptor-Mediated Endocytosis of Nanoparticles of Various Shapes, *Nano Lett.* 11 (2011) 5391–5395. doi:10.1021/nl2030213.
- [310] R. Vácha, F.J. Martinez-Veracoechea, D. Frenkel, Intracellular Release of Endocytosed Nanoparticles Upon a Change of Ligand–Receptor Interaction, *ACS Nano.* 6 (2012) 10598–10605. doi:10.1021/nn303508c.
- [311] M.P. Lambros, Y.E. Rahman, Effects of cyclosporin A on model lipid membranes, *Chem. Phys. Lipids.* 131 (2004) 63–69. doi:10.1016/j.chemphyslip.2004.04.002.
- [312] K.W.L. Christopher L Ahlback, Beyond cyclosporine A: Conformation-dependent passive membrane permeabilities of cyclic peptide natural products, *Future Med. Chem.* 7 (2015) 1–10. doi:10.4155/fmc.15.78.
- [313] A. Czogalla, Oral cyclosporine A - the current picture of its liposomal and other delivery systems, *Cell. Mol. Biol. Lett.* 14 (2008) 139–152. doi:10.2478/s11658-008-0041-6.
- [314] T. Ossman, G. Fabre, P. Trouillas, Interaction of wine anthocyanin derivatives with lipid bilayer membranes, *Comput. Theor. Chem.* 1077 (2016) 80–86. doi:10.1016/j.comptc.2015.10.034.
- [315] K.K. Biron, S.C. Stanat, J.B. Sorrell, J.A. Fyfe, P.M. Keller, C.U. Lambe, D.J. Nelson, Metabolic activation of the nucleoside analog 9-[(2-hydroxy-1-(hydroxymethyl)ethoxy)methyl]guanine in human diploid fibroblasts infected with human cytomegalovirus, *Proc. Natl. Acad. Sci. U. S. A.* 82 (1985) 2473–2477.
- [316] S.M. Flechner, R.K. Avery, R. Fisher, B.A. Mastroianni, D.A. Papajcik, K.J. O'Malley, M. Goormastic, D.A. Goldfarb, C.S. Modlin, A.C. Novick, A randomized prospective controlled trial of oral acyclovir versus oral ganciclovir for cytomegalovirus prophylaxis in high-risk kidney transplant recipients, *Transplantation.* 66 (1998) 1682–1688.
- [317] D.J. Winston, D. Wirin, A. Shaked, R.W. Busuttil, Randomised comparison of ganciclovir and high-dose acyclovir for long-term cytomegalovirus prophylaxis in liver-transplant recipients, *Lancet.* 346 (1995) 69–74.
- [318] C.V. Fletcher, H.H. Balfour, Evaluation of ganciclovir for cytomegalovirus disease, *DICP Ann. Pharmacother.* 23 (1989) 5–12.



- [319] H. Wiltshire, C.V. Paya, M.D. Pescovitz, A. Humar, E. Dominguez, K. Washburn, E. Blumberg, B. Alexander, R. Freeman, N. Heaton, K.P. Zuideveld, Valganciclovir Solid Organ Transplant Study Group, Pharmacodynamics of oral ganciclovir and valganciclovir in solid organ transplant recipients, *Transplantation*. 79 (2005) 1477–1483.
- [320] C. Fletcher, R. Sawchuk, B. Chinnock, P. de Miranda, H.H. Balfour, Human pharmacokinetics of the antiviral drug DHPG, *Clin. Pharmacol. Ther.* 40 (1986) 281–286.
- [321] N. Perrottet, L.A. Decosterd, P. Meylan, M. Pascual, J. Biollaz, T. Buclin, Valganciclovir in adult solid organ transplant recipients: pharmacokinetic and pharmacodynamic characteristics and clinical interpretation of plasma concentration measurements, *Clin. Pharmacokinet.* 48 (2009) 399–418. doi:10.2165/00003088-200948060-00006.
- [322] P.-A. Billat, J.-B. Woillard, M. Essig, F.-L. Sauvage, N. Picard, S. Alain, M. Neely, P. Marquet, F. Saint-Marcoux, Plasma and intracellular exposure to ganciclovir in adult renal transplant recipients: is there an association with haematological toxicity?, *J. Antimicrob. Chemother.* (2015). doi:10.1093/jac/dkv342.
- [323] W.B. Mahony, B.A. Domin, T.P. Zimmerman, Ganciclovir permeation of the human erythrocyte membrane, *Biochem. Pharmacol.* 41 (1991) 263–271.
- [324] J.H. Gray, R.P. Owen, K.M. Giacomini, The concentrative nucleoside transporter family, SLC28, *Pflüg. Arch. Eur. J. Physiol.* 447 (2004) 728–734. doi:10.1007/s00424-003-1107-y.
- [325] S.A. Baldwin, P.R. Beal, S.Y.M. Yao, A.E. King, C.E. Cass, J.D. Young, The equilibrative nucleoside transporter family, SLC29, *Pflüg. Arch. Eur. J. Physiol.* 447 (2004) 735–743. doi:10.1007/s00424-003-1103-2.
- [326] Y. Shu, C. Brown, R.A. Castro, R.J. Shi, E.T. Lin, R.P. Owen, S.A. Sheardown, L. Yue, E.G. Burchard, C.M. Brett, K.M. Giacomini, Effect of genetic variation in the organic cation transporter 1, OCT1, on metformin pharmacokinetics, *Clin. Pharmacol. Ther.* 83 (2008) 273–280. doi:10.1038/sj.cpt.6100275.
- [327] R.L. Prentice, L.P. Zhao, Estimating equations for parameters in means and covariances of multivariate discrete and continuous responses, *Biometrics*. 47 (1991) 825–839.
- [328] N. Picard, S.W. Yee, J.-B. Woillard, Y. Lebranchu, Y. Le Meur, K.M. Giacomini, P. Marquet, The role of organic anion-transporting polypeptides and their common genetic variants in mycophenolic acid pharmacokinetics, *Clin. Pharmacol. Ther.* 87 (2010) 100–108. doi:10.1038/clpt.2009.205.
- [329] J. Weiss, M. Herzog, S. König, C.H. Storch, N. Ketabi-Kiyanvash, W.E. Haefeli, Induction of multiple drug transporters by efavirenz, *J. Pharmacol. Sci.* 109 (2009) 242–250.
- [330] P.-A. Billat, F.-L. Sauvage, N. Picard, N. Tafzi, S. Alain, M. Essig, P. Marquet, F. Saint-Marcoux, Liquid chromatography tandem mass spectrometry quantitation of intracellular concentrations of ganciclovir and its phosphorylated forms, *Anal. Bioanal. Chem.* (2015). doi:10.1007/s00216-015-8554-0.
- [331] G. Fabre, I. Bayach, K. Berka, M. Palonciová, M. Starok, C. Rossi, J.-L. Duroux, M. Otyepka, P. Trouillas, Synergism of antioxidant action of vitamins E, C and quercetin is



related to formation of molecular associations in biomembranes, *Chem. Commun. Camb. Engl.* 51 (2015) 7713–7716. doi:10.1039/c5cc00636h.

[332] M. Palonciová, R. DeVane, B. Murch, K. Berka, M. Otyepka, Amphiphilic drug-like molecules accumulate in a membrane below the head group region, *J. Phys. Chem. B.* 118 (2014) 1030–1039. doi:10.1021/jp4112052.

[333] K. Kotrych, T. Sulikowski, L. Domański, M. Białecka, M. Drożdżik, Polymorphism in the P-glycoprotein drug transporter MDR1 gene in renal transplant patients treated with cyclosporin A in a Polish population, *Pharmacol. Rep. PR.* 59 (2007) 199–205.

[334] L. Cheung, D.M.T. Yu, Z. Neiron, T.W. Failes, G.M. Arndt, J.I. Fletcher, Identification of new MRP4 inhibitors from a library of FDA approved drugs using a high-throughput bioluminescence screen, *Biochem. Pharmacol.* 93 (2015) 380–388. doi:10.1016/j.bcp.2014.11.006.

[335] K. Matsumoto, A. Shigemi, K. Ikawa, N. Kanazawa, Y. Fujisaki, N. Morikawa, Y. Takeda, Risk Factors for Ganciclovir-Induced Thrombocytopenia and Leukopenia, *Biol. Pharm. Bull.* 38 (2015) 235–238. doi:10.1248/bpb.b14-00588.

[336] T.C. Merigan, D.G. Renlund, S. Keay, M.R. Bristow, V. Starnes, J.B. O’Connell, S. Resta, D. Dunn, P. Gamberg, R.M. Ratkovec, A controlled trial of ganciclovir to prevent cytomegalovirus disease after heart transplantation, *N. Engl. J. Med.* 326 (1992) 1182–1186. doi:10.1056/NEJM199204303261803.

[337] E. Gane, F. Saliba, G.J. Valdecasas, J. O’Grady, M.D. Pescovitz, S. Lyman, C.A. Robinson, Randomised trial of efficacy and safety of oral ganciclovir in the prevention of cytomegalovirus disease in liver-transplant recipients. The Oral Ganciclovir International Transplantation Study Group [corrected], *Lancet Lond. Engl.* 350 (1997) 1729–1733.

[338] J.K. McGavin, K.L. Goa, Ganciclovir: an update of its use in the prevention of cytomegalovirus infection and disease in transplant recipients, *Drugs.* 61 (2001) 1153–1183.

[339] D.W. Cockcroft, M.H. Gault, Prediction of creatinine clearance from serum creatinine, *Nephron.* 16 (1976) 31–41.

[340] N. Perrottet, C. Csajka, M. Pascual, O. Manuel, F. Lamoth, P. Meylan, J.D. Aubert, J.P. Venetz, P. Soccia, L.A. Decosterd, J. Biollaz, T. Buclin, Population Pharmacokinetics of Ganciclovir in Solid-Organ Transplant Recipients Receiving Oral Valganciclovir, *Antimicrob. Agents Chemother.* 53 (2009) 3017–3023. doi:10.1128/AAC.00836-08.

[341] N. Abula, L.W. Chinn, T. Nakamura, L. Liu, C.C. Huang, S.J. Johns, M. Kawamoto, D. Stryke, T.R. Taylor, T.E. Ferrin, K.M. Giacomini, D.L. Kroetz, The human multidrug resistance protein 4 (MRP4, ABCG4): functional analysis of a highly polymorphic gene, *J. Pharmacol. Exp. Ther.* 325 (2008) 859–868. doi:10.1124/jpet.108.136523.

[342] Z.-S. Chen, K. Lee, G.D. Kruh, Transport of Cyclic Nucleotides and Estradiol 17-β-d-Glucuronide by Multidrug Resistance Protein 4 RESISTANCE TO 6-MERCAPTOPYRIMIDINE AND 6-THIOGUANINE, *J. Biol. Chem.* 276 (2001) 33747–33754. doi:10.1074/jbc.M104833200.

[343] J.D. Schuetz, M.C. Connelly, D. Sun, S.G. Paibir, P.M. Flynn, R.V. Srinivas, A. Kumar, A. Fridland, MRP4: A previously unidentified factor in resistance to nucleoside-based antiviral drugs, *Nat. Med.* 5 (1999) 1048–1051. doi:10.1038/12487.



- [344] M. Adachi, J. Sampath, L. Lan, D. Sun, P. Hargrove, R. Flatley, A. Tatum, M.Z. Edwards, M. Wezeman, L. Matherly, R. Drake, J. Schuetz, Expression of MRP4 confers resistance to ganciclovir and compromises bystander cell killing, *J. Biol. Chem.* 277 (2002) 38998–39004. doi:10.1074/jbc.M203262200.
- [345] P.L. Anderson, J. Lamba, C.L. Aquilante, E. Schuetz, C.V. Fletcher, Pharmacogenetic characteristics of indinavir, zidovudine, and lamivudine therapy in HIV-infected adults: a pilot study, *J. Acquir. Immune Defic. Syndr.* 1999. 42 (2006) 441–449. doi:10.1097/01.qai.0000225013.53568.69.
- [346] J.J. Kiser, C.L. Aquilante, P.L. Anderson, T.M. King, M.L. Carten, C.V. Fletcher, Clinical and genetic determinants of intracellular tenofovir diphosphate concentrations in HIV-infected patients, *J. Acquir. Immune Defic. Syndr.* 1999. 47 (2008) 298–303.
- [347] M. Ansari, G. Sauty, M. Labuda, V. Gagné, C. Laverdière, A. Moghrabi, D. Sinnett, M. Krajcinovic, Polymorphisms in multidrug resistance-associated protein gene 4 is associated with outcome in childhood acute lymphoblastic leukemia, *Blood.* 114 (2009) 1383–1386. doi:10.1182/blood-2008-11-191098.
- [348] U. Gradhand, T. Lang, E. Schaeffeler, H. Glaeser, H. Tegude, K. Klein, P. Fritz, G. Jedlitschky, H.K. Kroemer, I. Bachmakov, B. Anwald, R. Kerb, U.M. Zanger, M. Eichelbaum, M. Schwab, M.F. Fromm, Variability in human hepatic MRP4 expression: influence of cholestasis and genotype, *Pharmacogenomics J.* 8 (2007) 42–52. doi:10.1038/sj.tpj.6500451.
- [349] E.L. Woodahl, M.H. Crouthamel, T. Bui, D.D. Shen, R.J.Y. Ho, MDR1 (ABCB1) G1199A (Ser400Asn) polymorphism alters transepithelial permeability and sensitivity to anticancer agents, *Cancer Chemother. Pharmacol.* 64 (2009) 183–188. doi:10.1007/s00280-008-0906-4.
- [350] G. Dessilly, L. Elens, N. Panin, A. Capron, A. Decottignies, J.-B. Demoulin, V. Haufroid, ABCB1 1199G>A genetic polymorphism (Rs2229109) influences the intracellular accumulation of tacrolimus in HEK293 and K562 recombinant cell lines, *PloS One.* 9 (2014) e91555. doi:10.1371/journal.pone.0091555.
- [351] H. Gréen, P. Söderkvist, P. Rosenberg, G. Horvath, C. Peterson, ABCB1 G1199A polymorphism and ovarian cancer response to paclitaxel, *J. Pharm. Sci.* 97 (2008) 2045–2048. doi:10.1002/jps.21169.
- [352] H. Gréen, I.J. Falk, K. Lotfi, E. Paul, M. Hermansson, R. Rosenquist, C. Paul, H. Nahi, Association of ABCB1 polymorphisms with survival and in vitro cytotoxicity in de novo acute myeloid leukemia with normal karyotype, *Pharmacogenomics J.* 12 (2012) 111–118. doi:10.1038/tpj.2010.79.
- [353] J. Gregers, H. Gréen, I.J. Christensen, K. Dalhoff, H. Schroeder, N. Carlsen, S. Rosthøj, B. Lausen, K. Schmiegelow, C. Peterson, Polymorphisms in the ABCB1 gene and effect on outcome and toxicity in childhood acute lymphoblastic leukemia, *Pharmacogenomics J.* (2015). doi:10.1038/tpj.2014.81.
- [354] R. Boulton, The copigmentation of anthocyanins and its role in the color of red wine: a critical review, *Am. J. Enol. Vitic.* 52 (2001) 67–87.



- [355] P. Trouillas, F. Di Meo, J. Gierschner, M. Linares, J.C. Sancho-García, M. Otyepka, Optical properties of wine pigments: theoretical guidelines with new methodological perspectives, *Tetrahedron*. 71 (2015) 3079–3088. doi:10.1016/j.tet.2014.10.046.
- [356] R. Brouillard, B. Delaporte, Chemistry of anthocyanin pigments. 2. Kinetic and thermodynamic study of proton transfer, hydration, and tautomeric reactions of malvidin 3-glucoside, *J. Am. Chem. Soc.* 99 (1977) 8461–8468. doi:10.1021/ja00468a015.
- [357] P.G.I. Robert E Asenstorfer, Charge equilibria and pK(a) of malvidin-3-glucoside by electrophoresis, *Anal. Biochem.* 318 (2003) 291–9. doi:10.1016/S0003-2697(03)00249-5.
- [358] T.K. McGhie, M.C. Walton, The bioavailability and absorption of anthocyanins: Towards a better understanding, *Mol. Nutr. Food Res.* 51 (2007) 702–713. doi:10.1002/mnfr.200700092.
- [359] J. He, A.R.F. Carvalho, N. Mateus, V. De Freitas, Spectral Features and Stability of Oligomeric Pyranoanthocyanin-flavanol Pigments Isolated from Red Wines, *J. Agric. Food Chem.* 58 (2010) 9249–9258. doi:10.1021/jf102085e.
- [360] V. Freitas, N. Mateus, Formation of pyranoanthocyanins in red wines: a new and diverse class of anthocyanin derivatives, *Anal. Bioanal. Chem.* 401 (2011) 1463–1473. doi:10.1007/s00216-010-4479-9.
- [361] R. Brouillard, G. Mazza, Z. Saad, A.M. Albrecht-Gary, A. Cheminat, The copigmentation reaction of anthocyanins: a microprobe for the structural study of aqueous solutions, *J. Am. Chem. Soc.* 111 (1989) 2604–2610. doi:10.1021/ja00189a039.
- [362] G. Fabre, I. Bayach, K. Berka, M. Palonciová, M. Starok, C. Rossi, J.-L. Duroux, M. Otyepka, P. Trouillas, Synergism of antioxidant action of vitamins E, C and quercetin is related to formation of molecular associations in biomembranes, *Chem. Commun.* 51 (2015) 7713–7716. doi:10.1039/C5CC00636H.
- [363] M.P. Kähkönen, M. Heinonen, Antioxidant Activity of Anthocyanins and Their Aglycons, *J. Agric. Food Chem.* 51 (2003) 628–633. doi:10.1021/jf025551i.
- [364] I.G. Roussis, I. Lambropoulos, K. Soulti, Scavenging capacities of some wines and wine phenolic extracts, *Food Technol. Biotechnol.* 43 (2005) 351–358.
- [365] C. Tsang, S. Higgins, G.G. Duthie, S.J. Duthie, M. Howie, W. Mullen, M.E.J. Lean, A. Crozier, The influence of moderate red wine consumption on antioxidant status and indices of oxidative stress associated with CHD in healthy volunteers, *Br. J. Nutr.* 93 (2005) 233–240. doi:10.1079/BJN20041311.
- [366] D. Villaño, M.S. Fernández-Pachón, A.M. Troncoso, M.C. García-Parrilla, Influence of enological practices on the antioxidant activity of wines, *Food Chem.* 95 (2006) 394–404. doi:10.1016/j.foodchem.2005.01.005.
- [367] M.D. Rivero-Pérez, P. Muñoz, M.L. González-Sanjosé, Contribution of anthocyanin fraction to the antioxidant properties of wine, *Food Chem. Toxicol.* 46 (2008) 2815–2822. doi:10.1016/j.fct.2008.05.014.
- [368] A. Ghiselli, M. Nardini, A. Baldi, C. Scaccini, Antioxidant activity of different phenolic fractions separated from Italian red wine, *J. Agric. Food Chem.* 46 (1998) 361–367.



- [369] P. Kar, D. Laight, K.M. Shaw, M.H. Cummings, Flavonoid-rich grapeseed extracts: A new approach in high cardiovascular risk patients?, *Int. J. Clin. Pract.* 60 (2006) 1484–1492. doi:10.1111/j.1742-1241.2006.01038.x.
- [370] H. Kamei, Y. Hashimoto, T. Koide, T. Kojima, M. Hasegawa, Anti-tumor effect of methanol extracts from red and white wines, *Cancer Biother. Radiopharm.* 13 (1998) 447–452.
- [371] A. Jankowski, B. Jankowska, J. Niedworok, The effect of anthocyanin dye from grapes on experimental diabetes, *Folia Med. Cracov.* 41 (2000) 5–15.
- [372] P. Pawłowicz, J. Wilczyński, G. Stachowiak, P. Hincz, Administration of natural anthocyanins derived from chokeberry retardation of idiopathic and preeclamptic origin. Influence on metabolism of plasma oxidized lipoproteins: the role of autoantibodies to oxidized low density lipoproteins, *Ginekol. Pol.* 71 (2000) 848–853.
- [373] C. Jhin, K.T. Hwang, Prediction of Radical Scavenging Activities of Anthocyanins Applying Adaptive Neuro-Fuzzy Inference System (ANFIS) with Quantum Chemical Descriptors, *Int. J. Mol. Sci.* 15 (2014) 14715–14727. doi:10.3390/ijms150814715.
- [374] F. Di Meo, V. Lemaury, J. Cornil, R. Lazzaroni, J.-L. Duroux, Y. Olivier, P. Trouillas, Free Radical Scavenging by Natural Polyphenols: Atom versus Electron Transfer, *J. Phys. Chem. A.* 117 (2013) 2082–2092. doi:10.1021/jp3116319.
- [375] T. Tsuda, K. Shiga, K. Ohshima, S. Kawakishi, T. Osawa, Inhibition of lipid peroxidation and the active oxygen radical scavenging effect of anthocyanin pigments isolated from *Phaseolus vulgaris* L., *Biochem. Pharmacol.* 52 (1996) 1033–1039. doi:10.1016/0006-2952(96)00421-2.
- [376] X. Zhang, Y. Shen, W. Prinyawiwatkul, J.M. King, Z. Xu, Comparison of the activities of hydrophilic anthocyanins and lipophilic tocopherols in black rice bran against lipid oxidation, *Food Chem.* 141 (2013) 111–116. doi:10.1016/j.foodchem.2013.03.034.
- [377] A. Arora, T.M. Byrem, M.G. Nair, G.M. Strasburg, Modulation of liposomal membrane fluidity by flavonoids and isoflavonoids, *Arch. Biochem. Biophys.* 373 (2000) 102–109. doi:10.1006/abbi.1999.1525.
- [378] A.F. Lenne-Gouverneur, A. Lobstein, G. Haan-Archipoff, G. Duportail, R. Anton, J.G. Kuhry, Interactions of the monomeric and dimeric flavones apigenin and amentoflavone with the plasma membrane of L929 cells; a fluorescence study, *Mol. Membr. Biol.* 16 (1999) 157–165.
- [379] M.J. Abraham, T. Murtola, R. Schulz, S. Páll, J.C. Smith, B. Hess, E. Lindahl, GROMACS: High performance molecular simulations through multi-level parallelism from laptops to supercomputers, *SoftwareX.* (n.d.). doi:10.1016/j.softx.2015.06.001.
- [380] A.W. Schüttelkopf, D.M.F. van Aalten, PRODRG: a tool for high-throughput crystallography of protein-ligand complexes, *Acta Crystallogr. D Biol. Crystallogr.* 60 (2004) 1355–1363. doi:10.1107/S0907444904011679.
- [381] J.A. Lemkul, W.J. Allen, D.R. Bevan, Practical Considerations for Building GROMOS-Compatible Small-Molecule Topologies, *J. Chem. Inf. Model.* 50 (2010) 2221–2235. doi:10.1021/ci100335w.



- [382] M. Frisch, G. Trucks, H. Schlegel, G. Scuseria, M. Robb, J. Cheeseman, G. Scalmani, V. Barone, B. Mennucci, G. Petersson, H. Nakatsuji, M. Caricato, X. Li, H. Hratchian, A. Izmaylov, J. Bloino, G. Zheng, J. Sonnenberg, M. Hada, M. Ehara, K. Toyota, R. Fukuda, J. Hasegawa, M. Ishida, T. Nakajima, Y. Honda, O. Kitao, H. Nakai, T. Vreven, J. Montgomery, J. Peralta, F. Ogliaro, M. Bearpark, J. Heyd, E. Brothers, K. Kudin, V. Staroverov, R. Kobayashi, J. Normand, K. Raghavachari, A. Rendell, J. Burant, S. Iyengar, J. Tomasi, M. Cossi, N. Rega, J. Millam, M. Klene, J. Knox, J. Cross, V. Bakken, C. Adamo, J. Jaramillo, R. Gomperts, R. Stratmann, O. Yazyev, A. Austin, R. Cammi, C. Pomelli, J. Ochterski, R. Martin, K. Morokuma, V. Zakrzewski, G. Voth, P. Salvador, J. Dannenberg, S. Dapprich, A. Daniels, Farkas, J. Foresman, J. Ortiz, J. Cioslowski, D. Fox, Gaussian 09, Revision A.02, (2009).
- [383] F.-Y. Dupradeau, A. Pigache, T. Zaffran, C. Savineau, R. Lelong, N. Grivel, D. Lelong, W. Rosanski, P. Cieplak, The R.E.D. tools: advances in RESP and ESP charge derivation and force field library building, *Phys. Chem. Chem. Phys.* 12 (2010) 7821–7839. doi:10.1039/C0CP00111B.
- [384] Y. Duan, C. Wu, S. Chowdhury, M.C. Lee, G. Xiong, W. Zhang, R. Yang, P. Cieplak, R. Luo, T. Lee, J. Caldwell, J. Wang, P. Kollman, A point-charge force field for molecular mechanics simulations of proteins based on condensed-phase quantum mechanical calculations, *J. Comput. Chem.* 24 (2003) 1999–2012. doi:10.1002/jcc.10349.
- [385] W.D. Cornell, P. Cieplak, C.I. Bayly, I.R. Gould, K.M. Merz, D.M. Ferguson, D.C. Spellmeyer, T. Fox, J.W. Caldwell, P.A. Kollman, A Second Generation Force Field for the Simulation of Proteins, Nucleic Acids, and Organic Molecules, *J. Am. Chem. Soc.* 117 (1995) 5179–5197. doi:10.1021/ja00124a002.
- [386] N.M. O'Boyle, T. Vandermeersch, C.J. Flynn, A.R. Maguire, G.R. Hutchison, Confab - Systematic generation of diverse low-energy conformers, *J. Cheminformatics.* 3 (2011) 8. doi:10.1186/1758-2946-3-8.
- [387] A.R. Braun, J.N. Sachs, J.F. Nagle, Comparing simulations of lipid bilayers to scattering data: the GROMOS 43A1-S3 force field, *J. Phys. Chem. B.* 117 (2013) 5065–5072. doi:10.1021/jp401718k.
- [388] T. Darden, D. York, L. Pedersen, Particle mesh Ewald: An N-log(N) method for Ewald sums in large systems, *J. Chem. Phys.* 98 (1993) 10089–10092. doi:10.1063/1.464397.
- [389] W. Humphrey, A. Dalke, K. Schulten, VMD: Visual molecular dynamics, *J. Mol. Graph.* 14 (1996) 33–38. doi:10.1016/0263-7855(96)00018-5.
- [390] A. Klamt, F. Eckert, W. Arlt, COSMO-RS: An Alternative to Simulation for Calculating Thermodynamic Properties of Liquid Mixtures, *Annu. Rev. Chem. Biomol. Eng.* 1 (2010) 101–122. doi:10.1146/annurev-chembioeng-073009-100903.
- [391] R. Ahlrichs, F. Furche, S. Grimme, Comment on “Assessment of exchange correlation functionals” [A.J. Cohen, N.C. Handy, *Chem. Phys. Lett.* 316 (2000) 160–166], *Chem. Phys. Lett.* 325 (2000) 317–321. doi:10.1016/S0009-2614(00)00654-0.
- [392] M.T. Satué-Gracia, M. Heinonen, E.N. Frankel, Anthocyanins as Antioxidants on Human Low-Density Lipoprotein and Lecithin-Liposome Systems, *J. Agric. Food Chem.* 45 (1997) 3362–3367. doi:10.1021/jf970234a.



- [393] I. Hubatsch, E.G.E. Ragnarsson, P. Artursson, Determination of drug permeability and prediction of drug absorption in Caco-2 monolayers, *Nat. Protoc.* 2 (2007) 2111–2119. doi:10.1038/nprot.2007.303.
- [394] X. Liu, B. Testa, A. Fahr, Lipophilicity and Its Relationship with Passive Drug Permeation, *Pharm. Res.* 28 (2010) 962–977. doi:10.1007/s11095-010-0303-7.
- [395] P. Matsson, L.A. Fenu, P. Lundquist, J.R. Wiśniewski, M. Kansy, P. Artursson, Quantifying the impact of transporters on cellular drug permeability, *Trends Pharmacol. Sci.* 36 (2015) 255–262. doi:10.1016/j.tips.2015.02.009.
- [396] D. Bemporad, J.W. Essex, C. Luttmann, Permeation of Small Molecules through a Lipid Bilayer: A Computer Simulation Study, *J. Phys. Chem. B.* 108 (2004) 4875–4884. doi:10.1021/jp035260s.
- [397] R. Gupta, D.B. Sridhar, B. Rai, Molecular Dynamics Simulation Study of Permeation of Molecules through Skin Lipid Bilayer, *J. Phys. Chem. B.* 120 (2016) 8987–8996. doi:10.1021/acs.jpcc.6b05451.
- [398] M. Orsi, J.W. Essex, Permeability of drugs and hormones through a lipid bilayer: insights from dual-resolution molecular dynamics, *Soft Matter.* 6 (2010) 3797. doi:10.1039/c0sm00136h.
- [399] S.J. Marrink, H.J.C. Berendsen, Permeation Process of Small Molecules across Lipid Membranes Studied by Molecular Dynamics Simulations, *J. Phys. Chem.* 100 (1996) 16729–16738. doi:10.1021/jp952956f.
- [400] D. Bemporad, C. Luttmann, J.W. Essex, Behaviour of small solutes and large drugs in a lipid bilayer from computer simulations, *Biochim. Biophys. Acta BBA - Biomembr.* 1718 (2005) 1–21. doi:10.1016/j.bbamem.2005.07.009.
- [401] S.-W. Chiu, S.A. Pandit, H.L. Scott, E. Jakobsson, An improved united atom force field for simulation of mixed lipid bilayers, *J. Phys. Chem. B.* 113 (2009) 2748–2763. doi:10.1021/jp807056c.
- [402] Gaussian 09 Citation, (n.d.). http://www.gaussian.com/g_tech/g_ur/m_citation.htm (accessed October 15, 2016).
- [403] S. Nosé, A unified formulation of the constant temperature molecular dynamics methods, *J. Chem. Phys.* 81 (1984) 511. doi:10.1063/1.447334.
- [404] W.G. Hoover, Canonical dynamics: Equilibrium phase-space distributions, *Phys. Rev. A.* 31 (1985) 1695–1697.
- [405] M. Parrinello, A. Rahman, Polymorphic transitions in single crystals: A new molecular dynamics method, *J. Appl. Phys.* 52 (1981) 7182–7190. doi:10.1063/1.328693.
- [406] T. Darden, D. York, L. Pedersen, Particle Mesh Ewald: An $N \cdot \log(N)$ Method for Ewald Sums in Large Systems, *J. Chem. Phys.* 98 (1993) 10089–10092. doi:10.1063/1.464397.
- [407] MemGen, (n.d.). <http://memgen.uni-goettingen.de/> (accessed October 15, 2016).
- [408] B. Roux, M. Karplus, Ion transport in a gramicidin-like channel: dynamics and mobility, *J. Phys. Chem.* 95 (1991) 4856–4868. doi:10.1021/j100165a049.
- [409] R. Kubo, The fluctuation-dissipation theorem, *Rep. Prog. Phys.* 29 (1966) 255. doi:10.1088/0034-4885/29/1/306.



- [410] T.-X. Xiang, B.D. Anderson, The relationship between permeant size and permeability in lipid bilayer membranes, *J. Membr. Biol.* 140 (n.d.) 111–122. doi:10.1007/BF00232899.
- [411] D. Bemporad, C. Luttmann, J.W. Essex, Computer Simulation of Small Molecule Permeation across a Lipid Bilayer: Dependence on Bilayer Properties and Solute Volume, Size, and Cross-Sectional Area, *Biophys. J.* 87 (2004) 1–13. doi:10.1529/biophysj.103.030601.
- [412] D. Bassolino-Klimas, H.E. Alper, T.R. Stouch, Mechanism of Solute Diffusion through Lipid Bilayer Membranes by Molecular Dynamics Simulation, *J. Am. Chem. Soc.* 117 (1995) 4118–4129. doi:10.1021/ja00119a028.
- [413] B. Thorens, M. Mueckler, Glucose transporters in the 21st Century, *Am. J. Physiol. - Endocrinol. Metab.* 298 (2010) E141–E145. doi:10.1152/ajpendo.00712.2009.
- [414] I. Oren, S.J. Fleishman, A. Kessel, N. Ben-Tal, Free Diffusion of Steroid Hormones Across Biomembranes: A Simplex Search with Implicit Solvent Model Calculations, *Biophys. J.* 87 (2004) 768–779. doi:10.1529/biophysj.103.035527.
- [415] C. Manach, A. Scalbert, C. Morand, C. Rémésy, L. Jiménez, Polyphenols: food sources and bioavailability, *Am. J. Clin. Nutr.* 79 (2004) 727–747.
- [416] G. Fabre, I. Bayach, K. Berka, M. Paloncýová, M. Starok, C. Rossi, J.-L. Duroux, M. Otyepka, P. Trouillas, Synergism of antioxidant action of vitamins E, C and quercetin is related to formation of molecular associations in biomembranes, *Chem. Commun.* 51 (2015) 7713–7716. doi:10.1039/C5CC00636H.
- [417] P. Košinová, K. Berka, M. Wykes, M. Otyepka, P. Trouillas, Positioning of antioxidant quercetin and its metabolites in lipid bilayer membranes: implication for their lipid-peroxidation inhibition, *J. Phys. Chem. B.* 116 (2012) 1309–1318. doi:10.1021/jp208731g.
- [418] J. Rautio, *Prodrugs and Targeted Delivery: Towards Better ADME Properties*, John Wiley & Sons, 2011.
- [419] M. Fujikawa, K. Nakao, R. Shimizu, M. Akamatsu, QSAR study on permeability of hydrophobic compounds with artificial membranes, *Bioorg. Med. Chem.* 15 (2007) 3756–3767. doi:10.1016/j.bmc.2007.03.040.



Physical-chemical understanding of membrane partitioning and permeation at an atomic resolution: towards *in silico* pharmacology

The mechanism of interaction between drugs or any xenobiotic and membrane is one of the key factors that affect its biological of action, and so its therapeutic activity. A thorough rationalization of the relationship between the intrinsic properties of the xenobiotics and their mechanism of interaction with membranes can now be assessed with atomistic details. Molecular dynamics (MD) is a powerful research tool to study xenobiotics-membrane interactions, which can access time and space scales that are not simultaneously accessible by experimental methods. Semi-quantitative molecular and thermodynamic descriptions of these interactions can be provided using *in silico* model of lipid bilayers, often in agreement with experimental measurements.

The main goal of our investigation consisted to get in depth insight into the mechanisms of interaction/partitioning/insertion/crossing with/in/into/through membrane and drug delivery using MD. In this thesis, we have focused on both drugs used in renal transplantation (e.g., antivirals, immunosuppressants) and antioxidants, which can also be used to protect organs along the transplantation processes. We have provided a series of clues showing that MD simulations can tackle the delicate process of drug passive permeation.

Both, unbiased and biased MD (*z*-constraint) simulations have been used to elucidate the xenobiotics-membrane interactions (i.e., positioning and orientation) and to evaluate crossing energies, diffusion coefficients, and permeability coefficients. These findings led us to draw qualitative structure-permeability relationships (SPR). We have carefully analyzed how the chemical and physical properties of xenobiotics affect the mechanism of interactions and thus permeability. The robustness of these MD-based methodologies has been determined to qualitatively predict these pharmacological parameters. Hydrophobic compounds showed a favorable partitioning into the lipid bilayer and relatively low Gibbs energy of crossing the center of membrane (ΔG_{cross}). Hydrophilic or charged compounds showed partitioning close to membrane surface, in interaction with the polar head groups and water molecules; this has been shown to dramatically increase ΔG_{cross} . Amphiphilic compounds are intermediate compounds in terms of membrane insertion/positioning/crossing. It clearly appears that they should be analyzed case by case, an analysis for which MD simulations could be particularly supportive. Also the influence of size at predicting permeation has been studied (i.e., relatively large drugs were tested). The molecular size has shown no significant influence on ΔG_{cross} whereas diffusion coefficients were significantly affected, depending on the membrane regions.

Keywords: (un)biased molecular dynamics; lipid bilayer membranes; partitioning; passive permeation; antivirals; immunosuppressants; antioxidants.



Compréhension physico-chimique de la partition et de la perméation membranaire à l'échelle atomique: vers la pharmacologie in silico

Le mécanisme d'interaction d'un composé *xénobiotique* avec la membrane est un des facteurs clés qui influence son mécanisme d'action biologique et donc son action thérapeutique pour un principe actif. Une analyse précise des interactions intermoléculaires à l'échelle atomique peut être obtenue par dynamique moléculaire, une méthode qui apparaît plus que jamais comme une alternative élégante aux techniques expérimentales. Les simulations de dynamique moléculaire permettent d'évaluer ces interactions avec une résolution temporelle et spatiale difficiles à atteindre avec les méthodes expérimentales. Ces informations constituent une pierre angulaire de la compréhension des mécanismes d'action des *xénobiotiques*. Les résultats obtenus corréleront généralement bien avec les données expérimentales.

Dans ce travail théorique, nous avons utilisé des dynamiques moléculaires non-biaisées et biaisées (z-Contraint). Nous avons étudié les modes d'insertion (positionnement et orientation), les coefficients de partition, et la capacité de différents xénobiotiques à traverser la bicouche lipidique (perméation passive). Plusieurs composés de différentes familles thérapeutiques ont été étudiés (antiviraux, immunosuppresseurs et antioxydants), tous étant utilisés en transplantation d'organes ; les antioxydants sont étudiés en tant que protecteurs d'organe contre les phénomènes d'ischémie-reperfusion. Pour la perméation passive, les profils d'énergies, les coefficients de diffusion locaux et la résistance à la traversée ont été calculés pour finalement obtenir des coefficients globaux de perméabilité. Nous avons montré que ces techniques de calcul donnent une description qualitative du processus d'insertion/perméation, montrant notamment le rôle de différentes propriétés physiques (ex., polarité, charge). Des résultats remarquables ont été obtenus pour les larges molécules. Malgré la taille, ces molécules peuvent s'insérer dans la bicouche lipidique relativement facilement (faibles barrières énergétiques). Par contre, leur diffusion dans les différentes régions de la membrane peut augmenter d'une manière significative.

Ce travail donne une confiance accrue dans les méthodes de dynamique moléculaire pour devenir prédictive dans les années à venir, et aide de façon concrète les pharmacologues dans la recherche de nouvelles stratégies thérapeutiques.

Mots-clés: Dynamiques moléculaires non-biaisées et biaisées; bicouche lipidique ; partition; perméation passive; antiviraux; immunosuppresseurs; antioxydants.

